

TECHNISCHE UNIVERSITÄT MÜNCHEN

Fakultät für Medizin
Klinikum rechts der Isar
Medizinische Klinik und Poliklinik für Innere Medizin II

Systematic analysis of the class I histone deacetylases HDAC1, HDAC2 and HDAC3 in pancreatic cancer

Sieglinde Theresia Hastreiter

Vollständiger Abdruck der von der Fakultät für Medizin der Technischen Universität
München zur Erlangung des akademischen Grades eines
Doktors der Naturwissenschaften
genehmigten Dissertation.

Vorsitzende/-r: Prof. Dr. Martin Göttlicher
Prüfende/-r der Dissertation: 1. Priv.-Doz. Dr. Günter Schneider
2. Prof. Dr. Dr. h.c. mult. Martin Hrabě de Angelis

Die Dissertation wurde am 12.11.2020 bei der Technischen Universität München
eingereicht und durch die Fakultät für Medizin am 16.03.2021 angenommen.

Table of contents

List of tables	IV
List of figures	V
List of supplementary tables	VI
List of supplementary figures	VI
List of appendix figures	VII
Abbreviations	VIII
1. Summary	1
2. Zusammenfassung	3
3. Introduction	5
3.1 Pancreatic ductal adenocarcinoma	6
3.1.1 Progression of PDAC	7
3.1.2 Mouse models of PDAC	9
3.1.3 Mechanisms of metastatic spread	11
3.2 Histone deacetylases	16
3.2.1 HDAC isoenzymes	17
3.2.2 Role of HDACs in cancer, especially in PDAC	19
4. Aims of the work	23
5. Technical equipment	24
6. Methods	30
6.1 Mouse models	30
6.2 Cell culture techniques	35
6.3 Molecular techniques	44
6.3.1 Genotyping	44
6.3.2 RNA analysis	48
6.3.3 Protein analysis	51
6.4 Histological analysis	56

6.5	Statistical testing.....	60
6.6	Software	62
7.	Results.....	63
7.1	HDAC inhibitor treatment in murine PDAC cell lines	63
7.2	Inducible knock-out of class I HDACs <i>Hdac1</i> , <i>Hdac2</i> and <i>Hdac3 in vitro</i>	64
7.2.1	Coincident genetic deletion of <i>Hdac1</i> , <i>Hdac2</i> and <i>Hdac3</i> in murine PDAC cell lines	64
7.2.2	Genetic deletion of <i>Hdac1</i> in a murine PDAC cell line.....	66
7.2.3	Genetic deletion of <i>Hdac2</i> in murine PDAC cell lines	68
7.2.4	Genetic deletion of <i>Hdac3</i> in murine PDAC cell lines	72
7.2.5	Cre toxicity.....	75
7.3	Epithelial and mesenchymal fractions of dual-recombination model based PDAC cell lines	77
7.3.1	Differential trypsinization to generate epithelial and mesenchymal fractions of PDAC cell lines	77
7.3.2	Genetic deletion of <i>Hdac2</i> in epithelial and mesenchymal fractions of dual-recombination model based PDAC cell lines.....	80
7.3.3	Pathway analysis in <i>Hdac2</i> deficient PDAC cells	82
7.3.4	TGF β pathway activation in <i>Hdac2</i> deficient PDAC cell lines	84
7.3.5	Specific role of HDAC2 in TGF β induced EMT.....	87
7.3.6	Rescue of TGF β induced decrease in cell survival and colony formation in <i>Hdac2</i> deficient PDAC cells	89
7.4	<i>In vivo</i> phenotype of <i>Hdac2</i> deficient KPC mice	92
7.4.1	Fewer metastases in <i>Hdac2</i> deficient mice	94
8.	Discussion	96
8.1	Effects of HDACis and inducible coincident and separate genetic deletion of class I HDACs <i>Hdac1</i> , <i>Hdac2</i> and <i>Hdac3 in vitro</i>	96
8.2	Epithelial and mesenchymal fraction of dual-recombinase based PDAC cell lines	107

8.3	<i>In vivo</i> phenotype of <i>Hdac2</i> deficient KPC mice	112
9.	Reference List.....	116
10.	Acknowledgements.....	135
11.	Supplementary Information.....	136
12.	Appendix.....	139

List of tables

Nomenclature of tables consists of the chapter the table is located in and the number of the table. For example, Table 3-1 is the first table in chapter 3.

Table 3-1: HDAC inhibitors in clinical trials.....	21
Table 5-1: Technical equipment.....	24
Table 5-2: Disposables.....	25
Table 5-3: Cell culture reagents and media.....	26
Table 5-4: Compounds.....	27
Table 5-5: Kits.....	27
Table 5-6: Reagents and enzymes.....	27
Table 5-7: Histology reagents.....	29
Table 6-1: Mice used for survival analysis.....	34
Table 6-2: Cell lines and genotypes.....	36
Table 6-3: Primer sequences for Mycoplasma test PCR.....	38
Table 6-4: Conditions for Mycoplasma test PCR.....	38
Table 6-5: Compounds used in MTT and Clonogenic Assay.....	42
Table 6-6: Voltage for cell cycle FACS analysis.....	44
Table 6-7: Conditions for lysis of tail biopsies.....	45
Table 6-8: Buffers for DNA isolation.....	45
Table 6-9: PCR mix and PCR conditions.....	46
Table 6-10: Primer sequences for genotyping PCR.....	46
Table 6-11: TAE buffer.....	48
Table 6-12: Reverse transcription mix and PCR conditions.....	49
Table 6-13: qRT-PCR reagents.....	50
Table 6-14: Primer sequences for qRT-PCR.....	50
Table 6-15: Laemmli buffer.....	52
Table 6-16: Buffers for western blot.....	53
Table 6-17: Conditions for SDS-PAGE gels.....	53
Table 6-18: Antibodies used for western blot.....	54
Table 6-19: Mice used for tumor grading and metastasis screening.....	58
Table 6-20: Software.....	62
Table 7-1: Differential trypsinization in PDAC cell lines.....	78
Table 7-2: Morphology of <i>Hdac2</i> pro- and deficient KPC cell lines.....	93
Table 7-3: Differential trypsinization <i>Hdac2</i> pro- and deficient KPC cell lines.....	93

List of figures

Nomenclature of figures consists of the chapter the figure is located in and the number of the figure. For example, Figure 3-1 is the first figure in chapter 3.

Figure 3-1: Expected number of cancer related deaths in the United States by 2030.	5
Figure 3-2: Progression model of PDAC	8
Figure 3-3: Affected pathways in PDAC progression	9
Figure 3-4: TGF β signaling pathway	14
Figure 3-5: Family of histone deacetylases	17
Figure 6-1: Genetic strategy of used KPC mouse model	31
Figure 6-2: Genetic strategy of used dual-recombinase mouse model	33
Figure 7-1: HDACi treatment in PDAC cell lines PPT-F1648, PPT-F2612 and PPT-F2800	63
Figure 7-2: Coincident genetic deletion of <i>Hdac1</i> , <i>Hdac2</i> and <i>Hdac3</i> in murine PDAC cell lines PPT-F5461, PPT-F5465 and PPT-F5470	65
Figure 7-3: Genetic deletion of <i>Hdac1</i> in murine PDAC cell line PPT-F3641	67
Figure 7-4: Genetic deletion of <i>Hdac2</i> in murine PDAC cell lines PPT-F1648, PPT-F2612 and PPT-F2800	68
Figure 7-5: FACS cell cycle analysis in <i>Hdac2</i> pro- and deficient PDAC cell line PPT-F1648	70
Figure 7-6: H3K27 acetylation in cell line PPT-F1648	71
Figure 7-7: Genetic deletion of <i>Hdac3</i> in PDAC cell lines PPT3-F4764, PPT3-F4402, PPT-F5061 and PPT2-F4699	72
Figure 7-8: FACS cell cycle analysis of <i>Hdac3</i> pro- and deficient PDAC cell lines PPT3-F4764, PPT3-F4402, PPT-F5061 and PPT2-F4699	74
Figure 7-9: Excluding Cre Toxicity and effect of heterozygous deletion of <i>Pdk1</i>	76
Figure 7-10: Differential trypsinization to generate epithelial and mesenchymal fractions of cell lines PPT-F2612 and PPT-F2800	79
Figure 7-11: <i>Hdac2</i> knock-out in epithelial and mesenchymal fractions of cell lines PPT-F2612 and PPT-F2800	81
Figure 7-12: Pathway analysis of <i>Hdac2</i> deficient PDAC cells	83
Figure 7-13: TGF β pathway activation in <i>Hdac2</i> pro- and deficient cell lines of KPC model	85

Figure 7-14: TGF β pathway activation in <i>Hdac2</i> pro- and deficient epithelial and mesenchymal fractions of cell lines PPT-F2612 and PPT-F2800	86
Figure 7-15: Activation of TGF β pathway in <i>Hdac1</i> pro- and deficient PPT-F3641 cells and in <i>Hdac3</i> pro- and deficient PPT2-F4699 cells	88
Figure 7-16: Inhibition of TGF β receptors in <i>Hdac2</i> pro- and deficient PPT-F1648 cells followed by TGF β pathway activation.....	90
Figure 7-17: Survival data and <i>in vivo</i> phenotype of <i>Hdac2</i> pro- and deficient KPC mice	92
Figure 7-18: Fewer metastasis in KPC, <i>Hdac2</i> ^{lox/lox} mice	94
Figure 7-19: Immunohistochemical analysis of HDAC2 expression in liver and lung metastasis of KPC, <i>Hdac2</i> ^{lox/lox} mice	95

List of supplementary tables

Nomenclature of supplementary tables consists of the chapter the table is located in and the number of the table. For example, Table S 1 is the first table in the chapter “supplementary data”.

Table S 1: Cultivation of picked clones of <i>Hdac1/2/3</i> deficient PDAC cell lines	136
Table S 2: Established epithelial and mesenchymal fractions of PDAC cell lines ...	136

List of supplementary figures

Nomenclature of supplementary figures consists of the chapter the figure is located in and the number of the figure. For example, Figure S 1 is the first figure in the chapter “supplementary data”.

Figure S 1: Proteome analysis of <i>Hdac2</i> pro- and deficient PPT-F1648 cells.....	137
Figure S 2: RGFP966 treatment in PDAC cell lines PPT-F1648, PPT-F2612, PPT-F1042 and PPT-F1146.....	137
Figure S 3: Western blot analysis of HDAC1 expression in PDAC cell lines PPT-F1648, PPT-F2612, PPT-F2800.....	138
Figure S 4: Immunohistochemical analysis of HDAC2 expression in KPC mice.....	138

List of appendix figures

Nomenclature of supplementary figures consists of the chapter the figure is located in and the number of the figure. For example, Figure A 1 is the first figure in the chapter “Appendix”.

Figure A 1: Original western blots and clonogenic assays of Figure 7-2.	139
Figure A 2: Original western blots and clonogenic assays of Figure 7-3.	139
Figure A 3: Original western blots and clonogenic assays of Figure 7-4, Figure 7-5 and Figure 7-6.	140
Figure A 4: Original western blots and clonogenic assays of Figure 7-7 and Figure 7-8.	141
Figure A 5: Original western blots and clonogenic assays of Figure 7-9.	142
Figure A 6: Original western blots of Figure 7-10.	143
Figure A 7: Original western blots and clonogenic assays of Figure 7-10.	144
Figure A 8: Light microscopy picture and clonogenic assays of Figure 7-13 and Figure 7-14.	145
Figure A 9: Original western blots and clonogenic assays of Figure 7-15.	146
Figure A 10: Original western blots and H&E stainings of <i>Hdac2</i> pro- and deficient KPC mice of Figure 7-17.	147
Figure A 11: H&E stainings of liver and lung of <i>Hdac2</i> pro- and deficient KPC mice of Figure 7-18 and Immunohistochemical analysis of HDAC2 expression in liver and lung metastasis of <i>Hdac2</i> deficient KPC mice of Figure 7-19.	148
Figure A 12: Original western blots of Figure S 3.	149
Figure A 13: Immunohistochemical analysis of HDAC2 expression in PPTs of KPC mice of Figure S 4.	149

Abbreviations

°C	Degree Celsius
4-OHT	4-Hydroxytamoxifen
ADM	Acinar-to-ductal metaplasia
AFL	Atypical flat lesion
APS	Ammonium persulfate
bp	Base pairs
BSA	Bovine serum albumin
cDNA	Complementary desoxyribonucleic acid
d	Days
DMEM	Dulbecco's Modified Eagles Medium
DMSO	Dimethylsulfoxide
DNA	Desoxyribonucleic acid
dNTP	Deoxyribonucleotide triphosphate
EDTA	Ethylenediaminetetraacetic acid
EGFR	Epidermal growth factor receptor
ER ^{T2}	Tamoxifen-inducible estrogen receptor
EMT	Epithelial-to-mesenchymal transition
EUCOMM	European Conditional Mouse Mutagenesis Program
EtOH	Ethanol
FACS	Fluorescence-activated cell sorting
FDA	US Food and Drug Administration
FCS	Fetal calf serum
Flp/frt	Flippase/frt
FSF	Frt-stop-frt
GSEA	Gene Set Enrichment Analysis
GEMM	Genetically engineered mouse model
h	Hours
H&E	Hematoxylin and eosin
HAT	Histone acetyltransferase
HDAC	Histone deacetylase
HDACi	HDAC inhibitor(s)
IPMN	Intraductal papillary mucinous neoplasm
kb	Kilo base pairs
KPC	<i>LSL-Kras^{G12D/+};LSL-Trp53^{R172H/+};Pdx1-Cre</i>
LSL	<i>loxP-Stop-loxP</i>
M	Mol/Molar
MCN	Mucinous cystic neoplasm
MEtOH	Methanol
MMP	Matrix metalloproteinases
MET	Mesenchymal-to-epithelial transition
mg	Milligram
min	Minute

ml	Milliliter
mM	Millimol/Millimolar
MTT	3-(4,5-dimethylthiazol-2-yl)-2,5-dipheyltetrazolium bromide
ng	Nanogram
nm	Nanometer
nM	Nanomol/Nanomolar
p-	Phospho-
PanIN	Pancreatic intraepithelial neoplasia
PBS	Phosphate buffered saline
PCR	Polymerasechainreaction
PDAC	Pancreatic ductal adenocarcinoma
PDGFR	Platelet-derived growth factor receptor
Pen/Strep	Penicillin/Streptomycin
PPT	Primary pancreatic tumor
PROTACs	PROteolysis-targeting Chimeras
PI	Propidium iodide
qRT-PCR	Quantitative real-time polymerase chain reaction
R26	Rosa26
RNA	Ribonucleic acid
RNA-Seq	Ribonucleic acid sequencing
Rpm	Rounds per minute
RT	Room temperature
SAHA	Suberoylanilide hydroxamic acid
SD	Standard deviation
SDS-PAGE	Sodium dodecyl sulfate polyacrylamide gel electrophoresis
sec	Seconds
SEM	Standard error of the mean
TAE	Tris acetate EDTA
TBS	TRIS buffered saline
TBS-T	TBS + Tween20
TEMED	<i>N,N,N',N'</i> -Tetramethylethylenediamine
TF	Transcription factor
TGFβ	Transforming growth factor β
Tris	Tris-(hydroxymethyl)-aminomethane
U	Units
V	Volt
v/v	Volume per volume
w/v	Weight per volume
WT	Wildtype
μl	Microliter
μm	Micrometer
μM	Micromolar

1. Summary

Over the last decades the understanding of tumor development and maintenance in general and for pancreatic ductal adenocarcinoma (PDAC) in particular has increased. Nevertheless, there are still many mechanisms which are not fully understood and there are no effective therapeutic options for PDAC still. Histone deacetylases (HDACs) are important players during chromatin remodeling and they are considered to be a therapeutic target in PDAC more and more. There is evidence that HDACs play an important role in PDAC development and maintenance, but it is still unclear which isoenzyme has which specific function.

During this work, the roles of specific HDAC isoenzymes HDAC1, HDAC2 and HDAC3 in PDAC maintenance were characterized. For this purpose, cell lines of PDAC mouse models were generated, allowing for the deletion of specific HDAC isoenzymes. Those pro- and deficient cells were then analyzed concerning proliferation, clonogenic ability and cell cycle progression. Several experiments showed the relevance of HDACs in PDAC maintenance, but it also became clear, that the deletion of every single analyzed isoenzyme has different effects on PDAC maintenance. A comparison between coincidental genetic deletion of *Hdac1*, *Hdac2* and *Hdac3* or treatment with class I HDACi revealed the much stronger effectiveness of the knock-out on cell viability. This observation underlines the need for a new kind of inhibitors that removes the target proteins from the cells.

Besides this, an important part was the separation of the mesenchymal and epithelial fractions of the parental cell lines. These separated fractions reflect the differently differentiated parts of a primary tumor. Due to this separation it was possible to analyze the well differentiated (epithelial) and undifferentiated (mesenchymal) subfraction of the same parental cell line separately. Since the dual-recombinase system is still intact in the fractions, it was also possible to investigate the HDAC isoenzyme's specific function in those morphological contexts by using the same analyzes as previously in the parental cell line. Through those experiments, the different dependencies of the epithelial and mesenchymal fractions became obvious, as they tolerated the loss of HDAC2 expression to different extent. In the same line with the higher sensitivity of mesenchymal fractions to *Hdac2* knock-out, another pivotal discovery was the unique role of HDAC2 during TGF β induced metastatic cascade. This could also be proved by the detailed analysis of the *Hdac2* pro- and deficient KPC mouse model. Therefore,

the *Hdac2* deficient group showed less metastasis in liver and lungs. Additionally, more *Hdac2* deficient mice displayed no metastasis in both organs.

Lessons learned from this work, are not only the relevance of isoenzyme specific treatment options, but also the need of new inhibitors that lead to degradation of the target proteins. Another aspect shown here, is the different effectiveness dependent on the morphological context of the tumor with mesenchymal cells being more sensitive to the loss of HDAC2 expression. The insights gained from the *in vitro* studies could be confirmed *in vivo*, emphasizing their importance.

2. Zusammenfassung

In den letzten Jahrzehnten wuchs das Wissen über die Tumorentstehung und dessen Aufrechterhaltung in vielen Tumorarten, unter anderem im duktalem Pankreaskarzinom (PDAC). Nichtsdestotrotz gibt es zahlreiche Mechanismen, die bis heute nicht entschlüsselt sind und es gibt auch weiterhin keine effektive Therapie für das Pankreaskarzinom.

Histondeacetylasen (HDACs) übernehmen bei der Chromatin-Remodellierung eine Schlüsselrolle und rücken immer mehr in den Fokus als mögliche therapeutische Ansätze zur Therapie des PDAC. Es ist bereits bekannt, dass HDACs bei der Entstehung und Aufrechterhaltung von PDAC relevant sind, allerdings kann den einzelnen Isoenzymen keine spezifische Funktion zugeordnet werden.

Im Rahmen dieser Arbeit wurde die spezifische Rolle der HDAC Isoenzyme HDAC1, HDAC2 und HDAC3 bei der Tumoraufrechterhaltung im Pankreaskarzinom untersucht. Dazu wurden Zelllinien generiert, welche die spezifische Deletion der entsprechenden Isoenzyme ermöglichen. Diese pro- und defizienten Zellen wurden dann bezüglich ihrer Proliferation, Koloniebildung und der Progression durch den Zellzyklus charakterisiert. Diverse Experimente bestätigten die Relevanz von HDACs in der Tumoraufrechterhaltung, zeigten aber auch, dass die Deletion der einzelnen untersuchten Isoenzyme unterschiedlich effektiv ist, um das Tumorwachstum einzuschränken. Ein Vergleich zwischen der gleichzeitigen genetischen Deletion von *Hdac1*, *Hdac2* und *Hdac3* im Gegensatz zur Verwendung von Klasse I HDAC Inhibitoren zeigte den deutlich stärkeren Effekt der genetischen Deletion auf die Zellviabilität im Vergleich zur Inhibierung der Isoenzyme. Diese Beobachtung unterstreicht die Notwendigkeit einer neuen Art von Inhibitoren, welche das Zielprotein aus der Zelle entfernen.

Ein weiterer wichtiger Teil war die Trennung der mesenchymalen und epithelialen Zellfraktionen einer parentalen Zelllinie. Diese aufgetrennten Fraktionen spiegeln die unterschiedlich differenzierten Bereiche des Primärtumors wieder. Dadurch wurde es möglich, die Deletion von HDAC Isoenzymen in den gut differenzierten (epithelialen) und undifferenzierten (mesenchymalen) Subfraktionen der gleichen parentalen Zelllinie getrennt voneinander zu analysieren. Da das duale Rekombinationssystem auch in den Subfraktionen funktional ist, war es so möglich die isoenzym-spezifische Funktion der HDACs in diesen Fraktionen zu analysieren, ebenso wie zuvor in der parentalen Zelllinie. Dadurch wurde deutlich, dass Tumore in unterschiedlichen

Differenzierungsstadien veränderte Abhängigkeiten von den Isoenzymen wie z.B. Hdac2 aufweisen. In die gleiche Richtung wie die beobachtete erhöhte Sensitivität von mesenchymalen Zellen gegenüber dem Verlust von *Hdac2*, geht eine weitere wichtige Entdeckung: die isoenzymspezifische Funktion von HDAC2 während der TGF β induzierten Metastasierung. Diese Beobachtung konnte auch *in vivo* im HDAC2 pro- und defizienten KPC Mausmodell bestätigt werden. So zeigten die HDAC2 defizienten Mäuse einen beeinträchtigten Metastasierungsprozess, wodurch sie weniger Metastasen in Leber und Lunge aufwiesen. Des Weiteren wies eine größere Anzahl von Mäusen der *Hdac2* defizienten Gruppe weniger Metastasen in beiden Organen auf.

Diese Arbeit zeigt sowohl die Notwendigkeit von isoenzymspezifischen Behandlungsmöglichkeiten, sowie auch die Dringlichkeit neue Inhibitoren zu entwickeln, welche zu einer Degradierung des Zielproteins führen. Ein weiterer Aspekt, der hier gezeigt wurde, ist die veränderte Abhängigkeit von diesen Isoenzymen entsprechend dem Differenzierungsstadiums des Tumors. Dabei reagieren mesenchymale Zellen sensitiver auf den Verlust von z. B. *Hdac2*. Die gewonnenen Erkenntnisse aus den *in vitro* Studien wurde in dem *in vivo* Modell bestätigt, wodurch die Bedeutung dieser Beobachtung unterstrichen wird.

3. Introduction

Cancer related death is the second leading cause of death worldwide (Global Burden of Disease Cancer *et al.*, 2015). Among these, pancreatic cancer is one of the most aggressive tumors with predicted 57,600 new cases and 47,050 deaths in the U.S. in 2020 (Rahib *et al.*, 2014; Siegel *et al.*, 2020). Due to new therapy options the 5-year survival rate of patients with pancreatic cancer increased to 9% over the last years, starting with a survival rate of only 2% in the late 1970's. How low this survival rate and how slow progress in improving the disease's outcome is, becomes even more clear when comparing pancreatic cancer to other cancer types. For prostate cancer the survival rate increased from 68% to 99% and for Non-Hodgkin lymphoma, a survival rate of 47% was first recorded in the late 1970's and has increased to 71% since then (Siegel *et al.*, 2014; Siegel *et al.*, 2019). So, the prognosis for patients with pancreatic cancer is still extremely bad and this type of cancer is expected to become the second leading cause of cancer related deaths in Germany and the United States by 2030 (Figure 3-1) (Quante *et al.*, 2016; Rahib *et al.*, 2014).

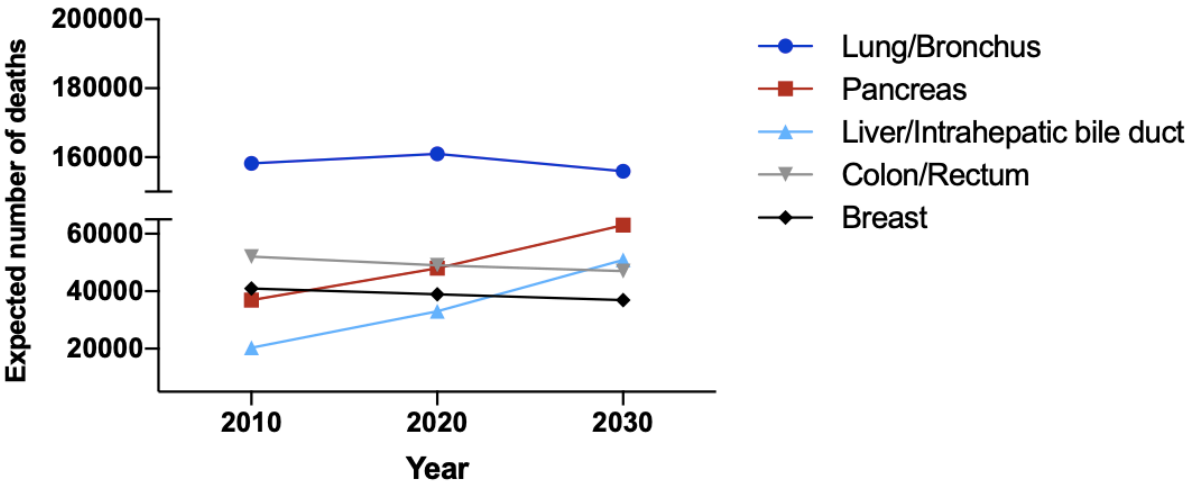


Figure 3-1: Expected number of cancer related deaths in the United States by 2030

The expected number of deaths has declined for most cancer types over the last years and is expected to drop further, however the number of deaths related to pancreatic cancer continues to increase. By 2030 pancreatic cancer is predicted to become the second leading cause of cancer related deaths in the United States (adapted from Rahib *et al.*, 2014).

3.1 Pancreatic ductal adenocarcinoma

Pancreatic cancer has different subtypes, with pancreatic ductal adenocarcinoma (PDAC) being the most common subtype (Warshaw and Fernandez-del Castillo, 1992). In 90% of the cases this disease develops sporadically, 7% of the patients diagnosed with PDAC show a familial background and only 3% have inherited cancer syndromes (Chari *et al.*, 2015). The majority of risk factors for PDAC belong to two groups: 5-10% of PDAC cases are related to genetic risk factors like BRCA2 mutations, Lynch syndrome, Peutz-Jeghers syndrome and hereditary pancreatitis, to name only a few (Goggins *et al.*, 1996; Kastrinos and Stoffel, 2014; Giardiello *et al.*, 2000; Raimondi *et al.*, 2010). However, the greater part of PDAC cases is caused by non-genetic risk factors such as smoking or chronic pancreatitis, a long-term progressive inflammatory disease that may be caused by excessive alcohol consumption (Iodice *et al.*, 2008; Yeo and Lowenfels, 2012; Raimondi *et al.*, 2010).

In most cases, pancreatic cancer is a disease linked to old age (Liszka *et al.*, 2010) and one tremendous problem is the late-stage detection. Additionally to the late onset of symptoms and subsequent rapid progression to death, early stages of the disease can only be detected with invasive measurements such as endoscopic ultrasound (Kenner *et al.*, 2016; Chari *et al.*, 2015).

At the moment, surgery in combination with adjuvant chemotherapy is the only potentially curative option for PDAC patients, however fewer than 20% of diagnosed patients are able to undergo such a life-saving surgery (Kenner *et al.*, 2016; Orth *et al.*, 2019). The recommended adjuvant treatment is a modified form of FOLFIRINOX (folinic acid-fluorouracil-irinotecan-oxaliplatin) (Janssen *et al.*, 2020). The current standard therapy for non-resectable or borderline resectable tumors are either single agents like FOLFIRINOX, gemcitabine, capecitabine, 5-fluorouracil (5-FU) as monotherapy or in combinations with chemo- or radiotherapy. Recently, treatments using neoadjuvant protocols are more often used to treat locally advanced and unresectable tumors, to improve their resectability. Sometimes it is also recommended to apply additional chemotherapy after surgery, depending on the patients' performance status and the response to the first treatment (Janssen *et al.*, 2020). In the metastasized stage the poly-chemotherapeutic regimen FOLFIRINOX showed positive effects on survival probability (Janssen *et al.*, 2020; Neoptolemos *et al.*, 2018; Orth *et al.*, 2019). Gemcitabine has been in use since 1997. It was shown, that it alleviates the disease-related symptoms and has some survival advantage over the

former standard therapy with 5-FU (fluorouracil) (Burriss *et al.*, 1997). In the last years several combination therapies with gemcitabine were tested, like its combination with nanoparticle albumin-bound paclitaxel (nab-paclitaxel) which increased overall survival significantly (Orth *et al.*, 2019; Adamska *et al.*, 2017). Another approach using the multidrug FOLFIRINOX regimen showed positive effects especially on patients with metastatic pancreatic cancer. FOLFIRINOX improved overall survival nearly twice-fold and progression-free survival significantly compared to gemcitabine treatment alone, but the treatment worsens the quality of life enormously showing increased toxicity of FOLFIRINOX (Conroy *et al.*, 2011; Orth *et al.*, 2019). Modifications of FOLFIRINOX treatment are under investigation at the moment (Adamska *et al.*, 2017).

Since the currently available treatments are not satisfactory, new therapeutic options for patients with pancreatic cancer are desperately needed.

3.1.1 Progression of PDAC

Taking a closer look at the progression of this deadly disease reveals that several precursor lesions, e. g. pancreatic intraepithelial neoplasms (PanINs), intraductal papillary mucinous neoplasms (IPMNs), mucinous cystic neoplasms (MCNs) or atypical flat lesions (AFLs) could act as the first step towards the development of PDAC (Hruban *et al.*, 2000; Wu *et al.*, 2011; Brugge *et al.*, 2004; Aichler *et al.*, 2012). One of the initiating events in murine PDAC formation is acinar-to-ductal metaplasia (ADM) and those ADM undergoing cells are precursors for PanINs, which act as a early step during progression towards PDAC (Storz, 2017; Zhu *et al.*, 2007). The role of ADM during progression of PDAC in mice has been proven, but how it contributes to human PDAC development needs to be elucidated (Storz, 2017).

It was shown further that 90% of all PDACs carry the *KRAS*^{G12D} mutation (Kanda *et al.*, 2012). *KRAS* is a member of the RAS protein family and therefore a small GTPase. It is able to switch between an active and an inactive state. The inactive state is characterized by binding of guanosine diphosphate (GDP), while in the active state guanosine triphosphate (GTP) is bound. Via extracellular stimuli, receptor tyrosine kinases are activated transforming the bound GDP to GTP. The GTP-bound *KRAS* is active and consequently multiple effector pathways are activated. The *KRAS*^{G12D} mutation is a well-documented point mutation in PDAC, leading to substitution of glycine with aspartate (G12D) and consequently, *KRAS* is constitutively active through persistent GTP-binding. Therefore, independent of growth factor stimulation this amino

acid change leads to overstimulation of downstream signaling pathways (Hezel *et al.*, 2006; Waters and Der, 2018).

The *KRAS* mutation is one of the earliest mutations that can be found in pancreatic cancer (Moskaluk *et al.*, 1997). Therefore it is considered to be the PDAC initiating mutation (Hezel *et al.*, 2006) which may be accompanied by mutations in several oncogenes, as well as mutations in or loss of tumor suppressors, such as *CDKN2A* (90%), *TRP53* (70%) and *SMAD4* (55%) (Figure 3-2) (Pelosi *et al.*, 2017).

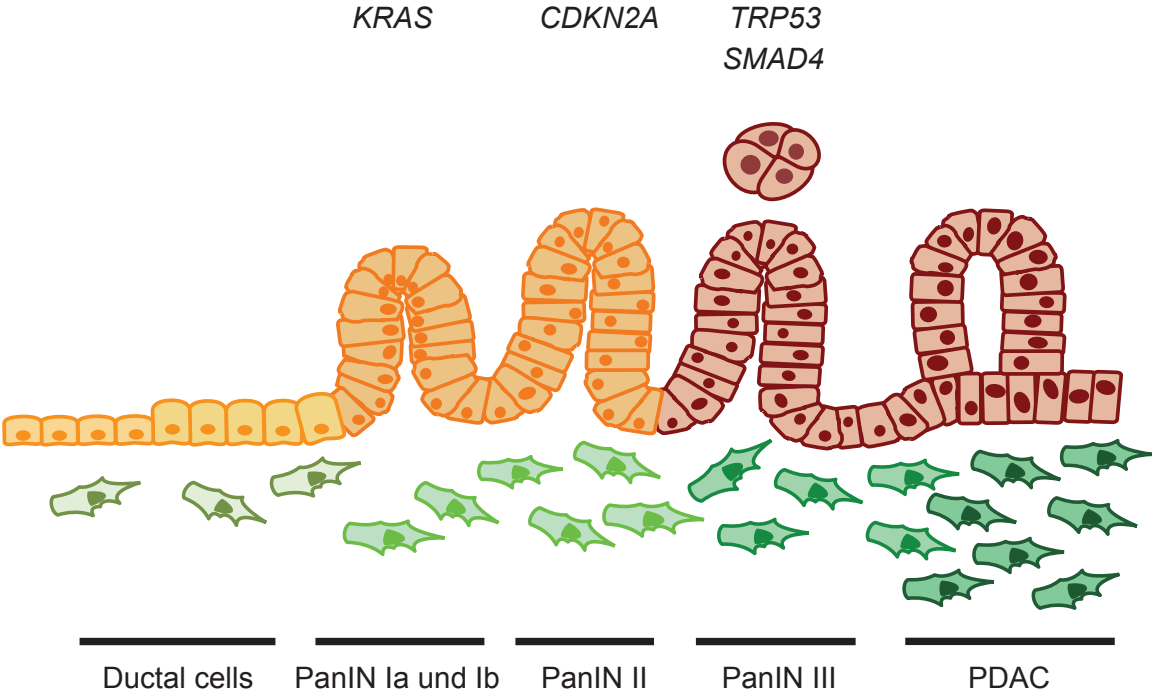


Figure 3-2: Progression model of PDAC
Ductal cells undergo transformation to PanIN lesions when mutations in the *KRAS* gene occur. Due to additional mutations in several genes like *CDKN2A*, *TRP53* and *SMAD4* cells progress via the different PanIN stages to PDAC (modified from Morris *et al.*, 2010).

During the progression from the precursor lesion to advanced PDAC, cancer cells gain several mutations, leading to activation or inactivation of various signaling pathways, thus making PDAC a dramatically heterogeneous disease (Figure 3-3) (Pelosi *et al.*, 2017).

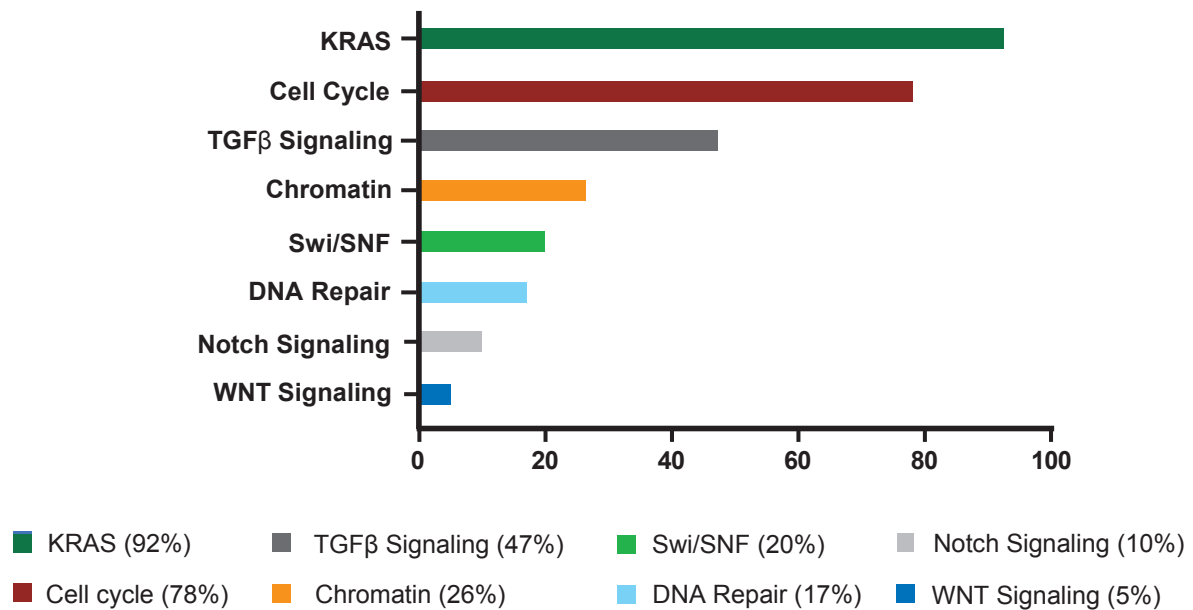


Figure 3-3: Affected pathways in PDAC progression

Most PDAC patients initially have mutations that modulate KRAS and TGFβ signaling as well as cell cycle progression. As the disease progresses, mutations that impair DNA repair or affect Chromatin remodeling, Swi/SNF complexes and Notch signaling have been reported (modified from Pelosi *et al.*, 2017).

Cancer cells are known to acquire different advantages over healthy cells which are summarized as hallmarks of cancer, namely self-sufficiency in growth signals, insensitivity to anti-growth signals, evasion of apoptosis, sustained angiogenesis, limitless replicative potential, tumor invasion and early metastatic spread (Hanahan and Weinberg, 2000; Hanahan and Weinberg, 2011).

To investigate the acquired advantages of tumor cells and the resulting changes in pathways as well as possible therapeutic targets, mouse models are often used.

3.1.2 Mouse models of PDAC

There are different genetically engineered mouse models (GEMM) available for investigating time- and tissue-specific roles of target genes during tumor development and maintenance.

The most promising and commonly used mouse model to study metastatic PDAC carries two mutations to mimic a realistic disease progression of human PDAC development. Those two mutations are the PDAC initiating *Kras*^{G12D} mutation (Hezel *et al.*, 2006; Jackson *et al.*, 2001) as well as a mutation in *Trp53* which is frequently affected in patients. In the mouse model this is reconstructed with the *Trp53*^{R172H}

mutation (Liu *et al.*, 2000). Those two mutations are both silenced by a *loxP-Stop-loxP* (*LSL*) cassette, which can be removed by a Cre recombinase, for example *Pdx1-Cre* (Hingorani *et al.*, 2005). Expression of this recombinase is limited to *Pdx1* expressing tissues like pancreatic tissue and consequently leads to the expression of the mutated *Kras* and *Trp53* exclusively in those tissues. All these alleles are combined in one GEMM: the *LSL-Kras^{G12D/+};LSL-Trp53^{R172H/+};Pdx1-Cre* (KPC) mouse model (Hingorani *et al.*, 2005).

To investigate time- and tissue-specific roles of genes, a common inducible dual-recombinase system is used. This mouse model combines the flippase/*frt* (*Flp/frt*) and the *Cre/loxP* system. In the transgenic *Pdx1-Flp* mouse line, the Flp recombinase is expressed under control of the *Pdx1* promoter to ensure its pancreas specific expression (Schonhuber *et al.*, 2014). Additionally, the PDAC initiating *Kras^{G12D}* mutation is silenced by a *frt-Stop-frt* (*FSF*) cassette (Schonhuber *et al.*, 2014) and a part of *Trp53* is flanked with *frt* sites (Lee *et al.*, 2012) in the inducible dual-recombinase mouse model. Both the *FSF* cassette and *frt* flanked exons can be deleted by the Flp recombinase, leading to the expression of the mutated *Kras* and deletion of *Trp53* in the Flp recombinase expressing pancreatic cells.

In the described mouse model, the Cre recombinase is aligned to the tamoxifen-inducible estrogen receptor (*ER^{T2}*) under the control of CAG promoter as a *Rosa26* knock-in. To ensure tissue-specific expression of the *CreER^{T2}* recombinase, the gene is also silenced by a *FSF* cassette (Schonhuber *et al.*, 2014). To enable the deletion of a gene of interest in this mouse model, its sequence is modified with *loxP* sites. The floxed sequence of the gene of interest is deleted by the Cre recombinase and therefore, gene transcription is impaired and a knock-out for the gene of interest is achieved. In summary, this mouse model allows for a time- and tissue-specific deletion of floxed sequences after 4-Hydroxytamoxifen (4-OHT) treatment.

Those two mouse models allow the investigation of PDAC development and maintenance of metastatic PDAC. In general, metastases are the reason for more than 90% of cancer deaths (Seyfried and Huysentruyt, 2013), particularly in PDAC where 91% of the patients display some form of metastasis at the time of diagnosis (Le Large *et al.*, 2017; Yachida *et al.*, 2010). Round about 80% of the patients that have been diagnosed with resectable PDAC and received curative therapy, relapsed with local

and/or distant metastasis and die within two years from that diagnosis. At the moment the patients with relapsed metastatic PDAC are treated like patients with newly diagnosed metastatic PDAC as there is a lack of treatment guidance for relapsed patients (Gbolahan *et al.*, 2019). In most cases metastases are located in the liver, but also the lung, the peritoneum and the lymph nodes are common sites of metastases (Deeb *et al.*, 2015; Le Large *et al.*, 2017). Since the metastatic spread is occurring in such a vast majority of the patients, this aspect needs to be considered when PDAC is studied. Therefore, mouse models that display metastatic PDAC are an important tool to gain further insights in the mechanism of metastatic spread in PDAC. The above described mouse models develop metastatic PDAC and for this reason, they can be used to investigate development, maintenance and metastatic spread of PDAC.

3.1.3 Mechanisms of metastatic spread

Metastases are defined as tumor cells spreading naturally to an organ distinct from the one in which they originated. Most often the metastases from primary pancreatic cancer occur in the liver and lung or in the peritoneum and lymph nodes (Hezel *et al.*, 2006; Yachida *et al.*, 2010). It was shown that the genetic heterogeneity observed in metastases reflects that of the primary tumor in PDAC (Seyfried and Huysentruyt, 2013; Yachida *et al.*, 2010). Lately, on the basis of data from breast cancer cell lines, it has been discussed, that metastatic spread is an evolutionary process since several conditions must be met for a metastasis to be established. This clonal evolution of the tumor cells is also reflected in the heterogeneity which is reduced during the steps of spontaneous metastatic spread that generate population bottlenecks (Sprouffske *et al.*, 2020). The primary tumor consists of different subclones which are likely to give rise to the numerous metastases, but it was shown, that they share all the same driver mutations, sustaining the argument for conserved clonal driver mutations during PDAC development (Yao *et al.*, 2020).

However, no significant differences in the genomic alterations on gene and pathway level were found between primary tumor and metastatic lesions (Brar *et al.*, 2019). No metastasis-specific driver mutations could be identified, but widespread epigenetic reprogramming was found during evolution of distant metastases, arguing for a non-genetic form of natural selection during PDAC progression. It has also been postulated, that subclones gain heterogenous metabolic, epigenetic and malignant properties which constitute an advantage during invasive tumor growth and metastatic spread. In

more detail, distant metastasis developed a dependence on the oxidative pentose phosphate pathway and its inhibition reversed reprogrammed chromatin, as well as malignant gene expression programs and tumorigenesis (McDonald *et al.*, 2017).

Causes of metastatic spread are not only genetic drivers, but also enhancer reprogramming as well as signaling from the tumor microenvironment to name only a few (Ohlund *et al.*, 2014; Roe *et al.*, 2017). Furthermore, a multi-parametric integrative analysis revealed that chromatin states differ between the less aggressive and the more aggressive subtype and that super-enhancer associated pathways play a role in the plasticity between the subtypes (Lomberk *et al.*, 2018). The Swi/SNF chromatin remodeling protein complex disrupts the tight contact of DNA and histones and is connected to metastatic PDAC, too. The loss of a member of this complex, ARID1A, was shown to lead to high grade and metastatic PDAC in the KPC mouse model (Hessmann and Ellenrieder, 2019). Recently it has been shown, that PDAC metastasis are promoted via microRNAs which activate the NF- κ B/MDM2 signaling axis (Zhu *et al.*, 2020).

The process of the metastatic spread is not yet fully understood. There are different models available to explain how the tumor cells can spread to other organs and which pathways are involved. There is evidence that, for example, hypoxia can drive metastatic spread (Li *et al.*, 2017; Muz *et al.*, 2015). Hypoxia is defined as a non-physiological level of oxygen tension (Muz *et al.*, 2015). Due to rapid growth of tumors the oxygen level in this tissue is often low. Therefore, the cancer cell metabolism is altered, leading to dysfunctional vascularization and acquisition of epithelial-to-mesenchymal transition (EMT). This results in cell mobility and thus metastases. A report where it was shown that acute hypoxia is associated with a more aggressive phenotype through induction of spontaneous metastatic spread, emphasizes the role of hypoxia during metastases formation (Muz *et al.*, 2015). Similarly, in PDAC it was found that *Blimp1* plays a pivotal role in metastasis formation under hypoxic conditions. Under hypoxia, HIF1 α is stabilized and can consequently induce *Blimp1* expression, which is necessary for the regulation of hypoxia-associated gene expression programs. Due to this, metastatic ability is promoted and cell division is suppressed (Chiou *et al.*, 2017).

There is also a link between metastatic spread and mitochondrial dysfunction. Cancer cells have respiratory insufficiency and therefore use fermentation as a compensatory source of energy, as first described by Warburg (Warburg, 1956). Metabolic changes

play a role in the metastatic process as metabolic intermediates like lactate, succinate and fumarate act as signaling agents that are capable of activating prometastatic pathways and therefore enhancing tumor growth and metastases formation (Payen *et al.*, 2016). In addition, metastases require strong extracellular matrix degradation ability which is connected to glycolysis (Li *et al.*, 2017). Metabolic rewiring plays a role in tumor aggressiveness by increased glucose uptake and glycolysis flux and is therefore discussed as an enhanced glycolytic phenotype of tumor cells (Kang *et al.*, 2019).

Another process that leads to metastases is epithelial-to-mesenchymal transition and its reverse process mesenchymal-to-epithelial transition (MET). During EMT epithelial cells turn into mesenchymal cells which are characterized by enhanced migratory capacity, invasiveness, elevated resistance to apoptosis and greatly increased production of extracellular matrix components. To undergo this process, epigenetic and genetic changes specifically in genes that favor clonal outgrowth are required. Carcinoma cells can pass through this process to different extents: either they become fully mesenchymal while others retain some epithelial traits or they display only a few mesenchymal characteristics (Kalluri and Weinberg, 2009).

In greater detail, EMT is a process which can be subdivided into several steps: First, loss of epithelial markers like E-cadherin and gain of mesenchymal markers like Vimentin occur. Next, the cell loses its baso-apical polarization and a front-rear polarization is acquired. Then cytoskeleton remodeling follows and finally cell-matrix adhesion is altered, a process that is accompanied by activation of proteolytic enzymes such as matrix metalloproteinases (MMPs). The tumor cells detach from the primary tumor and invade the surrounding tumor stroma and circulation. Thus, they are able to reach distant organs and establish metastases at secondary locations (Iwatsuki *et al.*, 2010).

One of the EMT-inducing cytokines is TGF β , which plays a dual role in tumor progression. At the early stage of tumor progression TGF β acts as a tumor suppressor. Later on, when the tumor has already reached an advanced stage, a functional switch occurs that transforms TGF β into a tumor promoter (Roberts and Wakefield, 2003). The first step of the signaling pathway is the binding of TGF β to the transmembrane TGF β -Receptor (TGF β -R) II and subsequent dimerization of the receptor with TGF β -RI which leads to phosphorylation of TGF β -RI (Bernabeu *et al.*, 2009; Wrana *et al.*, 1994). The activated TGF β -R complex then phosphorylates SMAD2 and SMAD3,

which in turn bind to SMAD4 forming the so-called Smad complex that will then translocate to the nucleus where it regulates the expression of several TGF β -dependent genes (Figure 3-4) (Ahmed *et al.*, 2017; Smith *et al.*, 2012).

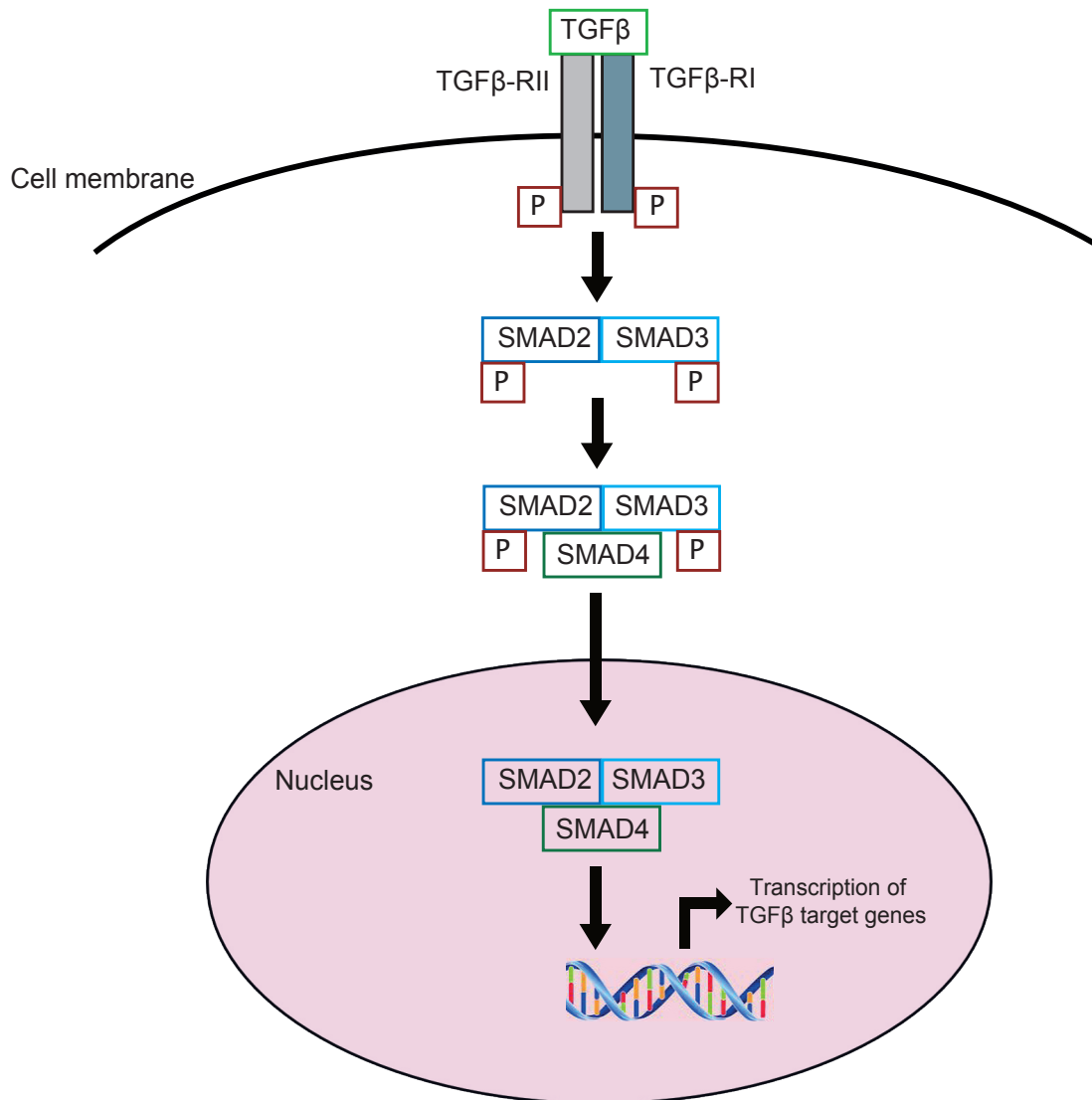


Figure 3-4: TGF β signaling pathway

TGF β binds to TGF β receptor II which leads to dimerization of TGF β receptor I and II and consequently the phosphorylation of TGF β receptor I. Thereby the TGF β receptor is activated and phosphorylates SMAD2 and SMAD3. The pSMAD2/3 can bind to SMAD4 and this complex enters the nucleus where it leads to the transcription of TGF β target genes (adapted from Ahmed *et al.*, 2017 and Smith *et al.*, 2012).

In pancreatic cancer cells a bilateral role of TGF β was demonstrated. On the one hand TGF β can induce EMT, but on the other hand it can also lead to apoptosis in TGF β sensitive PDAC cells. This EMT-induced apoptosis is called lethal EMT and it is mediated by repression of KLF5 which switches SOX4 function from pro-tumorigenic

to pro-apoptotic (David *et al.*, 2016). ID1 can preserve the PDAC cell against lethal EMT by uncoupling EMT from apoptosis in PDA progenitors. Thus there is a selection against the TGF β -induced inhibition of ID1 during PDAC progression (Huang *et al.*, 2020).

In addition it was reported, that TGF β stimulation in murine PDAC cells massively increases SNAIL1 expression, accompanied by a decrease in E-cadherin and other characteristics of lethal EMT (Su *et al.*, 2020).

There is also evidence, that histone deacetylases (HDACs) are involved in the process of metastatic spread. In cervical cancer it was shown that HDAC10 inhibits expression of matrix metalloproteinase 2 and 9 genes and therefore metastases are suppressed (Song *et al.*, 2013). Also, HDACs play a role during epithelial-to-mesenchymal transition in other cancer types. Highly metastatic PDAC cell populations were generated, characterized by higher expression of SNAIL and loss of E-cadherin. In those cells it was shown that the SNAIL/HDAC1/HDAC2 repressor complex leads to silencing of E-cadherin in PDAC (von Burstin *et al.*, 2009). In another study analyzing human PDAC samples, it was found that ZEB1/HDAC complexes are attached to the silent *Cdh1* promoter. Consequently, E-cadherin is not expressed and epithelial-to-mesenchymal transition is promoted. Deletion of ZEB1 inhibit binding of HDACs to the *Cdh1* promoter which is then transcriptionally active, resulting in expression of E-cadherin (Aghdassi *et al.*, 2012).

3.2 Histone deacetylases

Accessibility of the DNA is essential for gene transcription and therefore influences all processes within a cell. DNA accessibility is, for example, controlled by chromatin remodeling, a dynamic process which organizes the change between open and closed chromatin. Open chromatin is called euchromatin. During this state of hyperacetylated histones, the DNA is accessible for transcription factors (TFs) and gene transcription is possible. Histone deacetylation results in a closed chromatin state with densely packed DNA (heterochromatin) where gene transcription is silenced (Grozingler and Schreiber, 2002). For this epigenetic process two groups of enzymes are needed, the histone acetyltransferases (HATs) and their counterplayers, the histone deacetylases (HDACs) (Cress and Seto, 2000). Acetylation of lysine residues of histone tails neutralizes the histones positive charge and therefore their binding to negatively charged DNA is disturbed. As a consequence of the impaired binding of histones and DNA, the DNA is packed less densely, which results in open chromatin sites (Grozingler and Schreiber, 2002). This dynamic process of chromatin remodeling affects diverse cellular processes like proliferation, differentiation and DNA repair among others (Schneider *et al.*, 2010; Zhang *et al.*, 2016). In addition to the regulation of chromatin cross-talk, HDACs also influence post-translational modifications of other proteins, change gene expression and influence protein stability. Because of these functions, HDACs play a role in many human diseases like cancer, cardiac dysfunctions, neurobiological and metabolic disorders (Seto and Yoshida, 2014; Zhang *et al.*, 2017a).

Some of the above mentioned processes like DNA damage repair or cell proliferation are altered in cancer cells (Hanahan and Weinberg, 2000) and are also linked to HDACs (Li and Zhu, 2014). In case of DNA damage HDAC1 and HDAC2 are recruited to the affected sites to promote H3K56 hypoacetylation. This deacetylation facilitates non-homologous end-joining which is an important pathway for the repair of DNA double-strand breaks. If those HDAC isoenzymes are missing, tumor cells are more sensitive to DNA-damaging agents and less DNA double-strand breaks can be repaired (Miller *et al.*, 2010). Another altered pathway in cancer cells is cell cycle regulation. Therefore, it was shown that HDAC3 plays a crucial role since its knockdown leads to activation of spindle assembly checkpoint and sister chromatid dissociation (Eot-Houllier *et al.*, 2008). Those are only few examples, and there are

more studies, showing that interfering the altered pathways in cancer cells through targeting HDACs may be a therapeutic option (Li and Zhu, 2014).

3.2.1 HDAC isoenzymes

HDACs are expressed in almost all organisms and can be found in bacteria, fungi, plants and animals (Minucci and Pelicci, 2006). In 1969 the first HDAC enzyme was described by Inoue and Fujimoto. So far 18 different HDAC isoenzymes have been discovered in humans (Seto and Yoshida, 2014) and according to the sequence homology of their catalytic domain, they are grouped into four different classes: class I HDACs (HDAC1, 2, 3 and 8) are homologous to yeast Rpd3, class II HDACs (IIa: HDAC4, 5, 7 and 9; IIb: HDAC6 and 10) are homologous to yeast Hda1, class III HDACs (SIRT1-7) are homologous to yeast SIR2, and the class IV HDAC (HDAC11) shows homology to class I and II (Figure 3-5). The Sirtuins use NAD^+ as a cofactor instead of Zn^{2+} which is used by the other HDAC classes (Seto and Yoshida, 2014).

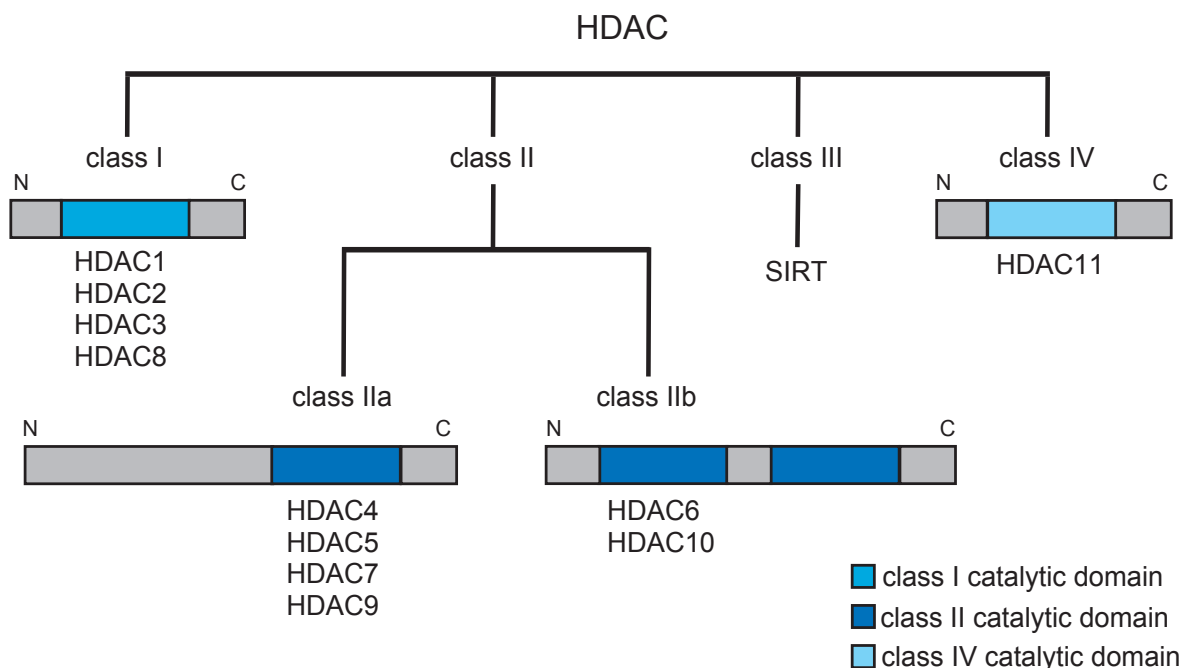


Figure 3-5: Family of histone deacetylases

HDACs are grouped into four different classes, according to the sequence homology of their catalytic domain. Class I consists of HDAC1, 2, 3 and 8 and class II can be subdivided to class IIa (HDAC4, 5, 7, 9) and class IIb (HDAC6, 10) with one or two catalytic domains respectively. Class III HDACs are called Sirtuins (SIRT1-7) and class IV consists of only one member, HDAC11 (adapted from Schneider *et al.*, 2010).

Taking a closer look at the isoenzymes and their target genes reveals, in addition to histones, several non-histone targets of HDACs. Those targets are relevant for diverse cellular processes like differentiation and apoptosis or are involved in cell cycle progression, DNA repair and replication (Minucci and Pelicci, 2006; Ropero and Esteller, 2007). Particularly, HDACs are able to deacetylate tumor relevant non-histone proteins like TRP53, β -Catenin or NF- κ B (Xu *et al.*, 2007).

HDAC1 was first isolated and cloned by Taunton *et al.*, 1996. It targets all four histones (Grozinger *et al.*, 1999) and several non-histone substrates like RB1, STAT3 and AMPK (Li and Zhu, 2014). If HDAC1 is part of the NuRD complex it plays a major role in regulating chromatin remodeling and targets the non-histone protein TRP53 and thus consequently influences several cellular processes like cell growth and apoptosis (Luo *et al.*, 2000). If it is part of the CoREST and Sin3A complex, HDAC1 can act as a transcriptional repressor (Gu *et al.*, 2005; Heideman *et al.*, 2014).

A few months after the first report of HDAC1 was published, HDAC2 was first described, however under the name mRPD3. (Yang *et al.*, 1996). Since then it has been shown that HDAC2 is part of protein complexes Sin3a, NuRD and CoREST (Ayer, 1999) and negatively regulates transcription by being recruited to DNA as a corepressor (Seto and Yoshida, 2014). HDAC2 is also involved in the regulation of several cellular processes, for example, it attenuates TRAIL-induced apoptosis (Schuler *et al.*, 2010).

About one year after the first description of HDAC2, HDAC3 was discovered. Similar to the previously identified histone deacetylases, *HDAC3* is expressed ubiquitously in several cell types (Yang *et al.*, 1997). It is part of the N-CoR/SMRT protein complex and selectively deacetylates histone H3 (Vermeulen *et al.*, 2004). Non-histone targets of this isoenzyme are, among others, p65, STAT3 and GATA1 (Li and Zhu, 2014). HDAC3 plays a role during cell cycle progression, as its impairment or loss can either induce S-Phase or G2/M-Phase arrest (Bhaskara *et al.*, 2008; Summers *et al.*, 2013; Wilson *et al.*, 2006). There is also evidence that DNA damage increases after loss of HDAC3 expression (Bhaskara *et al.*, 2008).

Reviewing the literature describing the HDAC isoenzymes, it becomes clear that the isoenzymes HDAC1 and HDAC2 are part of the same complexes and to some extent they have redundant functions (Haberland *et al.*, 2009a; Haberland *et al.*, 2009b; West and Johnstone, 2014). This can be explained partly by the high amino acid sequence

homology of 85% between HDAC1 and HDAC2 (Montgomery *et al.*, 2007), while HDAC3 has a sequence homology of 53% and 52% with HDAC1 and HDAC2, respectively (Yang *et al.*, 1997). It was also shown that knock-out of either *HDAC1* or *HDAC2* can be compensated by an upregulation of the corresponding other isoenzyme (Lagger *et al.*, 2002; Stojanovic *et al.*, 2017).

Particularly for HDAC1 and HDAC2 some similar or even redundant functions are described. For example, in ovarian cancer cells, as well as in colon cancer cells, inactivation of either HDAC1 or HDAC2 results in reduced proliferation. CLL cells show a higher sensitivity for Trail induced apoptosis when HDAC1 or HDAC2 are deleted. Combined deletion of HDAC1 and HDAC2 has strong effects on cell survival, differentiation as well as proliferation in heart, neurons or glial cells and B cells, while deletion of only HDAC1 or HDAC2 has no distinct effects (Jurkin *et al.*, 2011).

Besides the similar and redundant functions of HDAC1 and HDAC2, there are also some functions related to each isoenzyme specifically. For example, HDAC1 is necessary for embryonic development (Lagger *et al.*, 2002). Embryos lacking HDAC1 have increased levels of p21 and p27 and show a reduced proliferation rate. Additionally, loss of HDAC1 is connected to reduced growth in human breast cancer and osteosarcoma cells. Furthermore HDAC1 plays a role in restriction of cytokine expression in T lymphocytes and can induce autophagy in HeLaS3 cells (Jurkin *et al.*, 2011). However, HDAC2 plays a role in the prevention of apoptosis in colorectal cancer (Zhu *et al.*, 2004). The specific HDAC2 knock-down in breast cancer cells results in proliferation inhibition, cellular senescence and leads to increased sensitivity to topoisomerase inhibitor induced apoptosis. In PDAC cells HDAC2 decrease expression of NOXA leading to therapeutic resistance towards topoisomerase II inhibitor etoposide (Jurkin *et al.*, 2011).

3.2.2 Role of HDACs in cancer, especially in PDAC

Often in cancer the impaired histone acetylation pattern is observed and especially in gastrointestinal tumors it was shown that histone acetylation plays a role during tumor development and that it is also important for the tumor's invasive and metastatic potential (Ropero and Esteller, 2007). In addition, the number of publications showing aberrant expression of HDACs in several tumors are increasing (Li and Seto, 2016).

To name only a few studies to indicate the diversity of cancer types in which HDACs play a role, it was for example shown, that in gastric cancer *HDAC1* conduce to

successful cell proliferation and therefore deletion of this isoenzyme decreases proliferation and increases apoptosis (Yu *et al.*, 2019). While *HDAC2*-miRNA crosstalk plays an important role in acute myeloid leukemia (Conte *et al.*, 2019), deletion of *HDAC3* in the liver contributes to the tumorigenesis, as it was shown for hepatocellular carcinoma (Bhaskara *et al.*, 2010).

Several studies highlight the importance of HDACs as therapeutic targets for cancer therapy. This protein group is also a promising therapeutic option for pancreatic cancer since it influences proliferation, cell death and EMT programs in PDAC cells (Hessmann *et al.*, 2017).

In humans HDAC1 expression is correlated with poor PDAC survival rates (Miyake *et al.*, 2008) as well as increased tumor cell proliferation (Giaginis *et al.*, 2015) while HDAC2 expression increases with the progression of pancreatic cancer in humans (Fritsche *et al.*, 2009). The same was shown to be true for human colorectal cancer, where expression of class I HDACs HDAC1, HDAC2 and HDAC3 was significantly increased in dedifferentiated and highly proliferating tumors. Especially HDAC2 functions as a survival prognostic marker in those tumors (Weichert *et al.*, 2008). Comparisons between pancreatic ductal epithelial cells and pancreatic cancer cell lines revealed an increase in HDAC3 expression in the cancer cells (Jiao *et al.*, 2014). Taken together, these results point out that HDAC isoenzymes play an important role during pancreatic cancer development and maintenance, however the need to investigate the underlying mechanisms in greater detail remains.

Since the anti-tumor effect of HDACis was shown in numerous *in vitro* and also in *in vivo* studies, the next step was and still is the investigation of HDACis in clinical trials (Ropero and Esteller, 2007). HDAC inhibitors (HDACis) are based on different chemical structures which are hydroxamate, short-chain fatty acids, benzamide and cyclic peptides (Mottamal *et al.*, 2015). Unfortunately, almost all HDACis target two or more isoenzymes simultaneously, while pan-HDACis target one or more classes of HDACs (Eckschlager *et al.*, 2017). In the last years a few HDACi have been approved for cancer therapy by the *US Food and Drug Administration (FDA)*, mainly for T-cell lymphomas. In more detail, Vorinostat (SAHA) and Romidepsin (FK228) was approved for cutaneous T-Cell Lymphoma, Belinostat for relapsed or refractory peripheral T-Cell Lymphoma, while Panobinostat is approved for relapsed multiple myeloma (Mann *et al.*, 2007; Lee *et al.*, 2015; Raedler, 2016; VanderMolen *et al.*, 2011).

Table 3-1: HDAC inhibitors in clinical trials

HDACi	Targeted HDACs (Schneider <i>et al.</i> , 2010)	Cancer type	NCT number	FDA approved
SAHA	<i>pan</i> -HDAC	CTCL	NCT00771472	2006
AR-42	<i>pan</i> -HDAC	AML	NCT01798901	-
Panobinostat	<i>pan</i> -HDAC	Multiple myeloma	NCT02568943	2015
Chr-3996	Class I	Solid tumor	NCT00697879	-
Belinostat	<i>pan</i> -HDAC	PTCL	NCT01839097	2014
Entinostat	Class I	Solid tumors	NCT02897778	-
Pracinostat	<i>pan</i> -HDAC	AML	NCT01912274	-
RGFP966	HDAC3	-	-	-
Valproic acid	Class I	AML	NCT00414310	-
CI-994	Class I	Pancreatic cancer	NCT00004861	-
Dacinostat	<i>pan</i> -HDAC	-	-	-
Mocetinostat	Class I	Leukemia	NCT00431873	-
Romidepsin	Class I	Prostate cancer	NCT00106418	2009
CRA-026440	<i>pan</i> -HDAC	-	-	-
Trichostatin A	<i>pan</i> -HDAC	-	-	-
Merck60	HDAC1, 2	-	-	-

The effectiveness of novel HDACis (Table 3-1) is currently under investigation for several cancer types such as cutaneous T-cell lymphoma, diffuse B-cell lymphoma or myelodysplastic syndromes with some being subjected to clinical trials in different phases at present (Eckschlager *et al.*, 2017; Bolden *et al.*, 2006). Despite the evidence gained from pre-clinical data, that HDACi act as promising therapeutic compounds to treat pancreatic cancers (Ryu *et al.*, 2006; Sato *et al.*, 2004; Bai *et al.*, 2005; Garcia-Morales *et al.*, 2005; Laschankzy *et al.*, 2019; Cai *et al.*, 2018), the tested HDACis showed disappointing results in the clinical trials (Nguyen *et al.*, 2017). There is only limited amount of clinical studies that included PDAC patients. Vorinostat is tested in combination with proteasome inhibitors and seems to have potential to treat some

advanced solid tumors, but no effectiveness against PDAC was observed. Also other HDACis like CI-994 showed no significant anti-tumoral activity in PDAC patients, neither alone, nor in combination. At least a stable disease without further progression was observed in some PDAC patients treated with Romidepsin in combination with gemcitabine (Arlt and Schafer, 2016).

Those reports of clinical studies show the missing efficiency of HDACis in treatment of PDAC patients, despite the promising results of pre-clinical data. A crucial condition for the development of more effective inhibitors and potential therapeutics is a better understanding of how HDACs mechanistically affect the pathways which are involved in tumor development and maintenance. To reach this goal, knock-out models are a valuable tool to expand the knowledge in this field.

4. Aims of the work

Class I HDACs HDAC1, HDAC2 and HDAC3 are discussed as therapeutic targets for pancreatic cancer. Although the processes where HDACs are involved are known, their isoenzyme specific functions are still largely unclear.

This work was designed to systematically investigate the role of class I HDACs HDAC1, HDAC2 and HDAC3 for PDAC maintenance. Starting with the comparison of inhibition and genetic deletion of those class I HDACs, the goal was to elucidate the isoenzyme specific role of that class I HDACs in PDAC maintenance. Therefore, the dual-recombinase model was used, which allows the time- and tissue-specific deletion of the gene of interest. The basic characterization of the respective HDAC pro- and deficient PDAC cell line includes, next to the proof of the successful deletion of the isoenzyme, also the analysis of cell survival, ability to form colonies and cell cycle progression. This basic characterization was applied to the knock-out of each isoenzyme separately and as well to a combined knock-out of all three investigated isoenzymes.

Observing an effect of successful *Hdac* knock-out consequently led to the aim to investigate the mechanisms behind. Since published data highlighted the role of especially *Hdac2* in human undifferentiated tumors (Fritsche *et al.*, 2009), further analysis focused on this isoenzyme. Therefore, RNA-Seq as an unbiased approach was performed and revealed regulated transcripts after *Hdac2* knock-out which were used for identification of regulated pathways. Those insights gained from the pathway analysis paved the way for follow up studies *in vitro* and *in vivo*. For *in vivo* verification of the data from the *in vitro* experiments, the KPC mouse model with the constitutive *Hdac2* knock-out was used.

The use of the dual-recombinase model enabled the analysis of effects induced by isoenzyme specific deletion in an established PDAC, giving some hints how specific targeting of HDACs can influence the tumor and could be used for prospective therapeutic approaches in the clinic.

5. Technical equipment

Table 5-1: Technical equipment

Technical equipment	Source
AxioCam MRc	Carl Zeiss AG, Oberkochen
Axiovert 25 inverse microscope	Carl Zeiss AG, Oberkochen
Bioruptor Sonification System UCD-200TM	Diagenode, Seraing
CO ₂ incubator Heraeus 6000	Heraeus Instruments GmbH, Osterode
Electrophoresis power supply Power Pac 200	Bio-Rad Laboratories GmbH, München
FACS Calibur	BD Biosciences, San Jose, CA
Falcon® Pipet Controller	Corning, Corning, NY
FLUOstar OPTIMA	BMG LABTECH GmbH, Ortenberg
Gallios Flow Cytometer	Beckmann Coulter, Brea, CA
Heated paraffin embedding module EG1150 H	Leica Microsystems GmbH, Wetzlar
Hera safe	Heraeus Instruments GmbH, Osterode
Magnetic stirrer MR2000	Heidolph Instruments GmbH, Schwabach
Maxwell® 16 Instrument	Promega, Madison, WI
Microcentrifuge 5451 R	Eppendorf AG, Hamburg
Microscope Axio Imager. A1	Carl Zeiss AG, Oberkochen
Microtome Microm HM355S	Thermo Fisher Scientific Inc., Waltham, MA
Microwave	Siemens, München
Multiskan™ FC	Thermo Fisher Scientific Inc., Waltham, MA
Neubauer hemocytometer	LO-Laboroptik GmbH, Bad Homburg
Odyssey FC	LI-COR® Biosciences GmbH, Bad Homburg
Paraffin tissue floating bath Microm SB80	Thermo Fisher Scientific Inc., Waltham, MA
pH-Meter 521	WTW GmbH, Weilheim

Power supply E844, E822, EV243	Peqlab Biotechnologie GmbH, Erlangen
Rotina 46R	Hettich Zentrifugen, Tuttlingen
Slide scanner Apero AT2	Leica Microsystems GmbH, Wetzlar
Spectrophotometer NanoDrop 1000	Peqlab Biotechnologie GmbH, Erlangen
StepOnePlus™ Real-Time PCR System	Applied Biosystems Inc., Carlsbad, CA
Thermocycler TGradient	Biometra GmbH, Göttingen
Thermomixer compact	Eppendorf AG, Hamburg
Tissue processor ASP300	Leica Microsystems GmbH, Wetzlar
UVsolo TS2 Imaging System	Biometra, Jena
Vortex Genie 2™	Bender & Hobein AG, Zürich
Water bath 1083	GFL Gesellschaft für Labortechnik GmbH, Burgwedel
Western blot system SE 260 Mighty Small II	Hofer, Inc., Holliston, MA

Table 5-2: Disposables

Disposables	Source
6-well plates, 96-well plates	Corning Inc., Corning, NY
Amersham Protran 0.2 NC Nitrocellulose Blotting membrane	GE Healthcare Life Sciences, Freiburg
Cell culture plastics	BD Bioscience, Franklin Lakes, NJ; Greiner Bio-One, Frickenhausen
Cell scrapers	Sarstedt AG & Co., Nümbrecht
Combitips BioPur®	Eppendorf AG, Hamburg
Conical tubes, 15 ml	Greiner Bio-One, Frickenhausen
Conical tubes, 50 ml	Greiner Bio-One, Frickenhausen
Cover slips	Gerhard Menzel, Glasbearbeitungswerk GmbH & Co. KG, Braunschweig
CryoPure tubes	Sarstedt AG & Co., Nümbrecht
Disposable scalpels	Feather Safety Razor Co., Ltd, Osaka
Eppendorf PCR Tubes 0.2ml	Eppendorf AG, Hamburg
Filter tips	Kisker Biotech GmbH & Co. KG, Steinfurt

Disposables	Source
Fluorescence Activated Cell Sorting (FACS) tubes	Corning Inc., Corning, NY
Glass slides Superfrost® Plus	Gerhard Menzel, Glasbearbeitungswerk GmbH & Co. KG, Braunschweig
Pasteur pipettes	Hirschmann Laborgeräte GmbH & Co. KG, Eberstadt
PCR Microplate PCR-96-LP-AB-C	Axygen, Inc., Union City, CA
Pipette tips	Sarstedt AG & Co., Nümbrecht
Platemax® CycloSeal Sealing Film	Axygen, Inc., Union City, CA
Reaction tubes, 0.5 ml, 1.5 ml and 2 ml	Eppendorf AG, Hamburg
Serological pipettes	Sarstedt AG & Co., Nümbrecht
Tissue embedding cassette system	Medite GmbH, Burgdorf
Whatmann paper 3 mm chr	GE Healthcare Life Sciences, Freiburg

Table 5-3: Cell culture reagents and media

Cell culture reagents and media	Source
4-Hydroxytamoxifen (4-OHT)	Sigma-Aldrich, Steinheim
Collagenase Type II	Worthington Biochemical corporation, Lakewood, NJ
Dimethylsulfoxide (DMSO) cell culture	PanReac AppliChem, Darmstadt
Dulbecco's Modified Eagle Medium high glucose (DMEM)	Sigma-Aldrich, Steinheim
Dulbecco's phosphate buffered saline (PBS)	Sigma-Aldrich, Steinheim
Ethylenediamine-tetraacetic acid (EDTA)	Sigma-Aldrich, Steinheim
Fetal calf serum (FCS)	Biochrome AG, Berlin
Penicillin-Streptomycin (Pen/Strep)	Gibco™, Schwerte
Thiazolyl Blue Tetrazolium Bromide (MTT)	Sigma-Aldrich, Steinheim
Transforming growth factor β (TGF β)	PeproTech, Rocky Hill, NJ

Table 5-4: Compounds

Compounds	Catalogue number	Source
A83-01	72022	Stemcell Technologies, Vancouver
Galunisertib	S2230	Selleckchem, Houston, TX
LY2109761	S2704	Selleckchem, Houston, TX
Merck-60		Gift of Prof. Martin Göttlicher
MS-275	E3866	LC Laboratories, Woburn, MA
Panobinostat	S1030	Selleckchem, Houston, TX
SAHA	V8477	LC Laboratories, Woburn, MA

Table 5-5: Kits

Kits	Source
Antigen unmasking solution	Vector Laboratories, Burlingame, CA
Avidin/Biotin Blocking Kit	Vector Laboratories, Burlingame, CA
BM Cyclin	Roche, Basel
DAB peroxidase substrate Kit	Vector Laboratories, Burlingame, CA
GoTaq [®] qPCR Master Mix	Promega, Madison, WI
Maxwell [®] 16 LEV simplyRNA Purification Kit	Promega, Madison, WI
<i>PowerSYBR[®] Green PCR Master Mix</i>	Life Technologies LTD, Woolston Warrington
TaqMan [®] reverse transcription reagents	Applied Biosystems Inc., Foster City, CA
Vectastain [®] elite ABC Kit	Vector Laboratories, Burlingame, CA

Table 5-6: Reagents and enzymes

Reagents and enzymes	Source
β -Mercaptoethanol, 98%	Carl Roth GmbH + Co. KG GmbH, Karlsruhe
2-log DNA ladder	New England Biolabs, Frankfurt
30% Acrylamid/Bisacrylamid - stock solution (29:1)	Carl Roth GmbH + Co. KG GmbH, Karlsruhe

Reagents and enzymes	Source
Acetic acid (100%)	Merck KGaA, Darmstadt
Agarose	Sigma-Aldrich, Steinheim
Ammonium Persulfate (APS)	Sigma-Aldrich, Steinheim
Bovine serum albumin (BSA) fraction V	Serva, Heidelberg
Bradford reagent 5x	Serva, Heidelberg
Bromphenole Blue-Xylene Cyanole Dye solution	Sigma-Aldrich, Steinheim
Cell lysis buffer (9803S)	Cell Signaling Technology, Leiden
DNase I Kit	Sigma-Aldrich, Steinheim
dNTP-Mix	PeqLab, Erlangen
Ethidium bromide	Sigma-Aldrich, Steinheim
GeneRuler™ 100bp DNA ladder	Fermentas GmbH, St. Leon-Rot
Giemsa's Azur-Eosin-Methylene blue solution	Merck, Darmstadt
Glycerine	Carl Roth GmbH + Co. KG, Karlsruhe
Glycerol	Carl Roth GmbH + Co. KG, Karlsruhe
Glycine	Carl Roth GmbH + Co. KG, Karlsruhe
Glycine	Sigma-Aldrich, Steinheim
H ₂ O	Merck KGaA, Darmstadt
HCl (37%)	Merck, Darmstadt
Isopropanol	Carl Roth GmbH + Co. KG, Karlsruhe
KCl	Merck, Darmstadt
MgCl ₂	Merck, Darmstadt
Multiscribe reverse Transcriptase (50 U/μl)	Applied Biosystems, Darmstadt
Na ₂ (PO ₄)H ₂ O	Merck KGaA, Darmstadt
NaCl	Serva, Heidelberg
NuPAGE LDS sample buffer	Life Technologies LTD, Woolston Warrington
PageRuler Prestained Protein Ladder	Thermo Scientific, Schwerte
Phosphatase inhibitor mix	Serva, Heidelberg
Phosphate buffered saline (PBS) powder	Biochrome AG, Berlin
Propidiumjodid (PI)	Sigma-Aldrich, Steinheim

Reagents and enzymes	Source
Protease inhibitor cocktail tablets	Roche Diagnostics, Mannheim
Proteinase K solution	Sigma-Aldrich, Steinheim
PureLink™ RNase A	Thermo Fisher Scientific Inc., Waltham, MA
REDTaq® ReadyMix™ PCR reaction mix	Sigma-Aldrich, Steinheim
Skim milk powder	Sigma-Aldrich, Steinheim
Sodium Dodecyl Sulfate (SDS)	Serva, Heidelberg
Tetramethylethylenediamine (TEMED)	Carl Roth GmbH + Co. KG, Karlsruhe
Tris-(hydroxymethyl)-aminomethan (Tris)	Carl Roth GmbH + Co. KG, Karlsruhe
TritonX-100	Sigma-Aldrich, Steinheim
Tween20	Carl Roth GmbH + Co. KG, Karlsruhe

Table 5-7: Histology reagents

Histology reagents	Source
Eosin	Waldeck GmbH & co KG, Münster
Ethanol (EtOH) absolute	Otto Fischar, Saarbrücken
Hematoxylin	Merck KGaA, Darmstadt
Hydrogen peroxide 30%	Merck KGaA, Darmstadt
Methanol	Carl Roth GmbH + Co. KG, Karlsruhe
Pertex mounting medium	Medite GmbH, Burgdorf
Roti® Histofix 4%	Carl Roth GmbH + Co. KG, Karlsruhe
Roti® Histol	Carl Roth GmbH + Co. KG, Karlsruhe

6. Methods

6.1 Mouse models

All animal studies were conducted meeting the requirements of the European guidelines for the care and use of laboratory animals and were approved by the *Institutional Animal Care and Use Committees* of the *Technische Universität München* and *Regierung von Oberbayern*. All animals were on a mixed C57/Bl6;129S6/SvEv genetic background. All breeding and handling of living mice were performed by Dr. med. Patrick Wenzel.

KPC mouse model

The KPC mouse model was used to study the role of HDACs in metastatic PDAC.

These mice carry the *Kras*^{G12D} mutation and have a mutated *Trp53*^{R172H} gene which are both silenced by a *loxP-Stop-loxP* (*LSL*) cassette (Jackson *et al.*, 2001, Liu *et al.*, 2000; Olive *et al.*, 2004). To remove the *LSL* cassette a Cre recombinase is needed. There are different Cre recombinases available, e.g. the transgenetically generated *Pdx1-Cre* (Hingorani *et al.*, 2003) which is under control of the *Pdx1* promoter. Therefore, the Cre expression is limited to *Pdx1* expressing tissues like in pancreatic tissue and consequently the mutated *Kras* and *Trp53* are also expressed exclusively in these cells. All these alleles are combined in one GEMM – the *LSL-Kras*^{G12D/+};*LSL-Trp53*^{R172H/+};*Pdx1-Cre* (KPC) mouse model, which was used in this work to study tumor formation and progression (Hingorani *et al.*, 2005).

For analyzing the specific role of Histone deacetylases 2 (HDAC2) during tumor formation and progression, a KPC-based knock-out mouse model was generated. Therefore, a mouse line with floxed Exons 2 to 4 of *Hdac2* allele were paired with the KPC model, to achieve a mouse model with the constitutive *Hdac2* knock-out (Montgomery *et al.*, 2007) (see Figure 6-1).

LSL-Kras^{G12D/+};LSL-Trp53^{R172H/+};Pdx1-Cre;Hdac2^{lox/lox}

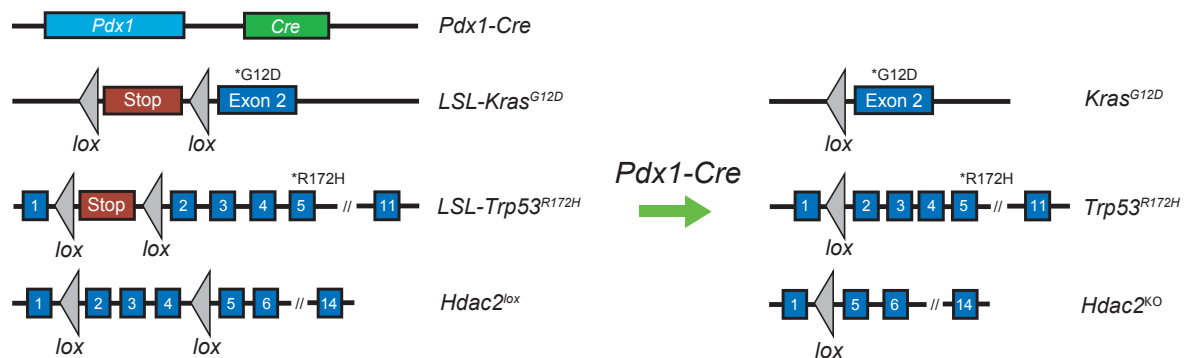


Figure 6-1: Genetic strategy of used KPC mouse model

KPC mice express *Pdx1*-Cre recombinase in pancreatic tissue, leading to expression of mutated *Kras* and *Trp53* and excision of Exon 2 to 4 of *Hdac2* allele whereby the *Hdac2* knock-out is generated. KO = knock-out, LSL = *loxP*-*Stop*-*loxP* (adapted from Hingorani *et al.*, 2005; Montgomery *et al.*, 2007; Schonhuber *et al.*, 2014).

Dual-recombinase mouse model

For investigating the role of histone deacetylases in PDAC maintenance, an inducible dual-recombinase system was used. This mouse model combines both the flippase/*frt* (*Flp/frt*) and the *Cre/loxP* system within one model.

The *Flp* recombinase is expressed under control of the *Pdx1* promoter to ensure the pancreas specific expression (Schonhuber *et al.*, 2014). The PDAC initiating *Kras^{G12D}* mutation is silenced by a *frt*-*Stop*-*frt* (*FSF*) cassette (Schonhuber *et al.*, 2014) and the Exons 2 to 6 of *Trp53* are flanked with *frt* sites (Lee *et al.*, 2012). Both *FSF* cassette and *frt* flanked exons can be deleted by the transgenetically generated *Pdx1*-*Flp*, leading to the expression of the mutated *Kras* and deletion of *Trp53* in *Pdx1*-*Flp* recombinase expressed in pancreatic cells.

In addition, the *Cre* recombinase is aligned to the tamoxifen-inducible estrogen receptor (*ER^{T2}*) under the control of *CAG* promoter as a *Rosa26* knock-in. To ensure tissue-specific expression of the *CreER^{T2}* recombinase, the gene is also silenced by an *FSF* cassette which can be deleted by *Pdx1*-*Flp* (Schonhuber *et al.*, 2014). To enable the deletion of a gene of interest, its sequence is modified with *loxP* sites. The floxed sequence of the gene on interest is deleted by the *Cre* recombinase when 4-Hydroxytamoxifen (4-OHT) is applied. Upon deletion of the floxed sequences the gene transcription is impaired and a knock-out for the gene of interest is achieved.

As shown in Figure 6-2 (A), once the *Pdx1*-Flp is expressed, the PDAC progression is initiated by the *Kras*^{G12D} mutation and the pancreas specific deletion of *Trp53* leads to a more realistic presentation of PDAC. The CreER^{T2} recombinase is expressed in the *Kras*^{G12D} lineage of the pancreatic tissue as well. The CreER^{T2} binds to HSP90 in the cytoplasm and is inactivated thereby (Figure 6-2 (B)). For time-specific deletion of a floxed gene of interest, 4-OHT has to be applied to the cells (1). 4-OHT displaces the binding of HSP90 to CreER^{T2}, leading to dissociation of Hsp90 from the CreER^{T2} (2) and translocation of CreER^{T2} to the nucleus (3) (Leone *et al.*, 2003; Schonhuber *et al.*, 2014). The gene of interest is modified with *loxP* sites. The floxed sequence is deleted by the Cre and therefore, the gene transcription is impaired and the knock-out for the gene of interest is achieved (4).

In this work the specific function of the class I HDACs HDAC1, HDAC2 and HDAC3 was investigated. Therefore, mice of the dual-recombinase system model were paired with mouse lines containing floxed *Hdac1*, *Hdac2* and *Hdac3* alleles respectively.

The *Hdac1* and *Hdac3* floxed mouse lines were generated by EUCOMM (HDAC1^{loxP} [*Hdac1*^{tm1a(EUCOMM)Wtsi}] and HDAC3^{loxP} [*Hdac3*^{tm1a(EUCOMM)Wtsi}]), the *Hdac2* floxed mouse line was generated by Montgomery *et al.*, 2007. While for knock-out of *Hdac1* and *Hdac3* the deletion of the respective Exon 3 is enough, for knock-out of *Hdac2* Exons 2 to 4 need to be deleted (*Hdac1*^{tm1a(EUCOMM)Wtsi}; *Hdac3*^{tm1a(EUCOMM)Wtsi}; Montgomery *et al.*, 2007) (Figure 6-2 (C)).

FSF-Kras^{G12D/+};FSF-Trp53^{frt/frt};Pdx1-Flp;R26^{CAG-FSF-CreERT2};Hdac^{lox/lox}

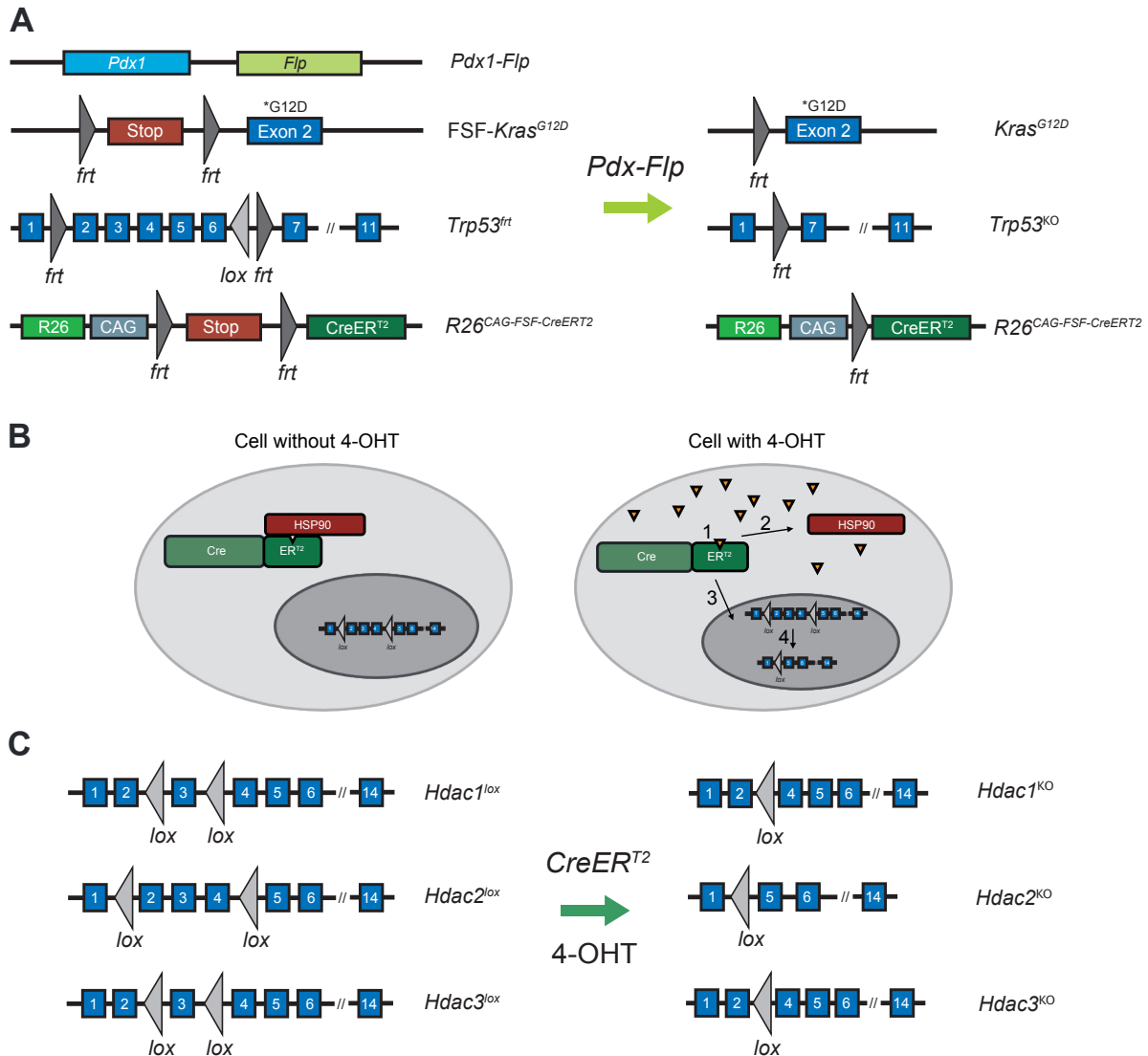


Figure 6-2: Genetic strategy of used dual-recombinase mouse model

A) In the dual-recombinase system, the *Pdx1-Flp* recombinase is expressed in pancreatic tissue, leading to expression of mutated *Kras*, deletion of *Trp53*, as well as expression of *CreERT²*. B) After application of 4-OHT, *CreERT²* is activated by replacement of HSP90 binding through 4-OHT (1+2) and translocated to the nucleus (3) where the recombinase leads to excision of floxed sequences (4). C) Active *CreERT²* removes floxed sequences of the *Hdac* genes which results in knock-out of *Hdac1*, *Hdac2* or *Hdac3*, respectively. FSF = *frt-Stop-frt*, KO = knock-out, 4-OHT = 4-Hydroxtamoxifen (adapted from Hingorani *et al.*, 2005; Montgomery *et al.*, 2007; Schonhuber *et al.*, 2014; Leone *et al.*, 2003; *Hdac1^{tm1a(EUCOMM)Wtsi}*; *Hdac3^{tm1a(EUCOMM)Wtsi}*).

Survival analysis

For survival analysis, the lifetime of KPC mice and KPC mice with hetero- or homozygous deletion of *Hdac2* was counted in days (d). For comparison of survival between the three groups, a Kaplan-Meier survival curve was performed. All animals used for survival analysis are listed in Table 6-1.

Table 6-1: Mice used for survival analysis

Mouse	Genotype
F1039	<i>Hdac2</i> ^{loxP/loxP} , <i>LSL-Kras</i> ^{G12D/+} , <i>LSL-Trp53</i> ^{R172H/+} , <i>Pdx1-Cre</i> , <i>LSL-Tva</i> ^{+/-}
F1042	<i>Hdac2</i> ^{loxP/loxP} , <i>LSL-Kras</i> ^{G12D/+} , <i>LSL-Trp53</i> ^{R172H/+} , <i>Pdx1-Cre</i>
F1047	<i>Hdac2</i> ^{loxP/loxP} , <i>LSL-Kras</i> ^{G12D/+} , <i>LSL-Trp53</i> ^{R172H/+} , <i>Pdx1-Cre</i> , <i>LSL-Tva</i> ^{+/-}
F1055	<i>Hdac2</i> ^{loxP/loxP} , <i>LSL-Kras</i> ^{G12D/+} , <i>LSL-Trp53</i> ^{R172H/+} , <i>Pdx1-Cre</i>
F1063	<i>Hdac2</i> ^{loxP/loxP} , <i>LSL-Kras</i> ^{G12D/+} , <i>LSL-Trp53</i> ^{R172H/+} , <i>Pdx1-Cre</i>
F1064	<i>Hdac2</i> ^{loxP/loxP} , <i>LSL-Kras</i> ^{G12D/+} , <i>LSL-Trp53</i> ^{R172H/+} , <i>Pdx1-Cre</i>
F1088	<i>Hdac2</i> ^{loxP/loxP} , <i>LSL-Kras</i> ^{G12D/+} , <i>LSL-Trp53</i> ^{R172H/+} , <i>Pdx1-Cre</i>
F1091	<i>Hdac2</i> ^{loxP/loxP} , <i>LSL-Kras</i> ^{G12D/+} , <i>LSL-Trp53</i> ^{R172H/+} , <i>Pdx1-Cre</i>
F1128	<i>Hdac2</i> ^{loxP/loxP} , <i>LSL-Kras</i> ^{G12D/+} , <i>LSL-Trp53</i> ^{R172H/+} , <i>Pdx1-Cre</i> , <i>LSL-Tva</i> ^{+/-}
F1129	<i>Hdac2</i> ^{loxP/loxP} , <i>LSL-Kras</i> ^{G12D/+} , <i>LSL-Trp53</i> ^{R172H/+} , <i>Pdx1-Cre</i> , <i>LSL-Tva</i> ^{+/-}
F1144	<i>Hdac2</i> ^{loxP/loxP} , <i>LSL-Kras</i> ^{G12D/+} , <i>LSL-Trp53</i> ^{R172H/+} , <i>Pdx1-Cre</i>
F1146	<i>Hdac2</i> ^{loxP/loxP} , <i>LSL-Kras</i> ^{G12D/+} , <i>LSL-Trp53</i> ^{R172H/+} , <i>Pdx1-Cre</i>
F1163	<i>Hdac2</i> ^{loxP/loxP} , <i>LSL-Kras</i> ^{G12D/+} , <i>LSL-Trp53</i> ^{R172H/+} , <i>Pdx1-Cre</i>
F1183	<i>Hdac2</i> ^{loxP/loxP} , <i>LSL-Kras</i> ^{G12D/+} , <i>LSL-Trp53</i> ^{R172H/+} , <i>Pdx1-Cre</i>
F1229	<i>Hdac2</i> ^{loxP/loxP} , <i>LSL-Kras</i> ^{G12D/+} , <i>LSL-Trp53</i> ^{R172H/+} , <i>Pdx1-Cre</i>
F1234	<i>Hdac2</i> ^{loxP/loxP} , <i>LSL-Kras</i> ^{G12D/+} , <i>LSL-Trp53</i> ^{R172H/+} , <i>Pdx1-Cre</i> , <i>LSL-Tva</i> ^{+/-}
F1252	<i>Hdac2</i> ^{loxP/loxP} , <i>LSL-Kras</i> ^{G12D/+} , <i>LSL-Trp53</i> ^{R172H/+} , <i>Pdx1-Cre</i>
F1259	<i>Hdac2</i> ^{loxP/loxP} , <i>LSL-Kras</i> ^{G12D/+} , <i>LSL-Trp53</i> ^{R172H/+} , <i>Pdx1-Cre</i> , <i>LSL-Tva</i> ^{+/+}
F1293	<i>Hdac2</i> ^{loxP/loxP} , <i>LSL-Kras</i> ^{G12D/+} , <i>LSL-Trp53</i> ^{R172H/+} , <i>Pdx1-Cre</i> , <i>LSL-Tva</i> ^{+/+}
F1296	<i>Hdac2</i> ^{loxP/loxP} , <i>LSL-Kras</i> ^{G12D/+} , <i>LSL-Trp53</i> ^{R172H/+} , <i>Pdx1-Cre</i> , <i>LSL-Tva</i> ^{+/+}
F1297	<i>Hdac2</i> ^{loxP/loxP} , <i>LSL-Kras</i> ^{G12D/+} , <i>LSL-Trp53</i> ^{R172H/+} , <i>Pdx1-Cre</i> , <i>LSL-Tva</i> ^{+/+}
F1374	<i>Hdac2</i> ^{loxP/loxP} , <i>LSL-Kras</i> ^{G12D/+} , <i>LSL-Trp53</i> ^{R172H/+} , <i>Pdx1-Cre</i>
F1915	<i>Hdac2</i> ^{loxP/loxP} , <i>LSL-Kras</i> ^{G12D/+} , <i>LSL-Trp53</i> ^{R172H/+} , <i>Pdx1-Cre</i> , <i>LSL-Tva</i> ^{+/-}
F2100	<i>Hdac2</i> ^{loxP/loxP} , <i>LSL-Kras</i> ^{G12D/+} , <i>LSL-Trp53</i> ^{R172H/+} , <i>Pdx1-Cre</i>
F2143	<i>Hdac2</i> ^{loxP/loxP} , <i>LSL-Kras</i> ^{G12D/+} , <i>LSL-Trp53</i> ^{R172H/+} , <i>Pdx1-Cre</i>
F2413	<i>Hdac2</i> ^{loxP/loxP} , <i>LSL-Kras</i> ^{G12D/+} , <i>LSL-Trp53</i> ^{R172H/+} , <i>Pdx1-Cre</i>
F2692	<i>Hdac2</i> ^{loxP/loxP} , <i>LSL-Kras</i> ^{G12D/+} , <i>LSL-Trp53</i> ^{R172H/+} , <i>Pdx1-Cre</i>
F2703	<i>Hdac2</i> ^{loxP/loxP} , <i>LSL-Kras</i> ^{G12D/+} , <i>LSL-Trp53</i> ^{R172H/+} , <i>Pdx1-Cre</i> , <i>LSL-Tva</i> ^{+/-}
F3399	<i>Hdac2</i> ^{loxP/loxP} , <i>LSL-Kras</i> ^{G12D/+} , <i>LSL-Trp53</i> ^{R172H/+} , <i>Pdx1-Cre</i>
F1033	<i>Hdac2</i> ^{loxP/+} , <i>LSL-Kras</i> ^{G12D/+} , <i>LSL-Trp53</i> ^{R172H/+} , <i>Pdx1-Cre</i>
F1037	<i>Hdac2</i> ^{loxP/+} , <i>LSL-Kras</i> ^{G12D/+} , <i>LSL-Trp53</i> ^{R172H/+} , <i>Pdx1-Cre</i>
F1276	<i>Hdac2</i> ^{loxP/+} , <i>LSL-Kras</i> ^{G12D/+} , <i>LSL-Trp53</i> ^{R172H/+} , <i>Pdx1-Cre</i>

Mouse	Genotype
F2002	<i>Hdac2</i> ^{loxP/+} , <i>LSL-Kras</i> ^{G12D/+} , <i>LSL-Trp53</i> ^{R172H/+} , <i>Pdx1-Cre</i>
F2409	<i>Hdac2</i> ^{loxP/+} , <i>LSL-Kras</i> ^{G12D/+} , <i>LSL-Trp53</i> ^{R172H/+} , <i>Pdx1-Cre</i>
F2417	<i>Hdac2</i> ^{loxP/+} , <i>LSL-Kras</i> ^{G12D/+} , <i>LSL-Trp53</i> ^{R172H/+} , <i>Pdx1-Cre</i>
F0793	<i>LSL-Kras</i> ^{G12D/+} , <i>LSL-Trp53</i> ^{R172H/+} , <i>Pdx1-Cre</i> , <i>LSL-Tva</i> ^{+/-}
BK50	<i>LSL-Kras</i> ^{G12D/+} , <i>LSL-Trp53</i> ^{R172H/+} , <i>Pdx1-Cre</i>
F1275	<i>LSL-Kras</i> ^{G12D/+} , <i>LSL-Trp53</i> ^{R172H/+} , <i>Pdx1-Cre</i>
AH1115	<i>LSL-Kras</i> ^{G12D/+} , <i>LSL-Trp53</i> ^{R172H/+} , <i>Pdx1-Cre</i>
AH1056	<i>LSL-Kras</i> ^{G12D/+} , <i>LSL-Trp53</i> ^{R172H/+} , <i>Pdx1-Cre</i>
F1416	<i>LSL-Kras</i> ^{G12D/+} , <i>LSL-Trp53</i> ^{R172H/+} , <i>Pdx1-Cre</i>
F2540	<i>LSL-Kras</i> ^{G12D/+} , <i>LSL-Trp53</i> ^{R172H/+} , <i>Pdx1-Cre</i>
F2854	<i>LSL-Kras</i> ^{G12D/+} , <i>LSL-Trp53</i> ^{R172H/+} , <i>Pdx1-Cre</i>
F2997	<i>LSL-Kras</i> ^{G12D/+} , <i>LSL-Trp53</i> ^{R172H/+} , <i>Pdx1-Cre</i>
F3045	<i>LSL-Kras</i> ^{G12D/+} , <i>LSL-Trp53</i> ^{R172H/+} , <i>Pdx1-Cre</i>
F3367	<i>LSL-Kras</i> ^{G12D/+} , <i>LSL-Trp53</i> ^{R172H/+} , <i>Pdx1-Cre</i>
S209	<i>LSL-Kras</i> ^{G12D/+} , <i>LSL-Trp53</i> ^{R172H/+} , <i>Pdx1-Cre</i> , <i>LSL-Tva</i> ^{+/-}
F1333	<i>LSL-Kras</i> ^{G12D/+} , <i>LSL-Trp53</i> ^{R172H/+} , <i>Pdx1-Cre</i>

LSL = *loxP-Stop-loxP*

6.2 Cell culture techniques

All used materials, reagents and kits, as well as their respective sources are listed in part 5 “Technical equipment”.

Primary cell culture

Tissue of primary pancreatic tumor (PPT) was washed in sterile PBS and cut to small pieces. Tissue was transferred to a 15 ml conical tube with DMEM with 10% (v/v) FCS and 1% (v/v) Pen/Strep and freshly added 0.1% (w/v) Collagenase type II. Tissue was incubated overnight at 37 °C. Suspension was centrifugated at 170 xg and room temperature (RT) for five minutes (min) and supernatant were removed. Cells were transferred with fresh medium to a cell culture flask and incubated for one week at 37 °C, 5% CO₂.

Culture conditions for PDAC cell lines

Murine PDAC cell lines were cultivated with DMEM supplemented with 10% (v/v) FCS and 1% (v/v) Pen/Strep at 37 °C, 5% CO₂. For re-cultivation 80 – 90% confluent cells were washed with 1x PBS, detached with 0.05% (v/v) EDTA and split 1:10 to a new flask and cultivated again until 80 – 90% confluence at 37 °C and 5% CO₂. Cells lines were used in as low passages as possible, but maximum to passage 25. Thawed cell lines were passaged at the maximum 10x before discarding the cells and thawing a new vial of the cell line. All experiments were started at 80% confluence, cells were routinely authenticated by genotyping. Cells were regularly tested for Mycoplasma and, if necessary, treated as well.

Table 6-2: Cell lines and genotypes

Cell line	Genotype
PPT-F1648	<i>FSF-Kras</i> ^{G12D/+} , <i>FSF-Trp53</i> ^{del/+} , <i>Pdx1-Flp</i> , <i>R26</i> ^{CAG-FSF-CreERT2/+} , <i>Pdk</i> ^{loxP/+} , <i>Hdac2</i> ^{loxP/loxP}
PPT-F2612	<i>FSF-Kras</i> ^{G12D/+} , <i>FSF-Trp53</i> ^{del/+} , <i>Pdx1-Flp</i> , <i>R26</i> ^{CAG-FSF-CreERT2/FSF-CreERT2} , <i>Hdac2</i> ^{loxP/loxP}
PPT-F2800	<i>FSF-Kras</i> ^{G12D/+} , <i>FSF-Trp53</i> ^{del/+} , <i>Pdx1-Flp</i> , <i>R26</i> ^{CAG-FSF-CreERT2/LSL-Tva} , <i>Hdac2</i> ^{loxP/loxP}
PPT3-F4764	<i>FSF-Kras</i> ^{G12D/+} , <i>Pdx1-Flp</i> , <i>R26</i> ^{CAG-FSF-CreERT2/+} , <i>Hdac3</i> ^{loxP/loxP} ,
PPT3-F4402	<i>FSF-Kras</i> ^{G12D/+} , <i>Pdx1-Flp</i> , <i>R26</i> ^{CAG-FSF-CreERT2/CreERT2} , <i>Hdac3</i> ^{loxP/loxP}
PPT-F5061	<i>FSF-Kras</i> ^{G12D/+} , <i>FSF-Trp53</i> ^{del/+} , <i>Pdx1-Flp</i> , <i>R26</i> ^{CAG-FSF-CreERT2/FSF-CreERT2} , <i>Hdac3</i> ^{loxP/loxP} ,
PPT2-F4699	<i>FSF-Kras</i> ^{G12D/+} , <i>FSF-Trp53</i> ^{del/+} , <i>Pdx1-Flp</i> , <i>R26</i> ^{CAG-FSF-CreERT2/FSF-CreERT2} , <i>Hdac3</i> ^{loxP/loxP}
PPT-F3262	<i>FSF-Kras</i> ^{G12D/+} , <i>FSF-Trp53</i> ^{del/frt} , <i>Pdx1-Flp</i> , <i>R26</i> ^{CAG-FSF-CreERT2/+} , <i>Hdac1</i> ^{loxP/loxP} , <i>Hdac2</i> ^{loxP/+} , <i>Hdac3</i> ^{loxP/+}
PPT-F3641	<i>FSF-Kras</i> ^{G12D/+} , <i>FSF-Trp53</i> ^{del/frt} , <i>Pdx1-Flp</i> , <i>R26</i> ^{CAG-FSF-CreERT2/+} , <i>Hdac1</i> ^{loxP/loxP} , <i>Hdac2</i> ^{loxP/+} , <i>Hdac3</i> ^{loxP/+}
PPT-F5461	<i>FSF-Kras</i> ^{G12D/+} , <i>FSF-Trp53</i> ^{del/frt} , <i>Pdx1-Flp</i> , <i>R26</i> ^{CAG-FSF-CreERT2/+} , <i>Hdac1</i> ^{loxP/loxP} , <i>Hdac2</i> ^{loxP/loxP} , <i>Hdac3</i> ^{loxP/loxP}
PPT-F5465	<i>FSF-Kras</i> ^{G12D/+} , <i>FSF-Trp53</i> ^{frt/del} , <i>Pdx1-Flp</i> , <i>R26</i> ^{CAG-FSF-CreERT2/FSF-CreERT2} , <i>Hdac1</i> ^{loxP/loxP} , <i>Hdac2</i> ^{loxP/loxP} , <i>Hdac3</i> ^{loxP/loxP}

Cell line	Genotype
PPT-F5470	<i>FSF-Kras^{G12D/+}, FSF-Trp53^{frt/del}, Pdx1-Flp, R26^{CAG-FSF-CreERT2/FSF-CreERT2}, Hdac1^{loxP/loxP}, Hdac2^{loxP/loxP}, Hdac3^{loxP/loxP}</i>
PPT-F1679	<i>FSF-Kras^{G12D/+}, FSF-Trp53^{del/+}, Pdx1-Flp, R26^{CAG-FSF-CreERT2/+}, Pdk^{loxP/+}</i>
PPT-15283	<i>FSF-Kras^{G12D/+}, FSF-Trp53^{frt/+}, Pdx1-Flp, R26^{CAG-FSF-CreERT2/dual}</i>
PPT-AA373	<i>LSL-Kras^{G12D/+}, LSL-Trp53^{R172H/+}, Pdx1-Cre, LSL-Tva^{+/-}</i>
PPT1-AH1056	<i>LSL-Kras^{G12D/+}, LSL-Trp53^{R172H/+}, Pdx1-Cre</i>
PPT-F0793	<i>LSL-Kras^{G12D/+}, LSL-Trp53^{R172H/+}, Pdx1-Cre, LSL-Tva^{+/-}</i>
PPT-F1042	<i>LSL-Kras^{G12D/+}, LSL-Trp53^{R172H/+}, Pdx1-Cre, Hdac2^{loxP/loxP}</i>
PPT4-F1234	<i>LSL-Kras^{G12D/+}, LSL-Trp53^{R172H/+}, Pdx1-Cre, LSL-Tva^{+/-}, Hdac2^{loxP/loxP}</i>
PPT-F2143	<i>LSL-Kras^{G12D/+}, LSL-Trp53^{R172H/+}, Pdx1-Cre, Hdac2^{loxP/loxP}</i>
PPT-F1146	<i>LSL-Kras^{G12D/+}, LSL-Trp53^{R172H/+}, Pdx1-Cre, Hdac2^{loxP/loxP}</i>
PPT-F1915	<i>LSL-Kras^{G12D/+}, LSL-Trp53^{R172H/+}, Pdx1-Cre, LSL-Tva^{+/-}, Hdac2^{loxP/loxP}</i>
PPT-F2100	<i>LSL-Kras^{G12D/+}, LSL-Trp53^{R172H/+}, Pdx1-Cre, Hdac2^{loxP/loxP}</i>
PPT-AA352	<i>LSL-Kras^{G12D/+}, LSL-Trp53^{R172H/+}, Pdx1-Cre, LSL-Tva^{+/-}</i>
PPT-BK50	<i>LSL-Kras^{G12D/+}, LSL-Trp53^{R172H/+}, Pdx1-Cre</i>
PPT-4917	<i>LSL-Kras^{G12D/+}, LSL-Trp53^{R172H/+}, Pdx1-Cre, LSL-Tva^{+/-}</i>
PPT-F1128	<i>LSL-Kras^{G12D/+}, LSL-Trp53^{R172H/+}, Pdx1-Cre, Hdac2^{loxP/loxP}</i>

PPT = primary pancreatic tumor, FSF = *frt-Stop-frt*, LSL = *loxP-Stop-loxP*

Mycoplasma test PCR

Cells were cultivated until they were almost 100% confluent. 2 ml of supernatant was harvested and centrifugated at 250 xg for two minutes. Supernatant was transferred to a new reaction tube and centrifugated at 20,000 xg for ten minutes. Supernatant was discarded and pellet was resuspended in 50 µl PBS followed by heat inactivation at 95 °C for three minutes. This was used as a DNA template. PCR was performed using reagents and conditions described in Table 6-3 and Table 6-4, respectively. Next, gel electrophoresis using 1.5% agarose gel was performed. Positive cells showed a band at 200 bp size.

Table 6-3: Primer sequences for Mycoplasma test PCR

Forward primers (5' -> 3')	Reverse primers (5' -> 3')
CGC CTG AGT AGT ACG TTC GC	GCG GTG TGT ACA AGA CCC GA
CGC CTG AGT AGT ACG TAC GC	GCG GTG TGT ACA AAA CCC GA
TGC CTG GGT AGT ACA TTC GC	GCG GTG TGT ACA AAC CCC GA
TGC CTG AGT AGT ACA TTC GC	
CGC CTG AGT AGT ATG CTC GC	
CAC CTG AGT AGT ATG CTC GC	
CGC CTG GGT AGT ACA TTC GC	

A forward primer mix containing 10 µl from each forward primer and 30 µl H₂O and a reverse primer mix containing 10 µl from each reverse primer and 70 µl H₂O was prepared. Primers had a stock concentration of 100 µM and were used with a final concentration of 10 µM.

Table 6-4: Conditions for Mycoplasma test PCR

Mycoplasma test PCR	Mycoplasma PCR conditions		
15 µl REDTaq® Ready mix™	95 °C	15 min	
2 µl forward primer mix	94 °C	1 min	40x
2 µl reverse primer mix	60 °C	1 min	
9 µl H ₂ O	74 °C	1 min	
2 µl DNA template	72 °C	10 min	
	25 °C	Constantly	

Treatment against Mycoplasma

Mycoplasma positive cell lines were treated with BM Cyclin. Therefore, medium was removed and new cell culture medium supplemented with 4 µl BM Cyclin 1 per ml medium (final concentration 10 µg/ml) was added to the cells. The cells were cultivated for three days as usual at 37 °C and 5% CO₂ with this medium. After three days this medium was removed and new cell culture medium containing 4 µl BM Cyclin 2 per ml medium (final concentration 5 µg/ml) was added to the cells. The cells were cultivated for four days in this medium as usual. This treatment cycle was repeated twice and the cells were split when they reach about 80% confluence. After all treatment cycles have been completed, the cells were cultivated for 14 days in the usual medium without BM

Cyclin supplementation. Afterwards the Mycoplasma test PCR was repeated to ensure successful treatment.

Freeze cells

Cells were washed with PBS and detached with 0.05% (v/v) EDTA. Detached cells were resuspended in PBS, followed by centrifugation (210 $\times g$, 5 min, 4 °C). Supernatant was discarded and the pellet was resuspended in cold freezing medium (DMEM + 20% (v/v) FCS + 10% (v/v) DMSO). Cell suspension was distributed to CryoPure tubes and stored at -80 °C. After three days the cells were transferred to liquid N₂.

Thaw cells

Cells were thawed in CryoPure tubes at room temperature (RT) and transferred to a new flask with DMEM and cultivated at 37 °C, 5% CO₂ until cells were 80 – 90% confluent.

Removing fibroblasts

Cells were washed with PBS. Then 0.05% (v/v) EDTA for short incubation was added. When fibroblasts began to detach, they were removed with PBS. The remaining cells were cultivated as usual.

Separation of mesenchymal and epithelial cell line fractions

Separation of mesenchymal and epithelial cell fractions of the cell lines PPT-F2612 and PPT-F2800 was performed as described previously (Mueller *et al.*, 2018). In brief, PDAC cells were grown to 80% confluence, then medium was removed and cells in the parental flask were washed with PBS followed by incubation with 0.05% (v/v) EDTA. Mesenchymal cells detach faster than cells with epithelial morphology when treated with 0.05% (v/v) EDTA. To notice the time when the majority of mesenchymal cells are detached and the epithelial cells still stick to the flask, the cells were constantly monitored under a light microscope. Depending on the cell line this takes around 3 – 5 minutes. When this status was reached, the EDTA solution containing the detached mesenchymal cells was transferred to a new flask. This mesenchymal fraction was cultivated with medium as usual. The remaining cells in the parental flask were treated again with 0.05% (v/v) EDTA to detach the residual

mesenchymal cells. When only pure epithelial cells were still attached to the flask, the EDTA was removed and the cells were washed once with PBS before cultivated as epithelial fraction with medium as usual.

When the cells in the new flask had grown to around 80% confluence, the 0.05% (v/v) EDTA treatment was repeated and again the mesenchymal cells of the first mesenchymal fraction were detached and further cultivated as described above. The first epithelial fraction was treated again with 0.05% EDTA as well to remove the mesenchymal cells the fraction might still contain. After this, the remaining epithelial fraction was cultivated as described above.

This procedure was repeated several times until pure fractions were achieved.

Cell counting

Cells were washed with PBS and detached with 0.05% (v/v) EDTA. Detached cells were resuspended in DMEM medium, followed by singularization. Singularized cells were counted using a Neubauer counting chamber and calculation of the number of cells/ μ l was performed as described in the following formula:

$$\frac{\text{Desired number of cells}}{(\text{Median of counted cells of 4 large chambers}) * 10} = \mu\text{l of cell suspension}$$

For Fluorescence Activated Cell Sorting (FACS) analysis, used medium and washing PBS was collected as well as the cells; for MTT Assay and Clonogenic Assay only the cells were collected.

4-Hydroxytamoxifen treatment

Medium was removed and cells were washed with 1x PBS and detached with 0.05% (v/v) EDTA. 1 Million cells were seeded in 10 cm cell culture dish and 6 ml medium supplemented with 600 nM 4-OHT or vehicle (100% ethanol). Fresh 4-OHT or ethanol was added daily to the medium for eight days. After four days of treatment, the cells were split to avoid overconfluence. Protein or RNA was harvested as described above after eight days when the knock-out of the HDAC isoenzymes was successful.

HDACi treatment

Medium was removed and cells were washed with 1x PBS and detached with 0.05% (v/v) EDTA. 1 Million cells were seeded in 10 cm cell culture dish in 6 ml medium and allowed to attach overnight. Next day, cells were treated with HDACi or vehicle (DMSO) as a control for 24 hours (h), 48 h or 72 h. HDACis and the respective used concentrations are listed in Table 6-5.

TGF β treatment

Medium was removed and cells were washed with 1x PBS and detached with 0.05% (v/v) EDTA. 1 Million cells were seeded in 10 cm cell culture dish in 6 ml medium and allowed to attach overnight. Next day, cells were treated with TGF β (final concentration 5 ng/ml, solved in 10 mM citric acid) or vehicle solution (10 mM citric acid) and incubated for 72 hours or seven days as usual. Protein or RNA was harvested as described above.

MTT Assay – growth detection after 4-OHT/vehicle treatment

After eight days of 4-OHT/vehicle treatment, cells were detached, singularized and counted using a Neubauer hemocytometer as described above. 2,000 cells were seeded in 100 μ l DMEM medium in quadruplicates in a 96-well plate and were allowed to attach to the bottom of the plate overnight. For day 0 measurement 10 μ l MTT reagent was added the next day, followed by incubation for four hours at 37 °C, 5% CO₂. After this, DMEM was removed and 200 μ l Lysis reagent (1:1 100% EtOH + DMSO) was added to lyse the cells and dissolve the formazan crystals. After incubation for ten minutes (shaking) measurement with 595 nm was performed. For investigation of differences in cell proliferation, MTT Assay was measured at day 0, after 24 h, 48 h and 72 h. Day 0 was measured after cells settled down overnight and this timepoint was set as 1 to erase the differences/errors in cell counting and cell seeding. Measurements after 24 h, 48 h and 72 h were then normalized to the day 0 measurement.

MTT Assay – growth detection with TGF β or inhibitor treatment

MTT Assay was performed as described above with the following modifications: 2,000 cells were seeded in a 96-well plate in triplicates and were allowed to attach to the bottom of the plate overnight. Next day, inhibitors or TGF β and respective vehicle

solutions for controls were added and the cells were incubated for 72 h at 37 °C, 5% CO₂. For HDACis DMSO was used as vehicle solution and for TGFβ 10 mM citric acid was used as vehicle solution. After 72 h 10 μl MTT reagent was added and development of the assay was performed as described above. Used inhibitors and TGFβ, as well as the respective concentrations are listed in Table 6-5.

Table 6-5: Compounds used in MTT and Clonogenic Assay

Compound	Final concentration
TGFβ	5 ng
MS-275	4.5 μM, 5 μM
SAHA	4 μM
Panobinostat	100 nM
Merck-60	400 nM
A83-01	10 μM
Galunisertib	2 μM
LY2109761	2 μM

Clonogenic Assay – Giemsa staining

After eight days of 600 nM 4-OHT/vehicle treatment, cells were detached, singularized and counted using a Neubauer hemocytometer. 2,000 cells were seeded in DMEM + 10% (v/v) FCS + 1% (v/v) Pen/Strep in triplicates in a 6-well plate and incubated for seven days until single colonies formed. Medium was changed every second or third day. Medium was removed and cells were washed in PBS, followed by fixation with ice-cold 100% methanol and incubation for 30 min at RT on a shaker. Methanol was removed and colonies were stained with 1:20 diluted Giemsa staining solution overnight. Destaining was performed with ddH₂O. For quantification the number of colonies was counted.

This variant of clonogenic Assay was used during basic characterization of the cell lines. Cell lines with mesenchymal morphology do not form distinct colonies, thereby for analysis of those cell lines, another variant of clonogenic Assay was performed.

Clonogenic Assay – Crystal violet staining

After eight days of 600 nM 4-OHT/vehicle treatment cells were incubated with DMEM + 10% (v/v) FCS + 1% (v/v) Pen/Strep until day 12 and then detached, singularized

and counted using a Neubauer hemocytometer. 2,000 cells were seeded in DMEM + 10% (v/v) FCS + 1% (v/v) Pen/Strep in triplicates in a 24-well plate and allowed to attach to the bottom of the plate overnight and incubated for seven days. After this, medium was removed and cells were washed in PBS, followed by staining with 0.1% crystal violet in 100% ethanol for 20 min at RT on a shaker. Destaining was done with ddH₂O to scan the plates for visualization. To quantify the difference in growth and colony formation ability, cells were dissolved in 1% (w/v) SDS solution and measured at 595 nm.

This variant of clonogenic Assay was used for cell lines with complete mesenchymal morphology, since they do not form distinct colonies.

Clonogenic Assay – procedure for TGF β or inhibitor treatment

Cells were washed with 1x PBS, detached, singularized and counted using a Neubauer hemocytometer. 2,000 cells were seeded in DMEM + 10% (v/v) FCS + 1% (v/v) Pen/Strep in triplicates in a 24-well plate and allowed to attach to the bottom of the plate overnight. Next day the cells were treated with inhibitors or TGF β (Table 6-5) and the respective vehicle solution and incubated for seven days. For inhibitors DMSO was used as vehicle solution and for TGF β 10 mM citric acid was used as vehicle solution. After incubation for seven days, medium was removed and cells were washed in PBS, followed by staining with 0.1% (v/v) crystal violet in 100% Ethanol for 20 min at RT on a shaker. Destaining was done with ddH₂O to scan the plates for visualization of the colonies. To quantify the difference in growth and colony formation ability, cells were solved in 1% (w/v) SDS solution and measured at 595 nm.

This variant of clonogenic Assay was applied for cell lines that were used in TGF β /inhibitor treatments, since TGF β treated cells do not form distinct colonies.

Cell cycle FACS analysis

After eight days of 600 nM 4-OHT/vehicle treatment, cells were washed with PBS, followed by detaching with EDTA and cell counting. 1,000,000 cells were separated and centrifugated (5 min, 190 xg, RT). Cells were resuspended in 1 ml 70% EtOH, followed by incubation overnight at 4 °C in a FACS tube. 1 ml ice-cold PBS was added and cells were centrifugated (5 min, 190 xg, 4 °C). Supernatant was removed and cells were resuspended in 500 μ l PBS. RNase was added (final concentration 50 μ g/ml (v/v)), followed by incubation for 30 min at 37 °C in the dark. For staining,

Propidium iodide (PI) (final concentration 25 µg/ml (v/v)) was added and cell distribution was measured after at least 5 min with Gallios Flow Cytometer or FACS Calibur instrument. Voltages used vary among the cell lines and are listed in Table 6-6. Analysis was performed with the Software FlowJo Version V10.

Table 6-6: Voltage for cell cycle FACS analysis

Cell line	Voltage
PPT-F3641	440V
PPT-F1648	440V, 475V
PPT-F2612	412V
PPT-F2800	415V
PPT3-F4402	415V
PPT2-F4699	417V
PPT3-F4764	405V
PPT-F5061	415V
PPT-F1679	395V
PPT-15283	415V

6.3 Molecular techniques

All used materials, reagents and kits, as well as their respective sources are listed in part 5 “Technical equipment”.

6.3.1 Genotyping

Isolation of genomic DNA of mouse tail biopsies

For genotyping of mice, 2 – 3 mm of mouse tails were lysed in Soriano buffer as described previously (Krämer and Springer Science+Business Media, 2017). In brief, the tail biopsy was placed at the bottom of a reaction tube, covered with 50 µl Soriano buffer + 1 µl Proteinase K solution, followed by lysis (Table 6-7). Centrifugation at 12,000 xg for ten minutes separates the DNA containing supernatant from the tissue residuals of the tail. 45 µl of supernatant was transferred to a new reaction tube and stored at -20 °C. This DNA was used for genotyping. Buffer conditions, genotyping primers and PCR conditions are listed in Table 6-8, Table 6-9 and Table 6-10, respectively.

Table 6-7: Conditions for lysis of tail biopsies

PCR conditions for tail lysis	
55 °C	90 min
95 °C	15 min
4 °C	Constantly

Isolation of genomic DNA from tumor cell lines

Cells were washed with PBS. For harvesting 500 µl PBS was added and cells were scraped off. The cell suspension was transferred to a reaction tube and centrifugated for five minutes at 16,100 xg. Supernatant was removed and the pellet was dispersed in 300 µl cell lysis buffer + 20 µl Proteinase K solution and incubated overnight at 55 °C. Cell suspension was centrifugated for ten minutes at 16,100 xg. 200 µl of supernatant was transferred to a new reaction tube with 200 µl isopropanol, followed by centrifugation for ten minutes, 16,100 xg. Supernatant was discarded and 300 µl ice cold 70% EtOH was added. The centrifugation step was repeated and supernatant discarded. The pellet was dried and then solved in 100 µl TE buffer overnight at 4 °C. This DNA template was used for genotyping of cell lines and recombination PCR analysis. PCR conditions and primer sequences for genotyping are listed in Table 6-9 and Table 6-10, respectively.

Table 6-8: Buffers for DNA isolation

Buffers for DNA isolation	
Soriano buffer	0.5% (v/v) TritonX-100 1% (v/v) β-Mercaptoethanol 1x Gitschier's buffer
1x Gitschier's buffer (pH 8.8)	67 mM Tris 16.6 mM (NH ₄) ₂ SO ₄ 6.7 mM MgCl ₂
Cell lysis buffer (pH 8.0)	10 mM Tris 5 mM EDTA 0.5% (w/v) SDS 0.4 M NaCl
TE buffer	10 mM Tris 1 mM EDTA

Polymerase chain reaction

For polymerase chain reaction (PCR) REDTaq® ReadyMix™ was used. 10 µM forward and 10 µM reverse primers were mixed with H₂O to generate the primer mix. DNA isolation was performed as described above. PCR conditions are described in Table 6-9 and primers used are listed in Table 6-10.

Table 6-9: PCR mix and PCR conditions

PCR mix	PCR Conditions		
10 µl REDTaq® ReadyMix™	95 °C	5 min	
10 µl Primer mix	95 °C	45 sec	
1.5 µl DNA	60 °C	1 min	40x
	72 °C	90 sec	
	8 °C	Constantly	

Table 6-10: Primer sequences for genotyping PCR

Gene	Forward (5' -> 3')	Reverse (5' -> 3')	Basepairs
<i>Hdac1^{loxP/+}</i>	AATTCCTGCGTTCTA	CACAGGAGCCCTAAC	WT: 260 bp
	TTCGCC	TGGACAAG	MUT: 322 bp
		and	
		AAGAGCATGAACTGA	
		TGGCGAG	
<i>Hdac2</i>	GCACAGGCTACTACT	CCACCACTGACATGT	472 bp
<i>wildtype</i>	GTGTAGTCC	ACCCAAC	
<i>Hdac2^{loxP}</i>	GTCCCTCGACCTGCA	CCACCACTGACATGT	500 bp
	GGAATTC	ACCCAAC	
<i>Hdac3^{loxP/+}</i>	CACTGCCTGATCGTT	GACATTCCCAATACC	WT: 600 bp
	TCC	ACG	MUT: 700 bp
<i>Pdx1-Flp</i>	AGAGAGAAAATTGAA	CGTTGTAAGGGATGA	620 bp
	ACAAGTGCAGGT	TGGTGA ACT	
<i>Kras^{FSF-}</i>	CACCAGCTTCGGCTT	AGCTAATGGCTCTCA	WT: 270 bp
<i>G12D/+</i>	CCTATT	AAGGAATGTA	MUT: 350 bp
		and	
		GCGAAGAGTTTGTCC	
		TCAACC	

Gene	Forward (5' -> 3')	Reverse (5' -> 3')	Basepairs
<i>Trp53^{del/+}</i>	ACAGCGTGGTGGTA CCTTAT and CTATCAGGACATAGC GTTGG	TATACTCAGAGCCGG CCT	WT: 450 bp MUT: 650 bp
<i>Trp53^{frt/+}</i>	CAAGAGAACTGTGCC TAAGAG	CTTTCTAACAGCAA GGCAAGC	WT: 258 bp MUT: 292 bp
<i>R26^{CAG-FSF-CreERT2/+}</i>	GAATGTGCCTGGCTA GAGATC	GCAGATTCATCATGC GGA	190 bp
<i>Pdk^{loxP/+}</i>	ATCCCAAGTTACTGA GTTGTGTTGGAAG	TGTGGACAAACAGCA ATGAACATACACGC	WT: 200 bp MUT: 280 bp
<i>Kras^{LSL-G12D/+}</i>	CACCAGCTTCGGCTT CCTATT	AGCTAATGGCTCTCA AAGGAATGTA and CCATGGCTTGAGTAA GTCTGC	WT: 270 bp MUT: 170 bp
<i>Trp53^{LSL-R172H/+}</i>	AGCCTTAGACATAAC ACACGAACT and GCCACCATGGCTTGA GTAA	CTTGAGACATAGCC ACACTG	WT: 570 bp MUT: 270 bp
<i>Pdx1-Cre</i>	TTGAAACAAGTGCAG GTGTTTCG	CAGGGTGTATAAGC AATCCC	800 bp
<i>R26^{LSL-TVA/+}</i>	AAAGTCGCTCTGAGT TGTTAT	GCGAAGAGTTTGTCC TCAACC and GGAGCGGGAGAAAT GGATATG	WT: 600 bp MUT: 310 bp

WT = wildtype allele, MUT = mutated allele, bp = basepairs, FSF = *frt-Stop-frt*, LSL = *loxP-Stop-loxP*

All primers were synthesized by the company Eurofins MWG (Ebersberg) and dissolved in ddH₂O to a final concentration of 10 μM.

Gel electrophoresis

After performing PCR, separation of the DNA strands was done by gel electrophoresis using 1.5 – 2% agarose gels, prepared with 1x TAE buffer (see Table 6-11) plus ethidium bromide (1 mg/ml). As a running buffer 1x TAE buffer with ethidium bromide was used as well. The gel was run at 120 V for approximately 1.5 hours (h), until the DNA strands had been separated properly, followed by analysis with UV transillumination using the UVsolo TS Imaging System.

Table 6-11: TAE buffer

TAE buffer

1x TAE buffer (pH 8.5)	40 mM Tris
	20 mM EDTA
	0.14% (v/v) Acetic acid (100%)

6.3.2 RNA analysis

RNA isolation of tumor cell lines

Cells on ice were washed with ice-cold PBS and for harvesting 100 µl Homogenization solution with 2 µl Thioglycerol (1:50 final concentration) of the Maxwell[®] 16 LEV simplyRNA Purification Kit was added. Cells were scraped off, transferred to a reaction tube and flash-frozen in liquid N₂ before stored at -80 °C. For total RNA isolation Maxwell PROMEGA Kit was used according to the manufacturer's protocol. In brief, before starting the RNA isolation, DNase I solution was prepared by adding 275 µl of nuclease-free H₂O to the vial of lyophilized DNase I, followed by gentle mixing. 5 µl of Blue Dye was added to the DNase I solution as a visual aid for pipetting. DNase I was stored at -20 °C until use. Shortly before processing samples on the Maxwell[®] 16 Instrument the lysed cells were thawed and mixed with the same volume of the Maxwell[®] Lysis Buffer 1:1, followed by short thorough mixing. A maximum volume of 400 µl of this lysate was transferred to well #1 of the Maxwell[®] 16 LEV Cartridge, which is the one closest to the cartridge label. 5 µl of DNase I solution (in blue) was added to well #4 (yellow reagent), turning the reagent in well #4 to green. Maxwell[®] LEV Plunger were placed in well #8 of the cartridge and 0.5 ml Elution tubes, filled with 30 µl of nuclease-free H₂O, are placed at the front row of the Maxwell[®] 16 Cartridge Rack. The simplyRNA protocol was ran. The isolated RNA was directly used for cDNA synthesis or stored at -80 °C.

Reverse transcription

RNA concentration was measured with the spectrophotometer NanoDrop 1000 before cDNA synthesis. For cDNA synthesis reagents of the cDNA synthesis TaqMan® reverse transcription kit were used. 2 µg of RNA was transferred to a new reaction tube and put on ice. All reagents were mixed and added to the RNA samples. The complete volume should be at the bottom of the tubes before reverse transcription is performed. cDNA was stored at –20 °C. Used reagents and conditions for reverse transcription are listed in Table 6-12.

Table 6-12: Reverse transcription mix and PCR conditions

Reverse transcription mix	Reverse transcription conditions	
1x TaqMan RT Buffer	25 °C	10 min
5.5 mM MgCl ₂	48 °C	60 min
2.5 mM dNTP-Mix	95 °C	5 min
2.5 µM random hexamers	4 °C	For ever
0.4 U/µl RNase inhibitor		
1.25 U/µl Multiscribe reverse transcriptase		
2 µg RNA		
Ad RNase free H ₂ O to a total volume of 100 µl		

Quantitative real-time PCR

Quantitative real-time PCR (qRT-PCR) was performed using the StepOnePlus™ real time PCR system and software. Promega GoTaq® qPCR Master Mix was used as fluorescent dye and PCR was performed with 10 ng of cDNA in a total volume of 12.5 µl as described in Table 6-13. Primers used are listed in Table 6-14. Each sample was tested in triplicates and the ubiquitously expressed housekeeping genes *βActin* and *Gapdh* acted as endogenous references.

Analysis of relative mRNA expression was performed using the $2^{-\Delta\Delta C_t}$ method (Pfaffl, 2001). Ct values of the gene of interest and the housekeeping gene were calculated as mean of the respective triplicates. In detail, the following calculations were used:

$\Delta Ct = Ct \text{ (gene of interest)} - Ct \text{ (housekeeping gene)}$

$\Delta\Delta Ct = \Delta Ct \text{ (treated sample)} - \Delta Ct \text{ (control sample)}$

$2^{-\Delta\Delta Ct}$ was used for data analysis and presentation of the results.

Table 6-13: qRT-PCR reagents

qRT-PCR reagents

1x SYBR Green Buffer
100 nM forward Primer
100 nM reverse Primer
10 ng cDNA
Ad RNase free H ₂ O to total volume of 12.5 μ l

Table 6-14: Primer sequences for qRT-PCR

Gene	Forward (5' -> 3')	Reverse (5' -> 3')
<i>βActin</i>	GTCGAGTCGCGTCCACC	GTCATCCATGGCGAACTGGT
<i>Gapdh</i>	CCTGCCAAGTATGATGAC	GGAGTTGCTGTTGAAGTC
<i>Hdac1</i>	CTGAATACAGCAAGCAGATGCA GAG	TCCCGTGGACAACACTGACAGAAC
<i>Hdac2</i>	CGGTGTTTGATGGACTCTTTG	CCTGATGCTTCTGACTTCTTG
<i>Hdac3</i>	GCACCCAGTGTCCAGATTCA	GACCTCTCTCTTCAGCGTCG
<i>Cdh1</i>	GAGCGTGCCCCAGTATCG	CGTAATCGAACACCAACAGAGA GT
<i>Vimentin</i>	CCAGAGAGAGGAAGCCGAAA	GACGTGCCAGAGAAGCATTCTG
<i>Pdgfrα</i>	AGTGGCTACATCATCCCCCT	CCGAAGTCTGTGAGCTGTGT
<i>Pdgfrβ</i>	CTGTGCAGTTGCCTTACGAC	CAGGTGGGGTCCAAGATGAC
<i>Egfr</i>	ATGACGCATTCCCTCCCTGTA	TGATAATGCAGGTCTCTTCCA

All primers were designed for the murine gene of interest using the Primer-BLAST software of *National Center for Biotechnology Information*. All primers were synthesized by the company Eurofins MWG (Ebersberg) and dissolved in ddH₂O to a final concentration of 10 μ M.

Primer efficiency was estimated by running qRT-PCR of a cDNA sample with eight different concentrations (1 ng – 100 ng cDNA) and then the Ct values were blotted

against cDNA concentration. The slope of the linear equation was used to calculate the primer efficiency according to the equation $E = 10^{(-1/\text{slope})}$ (Pfaffl, 2001).

All primers used have an efficiency of between 85% and 115%.

6.3.3 Protein analysis

Protein isolation of tumor cell lines

Cells were washed once with cold PBS. 60 μl Cell lysis buffer supplemented 1x Phosphatase inhibitor and 1x Protease stop were added and cells were scraped off the cell culture dish. Cell suspension was transferred to a reaction tube, followed by flash freezing in liquid N_2 .

Protein isolation of tumor cell lines for proteome analysis

After five days of 4-OHT/vehicle treatment the cells were washed 1x with cold PBS, followed by detachment and resuspension in cold Dulbecco's Modified Eagle Medium (high glucose) (DMEM). The cell suspension was centrifugated for five minutes at 3,090 xg and 4 $^{\circ}\text{C}$. The washing step was repeated with cold PBS and 50% of the suspension was separated for the standard procedure. The remaining 50% of the suspension was processed for the proteome analysis. The centrifugation step was repeated, followed by removal of supernatant. Pellet was flash frozen using liquid N_2 . Pellets can be stored at -80 $^{\circ}\text{C}$ or thawed on ice, followed by centrifugation at 16,100 xg and 4 $^{\circ}\text{C}$ for 15 min and removal of supernatant. Pellets were resuspended in 200 μl heated 1x NuPAGE LDS sample buffer, followed by sonification (20 sec pulse, 30 sec pause, high amplitude, two repeats) and heated up to 75 $^{\circ}\text{C}$ for ten minutes.

The proteome analysis was performed by Dr. Falk Butter, *Institute of Molecular Biology gGmbH*, Mainz.

Bradford assay

Harvested protein samples were centrifugated at 16,100 xg and 4 $^{\circ}\text{C}$ for 15 minutes. 1 μl of the supernatant was added to 300 μl of 1x Bradford reagent. For standard curve BSA 0 – 8 μg (1 $\mu\text{g}/\mu\text{l}$) was added to the 1x Bradford reagent. Samples were incubated for 10 min at RT. Measurement of the absorbance was performed at 600 nM using a microplate reader. A BSA standard series were used as a reference for calculation of the protein concentration. For dilution of the samples to a defined concentration,

1x and 5x Laemmli buffer were used. For denaturation the samples were boiled for five minutes at 95 °C. Protein lysates were stored at -20 °C until further use. BSA for standard curve was measured once for every concentration, the protein samples were tested in triplicates.

Table 6-15: Laemmli buffer

Laemmli buffer

1x Laemmli buffer (pH 6.8)	6 mM Tris 10% (v/v) Glycerine 70 mM SDS 0.015 mM Bromophenol blue 1% (v/v) β -Mercaptoethanol
----------------------------	---

Western blot

Sodium dodecyl sulfate polyacrylamide gel electrophoresis (SDS-PAGE) was performed to separate proteins according to size. At least 60 μ g protein was loaded and to concentrate the proteins in the stacking gel 80 V were used for approximately 30 min. For separation of proteins 10% or 15% separating gel and 100 V for approximately two hours was used. Transfer of proteins from the gel to nitrocellulose membrane was performed using a wet transfer system. For detailed information concerning buffer conditions and SDS-PAGE see Table 6-16 and Table 6-17. The proteins were transferred to the membrane at 350 mA for two hours in a tank blot system and afterwards unspecific binding sites were blocked with 5% (w/v) skim milk powder in PBS + 0.1% (v/v) Tween20. Primary antibody was diluted in 5% (w/v) skim milk powder in PBS + 0.1% (v/v) Tween20 and membranes were incubated with a primary antibody solution. After three washing steps with PBS + 0.1% (v/v) Tween20 for ten minutes each, the secondary antibody was diluted in 5% (w/v) skim milk powder in PBS + 0.1% (v/v) Tween20 and membranes were incubated with this secondary antibody solution. Incubation with a primary or secondary antibody solution was performed for one hour at RT or overnight at 4 °C. For detailed information about antibodies and dilutions see Table 6-18. After the secondary antibody incubation, the membranes were washed three times as described above. For detection of proteins Odyssey LiCOR system with wavelength 700 nm or 800 nm according to the used secondary antibody. For analysis LiCOR Software Image Studio was used.

Table 6-16: Buffers for western blot

Buffers for western blot	
Separating gel buffer (pH 8.8)	1.5 M Tris
Stacking gel buffer (pH 6.8)	0.5 M Tris
1x Running buffer	192 mM Glycine 25 mM Tris 3.5 mM SDS
1x Transfer buffer	192 mM Glycine 25 mM Tris 20% (v/v) Methanol

Table 6-17: Conditions for SDS-PAGE gels

	10% separating gel	15% separating gel	Stacking gel
H ₂ O	2050 µl	1250 µl	1500 µl
Separating gel buffer	1300 µl	1300 µl	-
Stacking gel buffer	-	-	650 µl
30% Acrylamide/Bisacrylamide- stock solution (29:1)	1650 µl	2500 µl	375 µl
10% (w/v) SDS	50 µl	50 µl	25 µl
10% (w/v) APS	25 µl	25 µl	12.5 µl
TEMED	7.5 µl	7.5 µl	5 µl

Table 6-18: Antibodies used for western blot

Antibody	Dilution	Species of origin	Catalogue number	Manufacturer
βActin	1:5,000	Mouse	A5316	Sigma-Aldrich
HDAC1 2E10	1:1,000	Mouse	05-100	Millipore
HDAC2 (D6S5P)	1:500	Rabbit	57156	Cell Signaling Technology
HDAC2	1:500	Rabbit	Sc-7899	Santa Cruz Biotechnology
HDAC3 (H-99)	1:1,000	Rabbit	Sc-11417	Santa Cruz Biotechnology
E-cadherin (H108)	1:1,000	Mouse	610181	BD
Vimentin	1:500	Rabbit	5741	Cell Signaling Technology
TRP53	1:1,000	Rabbit	NCL-L-p53-CM5p	Leica Biosystems
CDK7 (FL-346)	1:500	Rabbit	E0204	Santa Cruz Biotechnology
Histone H3 (D1H2)	1:1,000	Rabbit	4499	Cell Signaling Technology
H3K27ac	1:500	Rabbit	8173S	Cell Signaling Technology
Anti-mouse IgG (H+L) (DyLight™ 680 Conjugate)	1:10,000	Goat	5470	Cell Signaling Technology
Anti-rabbit IgG (H+L) (DyLight™ 680 Conjugate)	1:10,000	Goat	5366	Cell Signaling Technology
Anti-mouse IgG (H+L) (DyLight™ 800 4X PEG Conjugate)	1:10,000	Goat	5257	Cell Signaling Technology
Anti-rabbit IgG (H+L) (DyLight™ 800 4X PEG Conjugate)	1:10,000	Goat	5151	Cell Signaling Technology

All antibodies were diluted in 5% (w/v) skim milk powder in PBS + 0.1% (v/v) Tween20.

RNA Sequencing

For RNA sequencing (RNA-Seq) analysis, three independent replicates of *Hdac2* pro- and deficient PPT-F1648 cells were used. Therefore, three independent 4-OHT/vehicle treatments of the cell line PPT-F1648 were performed and after eight days of treatment RNA samples were harvested as described above. mRNA was extracted as described above and quality was controlled using agarose gel electrophoresis. Approximately 500 ng of RNA was loaded on a 1% agarose gel and the two bands for 28S and 18S rRNA were separated with 80 V. RNA samples of good quality showed two distinct bands and were used for RNA-Seq. In addition, quality control measures were performed by the *Genomics and Proteomics Core Facility* of the *DKFZ Heidelberg*.

RNA-Seq was carried out by the *Genomics and Proteomics Core Facility* of the *DKFZ* (Heidelberg, Germany; B25M reads/sample (single-end reads); Illumina HiSeq 2000, San Diego, CA, USA). Next-generation sequencing data were analyzed using the Galaxy platform (Afgan *et al.*, 2016; Goecks *et al.*, 2013) and TrimGalore! (Galaxy Version 0.4.2) was used to remove adapters from FASTQ files. Reads were mapped to the mouse reference genome mm10 using bowtie2 (Langmead and Salzberg, 2012). Aligned reads which overlap to features in the GTF annotation file, obtained from the UCSC genome browser (Kent *et al.*, 2002), were calculated using htseq-count 0.6.1galaxy3 (Anders *et al.*, 2015). Differential expression of count data was determined by DESeq2 (Love *et al.*, 2014). Processing the raw data was performed by the former lab member Dr. rer. nat. Matthias Wirth.

RNA-Seq data are accessible on ENA: PRJEB35204.

MicroArray Analysis

RNA of three *Hdac2* pro- and three *Hdac2* deficient cell lines, derived from the KPC mouse model, was isolated as described above. For *Hdac2* proficient samples the cell lines PPT-4917, PPT-AA373 and PPT-BK50 were used and for *Hdac2* deficient samples the cell lines PPT-F1042, PPT-F1146 and PPT-F1128. RNA samples were processed according to Affymetrix standard protocols and hybridized onto the GeneChip Affymetrix Mouse Gene ST 1.0 (Affymetrix, Santa Clara, CA, USA). MicroArray analysis was performed by the former lab member Dr. med. Patrick Wenzel and the differentially regulated gene expression was analyzed in this work.

MicroArray mRNA expression data are accessible on GEO: GSE144798.

Visualization of RNA-Seq and MicroArray data

VENNY 2.1 (<https://bioinfogp.cnb.csic.es/tools/venny/>), a software to create Venn diagrams (Oliveros, 2007-2015), was used to visualize at least 1.5 fold up- and downregulated genes ($\log_2FC \pm 0.58$) that overlap in RNA-Seq and MicroArray data sets.

Analysis of the downregulated genes ($\log_2FC < 0.58$) upon deletion of *Hdac2* of both data sets was performed using molecular signatures database v7.1 (MSigDB) (<https://www.gsea-msigdb.org/gsea/msigdb/index.jsp>) and gene set enrichment analysis (GSEA) tool. Enrichment plots are shown with normalized enrichment score (NES), p-value (p) and false discovery rate (FDR) are depicted in the figure. HALLMARK signatures are shown (FDR < 0.05) (Liberzon *et al.*, 2015; Subramanian *et al.*, 2005).

6.4 Histological analysis

All used materials, reagents and kits, as well as their respective sources are listed in part 5 “Technical equipment”.

Paraffin sections

For histopathological analyses, murine tissues were fixed in 4% Roti[®] Histofix for 16 hours, dehydrated using the tissue processor ASP300 and embedded in paraffin. Sections of 2.5 μm were cut using the microtome Microm HM355S.

Hematoxylin and eosin (H&E) staining of tissue sections

Paraffin-embedded tissue sections were dewaxed twice in Roti[®] Histol for five minutes each, for rehydration an ethanol series (2x 100%, 2x 96% and 2x 80%, two minutes each) was used. Tissue sections were washed in H₂O before staining in hematoxylin for 30 sec, followed by incubation with tap water for five minutes and staining with eosin for 15 sec. Next, tissue sections were washed in water for ten minutes and dehydrated using an ethanol series (2x 80%, 2x 96% and 2x 100%, one minute each) and two times Roti[®] Histol for three minute each. Mounting the sections was performed using Pertex mounting medium. Slides were scanned with slide scanner Leica AT2 and images were captured by Aperio ImageScope.

Immunohistochemistry

Paraffin-embedded tissue sections were dewaxed twice in Roti® Histol for five minutes each, for rehydration an ethanol series (2x 100%, 2x 96% and 2x 80%, 2 min each) was used. Demasking of the antigens was achieved by boiling the tissue sections for ten minutes in unmasking solution (9.5 ml unmasking stock solution in 1 l H₂O). The sections had to cool down, before being washed with PBS 3x. For Blocking 3% H₂O₂ solution was used in the dark for 20 minutes, followed by incubation for one hour with 3% serum in PBS and Avidin (1 drop Avidin per 250 µl of 3% serum in PBS). After three washing steps with PBS, the tissue was incubated with the first antibody against HDAC2. The HDAC2 antibody (ab12169 from rabbit, purchased from Abcam, Cambridge, UK) was diluted 1:400 in a solution of 3% serum in PBS and Biotin (1 drop Biotin per 250 µl of 3% serum in PBS) and incubation was done overnight at 4 °C. The next day, the tissue was washed three times with PBS, followed by incubation with the secondary biotin-conjugated anti-rabbit antibody (from Vector Laboratories Inc., Burlingame, CA, USA). This secondary antibody was diluted 1:500 in 3% serum with PBS and the tissue was incubated with it for one hour at RT. Detection/development of the antibody signal was accomplished using the Vectastain® elite ABC kit as well as the DAB peroxidase substrate kit. Therefore, beforehand two drops of reagent A of the ABC kit were mixed with 5 ml PBS and then two drops of reagent B of the same kit were already mixed and then incubated for 30 minutes in the dark. After the incubation with the secondary antibody and three washing steps with PBS the tissue was incubated with the previously prepared solution of the ABC kit for 30 minutes. Afterwards again three washing steps in PBS followed. DAB peroxidase substrate solution was prepared by adding DAB reagent 1 (2 drops), DAB reagent 2 (4 drops) and DAB reagent 3 (2 drops) of the respective kit to 5 ml of ddH₂O. The tissue was incubated with this DAB solution for one minute, followed by three washing steps in ddH₂O. In addition, the tissue sections were stained with hematoxylin, followed by dehydration in an ethanol series (2x 80%, 2x 96% and 2x 100%, one minute each) and two times in Roti® Histol for three min each. Mounting the sections was performed using Pertex mounting medium. Slides were scanned with slide scanner Leica AT2 and images were captured by Aperio ImageScope.

Grading of primary pancreatic tumors

Primary pancreatic tumor tissue was isolated, embedded in paraffin and H&E staining was performed as described above. All animals analyzed are listed in Table 6-19. Analysis and grading of tumor tissue of the *Hdac2* pro- and deficient mice followed, with G1 = well differentiated, G2 = moderately differentiated, G3 = poorly differentiated and G4 = undifferentiated tumors. All slides were analyzed twice, while second analysis was done by Dr. med. vet. Katja Steiger (*Institut of Pathology, TUM*).

Table 6-19: Mice used for tumor grading and metastasis screening

Mouse	Genotype
F1039	<i>Hdac2</i> ^{loxP/loxP} , <i>LSL-Kras</i> ^{G12D/+} , <i>LSL-Trp53</i> ^{R172H/+} , <i>Pdx1-Cre</i> , <i>LSL-Tva</i> ^{+/-}
F1042	<i>Hdac2</i> ^{loxP/loxP} , <i>LSL-Kras</i> ^{G12D/+} , <i>LSL-Trp53</i> ^{R172H/+} , <i>Pdx1-Cre</i>
F1047	<i>Hdac2</i> ^{loxP/loxP} , <i>LSL-Kras</i> ^{G12D/+} , <i>LSL-Trp53</i> ^{R172H/+} , <i>Pdx1-Cre</i> , <i>LSL-Tva</i> ^{+/-}
F1055	<i>Hdac2</i> ^{loxP/loxP} , <i>LSL-Kras</i> ^{G12D/+} , <i>LSL-Trp53</i> ^{R172H/+} , <i>Pdx1-Cre</i>
F1063	<i>Hdac2</i> ^{loxP/loxP} , <i>LSL-Kras</i> ^{G12D/+} , <i>LSL-Trp53</i> ^{R172H/+} , <i>Pdx1-Cre</i>
F1088	<i>Hdac2</i> ^{loxP/loxP} , <i>LSL-Kras</i> ^{G12D/+} , <i>LSL-Trp53</i> ^{R172H/+} , <i>Pdx1-Cre</i>
F1091	<i>Hdac2</i> ^{loxP/loxP} , <i>LSL-Kras</i> ^{G12D/+} , <i>LSL-Trp53</i> ^{R172H/+} , <i>Pdx1-Cre</i>
F1128	<i>Hdac2</i> ^{loxP/loxP} , <i>LSL-Kras</i> ^{G12D/+} , <i>LSL-Trp53</i> ^{R172H/+} , <i>Pdx1-Cre</i> , <i>LSL-Tva</i> ^{+/-}
F1129	<i>Hdac2</i> ^{loxP/loxP} , <i>LSL-Kras</i> ^{G12D/+} , <i>LSL-Trp53</i> ^{R172H/+} , <i>Pdx1-Cre</i> , <i>LSL-Tva</i> ^{+/-}
F1144	<i>Hdac2</i> ^{loxP/loxP} , <i>LSL-Kras</i> ^{G12D/+} , <i>LSL-Trp53</i> ^{R172H/+} , <i>Pdx1-Cre</i>
F1146	<i>Hdac2</i> ^{loxP/loxP} , <i>LSL-Kras</i> ^{G12D/+} , <i>LSL-Trp53</i> ^{R172H/+} , <i>Pdx1-Cre</i>
F1163	<i>Hdac2</i> ^{loxP/loxP} , <i>LSL-Kras</i> ^{G12D/+} , <i>LSL-Trp53</i> ^{R172H/+} , <i>Pdx1-Cre</i>
F1183	<i>Hdac2</i> ^{loxP/loxP} , <i>LSL-Kras</i> ^{G12D/+} , <i>LSL-Trp53</i> ^{R172H/+} , <i>Pdx1-Cre</i>
F1229	<i>Hdac2</i> ^{loxP/loxP} , <i>LSL-Kras</i> ^{G12D/+} , <i>LSL-Trp53</i> ^{R172H/+} , <i>Pdx1-Cre</i>
F1234	<i>Hdac2</i> ^{loxP/loxP} , <i>LSL-Kras</i> ^{G12D/+} , <i>LSL-Trp53</i> ^{R172H/+} , <i>Pdx1-Cre</i> , <i>LSL-Tva</i> ^{+/-}
F1252	<i>Hdac2</i> ^{loxP/loxP} , <i>LSL-Kras</i> ^{G12D/+} , <i>LSL-Trp53</i> ^{R172H/+} , <i>Pdx1-Cre</i>
F1259	<i>Hdac2</i> ^{loxP/loxP} , <i>LSL-Kras</i> ^{G12D/+} , <i>LSL-Trp53</i> ^{R172H/+} , <i>Pdx1-Cre</i> , <i>LSL-Tva</i> ^{+/+}
F1293	<i>Hdac2</i> ^{loxP/loxP} , <i>LSL-Kras</i> ^{G12D/+} , <i>LSL-Trp53</i> ^{R172H/+} , <i>Pdx1-Cre</i> , <i>LSL-Tva</i> ^{+/+}
F1296	<i>Hdac2</i> ^{loxP/loxP} , <i>LSL-Kras</i> ^{G12D/+} , <i>LSL-Trp53</i> ^{R172H/+} , <i>Pdx1-Cre</i> , <i>LSL-Tva</i> ^{+/+}
F1297	<i>Hdac2</i> ^{loxP/loxP} , <i>LSL-Kras</i> ^{G12D/+} , <i>LSL-Trp53</i> ^{R172H/+} , <i>Pdx1-Cre</i> , <i>LSL-Tva</i> ^{+/+}
F1374	<i>Hdac2</i> ^{loxP/loxP} , <i>LSL-Kras</i> ^{G12D/+} , <i>LSL-Trp53</i> ^{R172H/+} , <i>Pdx1-Cre</i>
F1915	<i>Hdac2</i> ^{loxP/loxP} , <i>LSL-Kras</i> ^{G12D/+} , <i>LSL-Trp53</i> ^{R172H/+} , <i>Pdx1-Cre</i> , <i>LSL-Tva</i> ^{+/-}
F2100	<i>Hdac2</i> ^{loxP/loxP} , <i>LSL-Kras</i> ^{G12D/+} , <i>LSL-Trp53</i> ^{R172H/+} , <i>Pdx1-Cre</i>
F2143	<i>Hdac2</i> ^{loxP/loxP} , <i>LSL-Kras</i> ^{G12D/+} , <i>LSL-Trp53</i> ^{R172H/+} , <i>Pdx1-Cre</i>

Mouse	Genotype
F0793	<i>LSL-Kras</i> ^{G12D/+} , <i>LSL-Trp53</i> ^{R172H/+} , <i>Pdx1-Cre</i> , <i>LSL-Tva</i> ^{+/-}
BK50	<i>LSL-Kras</i> ^{G12D/+} , <i>LSL-Trp53</i> ^{R172H/+} , <i>Pdx1-Cre</i>
F1275	<i>LSL-Kras</i> ^{G12D/+} , <i>LSL-Trp53</i> ^{R172H/+} , <i>Pdx1-Cre</i>
AH1115	<i>LSL-Kras</i> ^{G12D/+} , <i>LSL-Trp53</i> ^{R172H/+} , <i>Pdx1-Cre</i>
AH1056	<i>LSL-Kras</i> ^{G12D/+} , <i>LSL-Trp53</i> ^{R172H/+} , <i>Pdx1-Cre</i>
F1416	<i>LSL-Kras</i> ^{G12D/+} , <i>LSL-Trp53</i> ^{R172H/+} , <i>Pdx1-Cre</i>
1616	<i>LSL-Kras</i> ^{G12D/+} , <i>LSL-Trp53</i> ^{R172H/+} , <i>Pdx1-Cre</i> , <i>E-cadh</i> ^{loxP/+}
1724	<i>LSL-Kras</i> ^{G12D/+} , <i>LSL-Trp53</i> ^{R172H/+} , <i>Pdx1-Cre</i>
1812	<i>LSL-Kras</i> ^{G12D/+} , <i>LSL-Trp53</i> ^{R172H/+} , <i>Pdx1-Cre</i> , <i>E-cadh</i> ^{loxP/+}
2205	<i>LSL-Kras</i> ^{G12D/+} , <i>LSL-Trp53</i> ^{R172H/+} , <i>Pdx1-Cre</i> , <i>Raf</i> ^{+/-}
3983	<i>LSL-Kras</i> ^{G12D/+} , <i>LSL-Trp53</i> ^{R172H/+} , <i>Pdx1-Cre</i> , <i>LSL-Tva</i> ^{+/-}
4421	<i>LSL-Kras</i> ^{G12D/+} , <i>LSL-Trp53</i> ^{R172H/+} , <i>Pdx1-Cre</i>
4917	<i>LSL-Kras</i> ^{G12D/+} , <i>LSL-Trp53</i> ^{R172H/+} , <i>Pdx1-Cre</i> , <i>LSL-Tva</i> ^{+/-}
AA352	<i>LSL-Kras</i> ^{G12D/+} , <i>LSL-Trp53</i> ^{R172H/+} , <i>Pdx1-Cre</i> , <i>LSL-Tva</i> ^{+/-}
AA373	<i>LSL-Kras</i> ^{G12D/+} , <i>LSL-Trp53</i> ^{R172H/+} , <i>Pdx1-Cre</i> , <i>LSL-Tva</i> ^{+/-}
S209	<i>LSL-Kras</i> ^{G12D/+} , <i>LSL-Trp53</i> ^{R172H/+} , <i>Pdx1-Cre</i> , <i>LSL-Tva</i> ^{+/-}
6817	<i>LSL-Kras</i> ^{G12D/+} , <i>LSL-Trp53</i> ^{R172H/+} , <i>Pdx1-Cre</i> , <i>LSL-Tva</i> ^{+/-}
R4496	<i>LSL-Kras</i> ^{G12D/+} , <i>LSL-Trp53</i> ^{R172H/+} , <i>Pdx1-Cre</i> , <i>Pdk</i> ^{loxP/+} , <i>Braf</i> ^{loxP/+} , <i>Raf</i> ^{loxP/+}
J158	<i>LSL-Kras</i> ^{G12D/+} , <i>LSL-Trp53</i> ^{R172H/+} , <i>Pdx1-Cre</i> , <i>LSL-Tva</i> ^{+/-} , <i>Pdk</i> ^{loxP/+}
6051	<i>LSL-Kras</i> ^{G12D/+} , <i>LSL-Trp53</i> ^{R172H/+} , <i>Pdx1-Cre</i>
S243	<i>LSL-Kras</i> ^{G12D/+} , <i>LSL-Trp53</i> ^{R172H/+} , <i>Pdx1-Cre</i> , <i>Pdk</i> ^{loxP/+} , <i>Raf</i> ^{loxP/+}
F1333	<i>LSL-Kras</i> ^{G12D/+} , <i>LSL-Trp53</i> ^{R172H/+} , <i>Pdx1-Cre</i>
S247	<i>LSL-Kras</i> ^{G12D/+} , <i>LSL-Trp53</i> ^{R172H/+} , <i>Pdx1-Cre</i> , <i>Pdk</i> ^{loxP/+} , <i>Raf</i> ^{loxP/+}
1778	<i>LSL-Kras</i> ^{G12D/+} , <i>LSL-Trp53</i> ^{R172H/+} , <i>Pdx1-Cre</i> , <i>LSL-Tva</i> ^{+/-}
S114	<i>LSL-Kras</i> ^{G12D/+} , <i>LSL-Trp53</i> ^{R172H/+} , <i>Pdx1-Cre</i>
6719	<i>LSL-Kras</i> ^{G12D/+} , <i>LSL-Trp53</i> ^{R172H/+} , <i>Pdx1-Cre</i> , <i>LSL-Tva</i> ^{+/-}

Metastases Screening

For metastases screening, liver and lung of *Hdac2* pro- and deficient mice which developed PDAC were investigated macroscopically for metastases at necropsy. Liver and lung were additionally fixed and embedded in paraffin as described above and used for subsequent microscopical metastases screening. All animals used for metastases screening were previously used for grading of the PPTs and are listed in

Table 6-19. The tissues were cut in serial sections, meaning ten sections á 2.5 µm (= series 1), followed by one step section with 100 µm to reach deeper areas of the embedded organ, again followed by ten sections á 2.5 µm (= series 2) and so on. Per organ and mouse at least ten series were cut. The first cut of each series was stained with haematoxylin and eosin as described above and systematically screened for metastases. Invading metastases which resulted from the primary pancreatic tumor directly growing into the liver were excluded and not counted as metastases, since those cells did not undergo EMT. Even micrometastases of only very few PDAC cells were counted as metastases.

In case of detected metastasis, the second cut of the respective series was used for HDAC2 Immunohistochemistry method, as described above.

All slides were scanned with slide scanner Leica AT2 and images were captured with Aperio ImageScope. All slides were analyzed twice, while second analysis was done by Dr. med. vet. Katja Steiger (*Institute of Pathology, TUM*).

6.5 Statistical testing

Graphical depiction and statistical analysis were performed using GraphPad Prism6 software. Unless indicated otherwise, all data determined were collected from three independent experiments and presented as mean +/- standard deviation (SD).

The datasets were tested for statistical significance using one-way ANOVA or two-sided Student's t test, multiple testing was corrected according to Bonferroni.

Generally, MTT Assay and clonogenic Assay were performed in three independent replicates conducted at least as technical triplicates in each cell line tested. Statistical significance between the 4-OHT and vehicle treated cells regarding the survival and colony formation was calculated using the data collected at the end point of the experiment after 72 hours for MTT assay or after eight days for clonogenic Assay. Therefore, the mean of the triplicates was calculated for each replicate separately. Mean +/- standard deviation (SD) of the three EtOH replicates was calculated. Differences between 4-OHT and vehicle samples were calculated for each replicate separately, followed by mean +/- SD calculation of all three 4-OHT replicates in relation to the respective vehicle sample. To test for statistical significance two-tailed Student's t test was performed.

Cell cycle analysis was performed in three independent experiments in each cell line and was analyzed using the distribution of cells in the cell cycle which is known from the FACS cell cycle analysis. Mean +/- standard deviation (SD) was calculated for each phase by using the percentage of cells in the respective phase out of three replicates. Differences between 4-OHT and vehicle samples were calculated for each replicate separately, followed by mean +/- SD calculation of all three 4-OHT replicates in relation to the respective vehicle sample. For statistical testing two-tailed Student's t test was performed.

Western blot analysis was performed in three independent experiments. Expression was calculated by measuring band intensity using Image Studio software. Band intensity of the vehicle treated samples was set as 1. Band intensity of the respective 4-OHT treated samples was divided by the band intensity of its respective vehicle treated sample. Mean +/- SD of the 4-OHT treated samples in relation to their vehicle treated samples was calculated.

qRT-PCR was performed with samples of three independent replicates and conducted as triplicates. $2^{-\Delta\Delta C_t}$ was calculated as described above and used for mean +/- SD calculation. Therefore, $2^{-\Delta\Delta C_t}$ values of three vehicle samples and their 4-OHT samples were used for calculation of mean +/- SD calculation.

For survival analysis the Kaplan-Meier estimator was used and analyzed by Log-rank test. Statistical significance was considered for p-value (p) < 0.05.

Metastasis screening was analyzed using two-sided Chi-square test for each group (none, liver, lung, liver and lung), separately.

6.6 Software

Table 6-20: Software

Software	Version	Company
GraphPad Prism	6	GraphPad Software
Image Studio	Version 5.2.5	LiCOR
StepOnePlusTM		Applied Biosystems
AxioVision	Rel. 4.8	Carl Zeiss Vision
Aperio ImageScope	Version 12.3.3	Leica Biosystems
Primer-BLAST		National Center of Biotechnology Information
FlowJo	V10	FlowJo
VENNY	2.1	BioinfoGP
MSigDB	7.1	ITCR

7. Results

7.1 HDAC inhibitor treatment in murine PDAC cell lines

Currently there are several HDACis in clinical trials but with very limited success as described in the introduction. To analyze the effect of quite a few HDACis on cell survival in pancreatic cancer cell lines, those cell lines were treated with commonly used HDACis.

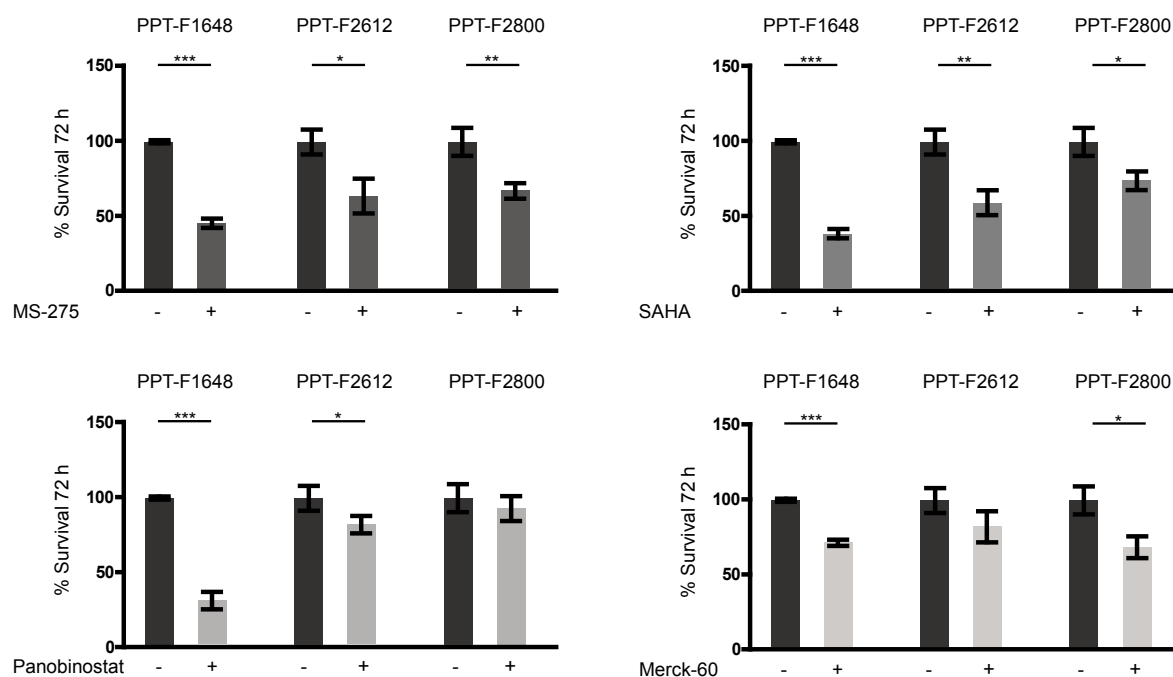


Figure 7-1: HDACi treatment in PDAC cell lines PPT-F1648, PPT-F2612 and PPT-F2800

MTT Assay of cell lines PPT-F1648, PPT-F2612 and PPT-F2800 treated with different HDAC inhibitors or vehicle (5 μ M MS-275, 4 μ M SAHA, 100 nM Panobinostat, 400 nM Merck-60, vehicle = DMSO). 2,000 cells were seeded and after attachment overnight treated with respective HDACi/vehicle for 72 hours. Experiments were performed as three biological replicates conducted as technical triplicates. Vehicle-treated samples were used as controls and their average was set as 100%. Data are shown as mean \pm SD, two-tailed unpaired Student's t test was performed, *: p-value (p) \leq 0.05, **: p \leq 0.01, ***: p \leq 0.001. H = hours.

Treatment with class I specific HDACi MS-275 reduced cell viability in all three tested cell lines, with the strongest effect in cell line PPT-F1648. Less than 50% viability was detected for those cells within 72 hours, while in the other two cell lines PPT-F2612 and PPT-F2800 viability was reduced to ca. 60 – 70%, respectively (Figure 7-1). Class I+II HDACi SAHA reduced cell viability as well, resulting in ca. 40% (PPT-F1648), ca. 60% (PPT-F2612) and ca. 75% (PPT-F2800) viable cells. HDACi effectiveness was severely different among the cell lines, especially for the pan-HDACi Panobinostat. In PPT-F1648 cells only around 30% of the cells were still viable after 72 hours treatment

with Panobinostat, while in the cell lines PPT-F2612 and PPT-F2800 viability was reduced by maximum 20%. The HDAC1/2 specific inhibitor Merck-60 reduced viability by maximum 30% in the three tested cell lines (Figure 7-1).

7.2 Inducible knock-out of class I HDACs *Hdac1*, *Hdac2* and *Hdac3* *in vitro*

The HDACi treatment shown in Figure 7-1 indicates an effect on cell survival but with different extent, dependent on the inhibitor used. It seems that the available HDACis are not potent enough to treat PDAC consistently. Since HDACs become more important as a possible therapeutic target for PDAC (Schneider *et al.*, 2010), there was a need to investigate the role of HDAC isoenzymes during tumor maintenance independent of the use of HDACis. The used dual-recombination mouse model allows the time-specific deletion of one or more HDAC isoenzymes in PDAC cell lines *in vitro*. Therefore, the mechanism behind the impaired survival can be investigated in detail. The genetic strategy of this mouse model and deletion of HDAC isoenzymes is explained in Figure 6-2 in the methods part.

7.2.1 Coincident genetic deletion of *Hdac1*, *Hdac2* and *Hdac3* in murine PDAC cell lines

To investigate the role of HDAC1, HDAC2 and HDAC3 in tumor maintenance floxed *Hdac1*, *Hdac2* and *Hdac3* alleles ($Hdac1^{tm1a(EUCOMM)Wtsi}$; $Hdac3^{tm1a(EUCOMM)Wtsi}$; Montgomery *et al.*, 2007) were combined within one mouse of the dual-recombination model (Schonhuber *et al.*, 2014). Thereby 4-OHT treatment leads to coincidental deletion of all three isoenzymes in the isolated murine PDAC cell lines obtained from this model. The successful deletion of the isoenzymes was proven by western blot. The effect on cell survival and colony formation was investigated using MTT Assay and clonogenic Assay.

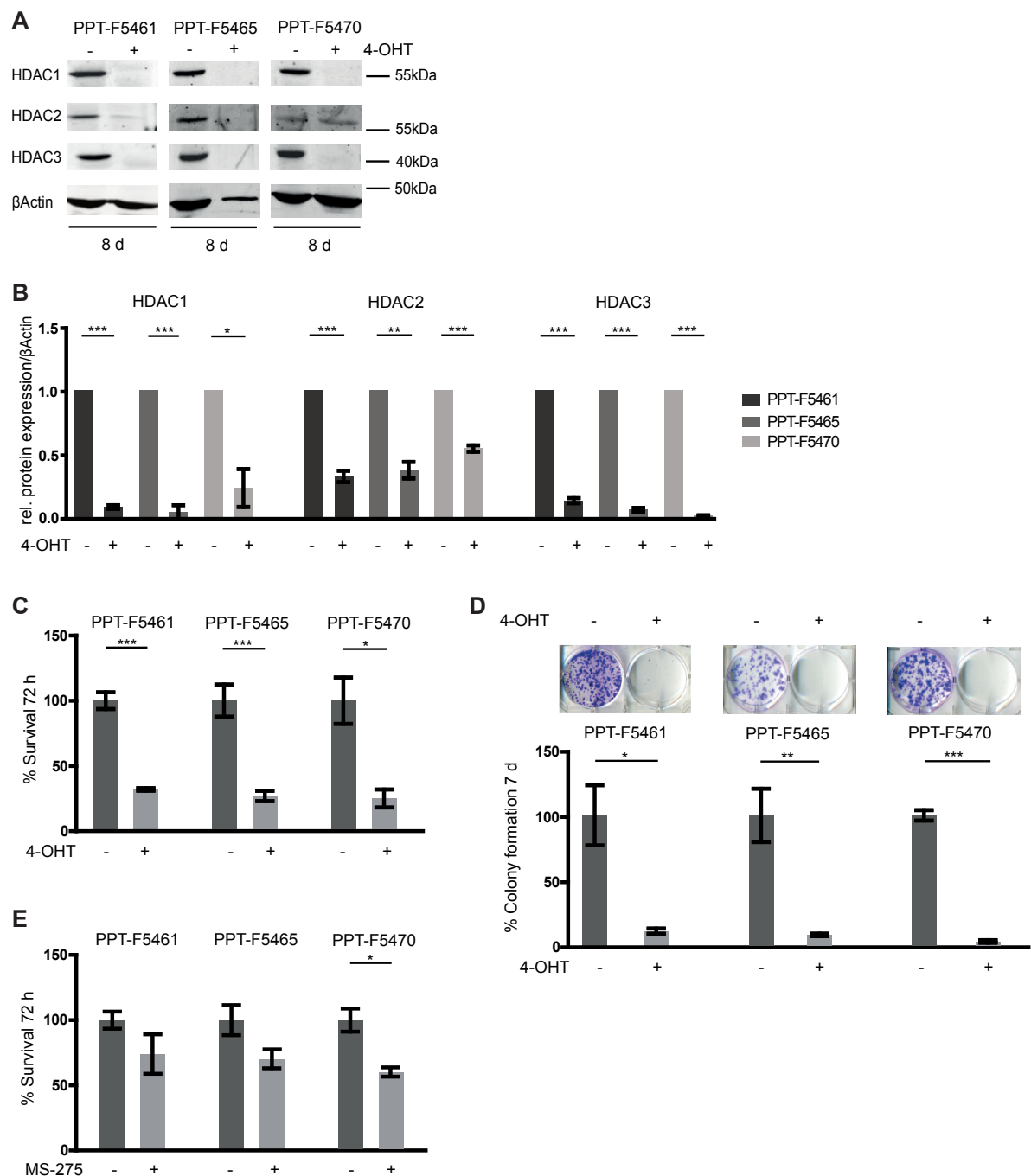


Figure 7-2: Coincident genetic deletion of *Hdac1*, *Hdac2* and *Hdac3* in murine PDAC cell lines PPT-F5461, PPT-F5465 and PPT-F5470

A) Western blot analysis of cell lines PPT-F5461, PPT-F5465 and PPT-F5470 after eight days of 4-OHT/vehicle treatment. One representative western blot is depicted, βActin = loading control. B) Quantification of Western blot analysis of three independent experiments per cell line, vehicle-treated cells = control, set as 1 for each cell line separately. C) MTT Assay and D) clonogenic Assay after eight days of 4-OHT/vehicle treatment. One representative clonogenic Assay is depicted (D). After eight days of 4-OHT/vehicle treatment 2,000 cells were seeded in triplicates and analyzed with MTT Assay after 72 hours and for clonogenic Assay after seven days. Quantification of three independent experiments per cell line was performed for both assays. Vehicle-treated cells = control, average of three experiments was set as 100%. E) MTT Assay after MS-275 treatment. 2,000 cells were seeded and after attachment overnight cells were treated with 4.5 μM MS-275 or vehicle for 72 hours. Experiment was performed as three biological replicates conducted as technical triplicates. Vehicle-treated cells = controls, average of three experiments was set as 100%. Data are shown as mean +/- SD, two-tailed unpaired Student's t test was performed, *: $p \leq 0.05$, **: $p \leq 0.01$, ***: $p \leq 0.001$. D = days, h = hours, 4-OHT = 4-Hydroxytamoxifen.

As shown in Figure 7-2 (A+B) after eight days (d) of 4-OHT treatment, the knock-out of *Hdac1* can be documented in all three cell lines PPT-F5461, PPT-F5465 and PPT-F5470. In the cell line PPT-F5470 there is no complete knock-out of *Hdac1* in all replicates, but a significant decrease of its expression. *Hdac2* could not be deleted completely in none of the cell lines, but its expression is significantly reduced. Downregulation was achieved to different extent in each cell line, with the least extent in PPT-F5470 and highest extend in PPT-F5461. *Hdac3* is deleted in all three cell lines. To monitor the cell survival after *Hdac* deletion, MTT Assay was used. The survival rate, shown in (Figure 7-2 (C)), is reduced by at least 60% in the cells deficient of *Hdac1*, *Hdac2* and *Hdac3*, compared to the respective proficient cells. Deletion of the isoenzymes is most effective in the cell line PPT-F5465. The clonogenic Assay (Figure 7-2 (D)) revealed that only around 10% of the deficient cells were able to form colonies in all three tested cell lines.

The coincident genetic deletion of *Hdac1*, *Hdac2* and *Hdac3* in cells of an established PDAC affects cell survival and colony formation. Comparing all three tested cell lines, it can be summarized as thus: the better the knock-out, the stronger the observed effect. Treatment with a class I specific HDACi like MS-275 also affects survival of these cell lines, but the effect of inhibition was weaker than the effect of genomic deletion of *Hdac1*, *Hdac2* and *Hdac3* (Figure 7-2 (E)).

7.2.2 Genetic deletion of *Hdac1* in a murine PDAC cell line

After the simultaneous deletion of all three investigated HDAC isoenzymes, also the deletion of each isoenzymes separately and the effects on tumor maintenance were tested using cell lines derived from the dual-recombinase mouse model with homozygous floxed *Hdac1* alleles ($Hdac1^{tm1a(EUCOMM)Wtsi}$).

Therefore, the same protocol of 4-OHT treatment was used as described above. The deletion of *Hdac1* leads to a downregulation of HDAC1, which was confirmed by western blot. Its effect on cell survival and colony formation assay was monitored as described above. In addition, the effect of *Hdac1* knock-out on cell cycle progression was investigated using FACS cell cycle analysis.

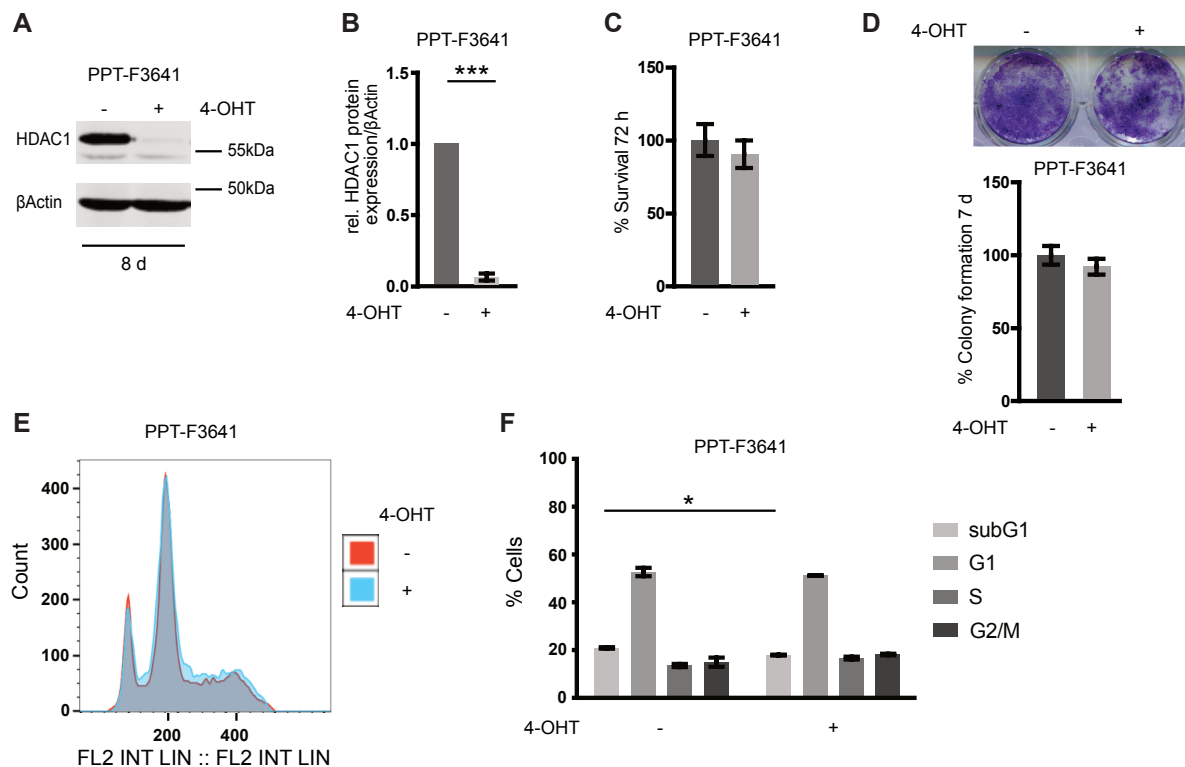


Figure 7-3: Genetic deletion of *Hdac1* in murine PDAC cell line PPT-F3641

A) Western blot analysis of cell line PPT-F3641 after eight days of 4-OHT/vehicle treatment. One representative western blot is depicted, β Actin = loading control. Quantification of three independent experiments is shown in B), vehicle-treated cells = controls, set as 1. C) MTT Assay and D) clonogenic Assay after eight days of 4-OHT/vehicle treatment. One representative clonogenic Assay is depicted (D). After eight days of 4-OHT/vehicle treatment 2,000 cells were seeded in triplicates and analyzed for MTT Assay after 72 hours and for clonogenic Assay after seven days. Quantification of three independent experiments per cell line was performed for both assays. Vehicle-treated cells = controls, average of three experiments was set as 100%. E) FACS cell cycle analysis after eight days of vehicle (red) or 4-OHT (blue) treatment. One representative FACS profile is depicted, quantification of two independent experiments is shown in F). Data are shown as mean \pm SD, two-tailed unpaired Student's t test was performed, *: $p \leq 0.05$, ***: $p \leq 0.001$. D = days, h = hours, 4-OHT = 4-Hydroxytamoxifen.

The knock-out of *Hdac1* after eight days of 4-OHT treatment was proven by western blot (Figure 7-3 (A+B)). Analyzing the effect of the HDAC1 loss on cell survival and colony formation revealed a reduced cell viability by 10% (Figure 7-3 (C)) in the *Hdac1* deficient PDAC cells. This observation is not found to be of statistical significance. Concerning the ability of colony formation (Figure 7-3 (D)), only a very slight reduction was detected. FACS cell cycle analysis was performed after *Hdac1* knock-out (Figure 7-3 (E)) and quantification of two independent replicates (Figure 7-3 (F)) shows slight but significant fewer amount of cells in subG1 phase and a very slight increase in S phase and G2/M phase after loss of HDAC1 expression.

7.2.3 Genetic deletion of *Hdac2* in murine PDAC cell lines

For investigation of the role of HDAC2 during tumor maintenance, mice with floxed *Hdac2* alleles (Montgomery *et al.*, 2007) were mated with control mice of the dual-recombination model (Schonhuber *et al.*, 2014) to generate a mouse model which allows time-specific deletion of *Hdac2* by eight days of 4-OHT treatment. *Hdac2* deletion leads to downregulation of HDAC2 which was proofed by western blot. According to the former analyzed cell lines, the *Hdac2* deficient PDAC cells were analyzed regarding cell survival and colony formation. In addition, also FACS cell cycle analysis was performed.

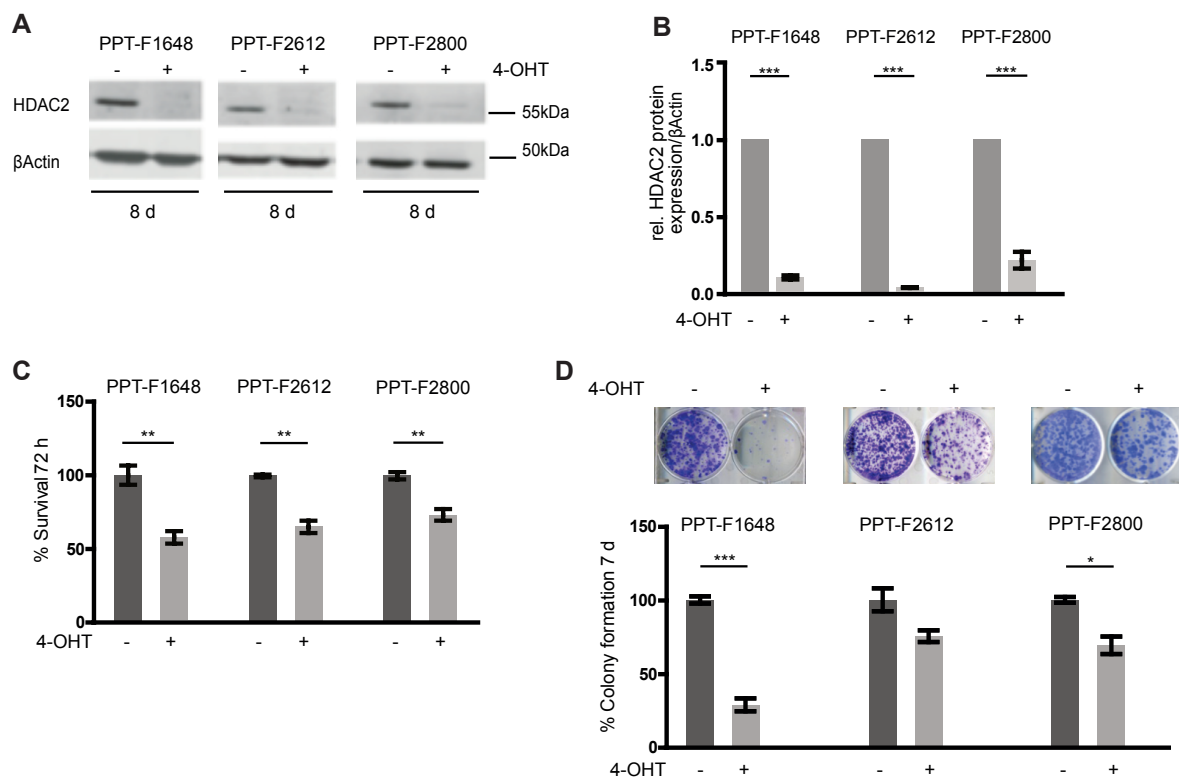


Figure 7-4: Genetic deletion of *Hdac2* in murine PDAC cell lines PPT-F1648, PPT-F2612 and PPT-F2800

A) Western blot of cell lines PPT-F1648, PPT-F2612 and PPT-F2800 after eight days of 4-OHT or vehicle treatment. One representative western blot is depicted, βActin = loading control. Quantification of three independent experiments is shown in B), Vehicle-treated cells = controls, set as 1 for each cell line separately. C) MTT Assay and D) clonogenic Assay after eight days of 4-OHT/vehicle treatment. One representative clonogenic Assay per cell line is depicted (D). After eight days of 4-OHT/vehicle treatment 2,000 cells were seeded in triplicates and analyzed for MTT Assay after 72 hours and for clonogenic Assay after seven days. Quantification of three independent experiments per cell line was performed for both assays. Vehicle-treated cells = controls, average of three experiments set as 100%. Data are shown as mean \pm SD, two-tailed unpaired Student's t test was performed *: $p \leq 0.05$, **: $p \leq 0.01$, ***: $p \leq 0.001$. D = days, h = hours, 4-OHT = 4-Hydroxytamoxifen.

Western blot analysis in Figure 7-4 (A) shows the downregulation of HDAC2 within eight days of 4-OHT treatment in all three PDAC cell lines PPT-F1648, PPT-F2612, PPT-F2800. Quantification of western blot analysis proves the significant loss of HDAC2 expression to different extents in all three cell lines (Figure 7-4 (A+B)). The loss of HDAC2 leads to a reduction in cell viability of approximately 20 – 40% (Figure 7-4 (C)), which differs between the three cell lines but is statistically significant for all of them. The cell line PPT-F1648 shows the greatest reduction in cell viability after *Hdac2* knock-out compared to the other two tested cell lines. Not only cell viability is affected, but also the colony formation is reduced (Figure 7-4 (D)) in the *Hdac2* deficient cells of the three tested cell lines. The ability to form colonies is impaired the most in the cell line PPT-F1648, while the cell lines PPT-F2612 and PPT-F2800 are affected less by *Hdac2* knock-out.

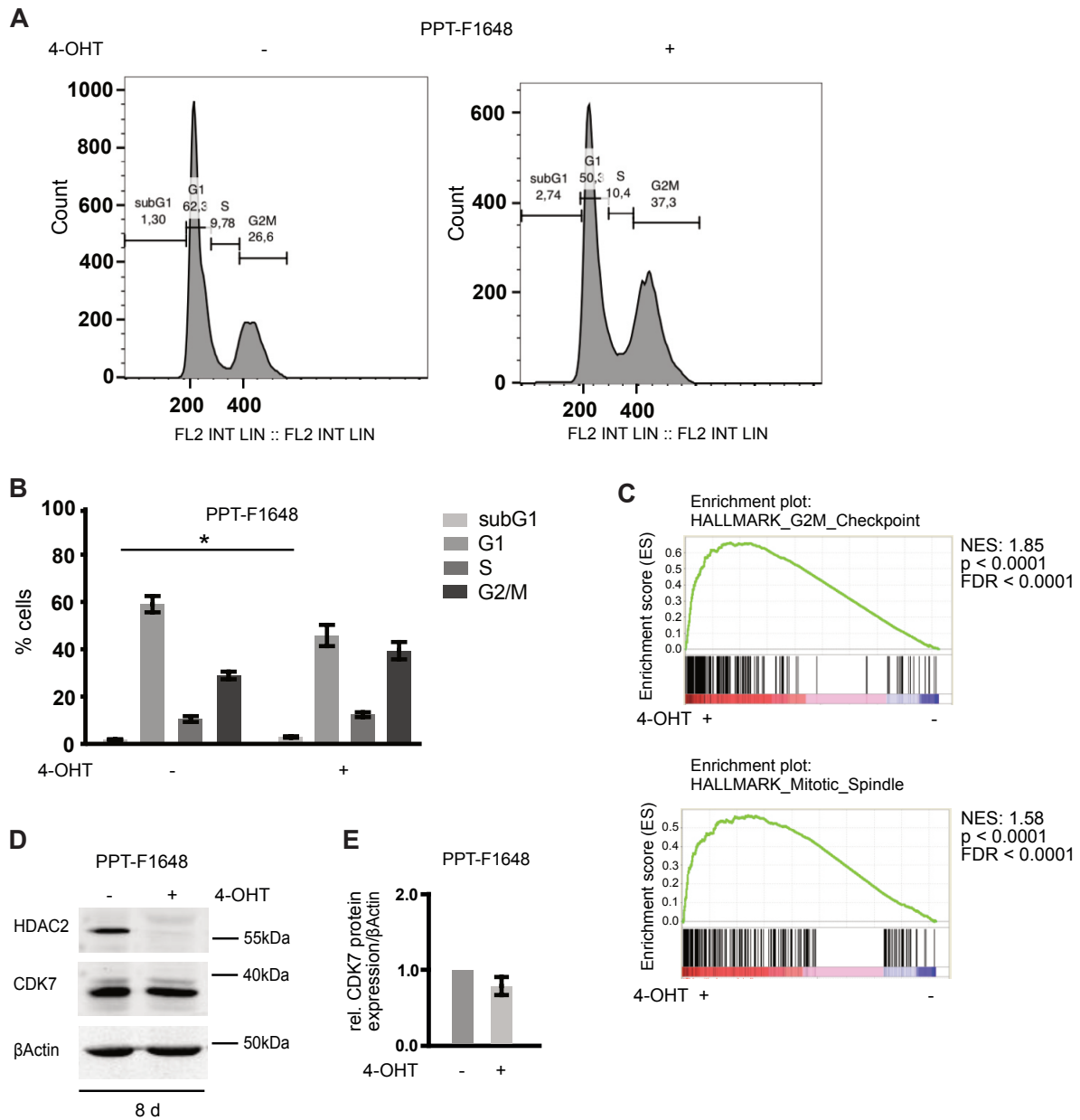


Figure 7-5: FACS cell cycle analysis in *Hdac2* pro- and deficient PDAC cell line PPT-F1648

A) FACS cell cycle analysis of PPT-F1648 cells after eight days of vehicle (left) or 4-OHT (right) treatment, one representative FACS cell cycle analysis is depicted. B) Quantification of FACS cell cycle analysis of three independent experiments. C) RNA-Seq of PPT-F1648 cells after eight days of 4-OHT/vehicle treatment was analyzed by GSEA, Enrichment plots for HALLMARK signatures are shown. D) Western blot analysis of PPT-F1648 cells after eight days of 4-OHT/vehicle treatment. One representative western blot is depicted, β Actin = loading control. Quantification of two independent experiments is shown in E), vehicle-treated cells = controls, set as 1. Data are shown as mean \pm SD, two-tailed unpaired Student's t test was performed, *: $p \leq 0.05$. D = days, h = hours, NES: normalized enrichment score; p: nominal p-value; FDR: false discovery rate, 4-OHT = 4-Hydroxytamoxifen.

To further analyze the effect of *Hdac2* knock-out in cell line PPT-F1648, FACS cell cycle analysis was performed. After successful deletion of HDAC2 a decrease in G1 phase and an increase in subG1 and G2/M phase was detected (Figure 7-5 A+B). In agreement with this observation, gene set enrichment analysis (GSEA) of RNA-Seq data from *Hdac2* pro- and deficient PPT-F1648 cells revealed enriched gene sets

linked to G2/M checkpoint and mitotic spindle in the *Hdac2* deficient state (Figure 7-5 C). Proteome analysis of PPT-F1648 *Hdac2* pro- and deficient cells after five days of 4-OHT treatment revealed a lower expression of CDK7 at this time point (Figure S 1), leading to the question whether loss of HDAC2 expression influences CDK7 expression and therefore leads to the observed G2/M arrest via impaired regulation of CDK7 targets. Validation after eight days of 4-OHT treatment showed no robust and significant downregulation of CDK7 (Figure 7-5 D+E).

Since HDACs play a role in chromatin remodeling (Cress and Seto, 2000) and acetylation of Histone H3 at Lysin 27 (H3K27ac) is a marker for active gene transcription (Kimura, 2013), H3K27ac was analyzed to characterize *Hdac2* deficient PPT-F1648 cells even more.

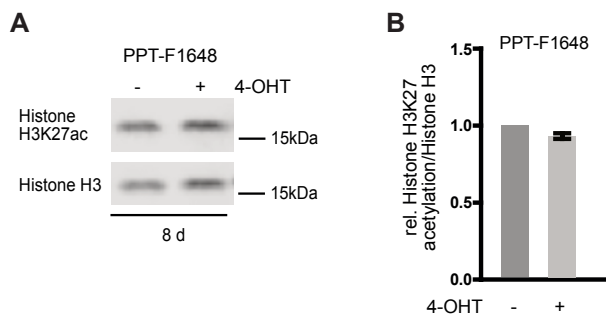


Figure 7-6: H3K27 acetylation in cell line PPT-F1648

A) Western blot analysis of PPT-F1648 cell after eight days of 4-OHT/vehicle treatment. One representative western blot is depicted, Histone H3 = loading control. The quantification of two independent experiments is shown in B), vehicle-treated cells = controls, set as 1. Data are shown as mean +/- SD. D = days, 4-OHT = 4-Hydroxytamoxifen.

Western blot analysis of PPT-F1648 *Hdac2* pro- and deficient cells show a very slight difference for H3K27 acetylation. The quantification of two independent experiments reveals a minimal decrease of H3K27 acetylation in *Hdac2* deficient cells (Figure 7-6 (A+B)).

7.2.4 Genetic deletion of *Hdac3* in murine PDAC cell lines

To investigate the role of HDAC3 in PDAC maintenance, mice with floxed *Hdac3* alleles (*Hdac3*^{tm1a(EUCOMM)Wtsi}) were mated with control mice of the dual-recombinase model (Schonhuber *et al.*, 2014). The isolated murine PDAC cell lines obtained from this model were treated with 4-OHT to knock-out *Hdac3* *in vitro* and the deletion was confirmed by western blot. Four cell lines were analyzed, while two cell lines carry wildtype *Trp53* (PPT3-F4764 and PPT3-F4402) and in two cell lines *Trp53* is deleted (PPT-F5061 and PPT2-F4699). Initially, the *Hdac3* pro- and deficient cells were characterized regarding cell survival and colony formation. Later, FACS cell cycle analysis completed the characterization of *Hdac3* deficient PDAC cells.

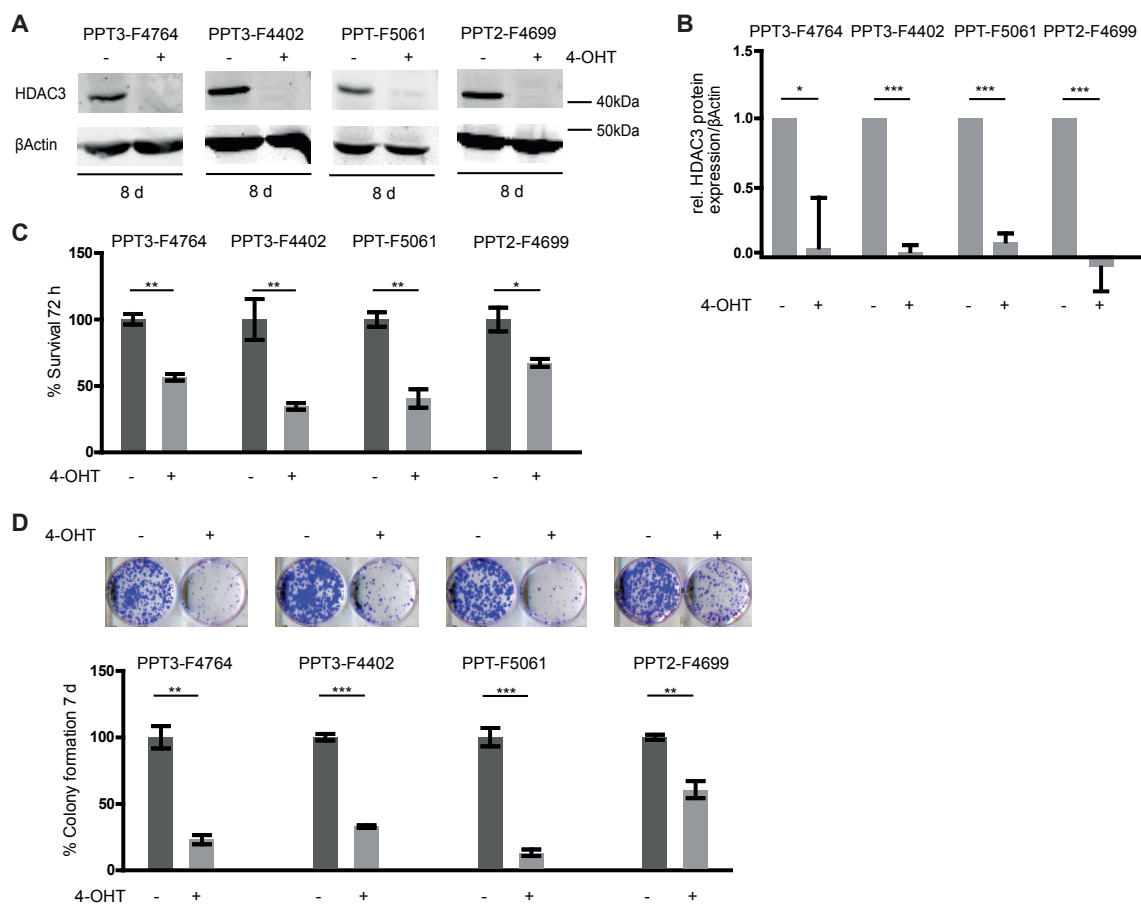


Figure 7-7: Genetic deletion of *Hdac3* in PDAC cell lines PPT3-F4764, PPT3-F4402, PPT-F5061 and PPT2-F4699.

A) Western Blot analysis of cell lines PPT3-F4764, PPT3-F4402, PPT-F5061 and PPT2-F4699 after eight days of 4-OHT/vehicle treatment. One representative western blot per cell line is depicted, β Actin = loading control. Quantification of three independent experiments is shown in B), vehicle-treated cells = controls, set as 1. C) MTT Assay and D) clonogenic Assay after eight days of 4-OHT/vehicle treatment. One representative clonogenic Assay is depicted (D). After eight days of 4-OHT/vehicle treatment 2,000 cells were seeded in triplicates and analyzed for MTT Assay after 72 hours and for clonogenic Assay after seven days. Quantification of three independent experiments per cell line was performed for both assays. Vehicle-treated cells = control, average of three experiments was set as 100%. Data are shown as mean \pm SD, two-tailed unpaired Student's t test was performed, *: $p \leq 0.05$, **: $p \leq 0.01$, ***: $p \leq 0.001$. D = days, h = hours, 4-OHT = 4-Hydroxytamoxifen.

The western blot in Figure 7-7 (A+B) proves the successful deletion of *Hdac3* after eight days of 4-OHT treatment. Analysis of *Hdac3* pro- and deficient cells reveals a significant lower survival (Figure 7-7 (C)) in all four cell lines with a decrease between 40% and 70% in the knock-out cells compared to the control cells of the respective cell line. The survival of the cell lines PPT3-F4402 and PPT-F5061 was affected most by loss of HDAC3 expression. Clonogenic Assay (Figure 7-7 (D)) was performed to check for the ability to create a new colony from a single cell and this ability is also significantly decreased in the *Hdac3* deficient cells of all tested cell lines. Approximately between 20% and 65% of the cells manage to form a colony if *Hdac3* is deleted, while colony formation is reduced most in *Hdac3* deficient cells of the cell lines PPT3-F4764 and PPT-F5061.

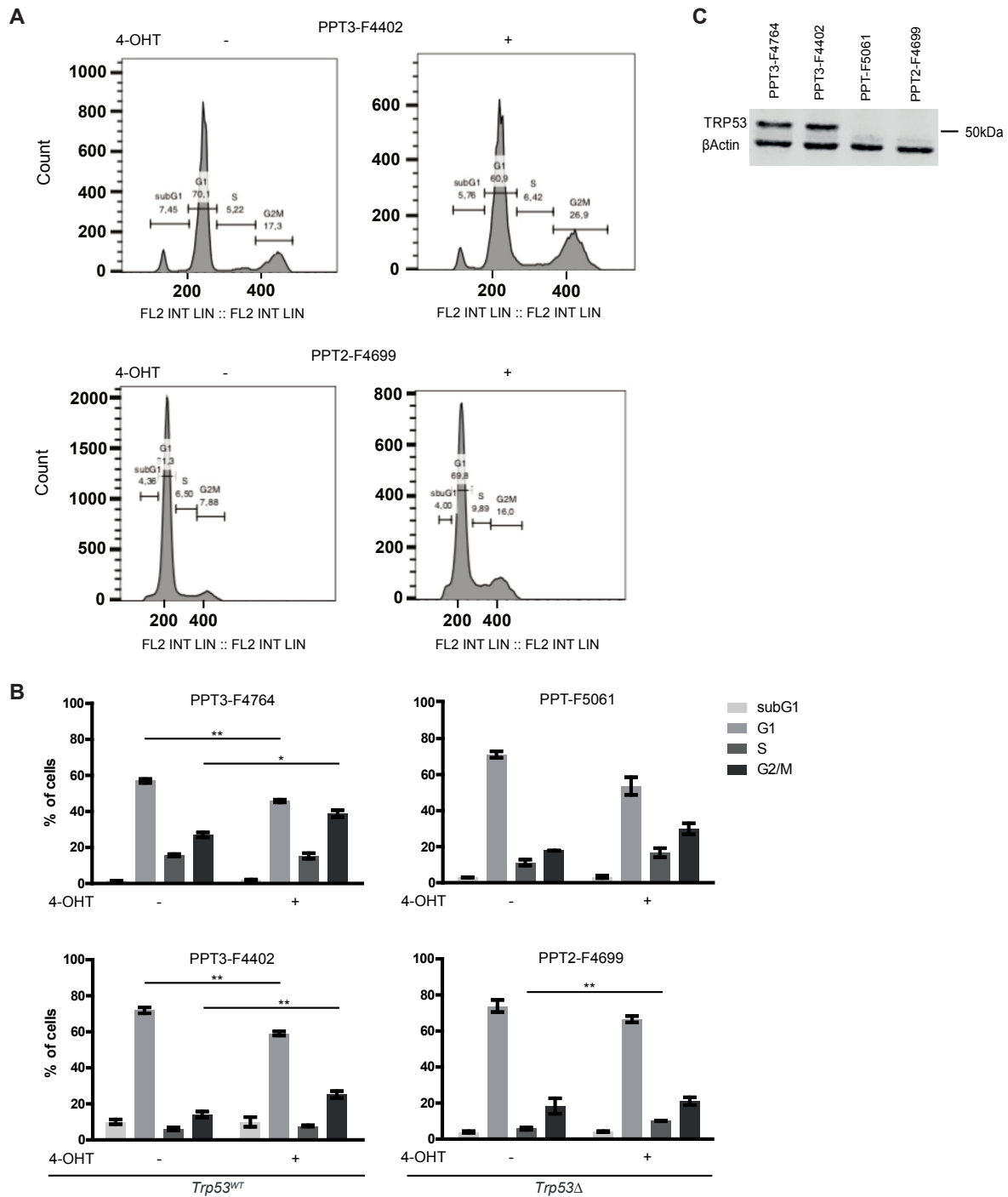


Figure 7-8: FACS cell cycle analysis of *Hdac3* pro- and deficient PDAC cell lines PPT3-F4764, PPT3-F4402, PPT-F5061 and PPT2-F4699.

A) FACS cell cycle analysis after eight days of 4-OHT/vehicle treatment of the cell lines PPT3-F4402 and PPT2-F4699. One representative FACS profile per cell line is shown. B) Quantification of FACS cell cycle analysis of three (PPT3-F4754, PPT3-F4402, PPT-F4699) or two (PPT-F5061) independent experiments after eight days of 4-OHT/vehicle treatment. C) Western blot analysis of cell lines PPT3-F4764, PPT3-F4402, PPT-F5061 and PPT2-F4699. One representative western blot is depicted. Data are shown as mean +/- SD, two-tailed unpaired Student's t test was performed, *: $p \leq 0.05$, **: $p \leq 0.01$, 4-OHT = 4-Hydroxytamoxifen, WT = wildtype, Δ = deleted.

To investigate the consequence of genetic *Hdac3* deletion and the mechanism that underlies the proliferation defect which was observed in the *Hdac3* deficient cells,

further, FACS cell cycle analysis was performed. Figure 7-8 (A+B) shows a reduction of cells in G1 phase and an enrichment of cells in S phase or/and G2/M phase, but no change for subG1 phase upon loss of HDAC3 expression. Considering the differences in cell cycle distribution between the *Hdac3* pro- and deficient cells in the four tested cell lines (Figure 7-8 (B)) their difference in TRP53 expression should be kept in mind (Figure 7-8 (C)). In both *Trp53* wildtype cell lines PPT3-F4764 and PPT3-F4402 a significant higher amount of cells can be found in G2/M phase after *Hdac3* knock-out. Furthermore, a minimal increase in the percentage of cells in the S phase is seen in cell line PPT3-F4402. The two *Trp53* deficient cell lines PPT-F5061 and PPT2-F4699 show an increased number of cells in the G2/M phase after *Hdac3* knock-out. In addition to this, both *Trp53* deficient cell lines show an accumulation of cells in the S phase after *Hdac3* deletion. This enrichment of cells in the S phase after *Hdac3* deletion reaches statistical significance in the cell line PPT2-F4699 (Figure 7-8 (B)).

7.2.5 Cre toxicity

In some studies, the expression of Cre recombinase is linked to growth-inhibition and genotoxic effects (Higashi *et al.*, 2009; Loonstra *et al.*, 2001). Furthermore, it was also described, that continuous low expression of Cre can lead to a cumulative increase in recombination lacking the toxic effects of the Cre recombinase (Janbandhu *et al.*, 2014; Loonstra *et al.*, 2001).

To exclude this so called Cre toxicity in the used dual-recombinase model, control cell lines PPT-15283 and PPT-F1679 were used. The cell line PPT-F1679 was used to analyze in addition if there is an effect on cell survival or colony formation upon heterozygous *Pdk1* deletion. The procedure of 4-OHT treatment and subsequent analysis of the cells was performed as described above.

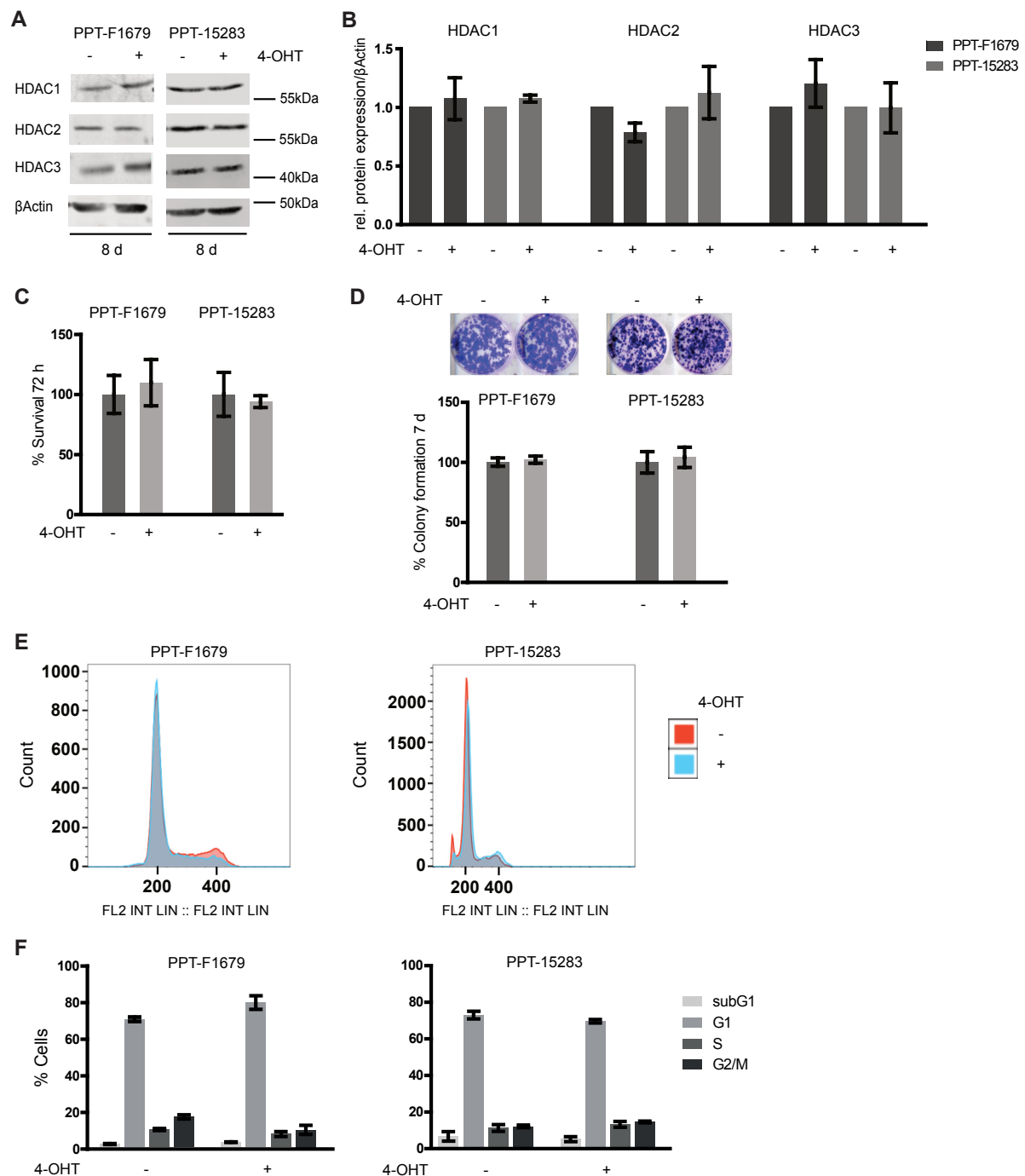


Figure 7-9: Excluding Cre Toxicity and effect of heterozygous deletion of *Pdk1*

A) Western blot analysis of cell lines PPT-F1679 and PPT-15283 after eight days of 4-OHT/vehicle treatment. One representative western blot is depicted, β Actin = loading control. Quantification of three independent experiments in (B), vehicle-treated cells = controls, set as 1. C) MTT Assay and D) clonogenic Assay after eight days of 4-OHT/vehicle treatment. One representative clonogenic Assay is depicted (D). After eight days of 4-OHT/vehicle treatment 2,000 cells were seeded in triplicates and analyzed for MTT Assay after 72 hours and for clonogenic Assay after seven days. Quantification of three independent experiments per cell line was performed for both assays. Vehicle-treated cells = controls, average of three experiments was set as 100%. E) FACS cell cycle analysis after eight days of vehicle (red) or 4-OHT (blue) treatment. One representative FACS profile is depicted, quantification of two (PPT-F1679) or three (PPT-15283) independent experiments is shown in F). All data are shown as mean \pm SD. D = days, h = hours, 4-OHT = 4-Hydroxytamoxifen.

Western blot analysis in Figure 7-9 (A+B) showed no effect on the expression of HDAC1, HDAC2 and HDAC3 due to eight days of 4-OHT treatment when the respective alleles are not floxed. Neither a significant effect on cell survival nor colony formation (Figure 7-9 (C+D)) could be observed. To completely cover the experimental spectrum, the other cell lines were also tested, cell cycle FACS analysis (Figure 7-9 (E)) was performed on the control cell lines, too. As expected, there was no significant difference in cell cycle distribution between the 4-OHT or vehicle treated cells of both cell lines.

7.3 Epithelial and mesenchymal fractions of dual-recombination model based PDAC cell lines

7.3.1 Differential trypsinization to generate epithelial and mesenchymal fractions of PDAC cell lines

PDAC is a heterogeneous disease and can be classified into several subtypes which reflect the differences in clinical outcomes and therapeutic response observed in the clinics. Originally, in humans three subtypes were defined based on transcriptomic data: classical, quasi-mesenchymal and exocrine-like subtype (Collisson *et al.*, 2011). The classical subtype is characterized by high expression of epithelial and adhesion-associated genes, while in the quasi-mesenchymal subtype mesenchyme associated genes were upregulated and the exocrine-like subtype showed a higher expression of tumor-cell-derived digestive enzyme genes (Collisson *et al.*, 2011). In the meantime, there were also other classifications available using unbiased hierarchical clustering, but they largely overlap with the initial classification. Those subtypes could be found in murine PDAC cell lines, too (Bailey *et al.*, 2016b; Moffitt *et al.*, 2015; Mueller *et al.*, 2018). Transcriptome analysis combined with detailed morphological analysis showed that the different morphologies of murine PDAC cell lines come along with broad differences in gene expression (Mueller *et al.*, 2018).

To investigate the role of HDACs in different murine tumor subtypes, the cell lines derived from the dual-recombination model were separated according to their morphology using differential trypsinization (Mueller *et al.*, 2018). Therefore, mesenchymal and epithelial fractions of the cell lines were isolated and cultivated

individually. With the help of the above described procedure, the role of HDACs in well differentiated (epithelial) cells and undifferentiated (mesenchymal) cells could be investigated, similar to the analyses that were performed with the parental cell lines.

Table 7-1: Differential trypsinization in PDAC cell lines

Floxed <i>Hdac</i>	Cell lines	Established separation
<i>Hdac1</i>	PPT-F3641, PPT-F3262	In 1 out of 2 cell lines
<i>Hdac2</i>	PPT-F1648, PPT-F2612, PPT-F2800	In 2 out of 3 cell lines
<i>Hdac3</i>	PPT3-F4764, PPT3-F4402, PPT2-F4699, PPT-F5061	In 2 out of 4 cell lines

Differential trypsinization was used to establish epithelial and mesenchymal fractions of the used PDAC cell lines and to investigate the role of HDACs in those fractions. As listed in Table 7-1, the separation of epithelial and mesenchymal subtype was not possible for all cell lines (see also Table S 2). 67% of the available *Hdac2* and 25% of the available *Hdac3* floxed cell lines could be clearly separated. For two *Hdac3* floxed cell lines only one fraction, either the epithelial or the mesenchymal fraction, could be established (Table S 2).

A more detailed analysis of separation of epithelial and mesenchymal fractions was performed in cell lines PPT-F2612 and PPT-F2800.

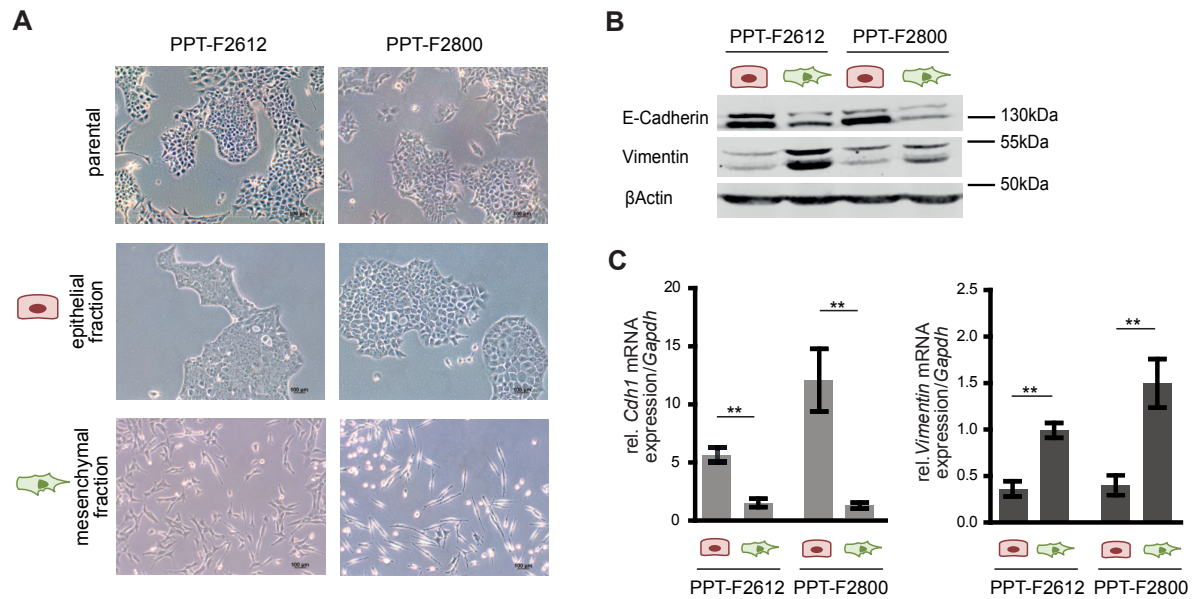


Figure 7-10: Differential trypsinization to generate epithelial and mesenchymal fractions of cell lines PPT-F2612 and PPT-F2800

A) Light microscopy picture of parental cell lines PPT-F2612 and PPT-F2800 and their separated epithelial and mesenchymal fractions. Scale bar depicts 100 μ m. B) Western blot analysis of the epithelial and mesenchymal fractions of the cell lines PPT-F2612 and PPT-F2800. One representative western blot is depicted, β Actin = loading control. C) qRT-PCR of epithelial and mesenchymal markers in the separated fractions of the cell lines PPT-F2612 and PPT-F2800. Quantification of three independent experiments conducted as triplicates are depicted as $2^{-\Delta\Delta Ct}$ value. Average of three replicates of PPT-F2612 mesenchymal fraction was set as 1. Data are shown as mean \pm SD, two-tailed unpaired Student's t test was performed, *: $p \leq 0.05$, **: $p \leq 0.01$, ***: $p \leq 0.001$. = epithelial, = mesenchymal.

Light microscopy pictures in Figure 7-10 (A) document the separation of epithelial and mesenchymal cells of the parental cell lines PPT-F2612 and PPT-F2800 by differential trypsinization. The establishment of the two morphological subtypes is confirmed by qPCR and western blot (Figure 7-10 (B+C, respectively)) which show an upregulation of the epithelial marker E-cadherin in the epithelial fraction and an upregulation of the mesenchymal marker Vimentin in the mesenchymal fraction of both cell lines. The upregulation of *Cdh1* on mRNA level is 6-fold (PPT-F2612) and 12-fold (PPT-F2800) in the epithelial fraction. The upregulation of *Vimentin* on mRNA level is at least 2-fold (PPT-F2612) and 3-fold (PPT-F2800) in the mesenchymal fraction compared to the respective other fraction of the cell line. The enhanced upregulation of the epithelial and mesenchymal marker in the subtypes of PPT-F2800 compared to PPT-F2612 reflects the morphology of the subtypes.

7.3.2 Genetic deletion of *Hdac2* in epithelial and mesenchymal fractions of dual-recombination model based PDAC cell lines

Since *HDAC2* was demonstrated to be expressed higher in undifferentiated human PDAC (Fritsche *et al.*, 2009), analysis of the role of HDAC2 in epithelial and mesenchymal fractions was performed. Therefore, the separated fractions of the *Hdac2*-deletable cell lines PPT-F2612 and PPT-F2800 were used. Like the parental cell lines, the separated fractions were treated with 4-OHT for eight days to knock-out *Hdac2* and the effect on cell viability and colony formation was tested as described above.

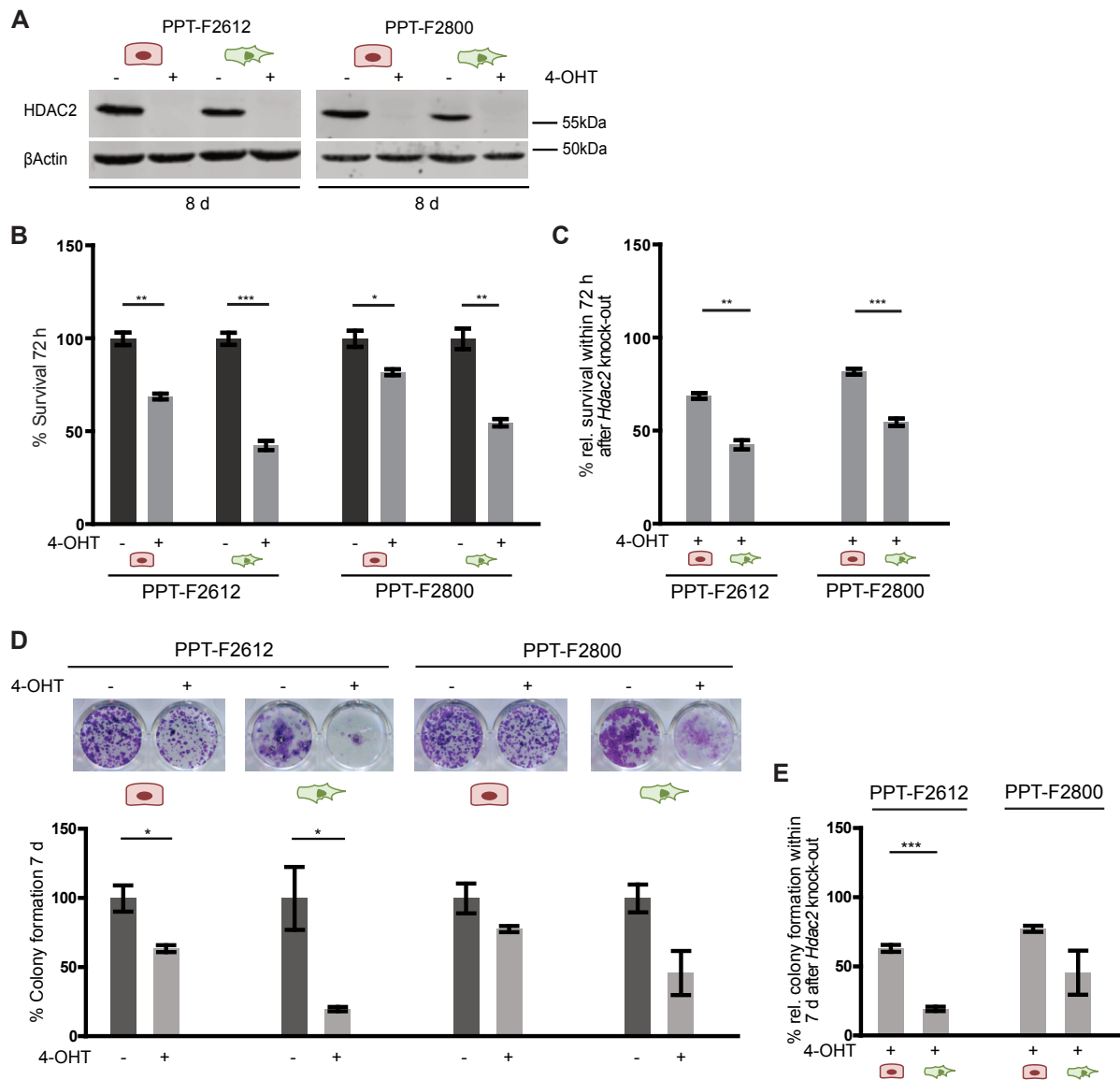


Figure 7-11: *Hdac2* knock-out in epithelial and mesenchymal fractions of cell lines PPT-F2612 and PPT-F2800

A) Western Blot analysis after eight days of 4-OHT/vehicle treatment in the epithelial and mesenchymal fraction of the cell line PPT-F2612. One representative western blot is depicted, β Actin = loading control. B+C) MTT Assay and D+E) clonogenic Assay after eight days of 4-OHT/vehicle treatment in the epithelial and mesenchymal fraction of the cell lines PPT-F2612 and PPT-F2800. One representative clonogenic Assay is depicted per cell line and fraction (D). After eight days of 4-OHT/vehicle treatment 2,000 cells were seeded in triplicates and analyzed for MTT Assay after 72 hours and for clonogenic Assay after seven days. Quantification of three independent experiments per cell line and fraction was performed for both Assays. Vehicle-treated cells = controls, average of three experiments was set as 100%. Data are shown as mean \pm SD, two-tailed unpaired Student's t test was performed *: $p \leq 0.05$, **: $p \leq 0.01$, ***: $p \leq 0.001$. D = days, h = hours, 4-OHT = 4-Hydroxytamoxifen,  = epithelial,  = mesenchymal.

Knock-out of *Hdac2* was possible in the epithelial, as well as in the mesenchymal fraction of both cell lines, which is shown by western blot analysis in Figure 7-11 (A). MTT Assay (Figure 7-11 (B)) reveals a significantly reduced cell survival after loss of HDAC2 expression. Around 70% cells in the epithelial fraction and only ca. 40% cells

in the mesenchymal fraction of cell line PPT-F2612 were viable after *Hdac2* knock-out. As well, in the second cell line PPT-F2800 cell survival is reduced by 18% in the epithelial and by 46% in the mesenchymal fraction. In both cell lines the decrease of cell survival is more pronounced in the mesenchymal fraction compared to the epithelial fraction (Figure 7-11 (C)). The same trend is seen in the ability of colony formation, which is decreased upon *Hdac2* deficiency in epithelial and mesenchymal fraction of both cell lines (Figure 7-11 (D)). In the epithelial fraction of PPT-F2612 colony formation is reduced to 63%, while in the mesenchymal fraction it is reduced to 18%. Also in cell line PPT-F2800 the decrease in colony formation ability is stronger in the mesenchymal fraction compared to the epithelial fraction. In the mesenchymal fraction 45% of cells are able to form colonies, while in the epithelial fraction 77% of the cells can still form colonies (Figure 7-11 (E)). In both assays the cell line PPT-F2612 shows a greater difference between epithelial and mesenchymal fraction than the cell line PPT-F2800.

7.3.3 Pathway analysis in *Hdac2* deficient PDAC cells

RNA-Seq of *Hdac2* pro- and deficient cells of the cell line PPT-F1648 was performed to investigate regulated gene expression and altered pathways after *Hdac2* knock-out in an already established PDAC. In addition to the analysis of the cell line derived from the dual-recombinase model, *Hdac2* pro- and deficient cell lines derived from the KPC model were also analyzed using MicroArray analysis. The genetic strategy behind the KPC mouse model and the dual-recombinase mouse model is explained in Figure 6-1 and Figure 6-2 in the methods part, respectively.

The combined analysis of both data sets allowed the detection of pathways that are affected by acute *Hdac2* deletion in the inducible knock-out model and constitutive *Hdac2* deletion in the KPC model. It is supposed that regulated genes and pathways detected in both models are highly dependent on HDAC2, since the effects of its deletion could not be compensated. Up- and downregulated data sets of both mouse models were compared.

Since HDAC2 is expressed higher in the pancreatic tumor tissue than compared to normal pancreatic tissue (Fritsche *et al.*, 2009), it seems like PDAC is dependent on HDAC2 expression. This hypothesis is also supported by the data shown above. Hence, the question arose which pathways are dependent on HDAC2 expression and

are no longer maintained in *Hdac2* deficient cells. Therefore, it was further analyzed which pathways are associated with in both analyses overlapping downregulated genes. In particular, those genes, like platelet-derived growth factor receptor alpha and beta ($PDGFR\alpha$ and $PDGFR\beta$) and epidermal growth factor receptor (EGFR), which were previously linked to the main regulated pathway, were chosen for further detailed validation (Jechlinger *et al.*, 2006; Kurahara *et al.*, 2016; Lo *et al.*, 2007; Weissmueller *et al.*, 2014).

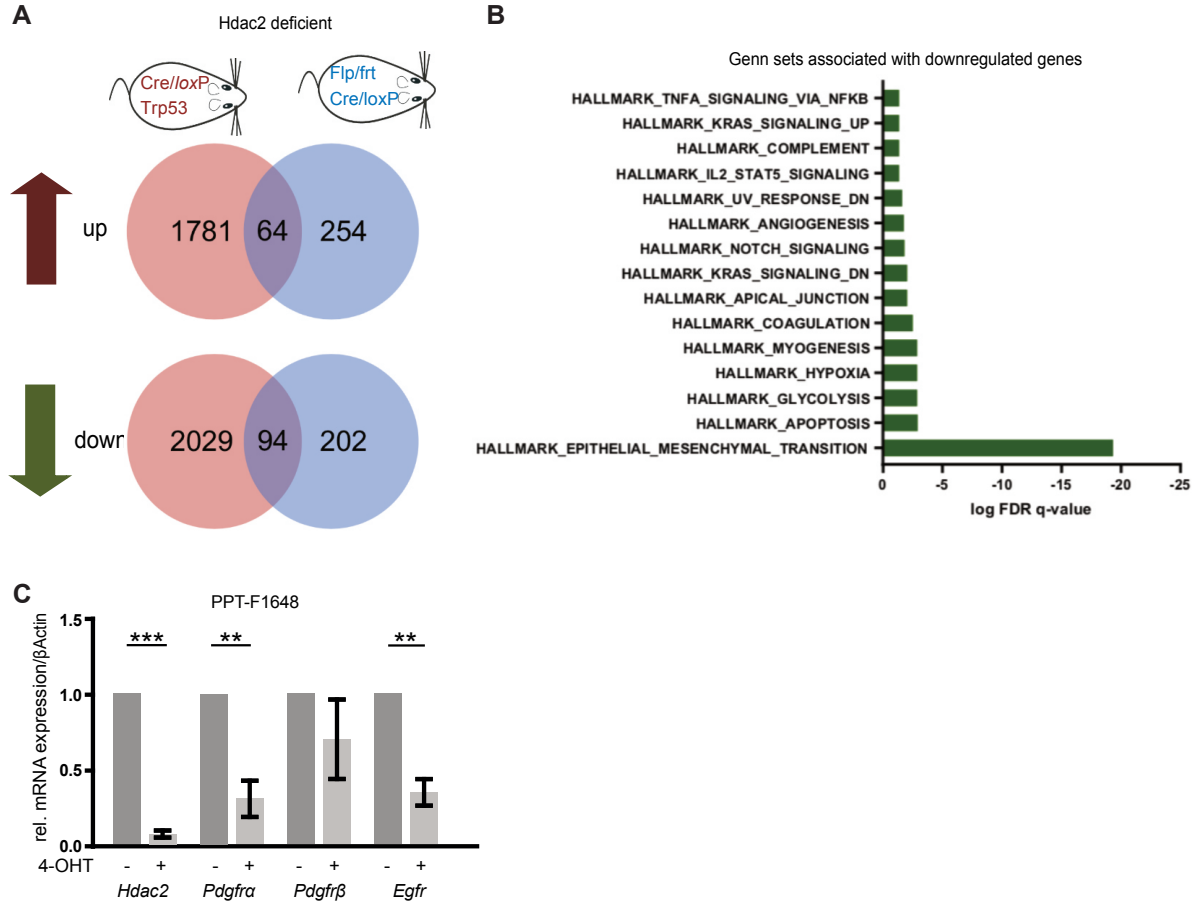


Figure 7-12: Pathway analysis of *Hdac2* deficient PDAC cells
 A) Venn diagrams show 1.5-fold up- or downregulated genes in RNA-Seq and MicroArray data sets of *Hdac2* deficient samples of the dual-recombinase model and the KPC model, respectively. RNA-Seq was performed of the dual-recombinase model cell line PPT-F1648, for MicroArray data the KPC derived cell lines PPT-4917, PPT-AA373, PPT-BK50, PPT-F1042, PPT-F1146 and PPT-F1128 were used. B) Pathway analysis of downregulated genes and C) qRT-PCR of PPT-F1648 cells after eight days of 4-OHT/vehicle treatment. Quantification of four (*Hdac2*) or three (*Pdgfra*, *Pdgfrb*, *Egfr*) independent experiments conducted as triplicates are depicted as $2^{-\Delta\Delta Ct}$ value, vehicle-treated cells = controls, set as 1. Data are shown as mean \pm SD, two-tailed unpaired Student's t test was performed, **: $p \leq 0.01$, ***: $p \leq 0.001$. 4-OHT = 4-Hydroxytamoxifen.

The Venn diagrams in Figure 7-12 (A) show the 1.5-fold up- and downregulated genes of RNA-Seq and MicroArray data sets, as well as the overlapping genes in both groups from the *Hdac2* deficient samples of both mouse models. Analyzing associated gene sets with those downregulated genes by using MSigDB revealed that most genes are associated with pathways like epithelial-to-mesenchymal transition, followed by apoptosis, glycolysis and hypoxia (Figure 7-12 (B)). PDGFR α and PDGFR β as well as EGFR are described to be related to epithelial-to-mesenchymal transition and were further validated in *Hdac2* pro- and deficient PPT-F1648 cells after eight days of 4-OHT/vehicle treatment (Figure 7-12 (C)). Reproducibility of the RNA-Seq and MicroArray data sets by the verified significant downregulated mRNA expression of those EMT-related genes is observed.

7.3.4 TGF β pathway activation in *Hdac2* deficient PDAC cell lines

The previously performed experiments have shown that HDAC2 plays a more important role in mesenchymal cells than in epithelial cells. However, a high expression of mesenchymal genes correlates with increased ability to metastasize, which is a malignancy defining hallmark (Fouad and Aanei, 2017; Giovannetti *et al.*, 2017). As described above, for the metastatic spread the epithelial-to-mesenchymal transition is a main driver and TGF β pathway is activating the process of EMT (Kalluri and Weinberg, 2009; Roberts and Wakefield, 2003). Since EMT is the main downregulated pathway after *Hdac2* knock-out in both mouse models was analyzed, so the question arose, if loss of HDAC2 expression has some effects on EMT by influencing its activation by TGF β pathway. To investigate the relation between *Hdac2* knock-out and EMT and if TGF β pathway is involved in this, the effects of combined *Hdac2* knock-out and TGF β pathway activation were performed in both available mouse models. Therefore, *Hdac2* deficient cells, either derived from the KPC model or generated by eight days of 4-OHT treatment of cell lines from the dual-recombinase model, were treated with TGF β . From the dual-recombinase model the epithelial and mesenchymal fractions of the cell lines PPT-F2612 and PPT-F2800 were used. Cell survival and colony formation was recorded by MTT Assay and clonogenic Assay as usual.

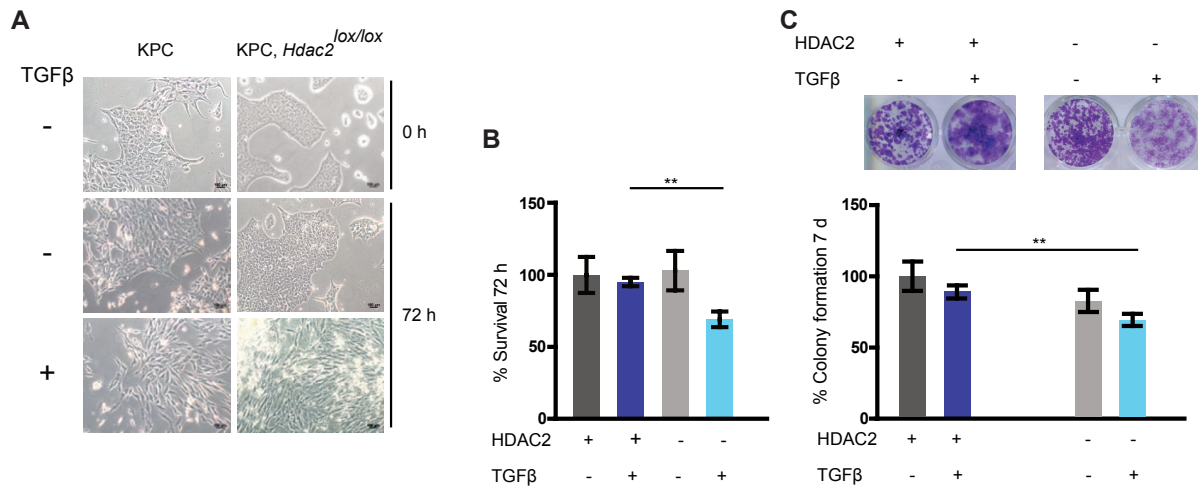


Figure 7-13: TGFβ pathway activation in *Hdac2* pro- and deficient cell lines of KPC model

A) Light microscopy picture of *Hdac2* pro- and deficient PDAC cell lines (PPT-AA352 and PPT-F2100, respectively) derived from the KPC mouse model under normal cultivation conditions and after treatment with 5 ng TGFβ or vehicle for 72 hours. Scale bar depicts 100 μm. B) MTT Assay and C) clonogenic Assay of *Hdac2* pro- and deficient KPC cell lines treated with 5 ng TGFβ or vehicle for 72 hours or seven days, respectively. One representative clonogenic Assay is depicted (C); *Hdac2* proficient: PPT-AA352, *Hdac2* deficient: PPT-F1234. 2,000 cells were seeded in triplicates and after attachment overnight cells were treated with TGFβ or vehicle and analyzed for MTT Assay after 72 hours and for clonogenic Assay after seven days. Quantification of three independent experiments per cell line (seven cell lines per group) was performed for both Assays. Vehicle-treated *Hdac2* proficient cells were used as controls and average was set as 100%. Data are shown as mean +/- SD, one-way ANOVA was performed, **: $p \leq 0.01$. D = days, h = hours, 4-OHT = 4-Hydroxytamoxifen.

TGFβ treatment of *Hdac2* pro- and deficient cell lines of the KPC mouse model, lead to morphological change in both groups. *Hdac2* pro- and deficient cell lines changed from epithelial to mesenchymal cell morphology within 72 hours of the TGFβ treatment (Figure 7-13 (A)). Cell survival as well as colony formation ability was not affected by TGFβ treatment in *Hdac2* proficient cell lines derived from the KPC mouse model. In addition, MTT Assay revealed no decrease in cell survival for the *Hdac2* deficient cell lines of this mouse model, but a slight decrease was observed in colony formation when compared to the *Hdac2* proficient cell lines. Both Assays point out, that TGFβ treatment leads to a significant decrease in cell survival as well as in colony formation in the *Hdac2* deficient cell lines, compared to the *Hdac2* proficient cell lines (Figure 7-13 (B–C)).

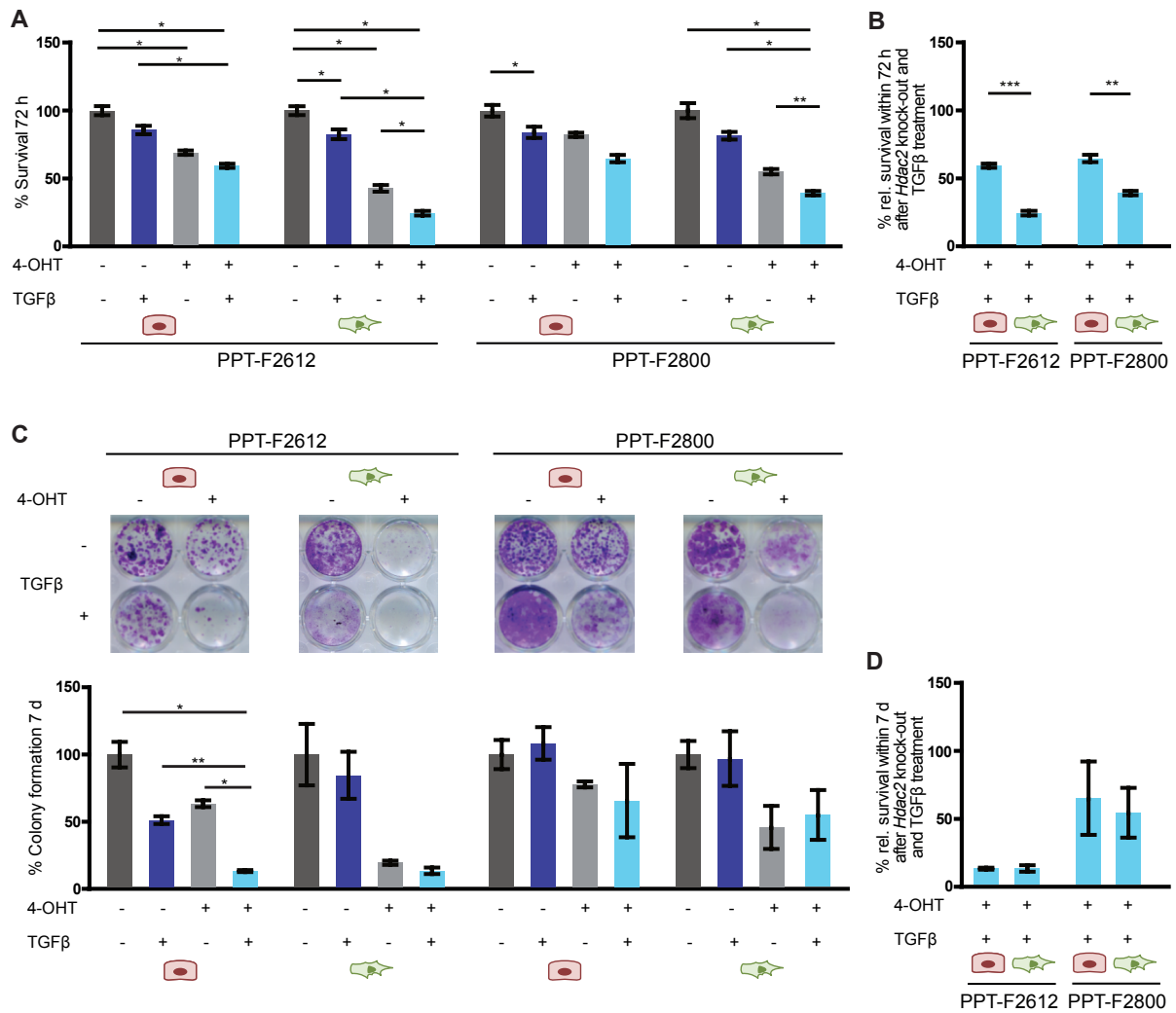


Figure 7-14: TGFβ pathway activation in *Hdac2* pro- and deficient epithelial and mesenchymal fractions of cell lines PPT-F2612 and PPT-F2800

A+B) MTT Assay and C+D) clonogenic Assay after eight days of 4-OHT/vehicle treatment in the epithelial and mesenchymal fraction of the cell lines PPT-F2612 and PPT-F2800, additionally treated with 5 ng TGFβ or vehicle. One representative clonogenic Assay is depicted per cell line and fraction (C). After eight days of 4-OHT/vehicle treatment 2,000 cells were seeded in triplicates. After attachment overnight cells were treated with TGFβ or vehicle and analyzed for MTT Assay after 72 hours and for clonogenic Assay after seven days. Quantification of three independent experiments per cell line and fraction was performed for both Assays. Vehicle-treated cells = controls, average of three experiments was set as 100%. Data are shown as mean +/- SD, two-tailed unpaired Student's t test or one-way ANOVA was performed, *: $p \leq 0.05$, **: $p \leq 0.01$, ***: $p \leq 0.001$. D = days, h = hours, 4-OHT = 4-Hydroxytamoxifen,  = epithelial,  = mesenchymal.

After eight days of 4-OHT/vehicle treatment, the mesenchymal and epithelial fractions of the cell lines PPT-F2612 and PPT-F2800 were additionally treated with TGFβ or vehicle for MTT Assay and clonogenic Assay. TGFβ reduced cell survival by maximum 18% in *Hdac2* proficient cells of both fractions. As well it was shown, that *Hdac2* knock-out decreased cell survival and it was even further decreased when cells were additionally treated with TGFβ after the *Hdac2* knock-out was generated. Furthermore it was observed, that the decrease of cell survival was stronger in the mesenchymal

fraction compared to the epithelial fraction. Those findings regarding cell survival were true for both tested cell lines (Figure 7-14 (A+B)). Colony formation was decreased upon TGF β treatment in *Hdac2* proficient epithelial and mesenchymal PPT-F2612 cells. In those mesenchymal cells *Hdac2* deficiency led to even stronger decrease in colony formation. In both fractions of PPT-F2612 loss of HDAC2 expression combined with TGF β treatment reduced colony formation most, resulting in only around 12% of epithelial and mesenchymal cells that were able to form colonies. Colony formation was slightly increased upon TGF β treatment in *Hdac2* proficient epithelial fraction of cell line PPT-F2800, whereas in the respective mesenchymal fraction colony formation was not changed upon TGF β treatment. *Hdac2* deficient epithelial and mesenchymal PPT-F2800 cells show a further reduced ability to form colonies. Additional treatment with TGF β reduced colony formation in epithelial fraction to 65%, while in the mesenchymal fraction additional TGF β treatment in *Hdac2* deficient PPT-F2800 reduced colony formation to around 55%. Colony formation ability was slightly increased in mesenchymal *Hdac2* deficient PPT-F2800 cells that were treated TGF β treated compared to the respective vehicle treated (Figure 7-14 (C+D)).

7.3.5 Specific role of HDAC2 in TGF β induced EMT

Hdac2 deficient PDAC cells have a survival deficit when the TGF β pathway is activated. Since there are always discussions about redundancies and specific functions of HDAC isoenzymes, cell survival and colony formation of TGF β treated *Hdac1* and *Hdac3* deficient PDAC cells were analyzed in the cell lines PPT-F3641 and PPT2-F4699, respectively.

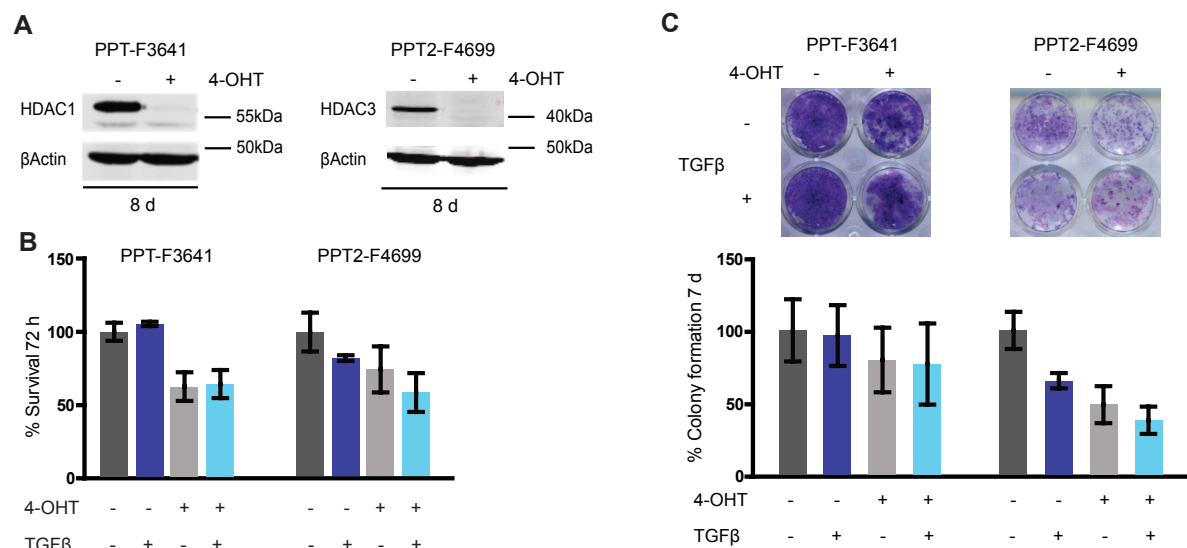


Figure 7-15: Activation of TGFβ pathway in *Hdac1* pro- and deficient PPT-F3641 cells and in *Hdac3* pro- and deficient PPT2-F4699 cells

A) Western Blot analysis of cell lines PPT-F3641 and PPT2-F4699 after eight days of 4-OHT/vehicle treatment. One representative western blot is depicted, βActin = loading control. B) MTT Assay and C) clonogenic Assay after eight days of 4-OHT/vehicle treatment in the cell lines PPT-F3641 and PPT2-F4699. After eight days of 4-OHT/vehicle treatment 2,000 cells were seeded in triplicates. After attachment overnight cells were treated with TGFβ or vehicle and analyzed for MTT Assay after 72 hours and for clonogenic Assay after seven days. One representative clonogenic Assay is depicted per cell line (C). Quantification of three independent experiments per cell line was performed for both Assays. Vehicle treated cells = controls, average of three experiments was set as 100%. Data are shown as mean +/- SD, one-way ANOVA was performed. D = days, h = hours, 4-OHT = 4-Hydroxytamoxifen.

After eight days of 4-OHT treatment knock-out of *Hdac1* or *Hdac3* (Figure 7-15 (A)) in the cell line PPT-F3641 and PPT2-F4699, respectively, was successful. In addition, the pro- and deficient cells were treated with TGFβ for 72 hours during MTT Assay or seven days during Clonogenic Assay. The loss of HDAC1 and HDAC3 expression affects the survival, but additional treatment with TGFβ had no further effect on both cell survival and colony formation (Figure 7-15 (B+C)) in PPT-F3641. Although in PPT2-F4699 the additional TGFβ treatment had no effect on cell survival, but a slightly stronger effect on colony formation after *Hdac3* knock-out. This is only a tendency and does not reach statistical significance.

7.3.6 Rescue of TGF β induced decrease in cell survival and colony formation in *Hdac2* deficient PDAC cells

The next step was then to investigate how inhibition of TGF β pathway could rescue the observed decreased survival and colony formation. Therefore, the cell line PPT-F1648 derived from the dual-recombinase mouse model was treated with 4-OHT, as usual, to knock-out *Hdac2* and afterwards seeded for MTT and clonogenic Assay. Then a four hours pre-treatment with the inhibitors was performed, before TGF β was added.

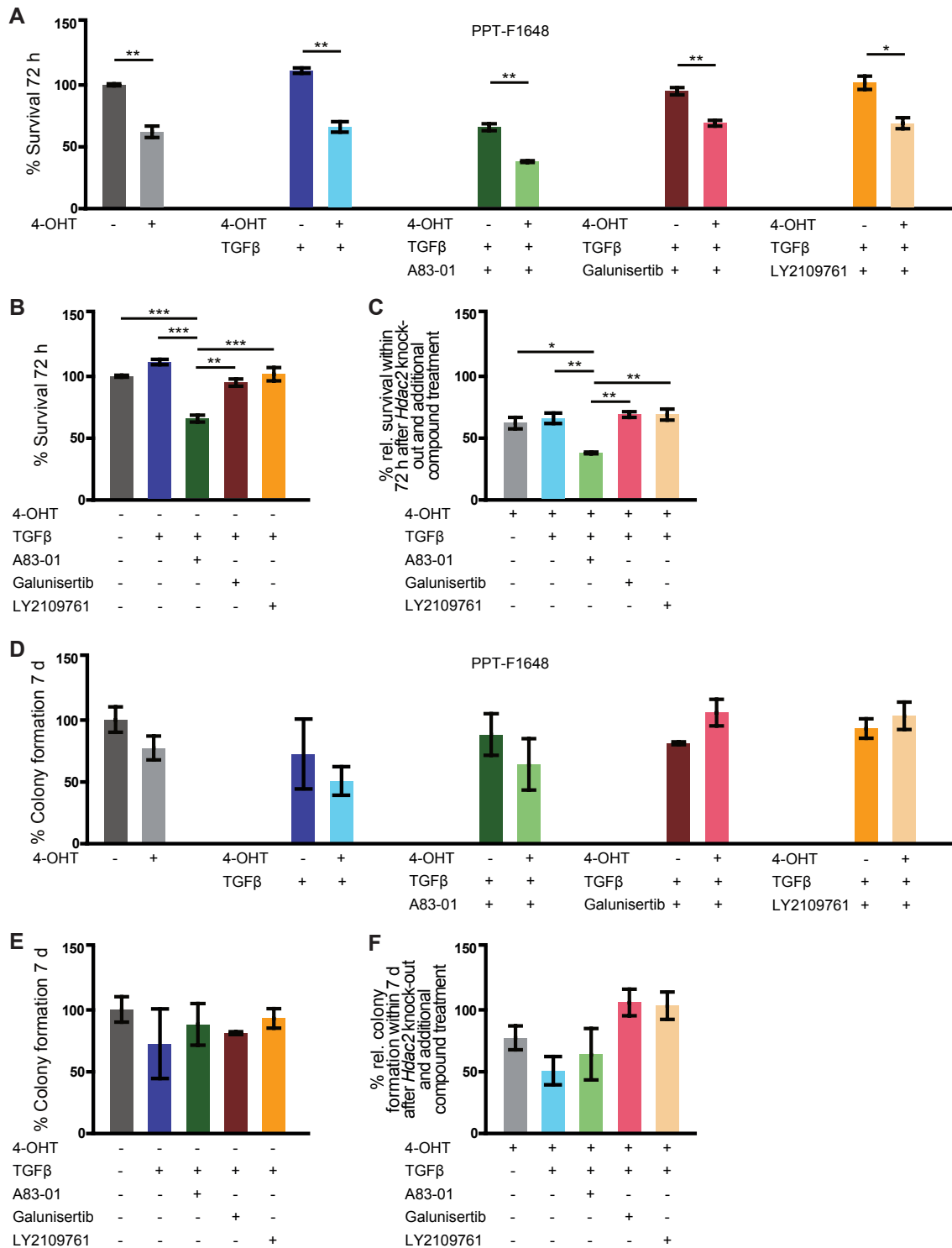


Figure 7-16: Inhibition of TGFβ receptors in *Hdac2* pro- and deficient PPT-F1648 cells followed by TGFβ pathway activation

A-C) MTT Assay and D-F) clonogenic Assay after eight days of 4-OHT/vehicle treatment in cell line PPT-F1648, followed by additionally treated with inhibitors and 5 ng TGFβ or vehicle. After eight days of vehicle or 4-OHT treatment, 2,000 *Hdac2* proficient and *Hdac2* deficient cells were seeded in triplicates per inhibitor/TGFβ combination. After attachment overnight cells were pre-treated for four hours with TGFβ receptor inhibitors (10 μM A83-01, 2 μM Galunisertib or 2 μM LY2109761) before treatment with 5 ng TGFβ or vehicle and analyzed for MTT Assay after 72 hours and for clonogenic Assay after seven days. Quantification of three independent experiments was performed for both Assays. *Hdac2* proficient vehicle treated cells were used as controls and average was set as 100%. Data are shown as mean \pm SD, two-tailed unpaired Student's t test or one-way ANOVA was performed, *: $p \leq 0.05$, **: $p \leq 0.01$, ***: $p \leq 0.001$. D = days, h = hours, 4-OHT = 4-Hydroxytamoxifen.

Cell viability is diminished in *Hdac2* deficient PPT-F1648 cells and the same is observed when those cells are additionally treated with TGF β for 72 hours. Pre-treatment with A83-01, which inhibits type I TGF β receptor (TGF β RI), followed by TGF β treatment decreases the viability in *Hdac2* deficient cells after 72 h, too. Pre-treatment with the other inhibitors Galunisertib (TGF β RI) and LY2109761 (TGF β RI/II) followed by TGF β treatment did also affect survival within 72 hours in *Hdac2* deficient cells of cell lines PPT-F1648 (Figure 7-16 (A)). In *Hdac2* proficient cells, as well as in *Hdac2* deficient cells, pre-treatment with compound A83-01 followed by TGF β treatment reduced cell survival significantly in comparison to the other used compounds (Figure 7-16 B+C). TGF β treatment alone and pre-treatment with Galunisertib and LY2109761 did not affect cell survival in comparison to *Hdac2* proficient vehicle treated cells (Figure 7-16 (B)). The same was seen in *Hdac2* deficient cells (Figure 7-16 (C)).

Colony formation was reduced in *Hdac2* deficient vehicle treated cells as well as after additional TGF β treatment. Also, pre-treatment with A83-01 followed by TGF β treatment reduced colony formation *Hdac2* deficient cells after seven days. This reduction could be rescued due to pre-treatment with TGF β RI inhibitor Galunisertib and TGF β RI/TGF β RII inhibitor LY2109761 before adding TGF β to the *Hdac2* deficient cells. By using those inhibitors, even the level of colony formation in *Hdac2* proficient cells could be reached (Figure 7-16 (D)). None of the used compounds or compound combinations could reduce colony formation within seven days in comparison to vehicle treated cells in *Hdac2* proficient cells of cell line PPT-F1648 (Figure 7-16 (E)). In *Hdac2* deficient PPT-F1648 cells, pre-treatment with Galunisertib and LY2109761 increased colony formation in comparison to pre-treatment with A83-01 or TGF β treatment alone, and even in comparison to vehicle treated *Hdac2* deficient cells, even though this increase did not reach statistical significance (Figure 7-16 (F)).

7.4 *In vivo* phenotype of *Hdac2* deficient KPC mice

After analyzing the effect of *Hdac2* knock-out *in vitro*, the results led to analyses of *in vivo* effects of *Hdac2* knock-out. Therefore, the KPC mouse model (Hingorani *et al.*, 2005) was combined with *Hdac2* floxed mice (Montgomery *et al.*, 2007) to generate a constitutive *Hdac2* deficient mouse model. Those animals were investigated in the first instance concerning survival and tumor development.

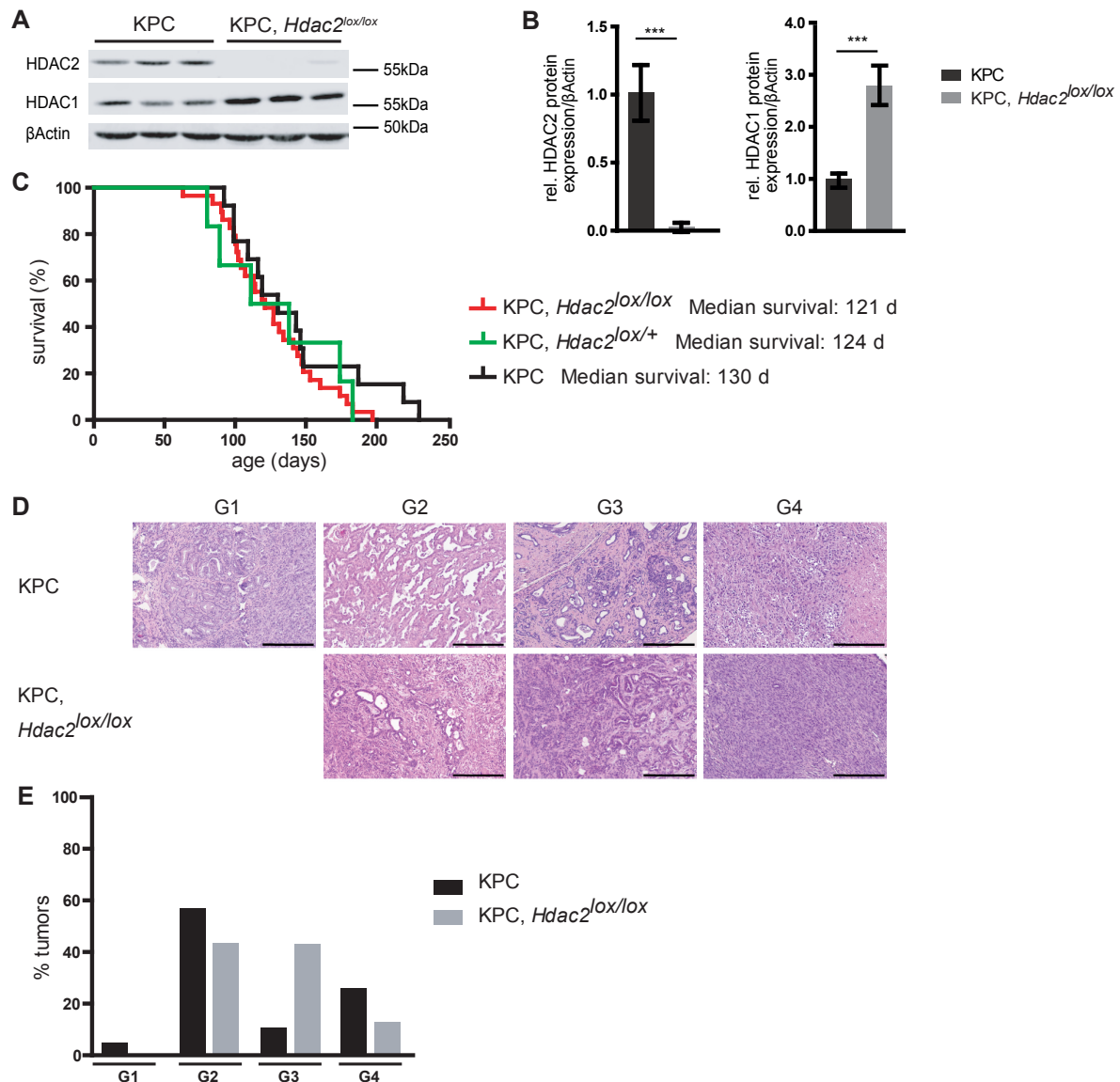


Figure 7-17: Survival data and *in vivo* phenotype of *Hdac2* pro- and deficient KPC mice

A) Western Blot analysis of each three *Hdac2* pro- and deficient cell lines derived from KPC mouse model. One representative western blot is depicted, βActin = loading control. B) Quantification of three *Hdac2* proficient and five *Hdac2* deficient samples, *Hdac2* proficient samples were used as controls, average was set as 1. C) Kaplan-Meier survival analysis of *Hdac2* proficient and hetero- and homozygous *Hdac2* deficient KPC mice (KPC, *Hdac2*^{lox/+} n = 6, KPC, *Hdac2*^{lox/lox} n = 29, KPC n = 13). D) H&E staining of PPTs of *Hdac2* pro- and deficient KPC mice (KPC: G1: AH1056, G2: F0793, G3: AH1056, G4: 6817, KPC, *Hdac2*^{lox/lox}: G2: F1297, G3: F1374, G4: F1128. Scale bar depicts 500 μm. E) Grading of H&E staining of PPTs: G1 = well differentiated, G2 = moderately differentiated, G3 = poorly differentiated and G4 = undifferentiated; KPC, *Hdac2*^{lox/lox} n = 24, KPC n = 25. Data are shown as mean +/- SD, two-tailed unpaired Student's t test was performed ***: p ≤ 0.001.

In Figure 7-17 (A+B) knock-out of *Hdac2* is proven by western blot and the compensation of the loss of HDAC2 expression through upregulation of *Hdac1* could be seen. The Kaplan-Meier survival curve (Figure 7-17 (C)) shows no difference between the control group and hetero- or homozygous knock-out of *Hdac2*. Since *Hdac2* pro- and deficient mice developed PDAC, the next step was to grade those PPTs while G1 are well differentiated, G2 are moderately differentiated, G3 are poorly differentiated and G4 are undifferentiated tumors. As shown in Figure 7-17 (D+E) for the deficient group, no G1 tumors could be found and compared to the control group fewer mice displayed tumors of G2 as well as G4 grade, but way more tumors of G3 grade. The histology of the tumors showed that there are fewer aggressive tumors of G4 grade in the *Hdac2* deficient cohort.

Table 7-2: Morphology of *Hdac2* pro- and deficient KPC cell lines

	Epithelial morphology	Mesenchymal morphology	Mixed morphology
KPC (n = 11)	27,3%	45,4%	27,3%
KPC, <i>Hdac2</i> ^{lox/lox} (n = 9)	44,5%	22,2%	33,3%

Analyzing the morphology of the available *Hdac2* pro- and deficient cell lines derived from the KPC mouse model (Table 7-2), revealed fewer mesenchymal cell lines in the *Hdac2* deficient group. This finding is accompanied by the observation of fewer undifferentiated tumors in the *Hdac2* deficient mice (Figure 7-17 (E)).

Table 7-3: Differential trypsinization *Hdac2* pro- and deficient KPC cell lines

	Established separation
KPC	3 out of 3
KPC, <i>Hdac2</i> ^{lox/lox}	0 out of 4

Differential trypsinization was successful in the *Hdac2* proficient KPC cell lines, but not in the *Hdac2* deficient KPC cell lines (Table 7-3), which further supports the theory, that HDAC2 is especially relevant in the mesenchymal subtype of PDAC.

significant, but there are significantly more mice in this deficient group that developed no metastases at all (Figure 7-18 (B)).

It was further analyzed, if the observed metastases in the KPC, *Hdac2*^{lox/lox} mice derived from *Hdac2* proficient cells, since there is a possibility that Cre recombinase did not fully recombine the floxed *Hdac2* alleles (Magnuson and Osipovich, 2013). Therefore, immunohistochemical staining of HDAC2 was performed in metastasis of KPC, *Hdac2*^{lox/lox} mice.

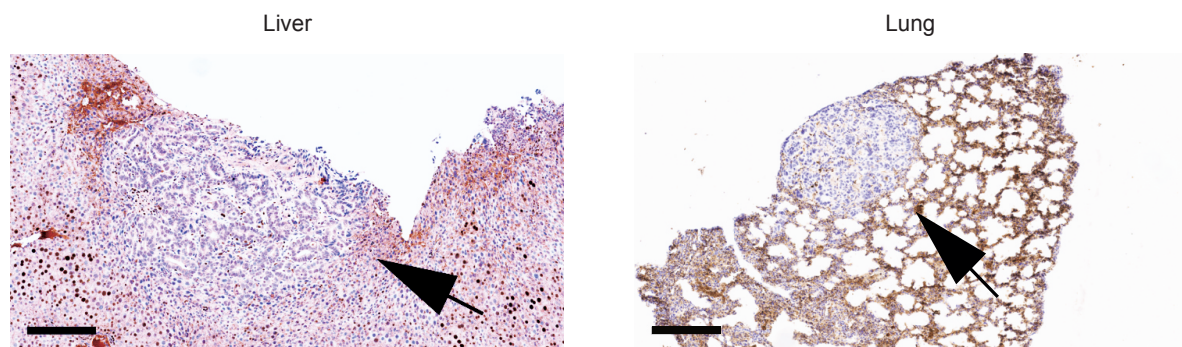


Figure 7-19: Immunohistochemical analysis of HDAC2 expression in liver and lung metastasis of KPC, *Hdac2*^{lox/lox} mice

Immunohistochemical *Hdac2* staining in liver and lung metastasis of KPC, *Hdac2*^{lox/lox} mice. Liver: F1039, lung: F1088. α -HDAC2 antibody: 1:400, scale bar depicts 200 μ M.

Figure 7-19 shows a representative immunohistochemical HDAC2 staining in liver and lung metastases of KPC, *Hdac2*^{lox/lox} mice. The tumor cells forming the metastases are negative for the HDAC2 staining in contrast to the surrounding liver or lung tissue. Hence, the constitutive knock-out of *Hdac2* in KPC, *Hdac2*^{lox/lox} mice seem to be not leaky but rather some *Hdac2* deficient tumor cells are still able to undergo the process of metastatic spread and colonize liver and/or lung tissue.

8. Discussion

The data shown in part 7 shed light on the importance of HDACs as a therapeutic target for PDAC. It also became clear that deletion of each tested isoenzyme separately or all together, affects the tumor maintenance differently, indicating that there are isoenzyme specific function of those HDAC isoenzymes. This encourages further investigations addressing the isoenzyme specificity as well as the relevance of the development of new isoenzyme specific HDACis. In addition, a relevance of especially HDAC2 was shown for the process of metastatic spread, but the detailed mechanism still remains undetected.

8.1 Effects of HDACis and inducible coincident and separate genetic deletion of class I HDACs *Hdac1*, *Hdac2* and *Hdac3* *in vitro*

Treatment with HDACis MS-275, SAHA, Panobinostat and Merck-60 reduced cell viability in all three cell lines PPT-F1648, PPT-F2612 and PPT-F2800 (Figure 7-1) within 72 hours. However, HDACi effectiveness was severely different among the cell lines, but cell line PPT-F1648 was most sensitive in comparison to the cell lines PPT-F2612 and PPT-F2800 to all tested HDACis and especially to the pan-HDACi Panobinostat. Panobinostat was less potent in the other tested cell lines, while class I specific HDACi MS-275 and class I+II specific HDACi SAHA led to a significant decrease of cell viability in all three tested cell lines. In other studies it was shown that Panobinostat has more potency to treat pancreatic cancer than other HDACis that inhibited only selective HDAC classes (Singh *et al.*, 2016). The same was seen in cell line PPT-F1648, while for the other cell lines this could not be observed. Since especially class I HDACs became a promising target for pancreatic cancer (Schneider *et al.*, 2010), the question arose how the deletion of only class I isoenzymes *Hdac1*, *Hdac2* and *Hdac3* contributes to the decrease of tumor cell survival.

To investigate the role of HDAC1, HDAC2 and HDAC3 in tumor maintenance, floxed *Hdac1*, *Hdac2* and *Hdac3* alleles were combined within the dual recombination model. The successful coincident knock-out of *Hdac1*, *Hdac2* and *Hdac3* (*Hdac1/2/3*) within a tumor cell severely decreases cell viability and colony formation. It was also observed that the better the knock-out, the stronger is the effect on cell survival and colony formation. The loss of cell viability and colony formation is intense, since it was not even possible to pick viable clones of the deficient cells of neither of the tested cell lines (Table S 1). Since there were almost no cells left after the successful deletion of

all three HDAC isoenzymes *Hdac1/2/3*, further experiments like FACS cell cycle analysis could not be performed. This observed enormous decrease in cell viability and colony formation proves the great potential of targeting HDACs as a therapeutic option to treat PDAC.

Comparing coincident knock-out of *Hdac1/2/3* with available class I specific HDAC inhibitors, like MS-275, shows a weakness of available inhibitors. Even if used in very high concentrations, the HDACi was not able to reduce cell growth completely (Figure 7-2), which was also observed by others (Nguyen *et al.*, 2017). This observation and also the findings shown in Figure 7-1 revealed a varying and dissatisfying potency of those inhibitors, especially in comparison to the effects of coincident knock-out of *Hdac1/2/3* on tumor cell survival. Besides this, HDACis are currently under investigation in several clinical trials to examine their therapeutic potential for solid tumors, like PDAC. Unfortunately, their effectiveness is not too overwhelming in those clinical trials, too, arguing for an urgent need for new, more effective and specific inhibitors (Hessmann *et al.*, 2017; Kim and Bae, 2011; Koutsounas *et al.*, 2013; Polireddy and Chen, 2016).

This ineffectiveness of HDACis could be explained with either an incomplete inhibition of the HDAC activity by the HDACis, or by a transient action of the inhibitors. But nonenzymatic functions of HDACs are also postulated. As HDACs are part of several complexes, their genetic deletion disrupt the complexes, whereas HDACis mainly block the enzymatic activity of the HDAC isoenzymes without destroying the complex (Haberland *et al.*, 2009b). Nonenzymatic functions of the different HDAC isoenzymes are addressed sparsely, especially in the context of cancer, and are mainly related to transcriptional activation. In human myeloid leukemia cells HDAC2 activates transcription through recruiting the transcriptional activator PAX5 to promoters of target genes independent of its deacetylase activity (Jung *et al.*, 2018). Furthermore, overexpression of HDAC1 or HDAC3 in mice's hearts causes cardiomyopathy, as well as their respective deacetylase-dead equivalents. In addition, it was shown that hepatosteatosis and repressed lipogenic gene expression in *Hdac3* deficient murine liver tissue can be rescued by deacetylase-inactive HDAC3 (Sun *et al.*, 2013).

All in all, it seems like only inhibition of enzymatic function is not enough to target PDAC efficiently. Since the results from the coincident genetic deletion of *Hdac1/2/3* are promising, it is likely that HDACs have some unexplored nonenzymatic functions and it can be concluded that eliminating the complete protein is more effective.

Maybe those nonenzymatic functions could be targeted using PROteolysis-TARgeting Chimeras (PROTACs). PROTAC is a novel method based on chemical protein knockdown strategy and is composed of three parts. A ligand that binds the target protein is connected via a linker molecule with a second ligand that recruits the E3 ligase. The protein of interest and the E3 ligase bind a ternary complex through the PROTAC, which is followed by ubiquitination of the protein of interest. When ubiquitination machinery and the ubiquitinated target protein are in close proximity, the protein of interest is degraded by the 26S proteasome. PROTACs are a possibility to target drug-resistant proteins and to impair nonenzymatic functions (Sun *et al.*, 2019). The high potency of PROTACs is shown *in vitro* and its activity was also proven *in vivo* in mouse models (Lai and Crews, 2017). Those characteristics are key advantages for PROTACs over classical inhibitors.

Yet hardly any PROTACs targeting HDACs have been developed. The first degrader for zinc-dependent HDACs was a HDAC6 selective PROTAC (Yang *et al.*, 2018). There was also a study investigating effective degraders targeting class I HDACs. In this study, the HDAC inhibitors MS-275, CI-994 and MGCD0103 were considered. Also, two linkers which differed in size (6 and 12 carbon alkyl linker) were tested, as well as two different E3 ligands, showing higher efficiency for the von-Hippel-Lindau ligand over the cereblon ligand. The most effective degrader consisted of benzamide HDACi CI-994, a 12 carbon alkyl linker and the von-Hippel-Lindau E3 ligand. It effectively decreased cell viability in colon cancer cells, providing an alternative to classical HDACis (Smalley *et al.*, 2020). Therefore, it is suggested to establish HDAC inhibitors that specifically target a combination of isoenzymes like HDAC1/2/3 and use them to develop PROTACs that lead to degradation of those subgroups of HDAC classes. It is supposed that this would be an option to achieve comparable results to the triple knock-out data.

The effects of simultaneous genetic deletion of *Hdac1/2/3* in murine PDAC cells are enormous, but still the isoenzyme specific functions of those class I HDACs are mostly unknown and were of great interest.

Isoenzyme specific functions are discussed frequently in literature. For example, a study showed that a double knock-out of *Hdac1* and *Hdac2* in developing mouse brains lead to apoptosis, DNA damage and impaired chromatin structure as well as embryonic lethality. Expression of a single allele of *Hdac1* in a *Hdac2* deficient state still caused

impaired brain development and perinatal lethality, while in a *Hdac1* deficient condition, one allele of *Hdac2* was enough to ensure normal brain development in mice. Therefore, it was concluded, that the role in chromatin structure maintenance is common for HDAC1 and HDAC2, but the function during development is unique for HDAC2 (Hagelkruys *et al.*, 2014). Not only in developmental processes, but also in context of tumor progression, it was shown that the functions of the HDAC isoenzymes differ. For instance, in breast cancer, *HDAC1* deletion reduces tumor cell growth, while *HDAC2* deletion increases sensitivity to topoisomerase inhibitor induced apoptosis (Jurkin *et al.*, 2011). Liver-specific deletion of *Hdac3* revealed a regulatory role of HDAC3 in STAT3-dependent cell proliferation which is important for liver regeneration and cancer (Lu *et al.*, 2018).

To shed some light on the isoenzyme specific function of the herein investigated HDACs in PDAC maintenance, the dual-recombinase mouse model was used. The cell lines derived from this model enabled the separate deletion of each isoenzyme in an established PDAC through 4-OHT treatment. The *Hdac1* specific genetic deletion in cell line PPT-F3641 resulted in a not significantly reduced cell growth within 72 h (Figure 7-3). This inhibition of cell growth was also observed in mammary carcinoma and osteosarcoma cell lines (Senese *et al.*, 2007). The inhibition of cell growth in *Hdac1* deficient cells is linked to an upregulation of p21/WAF1/CIP1 (p21), cyclins and cyclin-dependent kinases which are necessary for an appropriate cell cycle progression (Senese *et al.*, 2007). It is discussed that Sp1 is involved in the HDAC1 recruitment to the p21 promoter where it binds and represses the p21 activity (Lagger *et al.*, 2003). By deletion of *Hdac1*, p21 is no longer repressed and consequently the cell growth is no longer induced.

No difference was found for colony formation in the tested PDAC cell line (Figure 7-3), as it was previously shown for human hepatocarcinoma and colon cancer cell lines, but this is contrasted by what was seen in mammary carcinoma and osteosarcoma cell lines (Ler *et al.*, 2015; Senese *et al.*, 2007). This difference could be explained by the different tumor types that were analyzed, since it is possible that HDAC1 functions differ between the various tumor types and therefore its deletion might lead to divergent phenotypes.

Cell cycle progression remained unchanged upon *Hdac1* knock-out in the tested cell line, but a remarkable large number of cells in the subG1 phase was observed. Since this was seen with and without 4-OHT treatment, it seems like this is a characteristic

of the cell line PPT-F3641 and not dependent on the loss of HDAC1 expression. Even though a slight increase in S phase and G2/M phase was seen after quantification, all FACS profiles remained mostly unremarkable (Figure 7-3). This contrasts with what was found by others. So, it was shown that HDAC1 specific functions in mammary carcinoma and osteosarcoma cell lines are involved in G2/M transition and cell cycle progression. Those *Hdac1* deficient cells are not able to enter mitosis and consequently undergo apoptosis via capsase-3 activation (Senese *et al.*, 2007). A reason for the distinct results could be the cancer type analyzed. It could be that in pancreatic cancer, the role of HDAC1 during cell cycle progression is compensated by other cell cycle related proteins. Next to its role in cancer cell progression, HDAC1 is also necessary for embryonic development and its absence caused an increase of p21 and p27 and therefore reduced cellular proliferation rate in embryos and ES cells (Lagger *et al.*, 2002).

In the tested cell line PPT-F3641 a small decrease in cell viability was seen upon *Hdac1* knock-out but this was not significant and no effect was observed concerning colony formation or cell cycle progression. Since only one cell line was tested, it is recommended to verify these results in more cell lines, but so far, from the data presented here, it seems like HDAC1 does only marginally contribute to PDAC maintenance. Since there is no HDAC1 specific inhibitor available, the results of the genetic deletion cannot be compared to survival and colony formation ability when the enzymatic activity of HDAC1 is blocked.

Next, the genetic deletion of *Hdac2* and investigation of its effects on cell survival and colony formation followed. The three cell lines PPT-F1648, PPT-F2612 and PPT-F2800 were used, showing a significant decrease of cell survival within 72 h after *Hdac2* knock-out as well as significantly reduced colony formation (Figure 7-4). A reduction in cell viability of at least 20% was observed in all three cell lines, while for colony formation a reduction of 60% minimum was detected. This was also seen in human gastric cancer cell lines, where HDAC2 inactivation was followed by a reduction in tumor growth and clonal expansion (Kim *et al.*, 2013). Growth suppression was also seen in colon cancer cells *in vitro* when HDAC2 was inhibited using small interfering RNA (siRNA) (Weichert *et al.*, 2008). Another inhibition of HDAC2 via microRNA miR-500a-5p, which directly targets HDAC2, inhibits proliferation of colorectal cancer (Tang *et al.*, 2019). Those data show that HDAC2 is important for cell growth and colony

formation not only in PDAC but also in several other cancer types. The next steps would be the detailed analysis of mechanisms of cell viability and colony formation and how HDAC2 is involved or how its deletion interferes with those mechanisms.

Cell cycle analysis in the cell line PPT-F1648 revealed a significant increase in G2/M phase after *Hdac2* knock-out, accompanied by fewer cells in G1 phase (Figure 7-5). In literature the G2/M phase arrest is observed after HDACi treatment but is not described to be specific for HDAC2. The HDACis block the activation of G2/M regulatory complexes by decreased levels of cyclin A and cyclin B1 leading to G2/M arrest. G2/M transition is also dependent on Aurora A and PLK1 and can be downregulated by HDACis. Inhibition of *cdc2/cyclin B* by increased *Gadd45* expression results in G2/M arrest and is also associated with HDACi (Newbold *et al.*, 2016).

Proteome analysis of PPT-F1648 cells (Figure S 1) revealed a downregulation of CDK7 in *Hdac2* deficient cells after five days of 4-OHT treatment. CDK7 is described to have two functions: First, CDK7 is necessary for transcription by phosphorylation of RNA Polymerase II and other CDKs that are important for the transcriptional machinery. Second, CDK7 is also the only known CAK to activate CDKs that control cell division and require activation (T) loop phosphorylation (Schachter and Fisher, 2013). CDK7 is required for CDK1 phosphorylation and its inhibition in G2 phase leads to disruption of *Cdk1/cyclin B* complex and therefore blocks entry into mitosis (Laroche *et al.*, 2007). Therefore, CDK7 inhibition can indirectly lead to G2/M arrest via affecting the *Cdk1/cyclin B* complex. Validation of the proteome analysis after eight days of 4-OHT treatment did not confirm the CDK7 downregulation after five days of 4-OHT treatment, showing no robust and significant downregulation at that later point of time. According to this, the hypothesis of *Cdk7* downregulation, as a consequence of *Hdac2* knock-out leading to G2/M arrest via impaired regulation of CDK7 targets, could not be confirmed. It seems like there is another mechanism that leads to G2/M arrest after *Hdac2* knock-out, which needs to be elucidated. But in general, the detected G2/M arrest after loss of HDAC2 expression needs to be verified by analysis of cell cycle proteins to detect the mechanism behind this arrest and investigate the detailed contribution of HDAC2 in the G2/M arrest.

HDACs are involved in the process of chromatin remodeling, leading to closed chromatin state where gene transcription is silenced (Cress and Seto, 2000; Grozinger and Schreiber, 2002). Loss of HDACs is consequently assumed to result in more open

chromatin regions and active gene transcription. A marker for active gene transcription is for example the acetylation of Histone H3 at Lysin 27 (H3K27ac) (Kimura, 2013). To characterize *Hdac2* deficient PPT-F1648 cells even more, H3K27ac was analyzed in those cells. Surprisingly, no changes in H3K27ac were observed between *Hdac2* pro- and deficient PPT-F1648 cells (Figure 7-6). Since H3K27 is acetylated by the CBP/p300 complex and deacetylated by the HDAC1/2-NURD complex, an effect caused by *Hdac2* knock-out was expected (Morgan and Shilatifard, 2015). The phenomenon of unchanged histone acetylation was previously seen in murine embryonic stem cells, where the global histone acetylation level did not change after conditional knock-out of *Hdac2* (Dovey *et al.*, 2010). In contrast to this, coincidental deletion of *Hdac1* and *Hdac2* led to enhanced H3K27 acetylation in microglia (Datta *et al.*, 2018). The same was seen in human glioblastoma cell lines by inhibition of HDAC1 and HDAC2 together, but no significant change in H3K27ac was seen if only one isoenzyme was inhibited (Zhao *et al.*, 2020).

For sure, there is a need to verify the observation, that H3K27ac does not change after *Hdac2* deletion. Even if no change in H3K27 acetylation was seen, it would be important to investigate if acetylation patterns of other histones or non-histone targets of HDAC2 experience a change. This could be done by global acetylome analysis or by checking each acetylation site of the different histones separately, as well as by specifically analyzing acetylation status of HDAC2 targets.

Despite no change in H3K27 acetylation, regulation of pathways and regulation of mRNA was seen upon *Hdac2* knock-out. There is a link between acetylation and methylation as well as phosphorylation patterns described elsewhere. For instance, it is postulated that complexes which are responsible for H3K27 methylation and acetylation act in opposition to one another (Morgan and Shilatifard, 2015). For example, a direct link between acetylation and phosphorylation of AKT is related to deacetylase activity of HDAC3. When HDAC3 binds to AKT, it deacetylates AKT at Lysin 20, which leads to promotion of AKT phosphorylation (Long *et al.*, 2017). If and how the acetylation status of HDAC2 targets also influences their other protein modifications and therefore the activity of those proteins remains to be examined. Therefore, it is recommended to analyze not only acetylation but also global methylation and phosphorylation pattern to see if and how *Hdac2* knock-out influences gene expression directly or indirectly.

The strongest effect on cell survival was seen after *Hdac3* knock-out, but the decrease in cell viability was not affected by the *Trp53* status of the cell lines. The diminished cell viability after HDAC3 deletion was also observed in human colon cancer cell lines and cholangiocarcinoma cell lines (Wilson *et al.*, 2006; Yin *et al.*, 2017). In human gastric cancer cell lines it was observed, that *HDAC3* deletion correlates with expression of microRNA miR-454 which directly targets CHD5 and therefore decreases gastric cancer cell growth (Xu *et al.*, 2018).

Also, colony formation was reduced in the tested *Hdac3* deficient PDAC cell lines, as well as in human gastric cancer cells (Xu *et al.*, 2018). Using a novel HDAC3-specific inhibitor MI192 or siRNA against *HDAC3* in human cholangiocarcinoma showed a decrease in colony formation. It is discussed, that HDAC3 can rescue apoptosis signaling in this type of cancer and its deletion would lead to increased apoptosis and therefore no colonies could be formed (Yin *et al.*, 2017).

In summary, *Hdac3* knock-out in PDAC leads to a decrease in cell viability and colony formation, but it seems like these functions are independent of *Trp53*, since the data presented here show no obvious difference in survival and colony formation among the *Trp53* pro- and deficient tumors in the *Hdac3* deficient cells.

After loss of HDAC3 expression the cell cycle arrest differs between the four tested cell lines. While in all four cell lines an increase of cells in G2/M phase was observed after *Hdac3* deletion, only in the two cell lines PPT2-F4699 and PPT-F5061 a clear increase of cells in S phase was seen. In general, the observation that HDAC3 plays a role in cell cycle progression fits the published data (Bhaskara *et al.*, 2008; Summers *et al.*, 2013; Wilson *et al.*, 2006).

The observed differences between the four tested PDAC cell lines concerning cell cycle distribution after *Hdac3* knock-out, could give also a hint that there might be a TRP53 dependent cell cycle arrest. P53 is involved in the p53-p21-DREAM-E2F/CHR pathway (p53-DREAM pathway) and controls several genes associated with the cell cycle. The p53-DREAM pathway participates in the control of all checkpoints from DNA synthesis to cytokinesis, including G1/S, G2/M checkpoints as well as the spindle assembly checkpoint (Engeland, 2018). Besides the link of p53 with cell growth arrest and apoptosis, it is also associated with DNA damage. P53 is essential for G1/S checkpoint and prevents initiation of DNA replication in case of DNA damage by induction of p21 expression (Stewart and Pietsenpol, 2001). P21 consequently inhibits cdk2 complexes and promotes the assembly of cyclin D/cdk4 complexes leading to G1

arrest and avoiding transition to S phase (Giono and Manfredi, 2006). During S phase, p53 ensures that cells remain in S phase in case of DNA damage by blocking replication and delaying DNA synthesis. It is also discussed that CHK-1 is involved in regulation of DNA replication fork elongation and S phase progression in a p53-dependent way (Ahmed *et al.*, 2011). Additionally, p53 plays a role during G2 arrest induction and maintenance, by increased GADD45 expression and repression of Cdc25C, a mitosis promoting phosphatase, respectively. Finally, p53 is involved in the spindle assembly checkpoint, which ensures a correct alignment of all chromosomes at the cell equator, as well as correct microtubule attachment to the mitotic spindle, before anaphase is entered. It was also shown, that p53 plays a critical role in prevention of aneuploidy by blocking endoreduplication of tetraploid cells when mitotic failure happens (Giono and Manfredi, 2006).

Both *Trp53* wildtype cell lines PPT3-F4764 and PPT3-F4402 are significantly arrested in G2/M phase. In those *Hdac3* deficient cells a slight decrease in the percentage of cells in the S phase was observed, too. According to literature, HDAC3 is linked with DNA damage repair and is present at DNA replication forks (Wells *et al.*, 2013). It is also researched in human pancreatic cancer, that after *HDAC3* knockdown, p53 mRNA was upregulated (Jiao *et al.*, 2014). It could be the case that *Hdac3* deficiency leads to DNA damage, which is recognized by TRP53 and the respective checkpoints are activated until DNA damage is repaired and the cells can progress further through the cell cycle. A maybe increased TRP53 expression after *Hdac3* deletion might be helpful for that and therefore no S phase arrest could be seen in *Trp53* wildtype cell lines PPT3-F4764 and PPT3-F4402. The detected G2/M phase arrest fits to the published data, arguing that HDAC3 forms a complex with A-Kinase Anchor proteins AKAP95 and HA95 that are recruited to mitotic chromosomes and involved in mitotic progression. They also play an important role during the global histone deacetylation during mitosis together with HDAC3 (Li *et al.*, 2006). In case of *Hdac3* knock-out a correct progression through mitosis is not ensured, which could lead to activation of p53-dependent spindle-assembly checkpoint. It can be assumed that this function of HDAC3 in mitosis cannot be compensated or the damage caused by *Hdac3* deficiency needs more time, so that the cells are stuck in this phase. This would then result in a G2/M phase arrest, which would be in agreement with the observed G2/M phase arrest in the *Trp53* wildtype cell lines PPT3-F4764 and PPT3-F4402.

The two *Trp53* deficient cell lines PPT-F5061 and PPT2-F4699 show an increased number of cells in the G2/M phase after *Hdac3* knock-out as well (Figure 7-8 (B)). In addition to this, both *Trp53* deficient cell lines show an accumulation of cells in the S phase after loss of HDAC3 expression. In human nasopharyngeal carcinoma cells, S phase arrest can be induced via p53 independent mechanism by attenuating the PI3K/AKT signaling pathway (Lee *et al.*, 2018). HDAC3 can bind to AKT and deacetylates it, leading to AKT phosphorylation. Hence AKT is activated and DNA damage repair is promoted, at least in leukemia cells (Long *et al.*, 2017). Maybe also in pancreatic cancer, through loss of HDAC3, the AKT activation would be missing and the p53 independent cell cycle regulation via the PI3K/AKT pathway would not be functional, resulting in S phase arrest. Furthermore it was discussed, that p53 deficient cells progress slower through S phase, since DNA damage is not recognized and therefore not immediately repaired resulting in delayed DNA synthesis (Prost *et al.*, 1998). In case that DNA damage is not repaired as fast as in *Trpp53* wildtype cells, the delay in DNA synthesis would result in a S phase arrest. This is in agreement with the data presented herein, showing an accumulation of cells in S phase in *Trp53* deficient cells PPT2-F4699 and PPT-F5061 after *Hdac3* knock-out. Correct progression through G2/M phase is also secured by a p53 independent mechanism. This requires Cdk2 for direct phosphorylation of ATRIP and Cdc6, which in turn directly regulate G2/M transition via the ATR-Chk1-Cdc25A pathway (Chung and Bunz, 2010). Damages which are caused by *Hdac3* deficiency and avoid correct progression through G2/M phase, could be recognized by those p53 independent mechanisms, leading to a G2/M phase arrest. This can be a reason for the observed G2/M arrest in the *Trp53* deficient cell lines PPT-F5061 and PPT2-F4699.

In summary, it is likely that the differences observed in cell cycle progression are connected to the difference in *Trp53* status of the tested PDAC cell lines. To underpin this hypothesis a few experiments are necessary, starting with investigation of cell cycle markers to prove the results gained by FACS cell cycle analysis and validate the related TRP53 dependent and independent pathways. Until now, only two cell lines per group have been checked which are far too few to make an assured statement. Therefore, increasing the number of analyzed cell lines is strongly recommended.

If the difference in TRP53 expression is really the reason for the observed differences, remains to be seen. Since PDAC patients differ in the P53 status (Bailey *et al.*, 2016a), this observation is of high relevance for clinical studies. It opens up new opportunities

for patient specific combination therapies by targeting HDAC3 and maybe one of the respective pathways or checkpoints to push the cancer cells towards apoptosis.

Since there are no isoenzyme specific inhibitors available for HDAC1 and HDAC2, the observed effects on cell viability, colony formation and cell cycle distribution cannot be compared with inhibitor data. Therefore, it is not possible to draw any conclusions if the effect is due to the missing catalytic function of the specific HDAC isoenzyme or if the missing protein structure causes the effect. One reason for missing HDAC1 or HDAC2 specific inhibitors could be the high homologous sequence of the two isoenzymes. For HDAC3 a few specific inhibitors can be purchased and they seem to be potent in some cancer types (Beyer *et al.*, 2019; Yan *et al.*, 2018; Yu *et al.*, 2020). In the used cell lines, the tested HDAC3 specific inhibitor RGFP966 showed no effect on cell viability even if used in very high concentrations of 10 μ M (Figure S 2). For a better comparison between the effect of specific HDAC3 inhibition and *Hdac3* knock-out, those results need to be confirmed in *Hdac3* floxed cell lines PPT3-F4764, PPT3-F4402, PPT-F5061 and PPT2-F4699. This would be necessary to exclude cell line specific response to loss or inhibition of HDAC3 expression, too. Even if the response of the four tested cell lines to RGFP966 is very similar arguing against a distinct cell line specific response. Since the *Hdac3* knock-out results homogeneously in all four cell lines in a remarkable decrease in cell survival, and the inhibitor RGFP966 fails to decrease cell survival within 72 hours in four cell lines, it seems to be convincing that the inhibitor doesn't achieve results comparable to the knock-out. Nevertheless, a more detailed analysis of the differences between knock-out and inhibition is recommended by investigation and comparison of its effects on colony formation, cell cycle progression and acetylation pattern.

The term Cre toxicity describes the observation that Cre recombinase expression without any present floxed sequence can be responsible for genotoxic effects and reduced growth (Baba *et al.*, 2005; Higashi *et al.*, 2009; Loonstra *et al.*, 2001). As a reason, it is discussed that Cre can be expressed in several tissues, even if it is under control of a tissue-specific promoter (Wicksteed *et al.*, 2010). Another explanation could be, that in the mouse genome naturally occurring "cryptic" *loxP* sites exist, which differ in only a few nucleotides from the *loxP* sites. If those "cryptic" *loxP* sites are recognized and cut by the Cre recombinase, this causes DNA damage (Loonstra *et*

al., 2001). However next to cell death, DNA damage can lead to growth arrest, a main characteristic of Cre toxicity (Loonstra *et al.*, 2001; Su, 2006).

For these reasons it is important to include Cre expressing cell lines without any floxed sequences and to check for Cre toxicity in the used model. In this work, this was done by using two cell lines. Therefore, those control cell lines were treated with 4-OHT and EtOH, equivalent to the normal treatment used for deletion of HDAC isoenzymes. Since no effect was seen in the control cell lines PPT-15283 and PPT-F1679, neither on cell survival, nor on colony formation, Cre toxicity as a reason for decreased cell survival or colony formation can be ruled out. In one cell line PPT-F1679 also *Pdk1* is heterozygously floxed, as it is in the *Hdac2* floxed cell line PPT-F1648. Treating PPT-F1679 for eight days with 4-OHT revealed no difference in cell survival and colony formation. This confirms in addition, that heterozygous deletion of *Pdk1* has no phenotypic effect, which was also shown by others (Eser *et al.*, 2013), and therefore the documented differences between *Hdac2* pro- and deficient cells of the cell line PPT-F1648 can be traced back to the loss of HDAC2 expression and not to the heterozygous knock-out of *Pdk1*. In general, since Cre toxicity was excluded, the decreased cell viability and colony formation as well as the other effects that were detected in the floxed *Hdac* cell lines after 4-OHT treatment, can be attributed to the loss of the corresponding HDAC isoenzyme.

8.2 Epithelial and mesenchymal fraction of dual-recombinase based PDAC cell lines

To investigate the role of HDACs in different tumor subtypes, epithelial and mesenchymal fractions of the cell lines derived from the dual-recombinase model were generated through differential trypsinization (Mueller *et al.*, 2018). Therefore, the role of HDACs in well differentiated (epithelial) cells and undifferentiated (mesenchymal) cells could be investigated. Since it was shown previously that HDAC2 plays a role in undifferentiated tumors in humans (Fritsche *et al.*, 2009), further analysis of the role of HDAC2 in differentiated and undifferentiated subtype was performed. Recording cell survival and colony forming after *Hdac2* knock-out in epithelial and mesenchymal fractions revealed higher sensitivity against loss of HDAC2 expression in the mesenchymal subtypes of both tested cell lines. This let assume that mesenchymal PDAC cells are more dependent on HDAC2 expression.

This link between HDAC2 and mesenchymal cell morphology is also arguing for a relevance of HDAC2 in tumor differentiation and consequently also in metastatic spread. This was supported by the pathway analysis that was performed with *Hdac2* deficient cells derived from the dual-recombinase model and from the KPC model. RNA-Seq data from the inducible knock-out model were combined with MicroArray data from the constitutive knock-out model. Significantly downregulated genes of RNA-Seq analysis and MicroArray data show downregulation of EMT and EMT-related pathways in *Hdac2* deficient cells. Downregulated genes were analyzed to detect genes and pathways that are maintained by HDAC2 expression. Although HDACs are transcriptional repressors, some gene activating functions are described for class I HDACs (Somanath *et al.*, 2017; Zupkovitz *et al.*, 2006). Even if the responsible mechanisms are still unknown and it remains to be elucidate whether it is a direct or indirect mode of action, these first insights lead to an interesting new research topic (Somanath *et al.*, 2017).

The EMT-related pathways hypoxia and glycolysis were strongly downregulated after *Hdac2* knock-out and they are linked to the process of metastasis formation. Hypoxia is not only a result of rapid tumor growth but is also important for promoting tumor progression. PDAC is a highly hypoxic cancer and in those areas a decreased expression of E-cadherin accompanied by an increased expression of N-cadherin has been found, indicating the activation of EMT in hypoxic PDAC (Yuen and Diaz, 2014). Since it was already shown under normoxic conditions that a complex consisting of SNAIL, HDAC1 and HDAC2 is involved in suppression of E-cadherin in PDAC (von Burstin *et al.*, 2009), it would be worth to investigate if this could also be observed under hypoxic conditions. Maybe this could link HDAC2 with hypoxia related EMT. Another study identified a new HIF-2 α -miR301a-TP63 signaling pathway playing an important role in hypoxia-induced EMT in PDAC (Zhang *et al.*, 2020). If and how HDAC2 can influence this pathway by controlling p63 functions, as it was shown in epidermal progenitor cells, needs to be further investigated (LeBoeuf *et al.*, 2010). By far the strongest downregulated pathway in *Hdac2* deficient cells was epithelial-to-mesenchymal transition. On the one hand, EMT is one hallmark of undifferentiated tumors which are more sensitive to loss of HDAC2 expression and on the other hand, TGF β is one of the main driving forces in EMT. Therefore, the question arose if *Hdac2* knock-out prevents PDAC cells from undergoing EMT and formation of metastases when the TGF β pathway is activated. To study this hypothesis, *Hdac2* deficient cells

of both mouse models were treated additionally with TGF β to induce EMT and cell survival and colony formation was analyzed. Those assays showed that TGF β treatment in *Hdac2* deficient cells leads to reduced cell survival and colony formation, especially in the mesenchymal fractions.

It is discussed that TGF β is involved in several pathways which control cell survival and cell death, but its mode of action is highly dependent on cell type and cellular context and is not yet fully understood (Massague, 2012; Zhang *et al.*, 2017b). The role of TGF β as a survival signal was discussed in follicular dendritic cells, in microglia as well as in murine mammary carcinoma cells. On the contrary, in pancreatic epithelial cells, the TGF β response gene TIEG1 contributes to proapoptotic effects of TGF β via suppression of Bcl2 (Zhang *et al.*, 2017b). In pancreatic cancer cells with functional SMAD4 TGF β was shown to induce SNAIL and SOX4 expression. Through a resultant SMAD/SNAIL complex, KLF5 expression is repressed and in through the following absence of KLF5, SOX4 induced apoptosis (David *et al.*, 2016). In case of mutated *Smad4*, induction of SNAIL fails since SMAD4 containing transcriptional complex is not functional, but still SOX4 is expressed. As well, repression of KLF5 is no longer observed since the repressing SMAD/SNAIL complex is not existing. Consequently, SOX4 and KLF5 can cooperate and drive tumorigenesis as well as metastatic spread. This switch in SOX4 function modifies EMT to a lethal event in SMAD4 positive PDAC cells (David *et al.*, 2016). If the observed reduction in metastasis frequency in *Hdac2* deficient PDAC cells is connected to those mechanisms and is a consequence of lethal EMT requires further investigations.

In addition it was previously shown, that a SNAIL/HDAC1/HDAC2 repressor complex is crucial for E-cadherin downregulation and therefore contributes to the EMT process when TGF β is present. This could be prevented by combined treatment of TGF β and a class I specific HDACi valproic acid (von Burstin *et al.*, 2009), supporting also the findings presented here, that HDACs can contribute to metastatic spread.

Since redundant functions of HDAC isoenzymes are frequently discussed, the effect of TGF β treatment on *Hdac1* and *Hdac3* deficient PDAC cells was tested. The survival of those cells is affected within 72 h by loss of the HDAC isoenzyme but not further decreased by TGF β treatment in the respective cell line. Colony formation was also affected slightly after *Hdac1* knock-out in PPT-F3641 but stayed at the same level despite TGF β treatment. For *Hdac3* deficient cell line PPT2-F4699, a decrease in cell viability and colony formation was seen, but again no further decrease due to TGF β

treatment was observed in both assays. Those data presented herein show that specifically HDAC2 and not HDAC1 or HDAC3 is relevant in the TGF β signaling pathway.

Consequently, from all the described findings, the question arose how TGF β receptors are involved. To investigate this the cell line PPT-F1648 was chosen, since the pathway analysis was based on the RNA-Seq data derived from this cell line. Therefore, TGF β receptors were blocked using inhibitors against TGF β RI and/or TGF β RII in *Hdac2* deficient PDAC cells after eight days of 4-OHT treatment. The previous inhibition of TGF β RI by Galunisertib or TGF β RI/II by LY2109761 followed by an additional TGF β treatment in *Hdac2* deficient cells showed no effect on survival within 72 hours, but rescued the deficiency in colony formation ability to the level of *Hdac2* proficient cells. It was expected that TGF β treatment decreases survival even further in *Hdac2* deficient cells within 72 h. That this observation is lacking could be explained by the morphology of this cell line. PPT-F1648 cell population shows a mixed morphology of epithelial and mesenchymal cells. Maybe the effect on the highly sensitive mesenchymal subpopulation is unrecognized because the epithelial subpopulation is overgrowing due to less sensitivity. Treatment of seven days for colony formation assay reproduced the results of the previously investigated cell lines. Further analysis concerning the effectiveness of the tested TGF β receptor inhibitors in the other available cell lines of both mouse models is highly recommended.

In general, the observations gained by the inhibitor treatment lead to the conclusion, that HDAC2 is needed to transduce TGF β signaling via TGF β R and if HDAC2 is missing, the TGF β signaling pathway is not functional. An attempted explanation is that HDAC2 acts as a TGF β signal transducer and its absence leads to some kind of stress when TGF β is present. Which stress this could be and if this leads to apoptosis in a form of lethal EMT or activates other pathways leading to inhibition of colony formation is still an unsolved question and requires further investigation. Similar levels of colony formation upon TGF β receptor inhibition in *Hdac2* pro- deficient cells could be a hint, that the TGF β signaling is blocked previous to any intracellular activation and therefore it doesn't matter if HDAC2 is present or not. Since no effect on cell survival was seen after 72 hours, it seems to be an EMT related observation or maybe also the timeframe of 72 hours was too short to observe any changes.

In general, it is recommended to investigate if lethal EMT can be found in those cell lines and could serve as an explanation for decreased colony formation. Therefore, it is necessary to check if apoptosis is observed and if markers for lethal EMT can be found. Additionally, the analysis of SMAD4 status would be required. Despite this it is necessary to verify the rescue of TGF β induced reduction in colony formation upon inhibition of TGF β receptors in other cell lines.

It was also observed, that TGF β treatment in *Hdac2* deficient epithelial and mesenchymal fractions leads to a stronger decrease in cell survival and colony formation in the mesenchymal compared to the epithelial fraction. Maybe this could be explained by this context specificity of TGF β response, arguing for a higher dependency on HDAC2 mediation in TGF β signaling in mesenchymal cells. Further analyses are required to research, if mesenchymal and epithelial fractions differ in their response to TGF β treatment, when TGF β receptors are inhibited previously in combination with the absence of HDAC2.

It was summarized by Massague (2012) that three types of determinants are involved in the TGF β mediated response. Besides the factors that are involved in signal transduction and transcription, the epigenetic status of the cell contributes to the TGF β mediated response. The epigenetic status of a cell is responsible for open and closed chromatin conformation and consequently its accessibility for example for SMAD complexes (Massague, 2012). It could be possible that loss of HDAC2 expression affects those chromatin remodeling processes and therefore influences the TGF β signaling. Although surprisingly H3K27ac was not changed upon *Hdac2* knock-out in PPT-F1648 cells, it is necessary to further analyze the effects of *Hdac2* knock-out in the mesenchymal and epithelial fractions. This would also be necessary to reveal more specifically the role of HDAC2 in a more homogeneous cellular context.

In PDAC TGF β expression is associated with advanced tumor stages, shorter survival and liver metastases (Shen *et al.*, 2017; Teraoka *et al.*, 2001). Independent of TGF β , it was also found by other research groups, that HDACs play a role during the EMT process. For example in castration-resistant prostate cancer where HDACi LBH589 led to inhibition of epithelial-mesenchymal plasticity by suppression of HMGA2 expression (Ruscetti *et al.*, 2016). In addition, the HDACi TSA blocked the change from epithelial to spindle-like morphology in the presence of TGF β in renal epithelial cells (Yoshikawa *et al.*, 2007). It was also shown in metastatic renal cancer cells that HDACi treatment and knockout of HDAC1/HDAC2 reduced E-cadherin and PDGFR β

expression, with PDGFR β being a key driver of metastasis formation in this cancer type. But GO term revealed no changes in signaling pathways that are linked to EMT in renal cancer cells. This hints at HDACs being involved in regulation of EMT-associated proteins, but not directly in EMT in this cancer type (Kiweler *et al.*, 2018). In the herein tested PDAC cells, no robust change in PDGFR β expression could be found upon *Hdac2* knock-out, but those data were very heterogeneous and this discrepancy needs to be further investigated, for example by repetition of those experiments also in an increased number of cell lines. Maybe HDACs function and their contribution to EMT differs between the cancer types or is only relevant on other regulatory levels like protein stabilization etc.

Since HDAC2 is part of repressor complexes which are involved in chromatin remodeling, a different result has been expected. As described above, despite no observed changes in H3K27ac, there are other regulatory mechanisms like involving methylation and phosphorylation patterns that could cause the observed regulation of mRNA (Morgan and Shilatifard, 2015). Nevertheless, it is recommended, that the results of H3K27ac of PPT-F1648 need to be verified not only in other cell lines of the dual-recombinase model, but also in cell lines of the KPC mouse model.

In summary, those observations offer a first evidence, that HDAC2 is involved in TGF β induced EMT, even if the detailed mechanism is still obscure and requires further investigations. But nevertheless, the data indicate that targeting HDAC2 could be an opportunity to treat metastatic PDAC.

8.3 *In vivo* phenotype of *Hdac2* deficient KPC mice

After analyzing the effect of *Hdac2* knock-out *in vitro*, the consequence was to look for *in vivo* effects of *Hdac2* knock-out. Therefore, the KPC mouse model was combined with a *Hdac2* floxed mouse line, to generate a constitutive *Hdac2* deficient mouse model. Those animals were investigated in the first instance concerning survival and tumor development. The Kaplan-Meier survival curve shows no difference, due to homozygous or heterozygous knock-out of *Hdac2* compared to the KPC wildtype mice. This is contrary to the observed survival deficit in *Hdac2* deficient cells after acute knock-out of *Hdac2* in the Pdx-Flp model. Zimmermann and colleagues crossed HDAC2-mutant mice that have a catalytically inactive HDAC2 with tumor-prone APC^{min}

mice to investigate whether HDAC2 is necessary for development of intestinal tumor formation as well as development and function of the complete organism. Besides fewer intestinal tumors and smaller body size, no survival difference was found in HDAC2 inactive mice (Zimmermann *et al.*, 2007). The analysis of the role of HDACs for development, especially brain development, revealed catalytically inactive HDAC2 leading to a more severe phenotype than the heterozygous or homozygous deletion of *Hdac2* (Hagelkruys *et al.*, 2016). It seems that there are HDAC2 specific functions that cannot be compensated by other HDAC isoenzymes in certain tissues (Zimmermann *et al.*, 2007). The observed survival data in KPC mice with either no deletion or hetero-/homozygous knock-out of *Hdac2* could be explained by the compensatory role of HDAC1. Compared to the KPC model where HDAC1 is upregulated in the *Hdac2* deficient mice, in the acute knock-out model no difference in HDAC1 expression can be seen (Figure S 3). Probably the upregulation of HDAC1 and therefore a compensation of the survival deficit takes a while and is only visible in the constitutive knock-out model. If *Hdac2* deficient cells of the dual-recombination model were be cultivated over several weeks or months, a compensation of the survival deficit by upregulation of HDAC1 would be expected, but this remains to be proven.

Hdac2 pro- and deficient mice developed PDAC, but fewer undifferentiated tumors were detected in the *Hdac2* deficient group. The undifferentiated tumors have mainly mesenchymal characteristics and the observation of the decreased number of undifferentiated tumors when mice are lacking HDAC2 seems to indicate a relevance of HDAC2 for this differentiation state. This also follows the results of the epithelial and mesenchymal fractions of the dual-recombinase model, where the higher sensitivity of the mesenchymal subtype to *Hdac2* knock-out was documented, in comparison to the epithelial subtype. No variation in HDAC2 expression between the different stages of PDAC development is observed in *Hdac2* proficient KPC mice (Figure S 4), which is contrary to the results of human tissues, where a higher expression of HDAC2 in undifferentiated PDAC was detected (Fritsche *et al.*, 2009). A reason for this could be that the undifferentiated tumors of the KPC model already have a sufficient level of HDAC2 but are highly dependent on this isoenzyme and are not able to compensate its loss. Maybe it is also an explanation, that not the expression of HDAC2 itself, but its enzymatic activity is regulated in the murine PDAC stages. There are several options to regulate enzymatic activity of HDACs. For example, in HDAC containing

protein complexes, the binding of cofactors to the core complexes could be necessary for an active complex, and also posttranslational modifications like phosphorylation, acetylation, sumoylation etc. of HDACs depict a possibility for regulation of their activity (Seto and Yoshida, 2014). HDAC2 activity is promoted by phosphorylation and affects complex formation with Sin3 (Segre and Chiocca, 2011). It was also shown that HDAC2 sumoylation is needed for NF κ B activation in colon cancer cells and therefore protects those cells from genotoxic stress (Wagner *et al.*, 2015). If and how those regulations of HDAC activity especially for HDAC2 play a role in PDAC remains to be elucidated and needs further investigations.

To further validate the above described *in vitro* results and to verify the link between HDAC2 and formation of metastases, the *Hdac2* pro- and deficient cohorts of KPC mice were screened for metastases. In human PDAC patients, metastases occur frequently in lung and liver (Le Large *et al.*, 2017). Therefore, those two organs were screened systematically. And indeed, fewer metastases were observed in the *Hdac2* deficient KPC mice in both, liver and lungs. In addition, significantly more *Hdac2* deficient mice did not develop metastases at all, compared to the control cohort. This result emphasizes the importance of HDAC2 in the process of metastatic spread and fits to previous observations (von Burstin *et al.*, 2009). Immunohistochemical analysis of the metastasis in livers and lungs of *Hdac2* deficient mice revealed no HDAC2 expression in the tumor cells, compared to the surrounding liver or lung tissue. This argues for additional HDAC2 independent ways of metastatic spread. Nevertheless, blocking one road of metastasis formation decreases the chance of metastasis and therefore increases the patient's prognosis.

Comparison of the results from *Hdac2* acute und constitutive knock-out models shows that the growth arrest and survival deficit upon loss of HDAC2 expression is reversible, since the mice developed tumors and have the same life expectancy. But it was shown that HDAC2 plays a unique role in tumor progression and its importance for metastatic spread, which cannot be compensated and therefore should not be underestimated.

Future studies need to investigate the details of HDAC2 contribution in the formation of metastasis to fully understand the mechanism. The performed experiments using TGF β for induction of EMT present first results that HDAC2 plays a role during TGF β induced EMT as explained above. The detailed mechanism and how exactly HDAC2

is involved in this pathway is still unknown and further experiments to solve those unknown questions are required. Those experiments will be necessary to extend the knowledge gained from this work to target-aimed therapeutic options.

This work was designed to systematically analyze the role of the HDAC isoenzymes HDAC1, HDAC2 and HDAC3 in pancreatic cancer. In sum, the presented data show higher effects of coincident genetic deletion of the three HDAC isoenzymes *Hdac1/Hdac2/Hdac3* over their inhibition was shown, arguing for the development of a new inhibitor class like PROTACs to specifically target and eliminate the HDAC isoenzymes. In addition it is demonstrated, that isoenzyme specific deletion is a promising therapy option for PDAC, with HDAC1 being the least efficient isoenzyme for affecting PDAC maintenance, while deletion of HDAC3 attenuates cell survival and colony formation most. A validation of the different effects of *Hdac3* knock-out in a Trp53 dependent context is remaining and could be of clinical relevance and contribute to personalized therapy in the future. HDAC2 deletion also resulted in a relatively strong reduction in tumor cell survival and colony formation. Besides the unexpected finding of unchanged H3K27ac after *Hdac2* knock-out, which also needs verification, surprisingly additional insight in the role of HDACs as activators were given by the downregulated genes after *Hdac2* knock-out, that represent a gene set which are maintained by HDAC2 expression. This function of HDACs is still widely unknown, but recently gains increasing attention, opening new research topics. In addition, a dependency of mesenchymal cells on specifically HDAC2 was proven. It is also presented that HDAC2 contributes to TGF β induced EMT *in vitro* and *in vivo* and its deletion leads to reduced metastatic spread in liver and lung of mice suffering from PDAC. Also, significantly more animals were free of metastases in both organs when HDAC2 expression was lost. All in all, those data point towards a role of HDAC2 in the process of metastatic spread and the reduce metastasis probability according to *Hdac2* deletion could be of therapeutic relevance for PDAC patients in future.

9. Reference List

- Adamska, A., Domenichini, A., and Falasca, M. (2017). Pancreatic Ductal Adenocarcinoma: Current and Evolving Therapies. *Int J Mol Sci* 18.
- Afgan, E., Baker, D., van den Beek, M., Blankenberg, D., Bouvier, D., Cech, M., Chilton, J., Clements, D., Coraor, N., Eberhard, C., *et al.* (2016). The Galaxy platform for accessible, reproducible and collaborative biomedical analyses: 2016 update. *Nucleic Acids Res* 44, W3-W10.
- Aghdassi, A., Sandler, M., Guenther, A., Mayerle, J., Behn, C.O., Heidecke, C.D., Friess, H., Buchler, M., Evert, M., Lerch, M.M., *et al.* (2012). Recruitment of histone deacetylases HDAC1 and HDAC2 by the transcriptional repressor ZEB1 downregulates E-cadherin expression in pancreatic cancer. *Gut* 61, 439-448.
- Ahmed, A., Yang, J., Maya-Mendoza, A., Jackson, D.A., and Ashcroft, M. (2011). Pharmacological activation of a novel p53-dependent S-phase checkpoint involving CHK-1. *Cell Death Dis* 2, e160.
- Ahmed, S., Bradshaw, A.D., Gera, S., Dewan, M.Z., and Xu, R. (2017). The TGF-beta/Smad4 Signaling Pathway in Pancreatic Carcinogenesis and Its Clinical Significance. *J Clin Med* 6.
- Aichler, M., Seiler, C., Tost, M., Siveke, J., Mazur, P.K., Da Silva-Buttkus, P., Bartsch, D.K., Langer, P., Chiblak, S., Durr, A., *et al.* (2012). Origin of pancreatic ductal adenocarcinoma from atypical flat lesions: a comparative study in transgenic mice and human tissues. *J Pathol* 226, 723-734.
- Anders, S., Pyl, P.T., and Huber, W. (2015). HTSeq--a Python framework to work with high-throughput sequencing data. *Bioinformatics* 31, 166-169.
- Arlt, A., and Schafer, H. (2016). Investigational histone deacetylase inhibitors for treating pancreatic adenocarcinoma. *Expert Opin Investig Drugs* 25, 1251-1254.
- Ayer, D.E. (1999). Histone deacetylases: transcriptional repression with SINers and NuRDs. *Trends Cell Biol* 9, 193-198.
- Baba, Y., Nakano, M., Yamada, Y., Saito, I., and Kanegae, Y. (2005). Practical range of effective dose for Cre recombinase-expressing recombinant adenovirus without cell toxicity in mammalian cells. *Microbiol Immunol* 49, 559-570.
- Bai, J., Sui, J., Demirjian, A., Vollmer, C.M., Jr., Marasco, W., and Callery, M.P. (2005). Predominant Bcl-XL knockdown disables antiapoptotic mechanisms: tumor necrosis factor-related apoptosis-inducing ligand-based triple chemotherapy overcomes chemoresistance in pancreatic cancer cells in vitro. *Cancer Res* 65, 2344-2352.

Bailey, J.M., Hendley, A.M., Lafaro, K.J., Pruski, M.A., Jones, N.C., Alsina, J., Younes, M., Maitra, A., McAllister, F., Iacobuzio-Donahue, C.A., *et al.* (2016a). p53 mutations cooperate with oncogenic Kras to promote adenocarcinoma from pancreatic ductal cells. *Oncogene* 35, 4282-4288.

Bailey, P., Chang, D.K., Nones, K., Johns, A.L., Patch, A.M., Gingras, M.C., Miller, D.K., Christ, A.N., Bruxner, T.J., Quinn, M.C., *et al.* (2016b). Genomic analyses identify molecular subtypes of pancreatic cancer. *Nature* 531, 47-52.

Bernabeu, C., Lopez-Novoa, J.M., and Quintanilla, M. (2009). The emerging role of TGF-beta superfamily coreceptors in cancer. *Biochim Biophys Acta* 1792, 954-973.

Beyer, M., Romanski, A., Mustafa, A.M., Pons, M., Buchler, I., Vogel, A., Pautz, A., Sellmer, A., Schneider, G., Bug, G., *et al.* (2019). HDAC3 Activity is Essential for Human Leukemic Cell Growth and the Expression of beta-catenin, MYC, and WT1. *Cancers (Basel)* 11.

Bhaskara, S., Chyla, B.J., Amann, J.M., Knutson, S.K., Cortez, D., Sun, Z.W., and Hiebert, S.W. (2008). Deletion of histone deacetylase 3 reveals critical roles in S phase progression and DNA damage control. *Mol Cell* 30, 61-72.

Bhaskara, S., Knutson, S.K., Jiang, G., Chandrasekharan, M.B., Wilson, A.J., Zheng, S., Yenamandra, A., Locke, K., Yuan, J.L., Bonine-Summers, A.R., *et al.* (2010). Hdac3 is essential for the maintenance of chromatin structure and genome stability. *Cancer Cell* 18, 436-447.

Bolden, J.E., Peart, M.J., and Johnstone, R.W. (2006). Anticancer activities of histone deacetylase inhibitors. *Nat Rev Drug Discov* 5, 769-784.

Brar, G., Blais, E.M., Joseph Bender, R., Brody, J.R., Sohal, D., Madhavan, S., Picozzi, V.J., Hendifar, A.E., Chung, V.M., Halverson, D., *et al.* (2019). Multi-omic molecular comparison of primary versus metastatic pancreatic tumours. *Br J Cancer* 121, 264-270.

Brugge, W.R., Lauwers, G.Y., Sahani, D., Fernandez-del Castillo, C., and Warshaw, A.L. (2004). Cystic neoplasms of the pancreas. *N Engl J Med* 351, 1218-1226.

Burris, H.A., 3rd, Moore, M.J., Andersen, J., Green, M.R., Rothenberg, M.L., Modiano, M.R., Cripps, M.C., Portenoy, R.K., Storniolo, A.M., Tarassoff, P., *et al.* (1997). Improvements in survival and clinical benefit with gemcitabine as first-line therapy for patients with advanced pancreas cancer: a randomized trial. *J Clin Oncol* 15, 2403-2413.

Cai, M.H., Xu, X.G., Yan, S.L., Sun, Z., Ying, Y., Wang, B.K., and Tu, Y.X. (2018). Depletion of HDAC1, 7 and 8 by Histone Deacetylase Inhibition Confers Elimination of Pancreatic Cancer Stem Cells in Combination with Gemcitabine. *Sci Rep* 8, 1621.

Chari, S.T., Kelly, K., Hollingsworth, M.A., Thayer, S.P., Ahlquist, D.A., Andersen, D.K., Batra, S.K., Brentnall, T.A., Canto, M., Cleeter, D.F., *et al.* (2015). Early detection of sporadic pancreatic cancer: summative review. *Pancreas* 44, 693-712.

Chiou, S.H., Risca, V.I., Wang, G.X., Yang, D., Gruner, B.M., Kathiria, A.S., Ma, R.K., Vaka, D., Chu, P., Kozak, M., *et al.* (2017). BLIMP1 Induces Transient Metastatic Heterogeneity in Pancreatic Cancer. *Cancer Discov* 7, 1184-1199.

Chung, J.H., and Bunz, F. (2010). Cdk2 is required for p53-independent G2/M checkpoint control. *PLoS Genet* 6, e1000863.

Collisson, E.A., Sadanandam, A., Olson, P., Gibb, W.J., Truitt, M., Gu, S., Cooc, J., Weinkle, J., Kim, G.E., Jakkula, L., *et al.* (2011). Subtypes of pancreatic ductal adenocarcinoma and their differing responses to therapy. *Nat Med* 17, 500-503.

Conroy, T., Desseigne, F., Ychou, M., Bouche, O., Guimbaud, R., Becouarn, Y., Adenis, A., Raoul, J.L., Gourgou-Bourgade, S., de la Fouchardiere, C., *et al.* (2011). FOLFIRINOX versus gemcitabine for metastatic pancreatic cancer. *N Engl J Med* 364, 1817-1825.

Conte, M., Dell'Aversana, C., Sgueglia, G., Carissimo, A., and Altucci, L. (2019). HDAC2-dependent miRNA signature in acute myeloid leukemia. *FEBS Lett* 593, 2574-2584.

Cress, W.D., and Seto, E. (2000). Histone deacetylases, transcriptional control, and cancer. *J Cell Physiol* 184, 1-16.

Datta, M., Staszewski, O., Raschi, E., Frosch, M., Hagemeyer, N., Tay, T.L., Blank, T., Kreutzfeldt, M., Merkler, D., Ziegler-Waldkirch, S., *et al.* (2018). Histone Deacetylases 1 and 2 Regulate Microglia Function during Development, Homeostasis, and Neurodegeneration in a Context-Dependent Manner. *Immunity* 48, 514-529 e516.

David, C.J., Huang, Y.H., Chen, M., Su, J., Zou, Y., Bardeesy, N., Iacobuzio-Donahue, C.A., and Massague, J. (2016). TGF-beta Tumor Suppression through a Lethal EMT. *Cell* 164, 1015-1030.

Deeb, A., Haque, S.U., and Olowokure, O. (2015). Pulmonary metastases in pancreatic cancer, is there a survival influence? *J Gastrointest Oncol* 6, E48-51.

Dovey, O.M., Foster, C.T., and Cowley, S.M. (2010). Histone deacetylase 1 (HDAC1), but not HDAC2, controls embryonic stem cell differentiation. *Proc Natl Acad Sci U S A* 107, 8242-8247.

Eckschlager, T., Plch, J., Stiborova, M., and Hrabeta, J. (2017). Histone Deacetylase Inhibitors as Anticancer Drugs. *Int J Mol Sci* 18.

Engeland, K. (2018). Cell cycle arrest through indirect transcriptional repression by p53: I have a DREAM. *Cell Death Differ* 25, 114-132.

Eot-Houllier, G., Fulcrand, G., Watanabe, Y., Magnaghi-Jaulin, L., and Jaulin, C. (2008). Histone deacetylase 3 is required for centromeric H3K4 deacetylation and sister chromatid cohesion. *Genes Dev* 22, 2639-2644.

Eser, S., Reiff, N., Messer, M., Seidler, B., Gottschalk, K., Dobler, M., Hieber, M., Arbeiter, A., Klein, S., Kong, B., *et al.* (2013). Selective requirement of PI3K/PDK1 signaling for Kras oncogene-driven pancreatic cell plasticity and cancer. *Cancer Cell* 23, 406-420.

Fouad, Y.A., and Aanei, C. (2017). Revisiting the hallmarks of cancer. *Am J Cancer Res* 7, 1016-1036.

Fritsche, P., Seidler, B., Schuler, S., Schnieke, A., Gottlicher, M., Schmid, R.M., Saur, D., and Schneider, G. (2009). HDAC2 mediates therapeutic resistance of pancreatic cancer cells via the BH3-only protein NOXA. *Gut* 58, 1399-1409.

Garcia-Morales, P., Gomez-Martinez, A., Carrato, A., Martinez-Lacaci, I., Barbera, V.M., Soto, J.L., Carrasco-Garcia, E., Menendez-Gutierrez, M.P., Castro-Galache, M.D., Ferragut, J.A., *et al.* (2005). Histone deacetylase inhibitors induced caspase-independent apoptosis in human pancreatic adenocarcinoma cell lines. *Mol Cancer Ther* 4, 1222-1230.

Gbolahan, O.B., Tong, Y., Sehdev, A., O'Neil, B., and Shahda, S. (2019). Overall survival of patients with recurrent pancreatic cancer treated with systemic therapy: a retrospective study. *BMC Cancer* 19, 468.

Giaginis, C., Damaskos, C., Koutsounas, I., Zizi-Serbetzoglou, A., Tsoukalas, N., Patsouris, E., Kouraklis, G., and Theocharis, S. (2015). Histone deacetylase (HDAC)-1, -2, -4 and -6 expression in human pancreatic adenocarcinoma: associations with clinicopathological parameters, tumor proliferative capacity and patients' survival. *BMC Gastroenterol* 15, 148.

Giardiello, F.M., Brensinger, J.D., Tersmette, A.C., Goodman, S.N., Petersen, G.M., Booker, S.V., Cruz-Correa, M., and Offerhaus, J.A. (2000). Very high risk of cancer in familial Peutz-Jeghers syndrome. *Gastroenterology* 119, 1447-1453.

Giono, L.E., and Manfredi, J.J. (2006). The p53 tumor suppressor participates in multiple cell cycle checkpoints. *J Cell Physiol* 209, 13-20.

Giovannetti, E., van der Borden, C.L., Frampton, A.E., Ali, A., Firuzi, O., and Peters, G.J. (2017). Never let it go: Stopping key mechanisms underlying metastasis to fight pancreatic cancer. *Semin Cancer Biol* 44, 43-59.

Global Burden of Disease Cancer, C., Fitzmaurice, C., Dicker, D., Pain, A., Hamavid, H., Moradi-Lakeh, M., MacIntyre, M.F., Allen, C., Hansen, G., Woodbrook, R., *et al.* (2015). The Global Burden of Cancer 2013. *JAMA Oncol* 1, 505-527.

Goecks, J., Eberhard, C., Too, T., Galaxy, T., Nekrutenko, A., and Taylor, J. (2013). Web-based visual analysis for high-throughput genomics. *BMC Genomics* 14, 397.

Goggins, M., Schutte, M., Lu, J., Moskaluk, C.A., Weinstein, C.L., Petersen, G.M., Yeo, C.J., Jackson, C.E., Lynch, H.T., Hruban, R.H., *et al.* (1996). Germline BRCA2 gene mutations in patients with apparently sporadic pancreatic carcinomas. *Cancer Res* 56, 5360-5364.

Grozinger, C.M., Hassig, C.A., and Schreiber, S.L. (1999). Three proteins define a class of human histone deacetylases related to yeast Hda1p. *Proc Natl Acad Sci U S A* 96, 4868-4873.

Grozinger, C.M., and Schreiber, S.L. (2002). Deacetylase enzymes: biological functions and the use of small-molecule inhibitors. *Chem Biol* 9, 3-16.

Gu, H., Liang, Y., Mandel, G., and Roizman, B. (2005). Components of the REST/CoREST/histone deacetylase repressor complex are disrupted, modified, and translocated in HSV-1-infected cells. *Proc Natl Acad Sci U S A* 102, 7571-7576.

Haberland, M., Johnson, A., Mokalled, M.H., Montgomery, R.L., and Olson, E.N. (2009a). Genetic dissection of histone deacetylase requirement in tumor cells. *Proc Natl Acad Sci U S A* 106, 7751-7755.

Haberland, M., Montgomery, R.L., and Olson, E.N. (2009b). The many roles of histone deacetylases in development and physiology: implications for disease and therapy. *Nat Rev Genet* 10, 32-42.

Hagelkruys, A., Lagger, S., Krahmer, J., Leopoldi, A., Artaker, M., Pusch, O., Zezula, J., Weissmann, S., Xie, Y., Schofer, C., *et al.* (2014). A single allele of Hdac2 but not Hdac1 is sufficient for normal mouse brain development in the absence of its paralog. *Development* 141, 604-616.

Hagelkruys, A., Mattes, K., Moos, V., Rennmayr, M., Ringbauer, M., Sawicka, A., and Seiser, C. (2016). Essential Nonredundant Function of the Catalytic Activity of Histone Deacetylase 2 in Mouse Development. *Mol Cell Biol* 36, 462-474.

Hanahan, D., and Weinberg, R.A. (2000). The hallmarks of cancer. *Cell* 100, 57-70.

Hanahan, D., and Weinberg, R.A. (2011). Hallmarks of cancer: the next generation. *Cell* 144, 646-674.

Heideman, M.R., Lancini, C., Proost, N., Yanover, E., Jacobs, H., and Dannenberg, J.H. (2014). Sin3a-associated Hdac1 and Hdac2 are essential for hematopoietic stem cell homeostasis and contribute differentially to hematopoiesis. *Haematologica* 99, 1292-1303.

Hessmann, E., and Ellenrieder, V. (2019). Chromatin remodelling controls pancreatic tissue fate. *Gut* 68, 1139-1140.

Hessmann, E., Johnsen, S.A., Siveke, J.T., and Ellenrieder, V. (2017). Epigenetic treatment of pancreatic cancer: is there a therapeutic perspective on the horizon? *Gut* 66, 168-179.

Hezel, A.F., Kimmelman, A.C., Stanger, B.Z., Bardeesy, N., and Depinho, R.A. (2006). Genetics and biology of pancreatic ductal adenocarcinoma. *Genes Dev* 20, 1218-1249.

Higashi, A.Y., Ikawa, T., Muramatsu, M., Economides, A.N., Niwa, A., Okuda, T., Murphy, A.J., Rojas, J., Heike, T., Nakahata, T., *et al.* (2009). Direct hematological toxicity and illegitimate chromosomal recombination caused by the systemic activation of CreERT2. *J Immunol* 182, 5633-5640.

Hingorani, S.R., Petricoin, E.F., Maitra, A., Rajapakse, V., King, C., Jacobetz, M.A., Ross, S., Conrads, T.P., Veenstra, T.D., Hitt, B.A., *et al.* (2003). Preinvasive and invasive ductal pancreatic cancer and its early detection in the mouse. *Cancer Cell* 4, 437-450.

Hingorani, S.R., Wang, L., Multani, A.S., Combs, C., Deramaudt, T.B., Hruban, R.H., Rustgi, A.K., Chang, S., and Tuveson, D.A. (2005). Trp53R172H and KrasG12D cooperate to promote chromosomal instability and widely metastatic pancreatic ductal adenocarcinoma in mice. *Cancer Cell* 7, 469-483.

Hruban, R.H., Goggins, M., Parsons, J., and Kern, S.E. (2000). Progression model for pancreatic cancer. *Clin Cancer Res* 6, 2969-2972.

Huang, Y.H., Hu, J., Chen, F., Lecomte, N., Basnet, H., David, C.J., Witkin, M.D., Allen, P.J., Leach, S.D., Hollmann, T.J., *et al.* (2020). ID1 Mediates Escape from TGFbeta Tumor Suppression in Pancreatic Cancer. *Cancer Discov* 10, 142-157.

Iodice, S., Gandini, S., Maisonneuve, P., and Lowenfels, A.B. (2008). Tobacco and the risk of pancreatic cancer: a review and meta-analysis. *Langenbecks Arch Surg* 393, 535-545.

Iwatsuki, M., Mimori, K., Yokobori, T., Ishi, H., Beppu, T., Nakamori, S., Baba, H., and Mori, M. (2010). Epithelial-mesenchymal transition in cancer development and its clinical significance. *Cancer Sci* 101, 293-299.

Jackson, E.L., Willis, N., Mercer, K., Bronson, R.T., Crowley, D., Montoya, R., Jacks, T., and Tuveson, D.A. (2001). Analysis of lung tumor initiation and progression using conditional expression of oncogenic K-ras. *Genes Dev* 15, 3243-3248.

Janbandhu, V.C., Moik, D., and Fassler, R. (2014). Cre recombinase induces DNA damage and tetraploidy in the absence of loxP sites. *Cell Cycle* 13, 462-470.

Janssen, Q.P., O'Reilly, E.M., van Eijck, C.H.J., and Groot Koerkamp, B. (2020). Neoadjuvant Treatment in Patients With Resectable and Borderline Resectable Pancreatic Cancer. *Front Oncol* 10, 41.

Jechlinger, M., Sommer, A., Moriggl, R., Seither, P., Kraut, N., Capodiecci, P., Donovan, M., Cordon-Cardo, C., Beug, H., and Grunert, S. (2006). Autocrine PDGFR signaling promotes mammary cancer metastasis. *J Clin Invest* *116*, 1561-1570.

Jiao, F., Hu, H., Yuan, C., Jin, Z., Guo, Z., Wang, L., and Wang, L. (2014). Histone deacetylase 3 promotes pancreatic cancer cell proliferation, invasion and increases drug-resistance through histone modification of P27, P53 and Bax. *Int J Oncol* *45*, 1523-1530.

Jung, H., Kim, J.Y., Kim, K.B., Chae, Y.C., Hahn, Y., Kim, J.W., and Seo, S.B. (2018). Deacetylase activity-independent transcriptional activation by HDAC2 during TPA-induced HL-60 cell differentiation. *PLoS One* *13*, e0202935.

Jurkin, J., Zupkovitz, G., Lager, S., Grausenburger, R., Hagelkruys, A., Kenner, L., and Seiser, C. (2011). Distinct and redundant functions of histone deacetylases HDAC1 and HDAC2 in proliferation and tumorigenesis. *Cell Cycle* *10*, 406-412.

Kalluri, R., and Weinberg, R.A. (2009). The basics of epithelial-mesenchymal transition. *J Clin Invest* *119*, 1420-1428.

Kanda, M., Matthaei, H., Wu, J., Hong, S.M., Yu, J., Borges, M., Hruban, R.H., Maitra, A., Kinzler, K., Vogelstein, B., *et al.* (2012). Presence of somatic mutations in most early-stage pancreatic intraepithelial neoplasia. *Gastroenterology* *142*, 730-733 e739.

Kang, H., Kim, H., Lee, S., Youn, H., and Youn, B. (2019). Role of Metabolic Reprogramming in Epithelial(-)Mesenchymal Transition (EMT). *Int J Mol Sci* *20*.

Kastrinos, F., and Stoffel, E.M. (2014). History, genetics, and strategies for cancer prevention in Lynch syndrome. *Clin Gastroenterol Hepatol* *12*, 715-727; quiz e741-713.

Kenner, B.J., Chari, S.T., Maitra, A., Srivastava, S., Cleeter, D.F., Go, V.L., Rothschild, L.J., and Goldberg, A.E. (2016). Early Detection of Pancreatic Cancer-a Defined Future Using Lessons From Other Cancers: A White Paper. *Pancreas* *45*, 1073-1079.

Kent, W.J., Sugnet, C.W., Furey, T.S., Roskin, K.M., Pringle, T.H., Zahler, A.M., and Haussler, D. (2002). The human genome browser at UCSC. *Genome Res* *12*, 996-1006.

Kim, H.J., and Bae, S.C. (2011). Histone deacetylase inhibitors: molecular mechanisms of action and clinical trials as anti-cancer drugs. *Am J Transl Res* *3*, 166-179.

Kim, J.K., Noh, J.H., Eun, J.W., Jung, K.H., Bae, H.J., Shen, Q., Kim, M.G., Chang, Y.G., Kim, S.J., Park, W.S., *et al.* (2013). Targeted inactivation of HDAC2 restores p16INK4a activity and exerts antitumor effects on human gastric cancer. *Mol Cancer Res* *11*, 62-73.

Kimura, H. (2013). Histone modifications for human epigenome analysis. *J Hum Genet* 58, 439-445.

Kiweler, N., Brill, B., Wirth, M., Breuksch, I., Laguna, T., Dietrich, C., Strand, S., Schneider, G., Groner, B., Butter, F., *et al.* (2018). The histone deacetylases HDAC1 and HDAC2 are required for the growth and survival of renal carcinoma cells. *Arch Toxicol* 92, 2227-2243.

Koutsounas, I., Giaginis, C., Patsouris, E., and Theocharis, S. (2013). Current evidence for histone deacetylase inhibitors in pancreatic cancer. *World J Gastroenterol* 19, 813-828.

Krämer, O.H., and Springer Science+Business Media (2017). HDAC/HAT function assessment and inhibitor development : methods and protocols (New York: Humana Press).

Kurahara, H., Maemura, K., Mataka, Y., Sakoda, M., Shinchi, H., and Natsugoe, S. (2016). Impact of p53 and PDGFR-beta Expression on Metastasis and Prognosis of Patients with Pancreatic Cancer. *World J Surg* 40, 1977-1984.

Lagger, G., Doetzelhofer, A., Schuettengruber, B., Haidweger, E., Simboeck, E., Tischler, J., Chiocca, S., Suske, G., Rotheneder, H., Wintersberger, E., *et al.* (2003). The tumor suppressor p53 and histone deacetylase 1 are antagonistic regulators of the cyclin-dependent kinase inhibitor p21/WAF1/CIP1 gene. *Mol Cell Biol* 23, 2669-2679.

Lagger, G., O'Carroll, D., Rembold, M., Khier, H., Tischler, J., Weitzer, G., Schuettengruber, B., Hauser, C., Brunmeir, R., Jenuwein, T., *et al.* (2002). Essential function of histone deacetylase 1 in proliferation control and CDK inhibitor repression. *EMBO J* 21, 2672-2681.

Lai, A.C., and Crews, C.M. (2017). Induced protein degradation: an emerging drug discovery paradigm. *Nat Rev Drug Discov* 16, 101-114.

Langmead, B., and Salzberg, S.L. (2012). Fast gapped-read alignment with Bowtie 2. *Nat Methods* 9, 357-359.

Larochelle, S., Merrick, K.A., Terret, M.E., Wohlbold, L., Barboza, N.M., Zhang, C., Shokat, K.M., Jallepalli, P.V., and Fisher, R.P. (2007). Requirements for Cdk7 in the assembly of Cdk1/cyclin B and activation of Cdk2 revealed by chemical genetics in human cells. *Mol Cell* 25, 839-850.

Laschanzky, R.S., Humphrey, L.E., Ma, J., Smith, L.M., Enke, T.J., Shukla, S.K., Dasgupta, A., Singh, P.K., Howell, G.M., Brattain, M.G., *et al.* (2019). Selective Inhibition of Histone Deacetylases 1/2/6 in Combination with Gemcitabine: A Promising Combination for Pancreatic Cancer Therapy. *Cancers (Basel)* 11.

Le Large, T.Y.S., Bijlsma, M.F., Kazemier, G., van Laarhoven, H.W.M., Giovannetti, E., and Jimenez, C.R. (2017). Key biological processes driving metastatic spread of pancreatic cancer as identified by multi-omics studies. *Semin Cancer Biol* 44, 153-169.

LeBoeuf, M., Terrell, A., Trivedi, S., Sinha, S., Epstein, J.A., Olson, E.N., Morrissey, E.E., and Millar, S.E. (2010). Hdac1 and Hdac2 act redundantly to control p63 and p53 functions in epidermal progenitor cells. *Dev Cell* 19, 807-818.

Lee, C.C., Lin, M.L., Meng, M., and Chen, S.S. (2018). Galangin Induces p53-independent S-phase Arrest and Apoptosis in Human Nasopharyngeal Carcinoma Cells Through Inhibiting PI3K-AKT Signaling Pathway. *Anticancer Res* 38, 1377-1389.

Lee, C.L., Moding, E.J., Huang, X., Li, Y., Woodlief, L.Z., Rodrigues, R.C., Ma, Y., and Kirsch, D.G. (2012). Generation of primary tumors with Flp recombinase in FRT-flanked p53 mice. *Dis Model Mech* 5, 397-402.

Lee, H.Z., Kwitkowski, V.E., Del Valle, P.L., Ricci, M.S., Saber, H., Habtemariam, B.A., Bullock, J., Bloomquist, E., Li Shen, Y., Chen, X.H., *et al.* (2015). FDA Approval: Belinostat for the Treatment of Patients with Relapsed or Refractory Peripheral T-cell Lymphoma. *Clin Cancer Res* 21, 2666-2670.

Leone, D.P., Genoud, S., Atanasoski, S., Grausenburger, R., Berger, P., Metzger, D., Macklin, W.B., Chambon, P., and Suter, U. (2003). Tamoxifen-inducible glia-specific Cre mice for somatic mutagenesis in oligodendrocytes and Schwann cells. *Mol Cell Neurosci* 22, 430-440.

Ler, S.Y., Leung, C.H., Khin, L.W., Lu, G.D., Salto-Tellez, M., Hartman, M., Iau, P.T., Yap, C.T., and Hooi, S.C. (2015). HDAC1 and HDAC2 independently predict mortality in hepatocellular carcinoma by a competing risk regression model in a Southeast Asian population. *Oncol Rep* 34, 2238-2250.

Li, H.M., Yang, J.G., Liu, Z.J., Wang, W.M., Yu, Z.L., Ren, J.G., Chen, G., Zhang, W., and Jia, J. (2017). Blockage of glycolysis by targeting PFKFB3 suppresses tumor growth and metastasis in head and neck squamous cell carcinoma. *J Exp Clin Cancer Res* 36, 7.

Li, Y., Kao, G.D., Garcia, B.A., Shabanowitz, J., Hunt, D.F., Qin, J., Phelan, C., and Lazar, M.A. (2006). A novel histone deacetylase pathway regulates mitosis by modulating Aurora B kinase activity. *Genes Dev* 20, 2566-2579.

Li, Y., and Seto, E. (2016). HDACs and HDAC Inhibitors in Cancer Development and Therapy. *Cold Spring Harb Perspect Med* 6.

Li, Z., and Zhu, W.G. (2014). Targeting histone deacetylases for cancer therapy: from molecular mechanisms to clinical implications. *Int J Biol Sci* 10, 757-770.

Liberzon, A., Birger, C., Thorvaldsdottir, H., Ghandi, M., Mesirov, J.P., and Tamayo, P. (2015). The Molecular Signatures Database (MSigDB) hallmark gene set collection. *Cell Syst* 1, 417-425.

Liszka, L., Pajak, J., Mrowiec, S., Zielinska-Pajak, E., Lampe, P., and Golka, D. (2010). Age distribution patterns of patients with conventional ductal adenocarcinoma of the pancreas. A single-institution study of 580 cases re-evaluated using current histopathological diagnostic criteria. *Pol J Pathol* 61, 65-77.

Liu, G., McDonnell, T.J., Montes de Oca Luna, R., Kapoor, M., Mims, B., El-Naggar, A.K., and Lozano, G. (2000). High metastatic potential in mice inheriting a targeted p53 missense mutation. *Proc Natl Acad Sci U S A* 97, 4174-4179.

Lo, H.W., Hsu, S.C., Xia, W., Cao, X., Shih, J.Y., Wei, Y., Abbruzzese, J.L., Hortobagyi, G.N., and Hung, M.C. (2007). Epidermal growth factor receptor cooperates with signal transducer and activator of transcription 3 to induce epithelial-mesenchymal transition in cancer cells via up-regulation of TWIST gene expression. *Cancer Res* 67, 9066-9076.

Lomberk, G., Blum, Y., Nicolle, R., Nair, A., Gaonkar, K.S., Marisa, L., Mathison, A., Sun, Z., Yan, H., Elarouci, N., *et al.* (2018). Distinct epigenetic landscapes underlie the pathobiology of pancreatic cancer subtypes. *Nat Commun* 9, 1978.

Long, J., Fang, W.Y., Chang, L., Gao, W.H., Shen, Y., Jia, M.Y., Zhang, Y.X., Wang, Y., Dou, H.B., Zhang, W.J., *et al.* (2017). Targeting HDAC3, a new partner protein of AKT in the reversal of chemoresistance in acute myeloid leukemia via DNA damage response. *Leukemia* 31, 2761-2770.

Loonstra, A., Vooijs, M., Beverloo, H.B., Allak, B.A., van Drunen, E., Kanaar, R., Berns, A., and Jonkers, J. (2001). Growth inhibition and DNA damage induced by Cre recombinase in mammalian cells. *Proc Natl Acad Sci U S A* 98, 9209-9214.

Love, M.I., Huber, W., and Anders, S. (2014). Moderated estimation of fold change and dispersion for RNA-seq data with DESeq2. *Genome Biol* 15, 550.

Lu, X.F., Cao, X.Y., Zhu, Y.J., Wu, Z.R., Zhuang, X., Shao, M.Y., Xu, Q., Zhou, Y.J., Ji, H.J., Lu, Q.R., *et al.* (2018). Histone deacetylase 3 promotes liver regeneration and liver cancer cells proliferation through signal transducer and activator of transcription 3 signaling pathway. *Cell Death Dis* 9, 398.

Luo, J., Su, F., Chen, D., Shiloh, A., and Gu, W. (2000). Deacetylation of p53 modulates its effect on cell growth and apoptosis. *Nature* 408, 377-381.

Magnuson, M.A., and Osipovich, A.B. (2013). Pancreas-specific Cre driver lines and considerations for their prudent use. *Cell Metab* 18, 9-20.

Mann, B.S., Johnson, J.R., Cohen, M.H., Justice, R., and Pazdur, R. (2007). FDA approval summary: vorinostat for treatment of advanced primary cutaneous T-cell lymphoma. *Oncologist* 12, 1247-1252.

Massague, J. (2012). TGFbeta signalling in context. *Nat Rev Mol Cell Biol* 13, 616-630.

McDonald, O.G., Li, X., Saunders, T., Tryggvadottir, R., Mentch, S.J., Warmoes, M.O., Word, A.E., Carrer, A., Salz, T.H., Natsume, S., *et al.* (2017). Epigenomic reprogramming during pancreatic cancer progression links anabolic glucose metabolism to distant metastasis. *Nat Genet* 49, 367-376.

Miller, K.M., Tjeertes, J.V., Coates, J., Legube, G., Polo, S.E., Britton, S., and Jackson, S.P. (2010). Human HDAC1 and HDAC2 function in the DNA-damage response to promote DNA nonhomologous end-joining. *Nat Struct Mol Biol* 17, 1144-1151.

Minucci, S., and Pelicci, P.G. (2006). Histone deacetylase inhibitors and the promise of epigenetic (and more) treatments for cancer. *Nat Rev Cancer* 6, 38-51.

Miyake, K., Yoshizumi, T., Imura, S., Sugimoto, K., Batmunkh, E., Kanemura, H., Morine, Y., and Shimada, M. (2008). Expression of hypoxia-inducible factor-1alpha, histone deacetylase 1, and metastasis-associated protein 1 in pancreatic carcinoma: correlation with poor prognosis with possible regulation. *Pancreas* 36, e1-9.

Moffitt, R.A., Marayati, R., Flate, E.L., Volmar, K.E., Loeza, S.G., Hoadley, K.A., Rashid, N.U., Williams, L.A., Eaton, S.C., Chung, A.H., *et al.* (2015). Virtual microdissection identifies distinct tumor- and stroma-specific subtypes of pancreatic ductal adenocarcinoma. *Nat Genet* 47, 1168-1178.

Montgomery, R.L., Davis, C.A., Potthoff, M.J., Haberland, M., Fielitz, J., Qi, X., Hill, J.A., Richardson, J.A., and Olson, E.N. (2007). Histone deacetylases 1 and 2 redundantly regulate cardiac morphogenesis, growth, and contractility. *Genes Dev* 21, 1790-1802.

Morgan, M.A., and Shilatifard, A. (2015). Chromatin signatures of cancer. *Genes Dev* 29, 238-249.

Morris, J.P.t., Wang, S.C., and Hebrok, M. (2010). KRAS, Hedgehog, Wnt and the twisted developmental biology of pancreatic ductal adenocarcinoma. *Nat Rev Cancer* 10, 683-695.

Moskaluk, C.A., Hruban, R.H., and Kern, S.E. (1997). p16 and K-ras gene mutations in the intraductal precursors of human pancreatic adenocarcinoma. *Cancer Res* 57, 2140-2143.

Mottamal, M., Zheng, S., Huang, T.L., and Wang, G. (2015). Histone deacetylase inhibitors in clinical studies as templates for new anticancer agents. *Molecules* 20, 3898-3941.

Mueller, S., Engleitner, T., Maresch, R., Zukowska, M., Lange, S., Kaltenbacher, T., Konukiewitz, B., Ollinger, R., Zwiebel, M., Strong, A., *et al.* (2018). Evolutionary routes and KRAS dosage define pancreatic cancer phenotypes. *Nature* 554, 62-68.

Muz, B., de la Puente, P., Azab, F., and Azab, A.K. (2015). The role of hypoxia in cancer progression, angiogenesis, metastasis, and resistance to therapy. *Hypoxia (Auckl)* 3, 83-92.

Neoptolemos, J.P., Kleeff, J., Michl, P., Costello, E., Greenhalf, W., and Palmer, D.H. (2018). Therapeutic developments in pancreatic cancer: current and future perspectives. *Nat Rev Gastroenterol Hepatol* 15, 333-348.

Newbold, A., Falkenberg, K.J., Prince, H.M., and Johnstone, R.W. (2016). How do tumor cells respond to HDAC inhibition? *FEBS J* 283, 4032-4046.

Nguyen, A.H., Elliott, I.A., Wu, N., Matsumura, C., Vogelauer, M., Attar, N., Dann, A., Ghukasyan, R., Toste, P.A., Patel, S.G., *et al.* (2017). Histone deacetylase inhibitors provoke a tumor supportive phenotype in pancreatic cancer associated fibroblasts. *Oncotarget* 8, 19074-19088.

Ohlund, D., Elyada, E., and Tuveson, D. (2014). Fibroblast heterogeneity in the cancer wound. *J Exp Med* 211, 1503-1523.

Olive, K.P., Tuveson, D.A., Ruhe, Z.C., Yin, B., Willis, N.A., Bronson, R.T., Crowley, D., and Jacks, T. (2004). Mutant p53 gain of function in two mouse models of Li-Fraumeni syndrome. *Cell* 119, 847-860.

Oliveros, J.C. (2007-2015). Venny. An interactive tool for comparing lists with Venn's diagrams.

Orth, M., Metzger, P., Gerum, S., Mayerle, J., Schneider, G., Belka, C., Schnurr, M., and Lauber, K. (2019). Pancreatic ductal adenocarcinoma: biological hallmarks, current status, and future perspectives of combined modality treatment approaches. *Radiat Oncol* 14, 141.

Payen, V.L., Porporato, P.E., Baselet, B., and Sonveaux, P. (2016). Metabolic changes associated with tumor metastasis, part 1: tumor pH, glycolysis and the pentose phosphate pathway. *Cell Mol Life Sci* 73, 1333-1348.

Pelosi, E., Castelli, G., and Testa, U. (2017). Pancreatic Cancer: Molecular Characterization, Clonal Evolution and Cancer Stem Cells. *Biomedicines* 5.

Pfaffl, M.W. (2001). A new mathematical model for relative quantification in real-time RT-PCR. *Nucleic Acids Res* 29, e45.

Polireddy, K., and Chen, Q. (2016). Cancer of the Pancreas: Molecular Pathways and Current Advancement in Treatment. *J Cancer* 7, 1497-1514.

Prost, S., Bellamy, C.O., Clarke, A.R., Wyllie, A.H., and Harrison, D.J. (1998). p53-independent DNA repair and cell cycle arrest in embryonic stem cells. *FEBS Lett* 425, 499-504.

Quante, A.S., Ming, C., Rottmann, M., Engel, J., Boeck, S., Heinemann, V., Westphalen, C.B., and Strauch, K. (2016). Projections of cancer incidence and cancer-related deaths in Germany by 2020 and 2030. *Cancer Med* 5, 2649-2656.

Raedler, L.A. (2016). Farydak (Panobinostat): First HDAC Inhibitor Approved for Patients with Relapsed Multiple Myeloma. *Am Health Drug Benefits* 9, 84-87.

Rahib, L., Smith, B.D., Aizenberg, R., Rosenzweig, A.B., Fleshman, J.M., and Matrisian, L.M. (2014). Projecting cancer incidence and deaths to 2030: the unexpected burden of thyroid, liver, and pancreas cancers in the United States. *Cancer Res* 74, 2913-2921.

Raimondi, S., Lowenfels, A.B., Morselli-Labate, A.M., Maisonneuve, P., and Pezzilli, R. (2010). Pancreatic cancer in chronic pancreatitis; aetiology, incidence, and early detection. *Best Pract Res Clin Gastroenterol* 24, 349-358.

Roberts, A.B., and Wakefield, L.M. (2003). The two faces of transforming growth factor beta in carcinogenesis. *Proc Natl Acad Sci U S A* 100, 8621-8623.

Roe, J.S., Hwang, C.I., Somerville, T.D.D., Milazzo, J.P., Lee, E.J., Da Silva, B., Maiorino, L., Tiriach, H., Young, C.M., Miyabayashi, K., *et al.* (2017). Enhancer Reprogramming Promotes Pancreatic Cancer Metastasis. *Cell* 170, 875-888 e820.

Ropero, S., and Esteller, M. (2007). The role of histone deacetylases (HDACs) in human cancer. *Mol Oncol* 1, 19-25.

Ruscetti, M., Dadashian, E.L., Guo, W., Quach, B., Mulholland, D.J., Park, J.W., Tran, L.M., Kobayashi, N., Bianchi-Frias, D., Xing, Y., *et al.* (2016). HDAC inhibition impedes epithelial-mesenchymal plasticity and suppresses metastatic, castration-resistant prostate cancer. *Oncogene* 35, 3781-3795.

Ryu, J.K., Lee, W.J., Lee, K.H., Hwang, J.H., Kim, Y.T., Yoon, Y.B., and Kim, C.Y. (2006). SK-7041, a new histone deacetylase inhibitor, induces G2-M cell cycle arrest and apoptosis in pancreatic cancer cell lines. *Cancer Lett* 237, 143-154.

Sato, N., Ohta, T., Kitagawa, H., Kayahara, M., Ninomiya, I., Fushida, S., Fujimura, T., Nishimura, G., Shimizu, K., and Miwa, K. (2004). FR901228, a novel histone deacetylase inhibitor, induces cell cycle arrest and subsequent apoptosis in refractory human pancreatic cancer cells. *Int J Oncol* 24, 679-685.

Schachter, M.M., and Fisher, R.P. (2013). The CDK-activating kinase Cdk7: taking yes for an answer. *Cell Cycle* 12, 3239-3240.

Schneider, G., Kramer, O.H., Fritsche, P., Schuler, S., Schmid, R.M., and Saur, D. (2010). Targeting histone deacetylases in pancreatic ductal adenocarcinoma. *J Cell Mol Med* 14, 1255-1263.

Schonhuber, N., Seidler, B., Schuck, K., Veltkamp, C., Schachtler, C., Zukowska, M., Eser, S., Feyerabend, T.B., Paul, M.C., Eser, P., *et al.* (2014). A next-generation dual-recombinase system for time- and host-specific targeting of pancreatic cancer. *Nat Med* 20, 1340-1347.

Schuler, S., Fritsche, P., Diersch, S., Arlt, A., Schmid, R.M., Saur, D., and Schneider, G. (2010). HDAC2 attenuates TRAIL-induced apoptosis of pancreatic cancer cells. *Mol Cancer* 9, 80.

Segre, C.V., and Chiocca, S. (2011). Regulating the regulators: the post-translational code of class I HDAC1 and HDAC2. *J Biomed Biotechnol* 2011, 690848.

Senese, S., Zaragoza, K., Minardi, S., Muradore, I., Ronzoni, S., Passafaro, A., Bernard, L., Draetta, G.F., Alcalay, M., Seiser, C., *et al.* (2007). Role for histone deacetylase 1 in human tumor cell proliferation. *Mol Cell Biol* 27, 4784-4795.

Seto, E., and Yoshida, M. (2014). Erasers of histone acetylation: the histone deacetylase enzymes. *Cold Spring Harb Perspect Biol* 6, a018713.

Seyfried, T.N., and Huysentruyt, L.C. (2013). On the origin of cancer metastasis. *Crit Rev Oncog* 18, 43-73.

Shen, W., Tao, G.Q., Zhang, Y., Cai, B., Sun, J., and Tian, Z.Q. (2017). TGF-beta in pancreatic cancer initiation and progression: two sides of the same coin. *Cell Biosci* 7, 39.

Siegel, R., Ma, J., Zou, Z., and Jemal, A. (2014). Cancer statistics, 2014. *CA Cancer J Clin* 64, 9-29.

Siegel, R.L., Miller, K.D., and Jemal, A. (2019). Cancer statistics, 2019. *CA Cancer J Clin* 69, 7-34.

Siegel, R.L., Miller, K.D., and Jemal, A. (2020). Cancer statistics, 2020. *CA Cancer J Clin* 70, 7-30.

Singh, A., Patel, V.K., Jain, D.K., Patel, P., and Rajak, H. (2016). Panobinostat as Pan-deacetylase Inhibitor for the Treatment of Pancreatic Cancer: Recent Progress and Future Prospects. *Oncol Ther* 4, 73-89.

Smalley, J.P., Adams, G.E., Millard, C.J., Song, Y., Norris, J.K.S., Schwabe, J.W.R., Cowley, S.M., and Hodgkinson, J.T. (2020). PROTAC-mediated degradation of class I histone deacetylase enzymes in corepressor complexes. *Chem Commun (Camb)* 56, 4476-4479.

Smith, A.L., Robin, T.P., and Ford, H.L. (2012). Molecular pathways: targeting the TGF-beta pathway for cancer therapy. *Clin Cancer Res* 18, 4514-4521.

Somanath, P., Herndon Klein, R., and Knoepfler, P.S. (2017). CRISPR-mediated HDAC2 disruption identifies two distinct classes of target genes in human cells. *PLoS One* 12, e0185627.

Song, C., Zhu, S., Wu, C., and Kang, J. (2013). Histone deacetylase (HDAC) 10 suppresses cervical cancer metastasis through inhibition of matrix metalloproteinase (MMP) 2 and 9 expression. *J Biol Chem* 288, 28021-28033.

Sprouffske, K., Kerr, G., Li, C., Prahallad, A., Rebmann, R., Waehle, V., Naumann, U., Bitter, H., Jensen, M.R., Hofmann, F., *et al.* (2020). Genetic heterogeneity and clonal evolution during metastasis in breast cancer patient-derived tumor xenograft models. *Comput Struct Biotechnol J* 18, 323-331.

Stewart, Z.A., and Pietenpol, J.A. (2001). p53 Signaling and cell cycle checkpoints. *Chem Res Toxicol* 14, 243-263.

Stojanovic, N., Hassan, Z., Wirth, M., Wenzel, P., Beyer, M., Schafer, C., Brand, P., Kroemer, A., Stauber, R.H., Schmid, R.M., *et al.* (2017). HDAC1 and HDAC2 integrate the expression of p53 mutants in pancreatic cancer. *Oncogene* 36, 1804-1815.

Storz, P. (2017). Acinar cell plasticity and development of pancreatic ductal adenocarcinoma. *Nat Rev Gastroenterol Hepatol* 14, 296-304.

Su, J., Morgani, S.M., David, C.J., Wang, Q., Er, E.E., Huang, Y.H., Basnet, H., Zou, Y., Shu, W., Soni, R.K., *et al.* (2020). TGF-beta orchestrates fibrogenic and developmental EMTs via the RAS effector RREB1. *Nature* 577, 566-571.

Su, T.T. (2006). Cellular responses to DNA damage: one signal, multiple choices. *Annu Rev Genet* 40, 187-208.

Subramanian, A., Tamayo, P., Mootha, V.K., Mukherjee, S., Ebert, B.L., Gillette, M.A., Paulovich, A., Pomeroy, S.L., Golub, T.R., Lander, E.S., *et al.* (2005). Gene set enrichment analysis: a knowledge-based approach for interpreting genome-wide expression profiles. *Proc Natl Acad Sci U S A* 102, 15545-15550.

Summers, A.R., Fischer, M.A., Stengel, K.R., Zhao, Y., Kaiser, J.F., Wells, C.E., Hunt, A., Bhaskara, S., Luzwick, J.W., Sampathi, S., *et al.* (2013). HDAC3 is essential for DNA replication in hematopoietic progenitor cells. *J Clin Invest* 123, 3112-3123.

Sun, X., Gao, H., Yang, Y., He, M., Wu, Y., Song, Y., Tong, Y., and Rao, Y. (2019). PROTACs: great opportunities for academia and industry. *Signal Transduct Target Ther* 4, 64.

Sun, Z., Feng, D., Fang, B., Mullican, S.E., You, S.H., Lim, H.W., Everett, L.J., Nabel, C.S., Li, Y., Selvakumaran, V., *et al.* (2013). Deacetylase-independent function of HDAC3 in transcription and metabolism requires nuclear receptor corepressor. *Mol Cell* 52, 769-782.

Tang, W., Zhou, W., Xiang, L., Wu, X., Zhang, P., Wang, J., Liu, G., Zhang, W., Peng, Y., Huang, X., *et al.* (2019). The p300/YY1/miR-500a-5p/HDAC2 signalling axis regulates cell proliferation in human colorectal cancer. *Nat Commun* 10, 663.

Taunton, J., Hassig, C.A., and Schreiber, S.L. (1996). A mammalian histone deacetylase related to the yeast transcriptional regulator Rpd3p. *Science* 272, 408-411.

Teraoka, H., Sawada, T., Yamashita, Y., Nakata, B., Ohira, M., Ishikawa, T., Nishino, H., and Hirakawa, K. (2001). TGF-beta1 promotes liver metastasis of pancreatic cancer by modulating the capacity of cellular invasion. *Int J Oncol* 19, 709-715.

VanderMolen, K.M., McCulloch, W., Pearce, C.J., and Oberlies, N.H. (2011). Romidepsin (Istodax, NSC 630176, FR901228, FK228, depsipeptide): a natural product recently approved for cutaneous T-cell lymphoma. *J Antibiot (Tokyo)* 64, 525-531.

Vermeulen, M., Carrozza, M.J., Lasonder, E., Workman, J.L., Logie, C., and Stunnenberg, H.G. (2004). In vitro targeting reveals intrinsic histone tail specificity of the Sin3/histone deacetylase and N-CoR/SMRT corepressor complexes. *Mol Cell Biol* 24, 2364-2372.

von Burstin, J., Eser, S., Paul, M.C., Seidler, B., Brandl, M., Messer, M., von Werder, A., Schmidt, A., Mages, J., Pagel, P., *et al.* (2009). E-cadherin regulates metastasis of pancreatic cancer in vivo and is suppressed by a SNAIL/HDAC1/HDAC2 repressor complex. *Gastroenterology* 137, 361-371, 371 e361-365.

Wagner, T., Kiweler, N., Wolff, K., Knauer, S.K., Brandl, A., Hemmerich, P., Dannenberg, J.H., Heinzl, T., Schneider, G., and Kramer, O.H. (2015). Sumoylation of HDAC2 promotes NF-kappaB-dependent gene expression. *Oncotarget* 6, 7123-7135.

Warburg, O. (1956). On the origin of cancer cells. *Science* 123, 309-314.

Warshaw, A.L., and Fernandez-del Castillo, C. (1992). Pancreatic carcinoma. *N Engl J Med* 326, 455-465.

Waters, A.M., and Der, C.J. (2018). KRAS: The Critical Driver and Therapeutic Target for Pancreatic Cancer. *Cold Spring Harb Perspect Med* 8.

Weichert, W., Roske, A., Niesporek, S., Noske, A., Buckendahl, A.C., Dietel, M., Gekeler, V., Boehm, M., Beckers, T., and Denkert, C. (2008). Class I histone deacetylase expression has independent prognostic impact in human colorectal cancer: specific role of class I histone deacetylases in vitro and in vivo. *Clin Cancer Res* 14, 1669-1677.

Weissmueller, S., Manchado, E., Saborowski, M., Morris, J.P.t., Wagenblast, E., Davis, C.A., Moon, S.H., Pfister, N.T., Tschaharganeh, D.F., Kitzing, T., *et al.* (2014). Mutant p53 drives pancreatic cancer metastasis through cell-autonomous PDGF receptor beta signaling. *Cell* 157, 382-394.

Wells, C.E., Bhaskara, S., Stengel, K.R., Zhao, Y., Sirbu, B., Chagot, B., Cortez, D., Khabele, D., Chazin, W.J., Cooper, A., *et al.* (2013). Inhibition of histone deacetylase 3 causes replication stress in cutaneous T cell lymphoma. *PLoS One* 8, e68915.

West, A.C., and Johnstone, R.W. (2014). New and emerging HDAC inhibitors for cancer treatment. *J Clin Invest* 124, 30-39.

Wicksteed, B., Brissova, M., Yan, W., Opland, D.M., Plank, J.L., Reinert, R.B., Dickson, L.M., Tamarina, N.A., Philipson, L.H., Shostak, A., *et al.* (2010). Conditional gene targeting in mouse pancreatic ss-Cells: analysis of ectopic Cre transgene expression in the brain. *Diabetes* 59, 3090-3098.

Wilson, A.J., Byun, D.S., Popova, N., Murray, L.B., L'Italien, K., Sowa, Y., Arango, D., Velcich, A., Augenlicht, L.H., and Mariadason, J.M. (2006). Histone deacetylase 3 (HDAC3) and other class I HDACs regulate colon cell maturation and p21 expression and are deregulated in human colon cancer. *J Biol Chem* 281, 13548-13558.

Wrana, J.L., Attisano, L., Wieser, R., Ventura, F., and Massague, J. (1994). Mechanism of activation of the TGF-beta receptor. *Nature* 370, 341-347.

Wu, J., Matthaei, H., Maitra, A., Dal Molin, M., Wood, L.D., Eshleman, J.R., Goggins, M., Canto, M.I., Schulick, R.D., Edil, B.H., *et al.* (2011). Recurrent GNAS mutations define an unexpected pathway for pancreatic cyst development. *Sci Transl Med* 3, 92ra66.

Xu, G., Zhu, H., Zhang, M., and Xu, J. (2018). Histone deacetylase 3 is associated with gastric cancer cell growth via the miR-454-mediated targeting of CHD5. *Int J Mol Med* 41, 155-163.

Xu, W.S., Parmigiani, R.B., and Marks, P.A. (2007). Histone deacetylase inhibitors: molecular mechanisms of action. *Oncogene* 26, 5541-5552.

Yachida, S., Jones, S., Bozic, I., Antal, T., Leary, R., Fu, B., Kamiyama, M., Hruban, R.H., Eshleman, J.R., Nowak, M.A., *et al.* (2010). Distant metastasis occurs late during the genetic evolution of pancreatic cancer. *Nature* 467, 1114-1117.

Yan, Y., An, J., Yang, Y., Wu, D., Bai, Y., Cao, W., Ma, L., Chen, J., Yu, Z., He, Y., *et al.* (2018). Dual inhibition of AKT-mTOR and AR signaling by targeting HDAC3 in PTEN- or SPOP-mutated prostate cancer. *EMBO Mol Med* 10.

Yang, K., Song, Y., Xie, H., Wu, H., Wu, Y.T., Leisten, E.D., and Tang, W. (2018). Development of the first small molecule histone deacetylase 6 (HDAC6) degraders. *Bioorg Med Chem Lett* 28, 2493-2497.

Yang, W.M., Inouye, C., Zeng, Y., Bearss, D., and Seto, E. (1996). Transcriptional repression by YY1 is mediated by interaction with a mammalian homolog of the yeast global regulator RPD3. *Proc Natl Acad Sci U S A* 93, 12845-12850.

Yang, W.M., Yao, Y.L., Sun, J.M., Davie, J.R., and Seto, E. (1997). Isolation and characterization of cDNAs corresponding to an additional member of the human histone deacetylase gene family. *J Biol Chem* 272, 28001-28007.

Yao, W., Maitra, A., and Ying, H. (2020). Recent insights into the biology of pancreatic cancer. *EBioMedicine* 53, 102655.

Yeo, T.P., and Lowenfels, A.B. (2012). Demographics and epidemiology of pancreatic cancer. *Cancer J* 18, 477-484.

Yin, Y., Zhang, M., Dorfman, R.G., Li, Y., Zhao, Z., Pan, Y., Zhou, Q., Huang, S., Zhao, S., Yao, Y., *et al.* (2017). Histone deacetylase 3 overexpression in human cholangiocarcinoma and promotion of cell growth via apoptosis inhibition. *Cell Death Dis* 8, e2856.

Yoshikawa, M., Hishikawa, K., Marumo, T., and Fujita, T. (2007). Inhibition of histone deacetylase activity suppresses epithelial-to-mesenchymal transition induced by TGF-beta1 in human renal epithelial cells. *J Am Soc Nephrol* 18, 58-65.

Yu, X., Yang, F., Jiang, H., and Fan, L. (2020). RGFP966 Suppresses Tumor Growth and Migration Through Inhibition of EGFR Expression in Hepatocellular Carcinoma Cells in vitro. *Drug Des Devel Ther* 14, 121-128.

Yu, Z., Zeng, J., Liu, H., Wang, T., Yu, Z., and Chen, J. (2019). Role of HDAC1 in the progression of gastric cancer and the correlation with lncRNAs. *Oncol Lett* 17, 3296-3304.

Yuen, A., and Diaz, B. (2014). The impact of hypoxia in pancreatic cancer invasion and metastasis. *Hypoxia (Auckl)* 2, 91-106.

Zhang, K.D., Hu, B., Cen, G., Yang, Y.H., Chen, W.W., Guo, Z.Y., Wang, X.F., Zhao, Q., and Qiu, Z.J. (2020). MiR-301a transcriptionally activated by HIF-2alpha promotes hypoxia-induced epithelial-mesenchymal transition by targeting TP63 in pancreatic cancer. *World J Gastroenterol* 26, 2349-2373.

Zhang, L., Du, J., Yano, N., Wang, H., Zhao, Y.T., Dubielecka, P.M., Zhuang, S., Chin, Y.E., Qin, G., and Zhao, T.C. (2017a). Sodium Butyrate Protects -Against High Fat Diet-Induced Cardiac Dysfunction and Metabolic Disorders in Type II Diabetic Mice. *J Cell Biochem* 118, 2395-2408.

Zhang, P., Torres, K., Liu, X., Liu, C.G., and Pollock, R.E. (2016). An Overview of Chromatin-Regulating Proteins in Cells. *Curr Protein Pept Sci* 17, 401-410.

Zhang, Y., Alexander, P.B., and Wang, X.F. (2017b). TGF-beta Family Signaling in the Control of Cell Proliferation and Survival. *Cold Spring Harb Perspect Biol* 9.

Zhao, H., Wang, Y., Yang, C., Zhou, J., Wang, L., Yi, K., Li, Y., Wang, Q., Shi, J., Kang, C., *et al.* (2020). EGFR-vIII downregulated H2AZK4/7AC though the PI3K/AKT-HDAC2 axis to regulate cell cycle progression. *Clin Transl Med* 9, 10.

Zhu, D., Zheng, S., Fang, C., Guo, X., Han, D., Tang, M., Fu, H., Jiang, M., Xie, N., Nie, Y., *et al.* (2020). Dysbindin promotes pancreatic ductal adenocarcinoma metastasis by activating NF-kappaB/MDM2 via miR-342-3p. *Cancer Lett.*

Zhu, L., Shi, G., Schmidt, C.M., Hruban, R.H., and Konieczny, S.F. (2007). Acinar cells contribute to the molecular heterogeneity of pancreatic intraepithelial neoplasia. *Am J Pathol* 171, 263-273.

Zhu, P., Martin, E., Mengwasser, J., Schlag, P., Janssen, K.P., and Gottlicher, M. (2004). Induction of HDAC2 expression upon loss of APC in colorectal tumorigenesis. *Cancer Cell* 5, 455-463.

Zimmermann, S., Kiefer, F., Prudenziati, M., Spiller, C., Hansen, J., Floss, T., Wurst, W., Minucci, S., and Gottlicher, M. (2007). Reduced body size and decreased intestinal tumor rates in HDAC2-mutant mice. *Cancer Res* 67, 9047-9054.

Zupkovitz, G., Tischler, J., Posch, M., Sadzak, I., Ramsauer, K., Egger, G., Grausenburger, R., Schweifer, N., Chiocca, S., Decker, T., *et al.* (2006). Negative and positive regulation of gene expression by mouse histone deacetylase 1. *Mol Cell Biol* 26, 7913-7928.

10. Acknowledgements

I want to sincerely thank everybody who supported me during the time of my doctoral research in any possible way.

First of all, I thank Prof. Roland M. Schmid for giving me the opportunity to work in his department at the Klinikum rechts der Isar.

Especially, I'm very grateful to Prof. Martin Hrabě de Angelis for being my second advisor and for his support during all the years.

Furthermore, I thank Dr. Maximilian Reichert for being my mentor.

Above all, I want to thank Dr. Günter Schneider for giving me the opportunity to work on my doctoral research in his group. By offering such an interesting topic and always supporting me, he contributed a large part to this dissertation.

I further want to thank all members of AG Schneider, AG Geißler and AG Saur, as well as, AG Reichert for scientific input and discussion, as well as for the great working atmosphere. Especially I want to thank Dr. Katja Steiger for her educational help regarding the histological analysis, especially the metastasis screening. Also I want to thank Dr. Falk Butter for performing the proteome analysis.

Finally and most importantly, I want to thank my husband and my family for their constant support throughout all the years. Without their understanding, encouraging help, this dissertation would not have been possible.

11. Supplementary Information

Table S 1: Cultivation of picked clones of *Hdac1/2/3* deficient PDAC cell lines

Cell line	Viable clones after EtOH treatment	Viable clones after 4-OHT treatment
PPT-F5461	12 out of 12	0 out of 48
PPT-F5465	8 out of 8	0 out of 50
PPT-F5470	10 out of 12	0 out of 43

Table S 2: Established epithelial and mesenchymal fractions of PDAC cell lines

Cell line	Established epithelial fraction	Established mesenchymal fraction
PPT-F3262	No	No
PPT-F3641	Yes	Yes
PPT-F1648	No	No
PPT-F2612	Yes	Yes
PPT-F2800	Yes	Yes
PPT-F4402	No	Yes
PPT-F4699	Yes	No
PPT-F4764	Yes	No
PPT-F5061	No	Yes

For each cell line two attempts for separation of epithelial and mesenchymal fraction were performed.

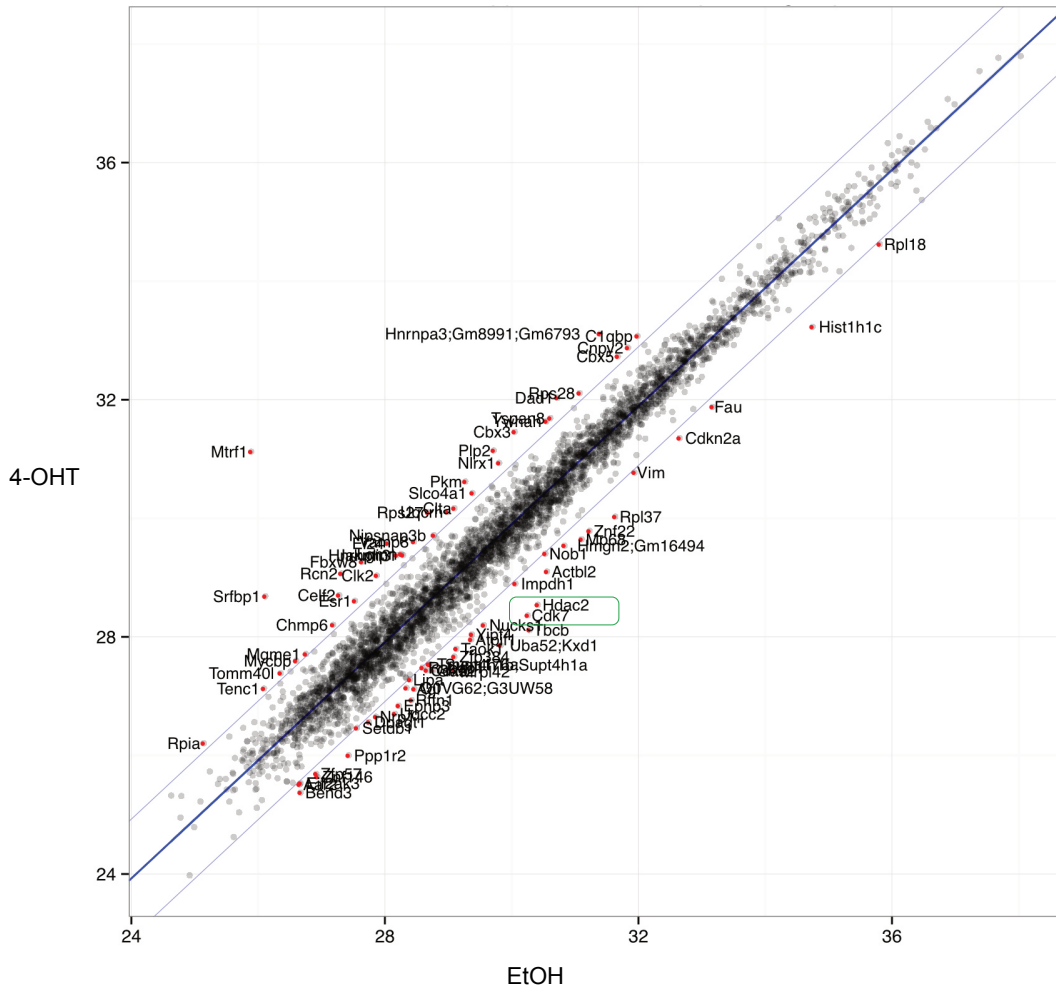


Figure S 1: Proteome analysis of *Hdac2* pro- and deficient PPT-F1648 cells.
 After five days of 4-OHT/vehicle treatment in PPT-F1648 cells proteome analysis was performed.

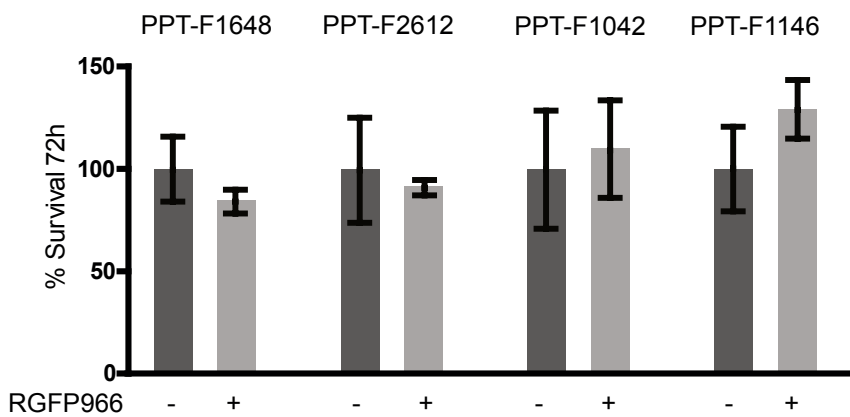


Figure S 2: RGFP966 treatment in PDAC cell lines PPT-F1648, PPT-F2612, PPT-F1042 and PPT-F1146.

MTT Assay of cell lines PPT-F1648, PPT-F2612, PPT-F1042, PPT-F1146 treated with 10 μ M HDAC3 specific inhibitor RGFP966 or DMSO as control. 2,000 cells were seeded and after attachment overnight treated with RGFP966 or DMSO. Experiments were performed as four (PPT-F1648, PPT-F2612) or three (PPT-F1042, PPT-F1146) biological replicates conducted as technical triplicates. DMSO treated samples were used as controls and average was set as 100%. Data are shown as mean \pm SD, two-tailed unpaired Student's t test was performed but no significance was detected.

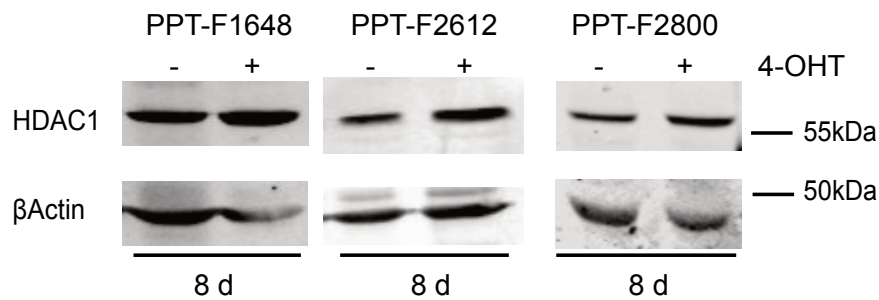


Figure S 3: Western blot analysis of HDAC1 expression in PDAC cell lines PPT-F1648, PPT-F2612, PPT-F2800.

Western Blot analysis of cell lines PPT-F1648, PPT-F2612 and PPT-F2800 after eight days of 4-OHT/vehicle treatment. The western blot show the HDAC1 expression in the same samples that were proven for successful *Hdac2* knock-out in Figure 7-4. βActin = loading control.

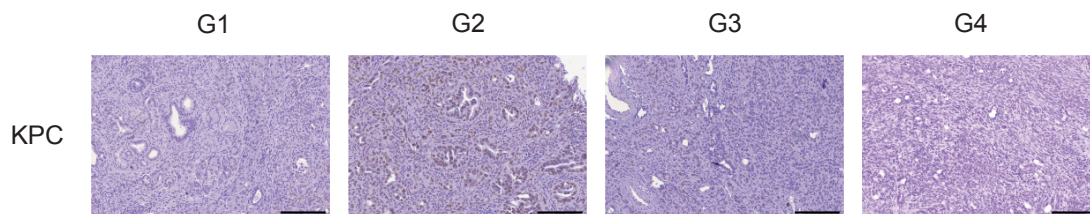


Figure S 4: Immunohistochemical analysis of HDAC2 expression in KPC mice.

Immunohistochemical analysis of HDAC2 expression in PPT of KPC mice with differently graded PPTs. Scale bar depicts 500 μm.

12. Appendix

In the appendix, the original western Blots, clonogenic assay plates etc. from the figures shown in part 7, are depicted.

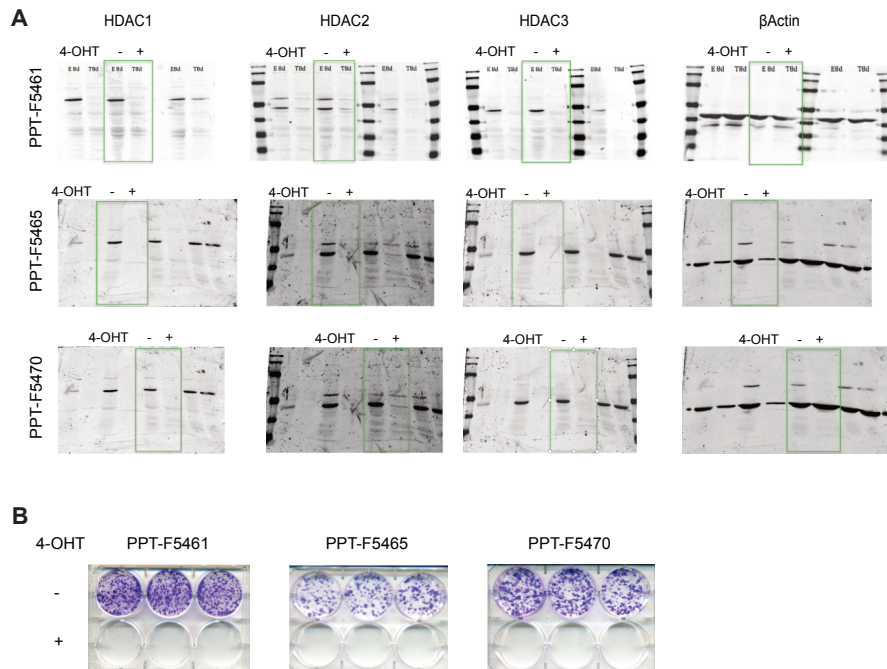


Figure A 1: Original western blots and clonogenic assays of Figure 7-2.

A) The complete original western blot showing successful knock-out of *Hdac1*, *Hdac2* and *Hdac3* of the cell line PPT-F5461, PPT-F5465 and PPT-F5470. As well western blot of loading control β Actin is shown, which was used for quantification. The lanes depicted in Figure 7-2 are framed in green. B) Original clonogenic assay of the cell lines PPT-F5461, PPT-F5465 and PPT-F5470 after eight days of 4-OHT/vehicle treatment. After eight days of 4-OHT/vehicle treatment 2,000 cells were seeded in triplicates and analyzed for clonogenic assay after seven days. 4-OHT = 4-Hydroxytamoxifen.

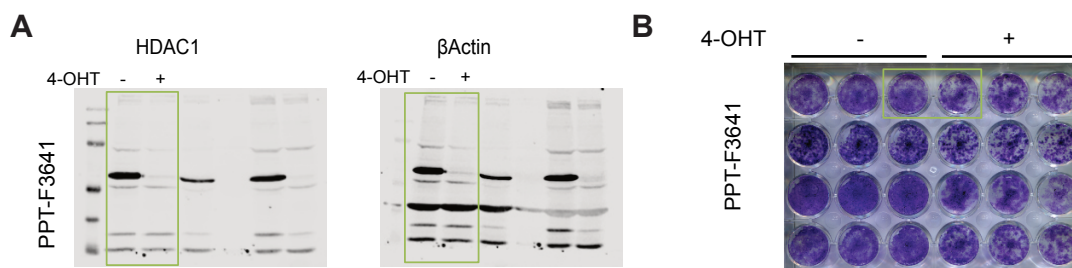


Figure A 2: Original western blots and clonogenic assays of Figure 7-3.

A) The complete original western blot showing successful knock-out of *Hdac1* in the cell line PPT-F3641. As well western blot of loading control β Actin is shown, which was used for quantification. The lanes depicted in Figure 7-3 are framed in green. B) Original clonogenic assay of the cell line PPT-F3641 after eight days of 4-OHT/vehicle treatment. After eight days of 4-OHT/vehicle treatment 2,000 cells were seeded in triplicates and analyzed for clonogenic assay after seven days. 4-OHT = 4-Hydroxytamoxifen.

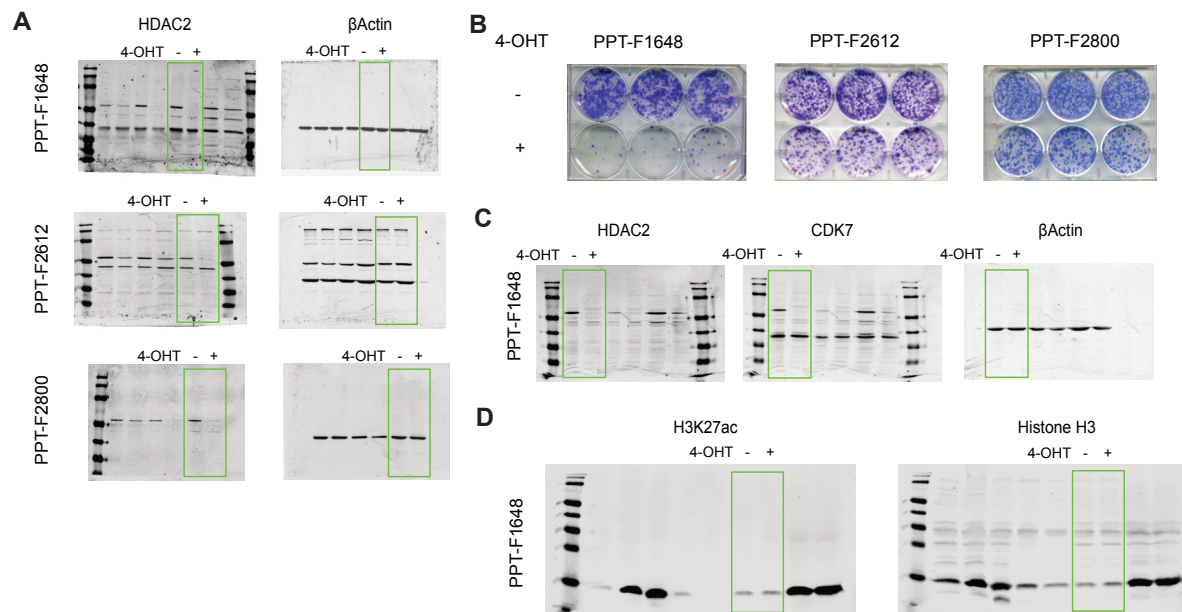


Figure A 3: Original western blots and clonogenic assays of Figure 7-4, Figure 7-5 and Figure 7-6.

A) The complete original western blot of Figure 7-4 showing successful knock-out of *Hdac2* in the cell line PPT-F1648, PPT-F2612 and PPT-F2800. As well western blot of loading control β Actin is shown, which was used for quantification. B) Original clonogenic assay of the cell line PPT-F1648, PPT-F2612 and PPT-F2800 after eight days of 4-OHT/vehicle treatment, presented in Figure 7-4. After eight days of 4-OHT/vehicle treatment 2,000 cells were seeded in triplicates and analyzed for clonogenic assay after seven days. C) The complete original western blot of Figure 7-5, showing successful knock-out of *Hdac2* and no differences in CDK7 expression in the cell line PPT-F1648. As well western blot of loading control β Actin is shown, which was used for quantification. D) The complete original western blot of Figure 7-6, showing no differences in H3K27ac after eight days of 4-OHT treatment in cell line PPT-F1648. As well western blot of loading control Histone H3 is shown, which was used for quantification. The western blot lanes depicted in Figure 7-4, Figure 7-5 and Figure 7-6 are framed in green. 4-OHT = 4-Hydroxytamoxifen.

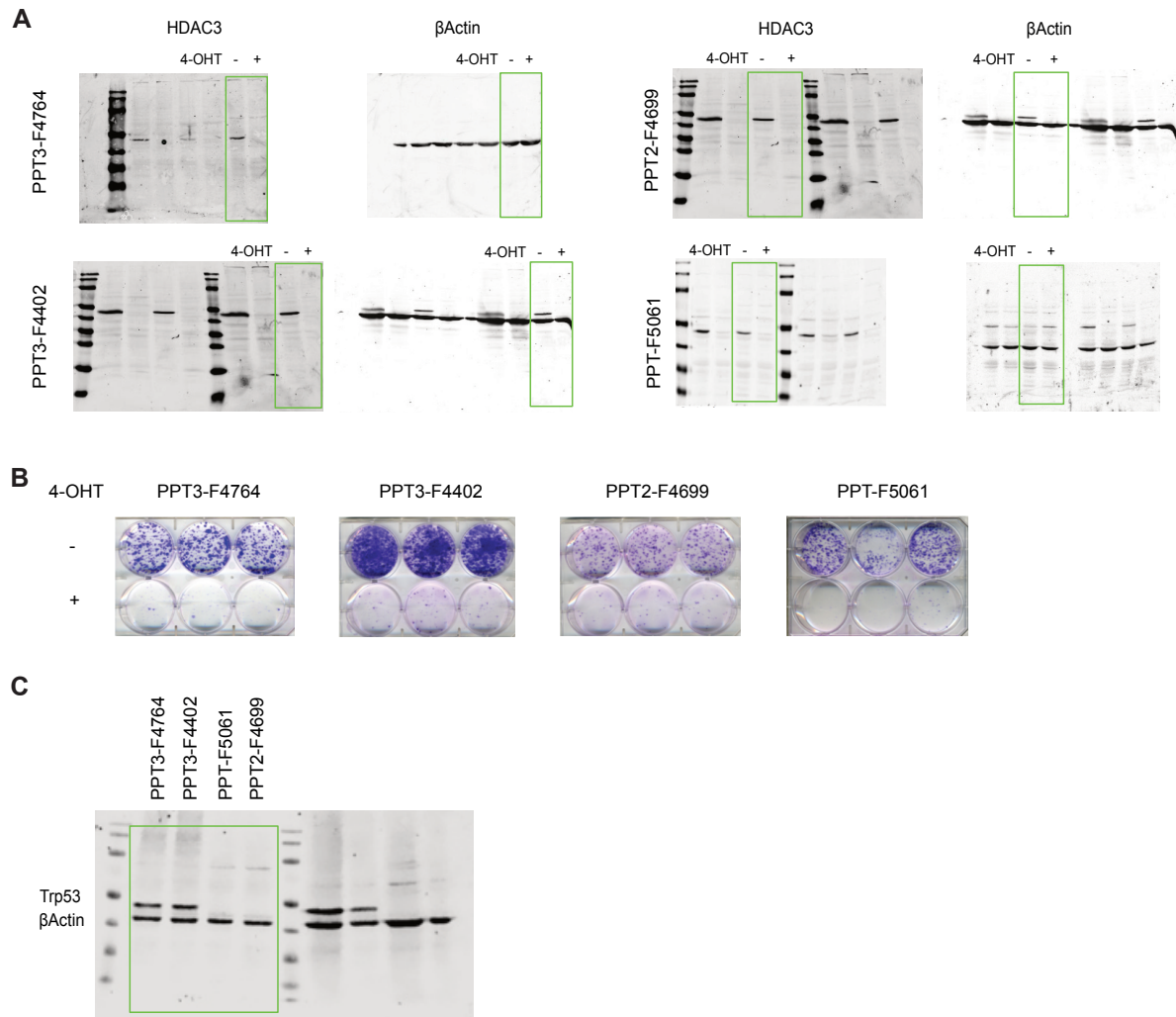


Figure A 4: Original western blots and clonogenic assays of Figure 7-7 and Figure 7-8.

A) The complete original western blot of Figure 7-7 showing successful knock-out of *Hdac3* in the cell lines PPT3-F4764, PPT3-F4402, PPT2-F4699 and PPT-F5061. As well western blot of loading control β Actin is shown, which was used for quantification. B) Original clonogenic assay of the cell lines PPT3-F4764, PPT3-F4402, PPT2-F4699 and PPT-F5061 after eight days of 4-OHT/vehicle treatment, presented in Figure 7-7. After eight days of 4-OHT/vehicle treatment 2,000 cells were seeded in triplicates and analyzed for clonogenic assay after seven days. C) The complete original western blot of Figure 7-8, showing successful TRP53 expression in cell lines PPT3-F4764, PPT3-F4402, PPT2-F4699 and PPT-F5061 as well as loading control β Actin, which was used for quantification. The western blot lanes depicted in Figure 7-7 and Figure 7-8 are framed in green. 4-OHT = 4-Hydroxytamoxifen.

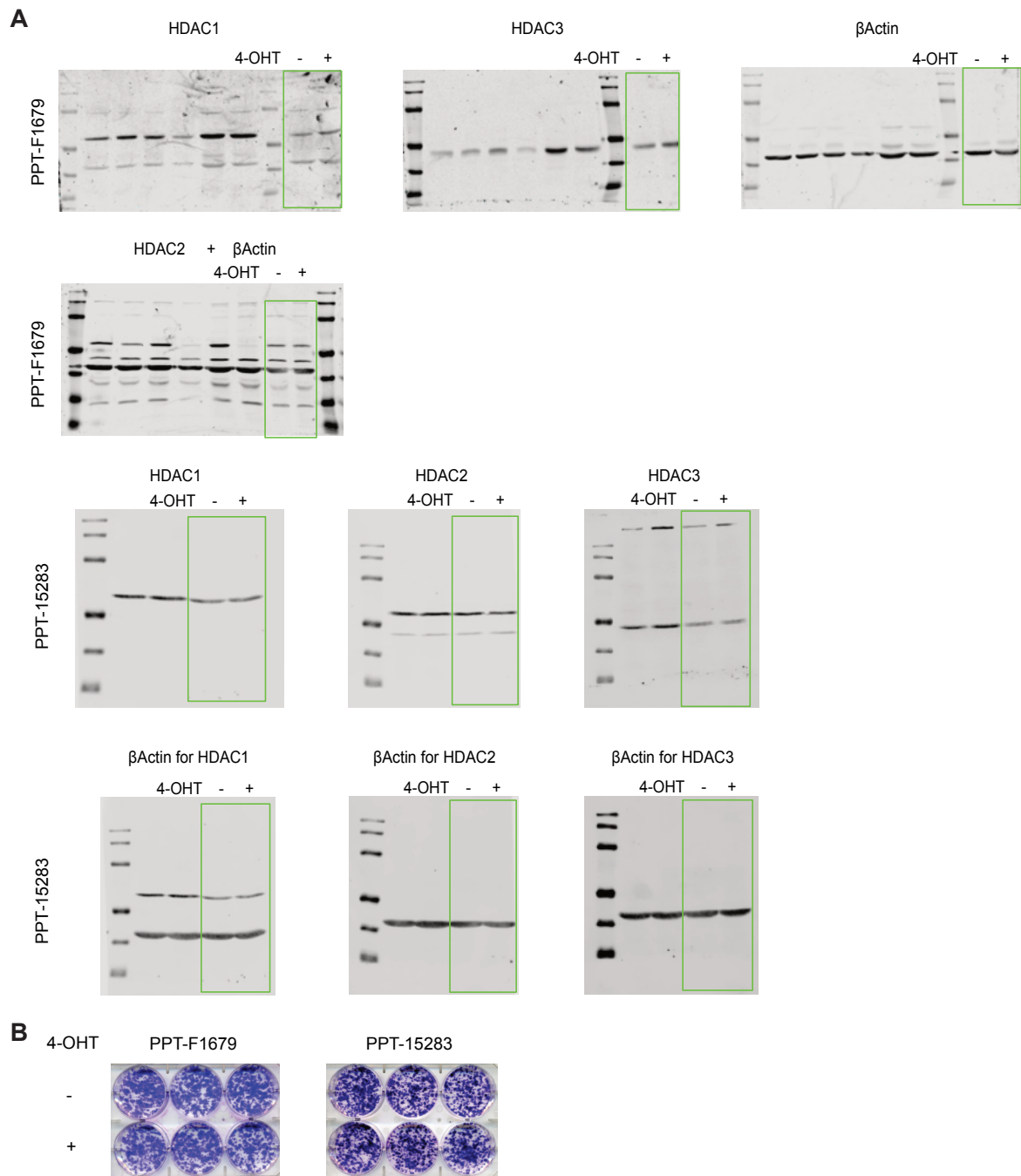


Figure A 5: Original western blots and clonogenic assays of Figure 7-9.

A) The complete original western blot of Figure 7-9 showing no change in HDAC1, Hdac2 and HDAC3 expression in the cell line PPT-F1670 and PPT-15283 used to test for Cre toxicity. As well western blot of loading control β Actin is shown, which was used for quantification. B) Original clonogenic assay of the cell line PPT-F1679 and PPT-15283 after eight days of 4-OHT/vehicle treatment, presented in Figure 7-9. After eight days of 4-OHT/vehicle treatment 2,000 cells were seeded in triplicates and analyzed for clonogenic assay after seven days. The western blot lanes depicted in Figure 7-9 are framed in green. 4-OHT = 4-Hydroxytamoxifen.

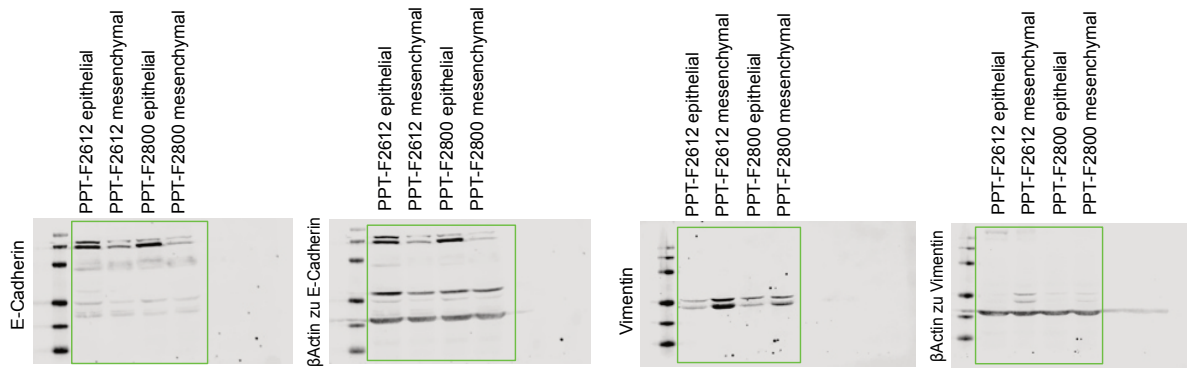


Figure A 6: Original western blots of Figure 7-10.

The complete original western blot of Figure 7-10 showing expression of E-Cadherin and Vimentin in epithelial and mesenchymal fractions of cell lines PPT-F2612 and PPT-F2800. As well western blot of loading control βActin is shown, which was used for quantification. The western blot lanes depicted in Figure 7-9 are framed in green. 4-OHT = 4-Hydroxytamoxifen.

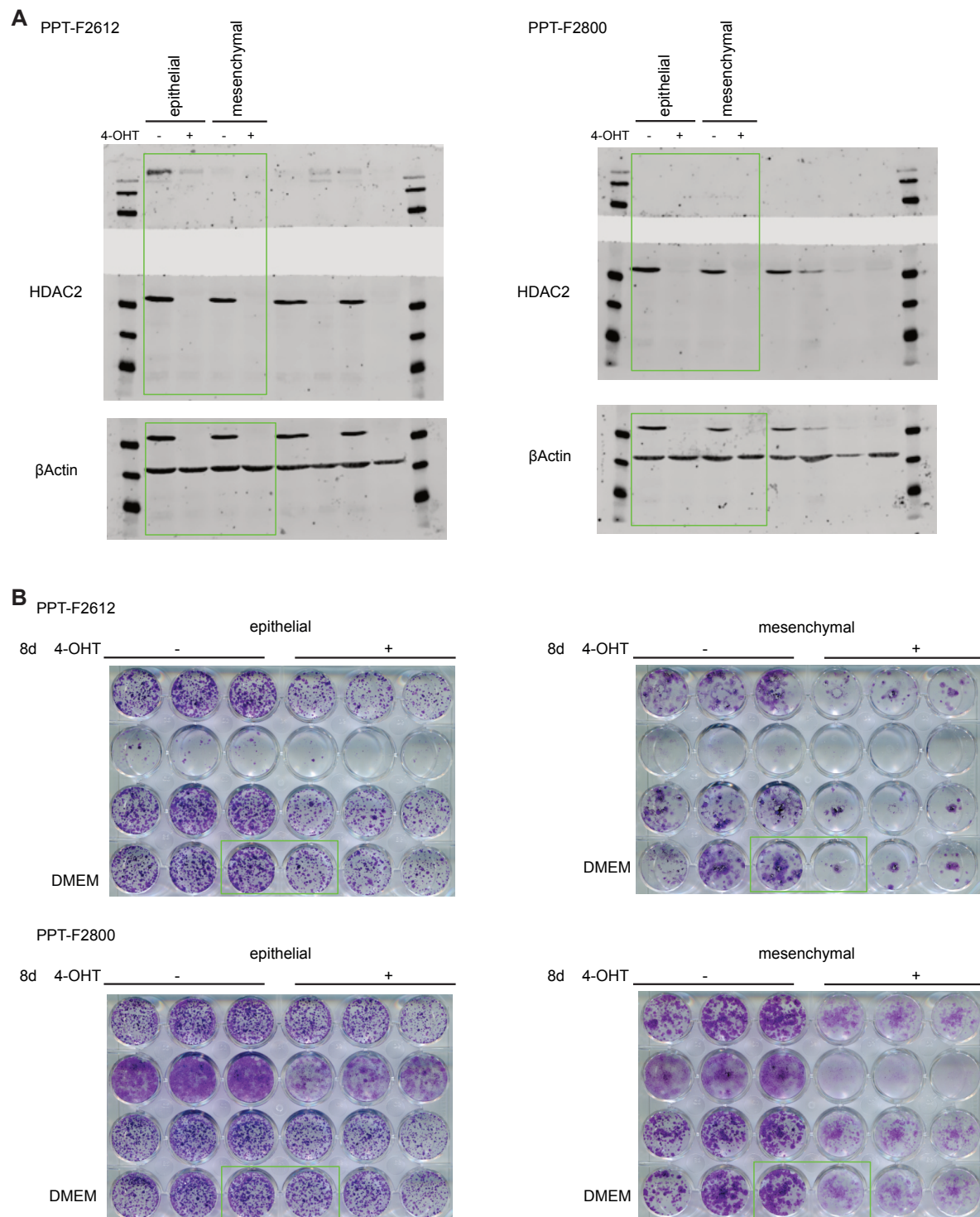


Figure A 7: Original western blots and clonogenic assays of Figure 7-10.

A) The complete original western blot of Figure 7-11 showing successful knock-out of *Hdac2* in epithelial and mesenchymal fractions of cell lines PPT-F2612 and PPT-F2800. As well western blot of loading control β Actin is shown, which was used for quantification. The western blot lanes depicted in Figure 7-10 are framed in green. B) Original clonogenic assay of the epithelial and mesenchymal fractions of the cell line PPT-F2612 and PPT-F2800 after eight days of 4-OHT/vehicle treatment, presented in Figure 7-10. After eight days of 4-OHT/vehicle treatment 2,000 cells were seeded in triplicates and analyzed for clonogenic assay after seven days. 4-OHT = 4-Hydroxytamoxifen.

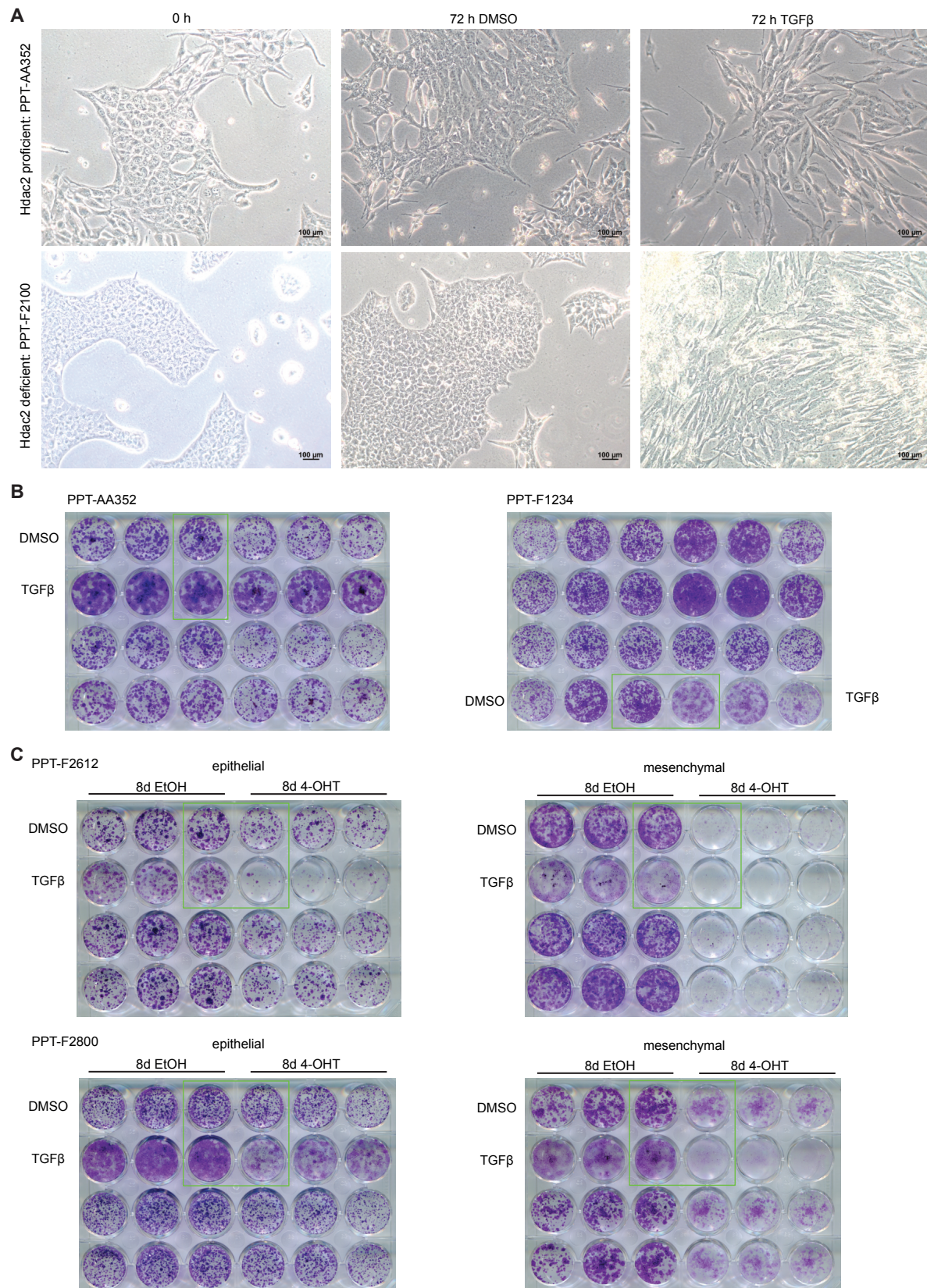


Figure A 8: Light microscopy picture and clonogenic assays of Figure 7-13 and Figure 7-14.

A) Enlarged light microscopy picture of KPC mouse model derived cell lines, treated for 72 hours with TGF β or vehicle as depicted in Figure 7-13. PPT-AA352 represent *Hdac2* proficient cells, PPT-F2100 represents *Hdac2* deficient cells. Scale bar depicts 100 μ m. B) Original clonogenic assay of *Hdac2* proficient cell line (PPT-AA352) and *Hdac2* deficient cell line (PPT-F1234) after seven days of TGF β or vehicle treatment. 2,000 cells were seeded in triplicates, treated with TGF β or vehicle after attachment overnight and analyzed for clonogenic assay after seven days. C) Original clonogenic assay of the

epithelial and mesenchymal fractions of the cell line PPT-F2612 and PPT-F2800 after eight days of 4-OHT/vehicle treatment followed by TGF β or vehicle treatment for seven days. After eight days of 4-OHT/vehicle treatment 2,000 cells were seeded in triplicates, treated with TGF β or vehicle after attachment overnight and analyzed for clonogenic assay after seven days. 4-OHT = 4-Hydroxytamoxifen.

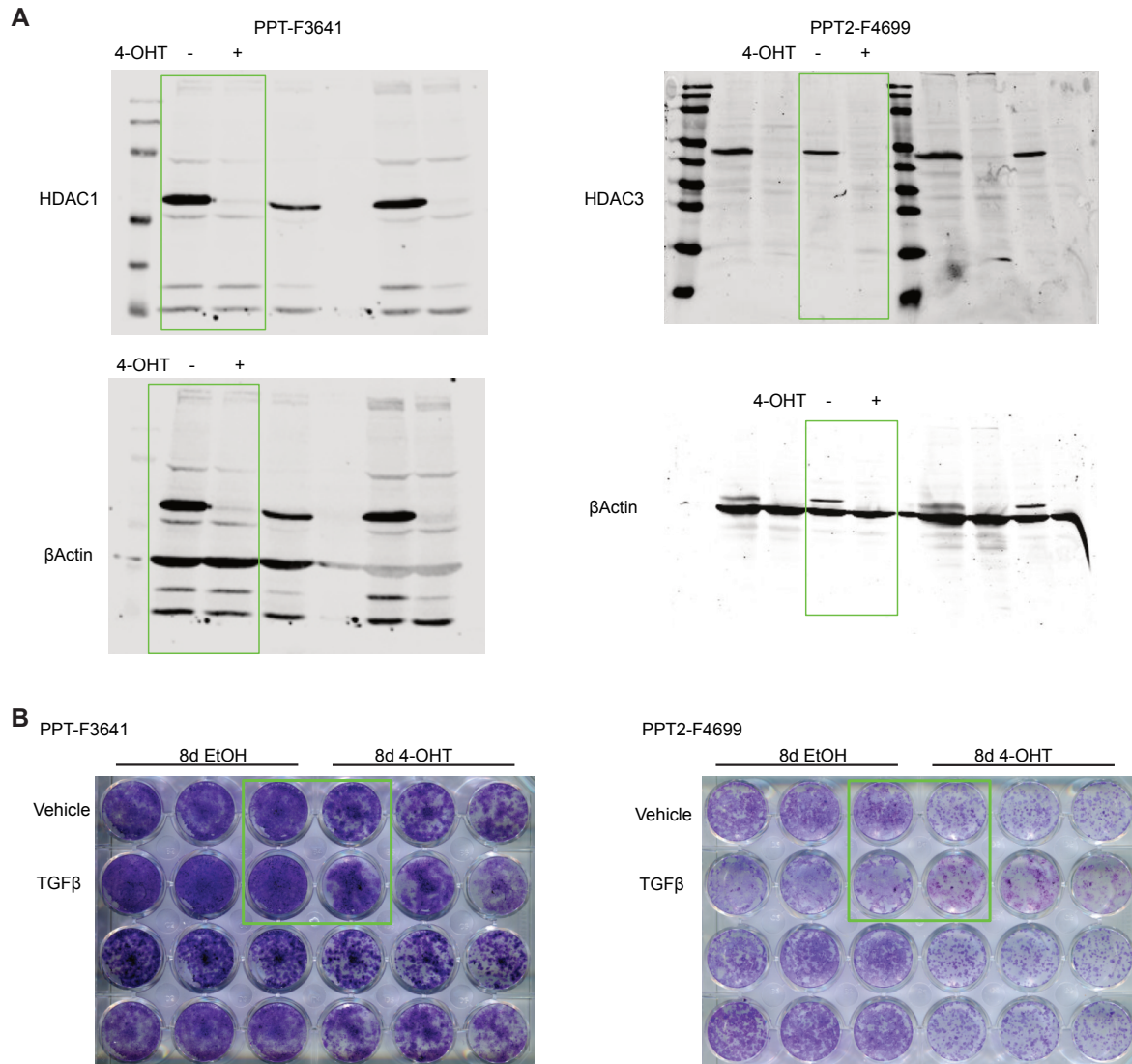


Figure A 9: Original western blots and clonogenic assays of Figure 7-15.

A) The complete original western blot of Figure 7-15 showing successful knock-out of *Hdac1* and *Hdac3* in cell lines PPT-F3641 and PPT2-F4699, respectively. As well western blot of loading control β Actin is shown, which was used for quantification. The western blot lanes depicted in Figure 7-15 are framed in green. B) Original clonogenic assay of the cell lines PPT-F3641 and PPT2-F4699 after eight days of 4-OHT/vehicle treatment followed by TGF β or vehicle treatment for seven days. After eight days of 4-OHT/vehicle treatment 2,000 cells were seeded in triplicates, treated with TGF β or vehicle after attachment overnight and analyzed for clonogenic assay after seven days. 4-OHT = 4-Hydroxytamoxifen.

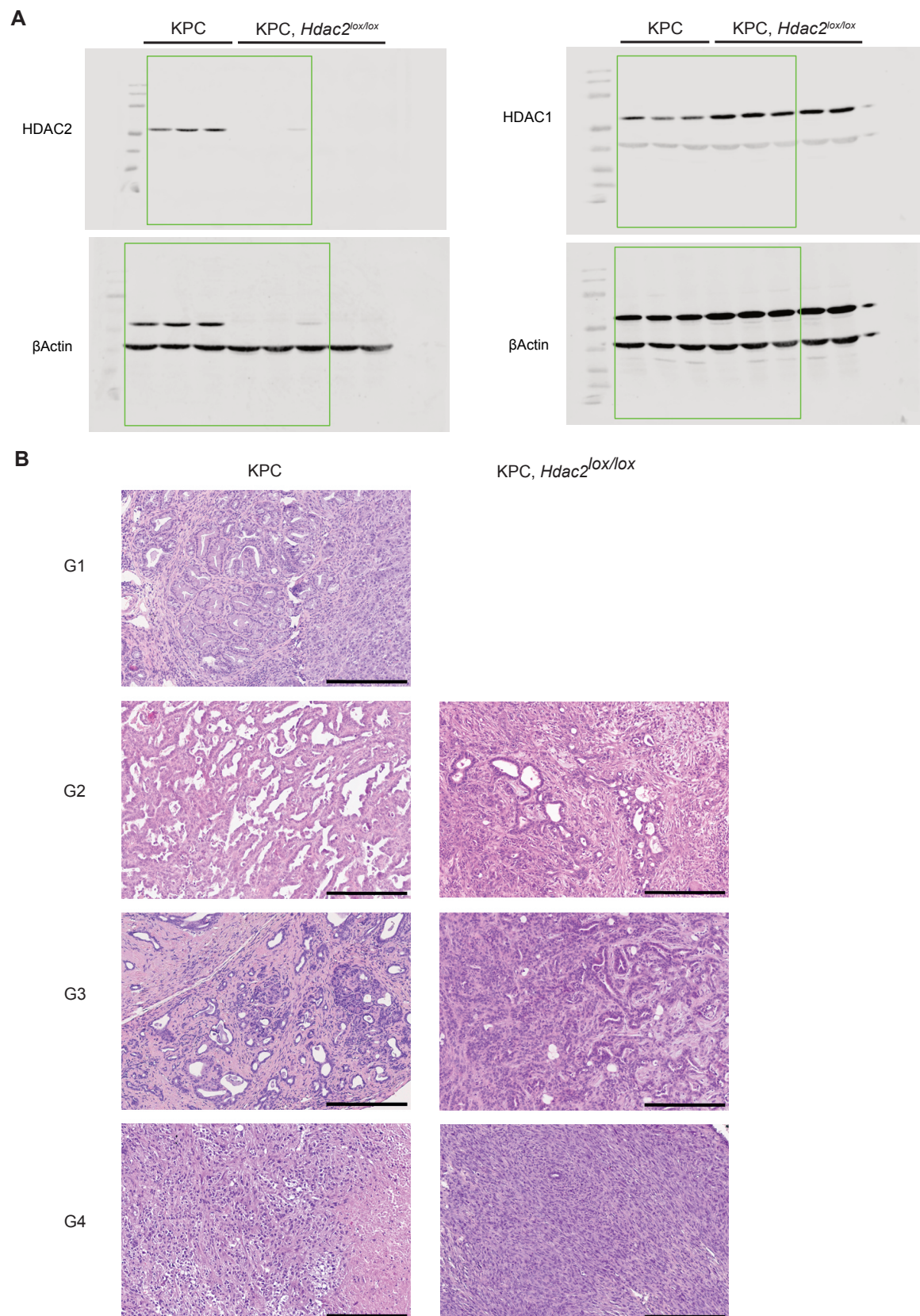


Figure A 10: Original western blots and H&E stainings of *Hdac2* pro- and deficient KPC mice of Figure 7-17.

A) The complete original western blot of Figure 7-17 showing no expression of HDAC2 and increased expression of HDAC1 in KPC mice with homozygously floxed *Hdac2* alleles. As well western blot of loading control βActin is shown, which was used for quantification. The western blot lanes depicted in Figure 7-17 are framed in green. B) H&E stainings of primary pancreatic tumors of *Hdac2* pro- and deficient KPC mice, according to their grading.

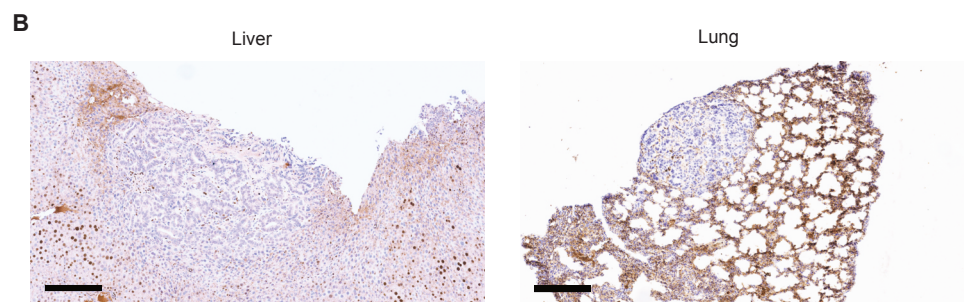
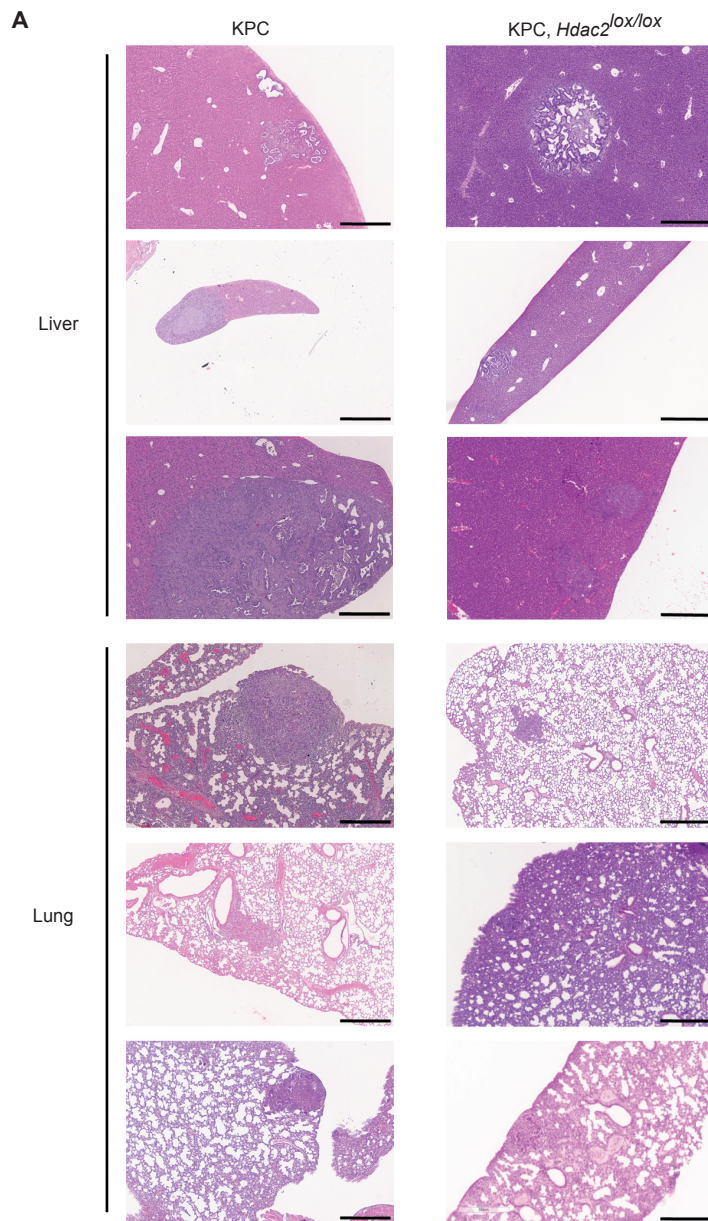


Figure A 11: H&E stainings of liver and lung of *Hdac2* pro- and deficient KPC mice of Figure 7-18 and Immunohistochemical analysis of HDAC2 expression in liver and lung metastasis of *Hdac2* deficient KPC mice of Figure 7-19.

A) Enlarged picture of H&E stainings of serial cuts from liver and lung tissue of *Hdac2* pro- and deficient KPC mice, that were used for metastasis screening as presented in Figure 7-18. Scale bar depict 500 μ m. KPC mice: liver metastasis of mice S114, S243, F0793; lung metastasis of mice 4421, 1812, 6719. KPC, *Hdac2*^{lox/lox} mice: liver metastasis of mice F1039, F1128, F2100; lung metastasis of mice F1915, F1039, F1091. B) Immunohistochemical analysis of HDAC2 expression in liver and lung metastasis of *Hdac2* deficient KPC mice. Scale bar depicts 200 μ m.

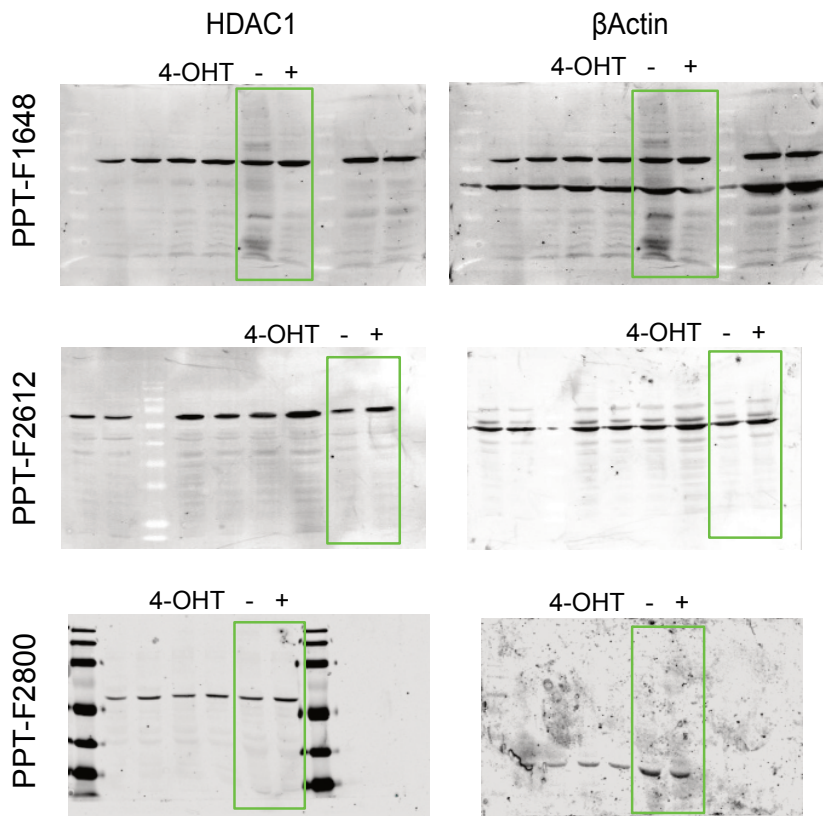


Figure A 12: Original western blots of Figure S 3.

The complete original western blot of Figure S 3 showing no difference in HDAC1 expression after 4-OHT/vehicle treatment in the cell line PPT-F1648, PPT-F2612 and PPT-F2800. As well western blot of loading control β Actin is shown. B successful knock-out of *Hdac2* in the same samples of the cell lines was already shown in Figure 7-4. The western blot lanes depicted in Figure S 3 are framed in green. 4-OHT = 4-Hydroxytamoxifen.

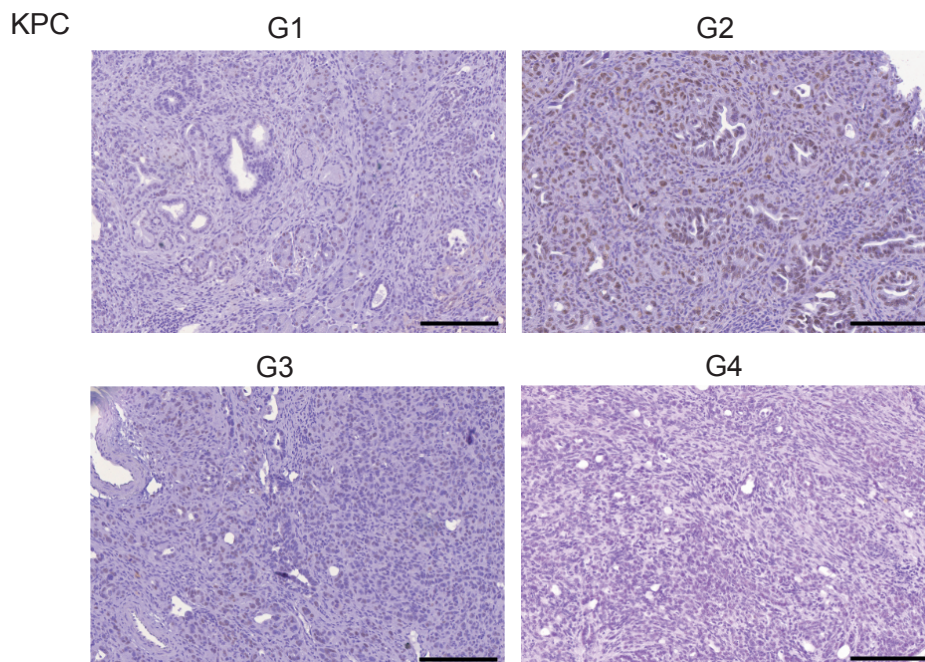


Figure A 13: Immunohistochemical analysis of HDAC2 expression in PPTs of KPC mice of Figure S 4.

Enlarged picture of Immunohistochemical analysis of HDAC2 expression in PPTs of *Hdac2* proficient KPC mice of each differentiation state (G1-G4). Scale bar depicts 500 μ m.